DOCTOR OF PHILOSOPHY

Investigating the relationship between clock gene stability and the pace of the vertebrate segmentation clock

Wiedermann, Guy

Award date:
2014

DOCTOR OF PHILOSOPHY

Investigating the relationship between clock gene stability and the pace of the vertebrate segmentation clock

Guy Wiedermann

2014

University of Dundee

Investigating the relationship between clock gene stability and the pace of the vertebrate segmentation clock

Guy Wiedermann

Doctor of Philosophy

University of Dundee

March 2014

Table of Contents

Table of Figures

Abbreviations

ADAM	A Disintegrin And Metalloproteinase
ANK	Ankyrin repeats
AP	Antero-posterior
APC	Adenomatous polyposis coli
bHLH	basic helix-loop-helix
BMP	Bone morphogenic protein
CDK	Cyclin-dependent kinase
CHX	Cycloheximide
CK1	Casein Kinase 1
CNH	Chordo-neural hinge
CREB	cAMP-response element-binding protein
CSL	CBF1, Su(H) and LAG-1 (a.k.a RBPJκ)
DLL	Delta-like
DMSO	Dimethyl sulfoxide
DRB	5,6-Dichloro-1-beta-D-ribofuranosylbenzimidazole
DSL	Delta, Serrate, and Lag-2
Dsh	Disheveled
E10.5	Embryonic day 10.5
EGF	Epidermal growth factor
ERK	Extracellular signal-regulated kinase
EtOH	Ethanol
FBW7	F-box and WD repeat domain-containing 7
FGF	Fibroblast Growth Factor
FGFR	Fibroblast Growth Factor Receptor
Fz	Frizzled
GSK3β	Glycogen synthase kinase 3 beta
HES	Hairy and enhancer of split

HH10	Hamburger and Hamilton stage 10
HOX	Homeobox
Hpf	Hours post-fertilisation
IgG	Immunoglobulin G
IP	Immunoprecipitation
ISH	*In situ* hybridisation
LEF	Lymphoid enhancer-binding factor
LFNG	Lunatic Fringe
LPM	Lateral plate mesoderm
MAM	Mastermind
MAPK	Mitogen activated protein kinase
MESP	Mesoderm posterior
MIB	Mindbomb
NC	Notochord
NECD	Notch extracellular domain
NICD	Notch intracellular domain
NLS	Nuclear localisation sequence
NSB	Node-streak border
NT	Neural tube
OPA	Glutamine-rich repeat
PEST	Proline/glutamic acid/serine/threonine-rich
PS	Primitive Streak
PSEN	Presenilin
PSM	Pre-somitic mesoderm
Ptch	Patched
RA	Retinoic acid
RAM	RBPJκ association module
RBPJκ	Recombination signal-Binding Protein 1 for J Kappa (a.k.a. CSL)

RC	Rostro-caudal
SHH	Sonic Hedgehog
Smo	Smoothened
T	Brachyury gene
TAD	Transactivation domain
TMD	Trans-membrane domain
WNT	Wingless-related integration site

Acknowledgements

I would like to thank the members of the Dale lab for all their help and moral support throughout my PhD. There are many people to thank. I would like to thank Kim for her constant support and motivating words, as well as first teaching me many procedures crucial to this project and also for assisting many times with those big dissection days. From the lab, I need to thank most notably Rob for the excellent banter during many many dissections days together and help with various aspects of the project. Sarah passed this project onto me and taught me many things during the very short time in which we overlapped. Mia kindly assisted me with the cNICD immunos and slide preparations. Miguel and Ian Newton were very helpful with advice on western blotting. Marianne is undoubtedly the most friendly and efficient lab manager in the building, which made life much easier during the last few years.

The labs of Kate Storey and Inke Nathke were very helpful with advice and reagents throughout my PhD. James and Fiona from the DSTT generated some of the antibodies that were essential for this project. I would like to thank Vicky Cowling and her lab for teaching me Immunoprecipitation and Liz Farrell from Dundee Cell Products for cloning some of the vectors for this project. Amit Garg kindly trawled the published microarray datasets on cycling gene to give us candidates to pursue further. Dave Chambers from KCL ran the custom chicken microarrays and the GSU at the University of Dundee ran the RNA-seq analyses. Pieta Schofield carried out all of the data normalisation and analysis from these datasets, for which I am very grateful. Doug Lamont was very cooperative with discussions about proteomics and for carrying out the mass spectrometry analyses.

Finally, I would like to dedicate my greatest thanks to my amazing fiancée Christina. I cannot put into words how important her support has been during the last few years, near and far, and I could not have done it without her. Her emotional support has undoubtedly helped me navigate my way through the ups and downs of my PhD.

Signed Declaration

I, the candidate, am the author of this thesis and have consulted all references cited. The work presented here is a record of my individual work, except where otherwise stated and this work has not previously been accepted for a higher degree.

Signed,

Guy Wiedermann

Supervisor Statement

The conditions of the relevant Ordinance and Regulations have been fulfilled.

Signed,

J. Kim Dale

Abstract

Somites are precursors of the vertebrae, ribs, and associated musculature and their formation relies on ordered and timely segmentation during early embryonic development. Somites form as they 'pinch' away from the pre-somitic mesoderm (PSM) with a species-specific periodicity, coinciding with waves of cycling mRNA expression of 'clock' genes sweeping across the PSM that are regulated by a molecular oscillator. Mathematical models suggest that sustained rapid oscillations of Notch-regulated gene transcription in the PSM depend on transient negative feedback loops that rely on unstable protein products. However, the pacemaker mechanism that underlies this segmentation clock is poorly understood and little experimental evidence exists linking the level of clock proteins to the periodicity of clock gene oscillations. It was previously shown that pharmacological inhibition of Wnt signalling slows oscillating transcription of the Notch target *Lfng* in the PSM of the chicken and mouse embryos. We have shown that another Wnt inhibitor XAV939 and a number of cdk inhibitors can phenocopy this effect in the PSM. This effect appears independent of the cell cycle and these inhibitors appear to have a general effect on transcription in the chicken PSM. In contrast to a previous report, we find that direct inhibition of Sonic hedgehog (Shh) signalling has no effect on oscillating clock gene transcription in the chicken PSM.

A custom-made antibody reveals that the level of a key clock protein is increased in the chicken PSM when treated with XAV939, or either of the cdk inhibitors which also slow oscillating clock gene transcription. This molecular evidence supports models which predict that the level of clock proteins in the PSM is fundamental to maintain rapid clock oscillations and timely somite formation. The Microarray and RNA-seq analyses of chicken PSM tissues discovered a set of genes whose transcription is affected by all three inhibitor treatments relative to corresponding controls. These candidates will be studied further as potential regulators of the segmentation clock period. Immunoprecipitation with the custom-made antibody followed by mass spectrometry analysis of lysates from chicken PSM tissues treated

with reagents that modify clock pace will uncover any post-translational modifications of this key protein which are altered by these inhibitors with the aim of identifying any key enzymatic regulators of its stability which act as part of the segmentation clock pacemaker mechanism.

Introduction

Early Tissue Formation in the Vertebrate Embryo

Segmentation of the vertebrate embryo, known as somitogenesis, is an essential process that is required during early embryogenesis to ensure the formation of the segmented skeleton and associated musculature in the adult (Dequeant and Pourquie, 2008). The entire process relies on a carefully orchestrated program of events that lead to the patterning of different tissues with specific timing that starts from very early stages of development. Signalling cues from an array of genetic pathways ensure normal embryonic development, which when disrupted can lead to congenital birth defects or even embryonic lethality (Giampietro et al, 2009).

Although the exact frequency of congenital vertebral malformations (CVM) is not clear, estimates have suggested between 0.5-1 in every 1000 humans exhibit some form of CVM (Giampietro et al, 2009). Some of the major human CVM disorders include congenital scoliosis, which occurs in ~1/1000 human births and is defined as lateral curvature of the spine more than 10 degrees caused by structural vertebral defects (Hedequist and Emans, 2007; Sparrow et al, 2012). Rarer syndromes include spondylocostal dysostosis (SCD) and spondylothoracic dysostosis (STD). SCD defines a range of defects generally affecting the segmentation of multiple vertebrae, which can involve more than 10 adjoining segments and often disrupting all vertebral regions with some rib alignment defects from the thoracic vertebrae (Sparrow et al, 2008). The defects of STD include a shortened trunk, with severe segmentation abnormalities affecting multiple neighbouring vertebrae and posterior rib fusion defects (Giampietro et al, 2009). These abnormalities are not a result of abberant bone formation but in fact occur much earlier due to errors during embryonic segmentation (Sparrow et al, 2012). Studies into the genetic etiologies of different types of CVM in humans to date are limited and further studies into embryonic segmentation are required if we are to gain a comprehensive understanding of the genetic basis behind these congenital birth defects.

This study will focus on segmentation within two different model species. The *Gallus gallus* (chicken) is an avian species, while the *Mus musculus* (mouse) is a mammalian species and therefore often used as a model due to strong similarities with human development. These model species are both examples of amniotes, which are a sub-set of tetrapod vertebrates including mammals, birds, and reptiles, the embryo of which develops within the protective amnion layer (Dequeant and Pourquie, 2008).

Vertebrates share many similarities in the processes that underlie early development and axial tissue formation during embryogenesis. The chicken has been a popular model species for studying early development of the vertebrate embryo. It is readily available at all times of the year and the Hamburger Hamilton developmental stage of the embryo can be accurately predicted based off the length of time and temperature that the egg is incubated for (Hamburger and Hamilton, 1951). The chicken embryo is also accessible for *in ovo* culture assays such as electroporation, as well as surgical and genetic manipulation in order to understand gene function in the regulation of key developmental processes (Gilbert, 2006).

The fertilised chick egg is telolecithal like the eggs of fish and reptiles, as it contains just a small disc of cytoplasm called the blastodisc that sits at the animal pole of the egg above a large yolk. Similar to the fish also, the chick egg undergoes discoidal meroblastic cleavage cell division as the egg is only partly divided and cleavage only occurs in the blastodisc (Fig.A.a; Gilbert, 2006). Once the first cleavage furrow appears centrally in the blastodisc, further cleavages occur but do not extend into the yolk and therefore form the blastoderm tissue of 5-6 cells in thickness at the future dorsal side of the embryo (Fig.A.b; Bellairs et al, 1978). The deeper cells at the centre of the blastoderm are then shed and die, which leaves a one-cell thick layer of cells known as the Area Pellucida which will later form most of the embryo proper. The periphery of the blastoderm maintains its thickness however and is known as the Area Opaca. The Marginal Zone is the domain that sits between the Area Pellucida and Area Opaca of the chicken embryo that also later contributes to embryonic cell fate (Gilbert, 2006).

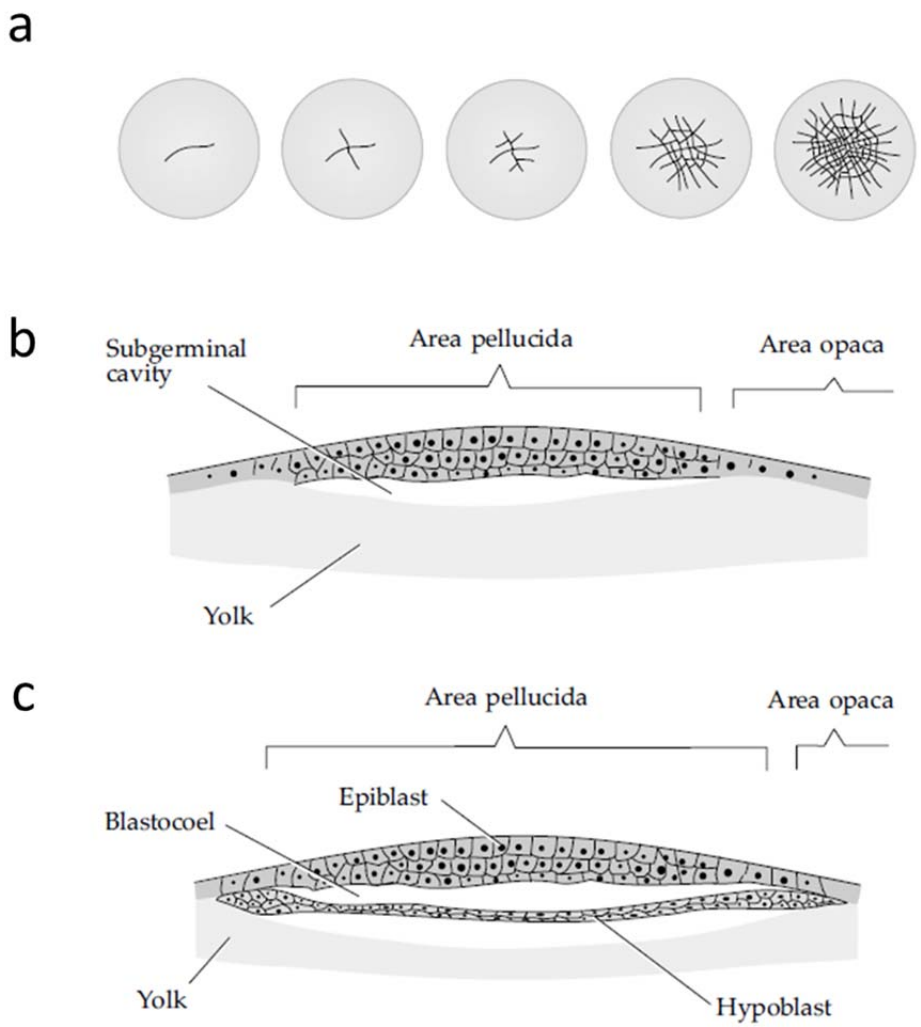

Figure A) Cleavage in the early chicken embryo. a) Schematic view above the animal pole of the early cleavage stage chick embryo, starting at the two-cell stage and progressing. The chick embryo undergoes discoidal meroblastic cleavage, as only the blastodisc cells at the animal pole of the egg divide. **b**) Transverse section schematic through the animal pole of a late cleavage stage chick embryo. The central Area pellucida will give rise to the embryo proper, while the peripheral Area opaca contributes to the extra-embryonic membranes. **c**) Transverse section schematic through the animal pole of an early gastrula stage chick embryo. The epiblast overlies the hypoblast layer of cells, with the intervening blastocoel cavity providing space for ingressing epiblast cells to form the 3 germ layers during gastrulation. (Adapted from **Gilbert, 2006**)

The majority of the cells in the Area Pellucida remain at the surface and form the epiblast which exclusively gives rise to all three germ layers of the chick embryo proper: the ectoderm, mesoderm, and endoderm; as well as contributing to some of the extra-embryonic membranes (Schoenwolf, 1991). However, some individual cells delaminate from the Area Pellucida and migrate ventrally to form 'islands' of primary hypoblast cells. Soon afterwards, cells from the posterior edge of the blastoderm migrate anteriorly as a sheet and push the primary hypoblast anteriorly in the process to create the secondary hypoblast (Stern, 2004). The epiblast and underlying hypoblast layers are both joined at the Marginal Zone, thus creating a space in between which is called the blastocoel (Fig.A.c; Gilbert, 2006).

A common feature of gastrulation in amniotes is the formation of the primitive streak (PS) from the epiblast layer of cells. In the chick embryo, the PS is first visible in the egg at 3-4 hours after laying as a thickening of cells in the medial epiblast at the posterior Marginal Zone. The PS cells become motile and undergo convergent extension movements that aid the progression of the PS anteriorly along the midline of the embryo, while becoming increasingly narrow (Fig. B.a) (Gilbert, 2006; Wilson et al, 2009). By 15-16 hours a depression known as the primitive groove can be seen inside the chick PS, which allows ingressing epiblast cells to migrate into the blastocoel below to give rise to the endodermal and mesodermal germ layers (Stern, 2004). The PS is analogous to the blastopore of the amphibian embryo and marks the site of gastrulation where the three germ layers of the embryo are established. A region of cells at the anterior limit of PS then form an organising centre containing progenitors of axial tissues which is known as the Hensen's node in the chick, or the node in the mouse embryo (Wilson et al, 2009). At 24 hours of incubation, or stage ~HH5, the chick PS reaches it is full extension of 60-75% of the Area Pellucida length before starting to regress towards the posterior of the embryo (Gilbert, 2006). As the PS regresses, the axial tissues are specified synchronously in an anterior-to-posterior direction and the embryo continues to extend its axis from the caudal end (Fig. B.b). The first cells to migrate through the node form the endoderm layer which lies most ventrally and will form the much of the internal organs. The next group of

ingressing cells through the node and PS form a loose layer of mesodermal cells which lie above the ventral endoderm layer and below the more dorsal epiblast. The mesoderm is then separated into the paraxial mesoderm, the intermediate mesoderm, and the lateral plate mesoderm (LPM) (Stern, 2004).

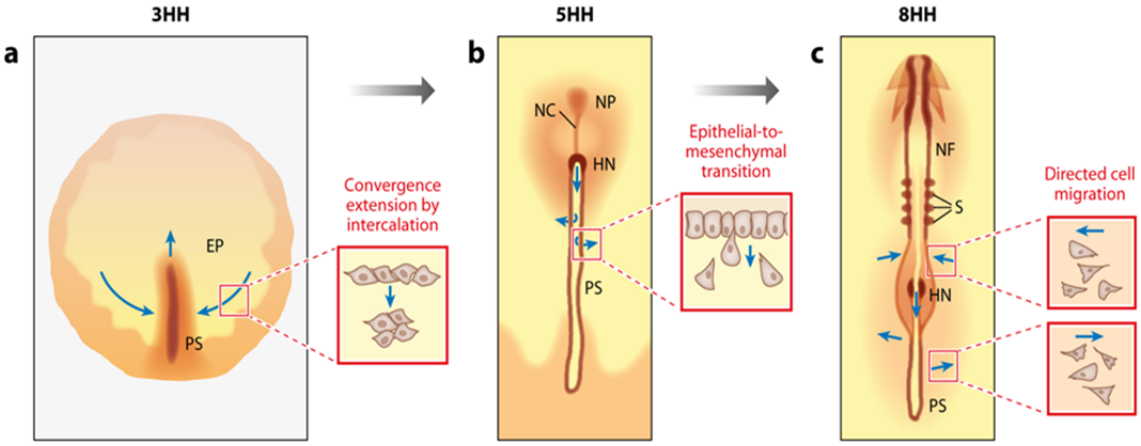

Figure B) Cellular movements during gastrulation and early embryonic axis elongation. Schematic dorsal views of the chicken embryo at stage Hamburger-Hamilton (HH) 3 (**a**), 5 (**b**), and 8 (**c**). **a**) Convergent-extension movements of epiblast (EP) cells at HH3 allow the primitive streak (PS) to extend towards the anterior embryo. **b**) By HH5 the PS has reached its full extension and starts to regress towards the posterior embryo while laying down the notochord (NC) and neural plate (NP) tissues from the Hensen's node (HN) at the anterior tip of the PS. Posterior to the HN, EP cells ingressing through the PS undergo EMT to form the mesodermal lineages. **c**) At HH8, directed migration and ingression reorganises the mesoderm. Convergent extension of paraxial mesoderm cells occurs towards the midline as this tissue generates the somites (S) from its anterior end. (Taken from **Benazeraf and Pourquie, 2013**)

Cell fate studies have uncovered specific regions of the PS, node, and epiblast which contribute to different axial tissues. The notochord (NC) - a rod of chordamesoderm which provides rigidity to the forming embryo - is formed from the node at the anterior limit of the PS and is left behind in the wake of the regressing PS (Wilson et al, 2009). This structure is a defining feature of chordates, although in most vertebrates the NC is not maintained in the adult, rather it forms the nucleus pulposus of the intervertebral discs (Gilbert, 2006). The central nervous system, which includes the brain and spinal cord of the adult, is initially formed by primary neurulation of ectoderm in the vertebrate embryo. This involves the production of a neural plate along the midline of the embryo which lies dorsal to the NC. More lateral neural cells then form neural folds either side of the midline that gradually fold up until they eventually meet at the dorsal edge to close off and form the neural tube (NT). Cells from the dorsal node have been shown to exclusively give rise to the ventral midline of the NT (Charrier et al, 1999), while epiblast cells surrounding the PS caudal and lateral to the node are found to contribute to the rest of the NT and to the paraxial mesoderm lineages (Fig. B.c) (Cambray and Wilson, 2007; Delfino-Machin et al, 2005).

Cells ingressing through more caudal regions of the PS contribute to increasingly more lateral mesodermal tissues including the paraxial mesoderm, heart, kidneys, LPM, and the extra-embryonic mesoderm (Psychoyos and Stern, 1996). The paraxial mesoderm flanking either side of both the NC and neural tissues contributes to the head mesoderm, as well as giving rise to the pre-somitic mesoderm (PSM) in amniotes (Dequeant and Pourquie, 2008; Maroto et al, 2012). The LPM contributes to the circulatory system, limb buds and heart mesoderm (Gilbert, 2006). More recent studies have given evidence for the existence of self-renewing, multipotent axial stem cells within an area including the caudal node and rostral limit of the neighbouring PS - termed the node-streak border (NSB) (Cambray and Wilson, 2002; Cambray and Wilson, 2007). Cells from the NSB and later in the chordo-neural hinge (CNH) derivative region of the tailbud have been shown to contribute to the NC, PSM, and the NT in the chick and mouse embryos (Cambray and Wilson, 2002; Charrier et al, 1999; McGrew et al, 2008).

As the axial tissues are laid down the embryo extends its axis from the caudal end of the PS, and later in the tailbud, with the aid of self-renewing axial stem cell progenitors which proliferate to replenish cells migrating through the PS (Cambray and Wilson, 2002, Maroto et al, 2012). The formation of the tailbud region later in development at stage HH14 in the chick and at embryonic day 9.5-10 (E9.5-10) in the mouse was previously thought to represent the creation of a pool of caudal axial progenitors (Criley, 1969; Schoenwolf, 1984). However, Wilson et al (2009) have postulated that the growing evidence for self-renewing stem cells suggest that this progenitor cell population is present earlier in development in the NSB and PS regions and that the process is continuous rather than from separate cell populations.

Somitogenesis in the vertebrate embryo

While the PS continues to regress towards the tail end, the anterior axial tissues are more specified than in the posterior embryo as they have formed earlier and have therefore had more time to undergo further differentiation and maturation. For example, in the stage HH10 chick embryo the neurectoderm in the caudal embryo at the level of the PSM has recently formed and is present as a relatively flat neural plate with a just slight indent at the midline. However, in the rostral embryo the neural folds have risen and converged to create the fully closed NT structure. In this sense, the embryo can be seen as a time-series of development with the oldest part at the head end and increasingly younger towards the primitive groove at the tail end (Fig. C). This is true of other axial tissues as well such as the neighbouring paraxial mesoderm tissue.

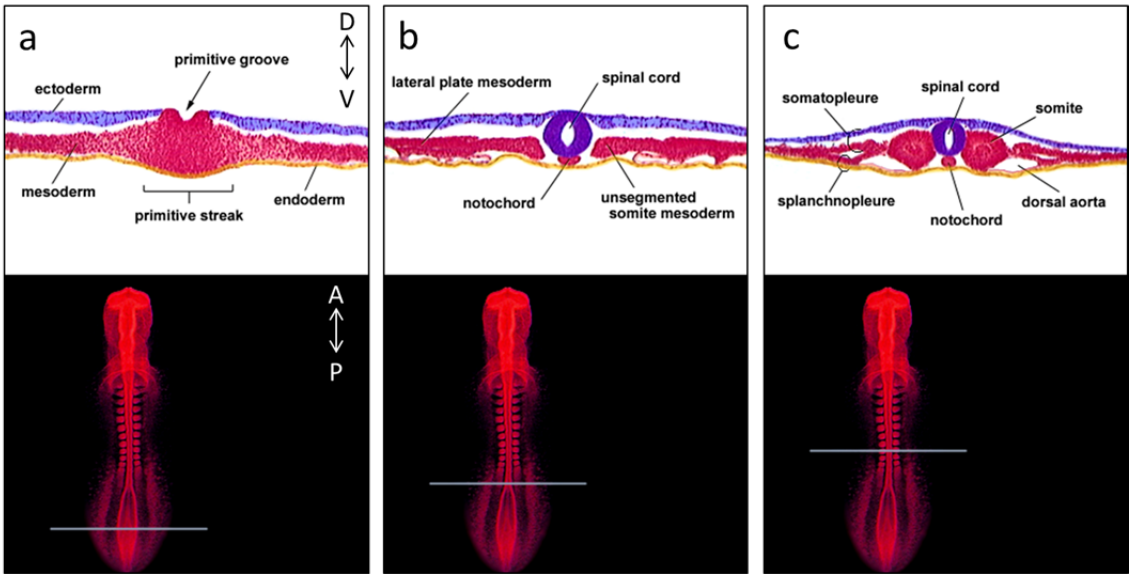

Figure C) Axial tissue formation and specification along the vertebrate embryonic axis. a-c) Transverse sections through the primitive streak (PS) region (**a**), pre-somitic mesoderm (PSM) region (**b**), and somite region (**c**) of a stage HH10 chicken embryo. **a**) In the PS region of the caudal embryo, the dorsal ectoderm layer and PS at the midline lie above the mesenchymal mesoderm layer, with the ventral endodermal cell layer underneath. **b**) At the level of the anterior PSM, the neural tube/spinal cord has closed up fully into a tube at the midline, with the mesoderm-derived notochord lying ventrally beneath the neural tube. The unsegmented PSM lies laterally either side of the neural tube and notochord, with the lateral plate mesoderm lying more laterally still either side of the PSM. **c**) Anterior to the PSM, the somites have segmented away from the paraxial mesoderm in pairs either side of the neural tube and form an epithelial outer layer. (Adapted from **Gilbert, 2006**)

The neighbouring PSM is a loosely organised tissue of mesenchymal cells that forms from the paraxial mesoderm either side of the forming neural plate/tube of the amniote embryo. However in lower vertebrates such as the zebrafish, the PSM lineage forms from the dorsal mesoderm (Dequeant and Pourquie, 2008). The PSM is an unsegmented tissue which forms segments of mesoderm, known as somites. The developmental process of vertebrate segmentation (or the generation of the somites) is also called somitogenesis. The somites are epithelialised blocks of mesoderm that periodically segment away from the anterior end of the PSM in pairs (Fig. D). The formation of a new pair of somites occurs sequentially at regular intervals and with a timing that is specific to each species. For example, a new pair of somites forms every 30 minutes in the zebrafish, in the chick embryo every 90 minutes, while in the mouse every 120 minutes and in the human every 4-5 hours (Dequeant and Pourquie, 2008). At the end of somitogenesis the number of somites formed also depends on the species: the chick embryo forms about 55 pairs of somites in total, the mouse has 65, the human forms 33, and some snakes have several hundred pairs of somites (Gomez et al, 2008).

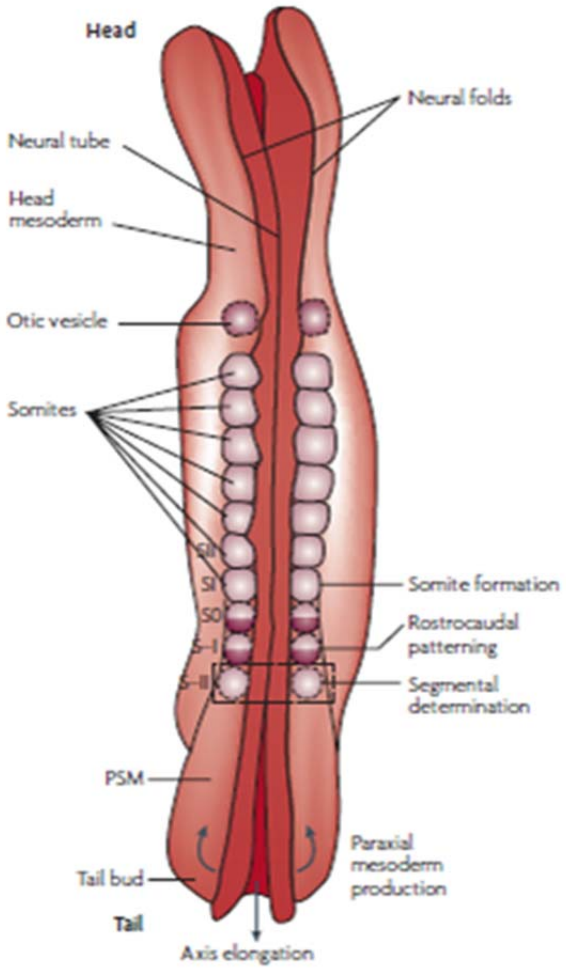

Figure D) Segmentation in the early vertebrate embryo. Dorsal schematic view of a 4-week old human embryo. The somites form sequentially in pairs in an anterior-to-posterior direction as they bud off from the anterior end of the PSM. The unsegmented PSM is replenished by progenitors from the tailbud ingressing from the primitive streak, which also allow axial elongation from the tail end (see arrows). Following segmental determination, the prospective somite region of the anterior PSM has rostro-caudal patterning specified prior to segmentation. The latest somite to form is termed the S0, with the S1 being the previous pair and so on. The next prospective somite regions of the PSM in order are termed the S-1, S-2, and so on. (Taken from **Dequeant and Pourquie, 2008**)

Invertebrate embryonic segmentation

Invertebrate segmentation differs from vertebrates in a number of fundamental ways. Studies on segmentation in the embryo of the fruit fly *Drosophila melanogaster* preceded major studies on vertebrates and uncovered a number of key signalling components whose homologues also have regulatory roles in vertebrate segmentation. Screens for segmentation abnormalities in the fly were the first studies to identify crucial signalling cascades that initiate the process of segmentation (Fig. E) (Nüsslein-Volhard and Wieschaus, 1980). The maternal messenger ribonucleic acids (mRNAs) *bicoid* and *nanos* are bound to the cytoskeleton on microtubules and are present in the anterior and poster poles of the oocyte, respectively (Gilbert, 2006). Once ovulation and fertilisation are complete, the protein products of these genes then diffuse across the syncytial blastoderm to form opposing morphogen gradients that are crucial for the establishment of AP patterning (Driever and Nusslein-Volhard, 1988; Wharton and Struhl, 1991). In addition, the maternal effect mRNAs *hunchback* and *caudal* are transported from the nurse cells of the fly ovary to the oocyte where they are present evenly across the AP axis of the syncytial blastoderm (Lehmann and Nüsslein-Volhard, 1987; Wu and Lengyel, 1998). Pumilio binding to the 3’ end of maternal *Hunchback* mRNA recruits Nanos to then bind the 3 prime untranslated region (3’ UTR) of Hunchback and inhibit its translation in the posterior embryo (Murata and Wharton, 1995). Hunchback protein is then restricted to a gradient of expression which is highest in the anterior end, while Nanos-dependent inhibition of *hunchback* translation prevents Hunchback protein expression in the posterior end of the embryo (Tautz et al, 1988). Hunchback protein is then restricted to a gradient of expression which is highest in the anterior end, while Nanos-dependent inhibition of *hunchback* translation prevents Hunchback protein expression in the posterior end of the embryo (Tautz et al, 1988). Conversely, *caudal* translation occurs in the posterior end of the embryo only due to Bicoid binding to the 3’ UTR of *caudal* mRNA in the anterior end of the embryo and preventing its translation here (Rivera-Pomar et al, 1996).

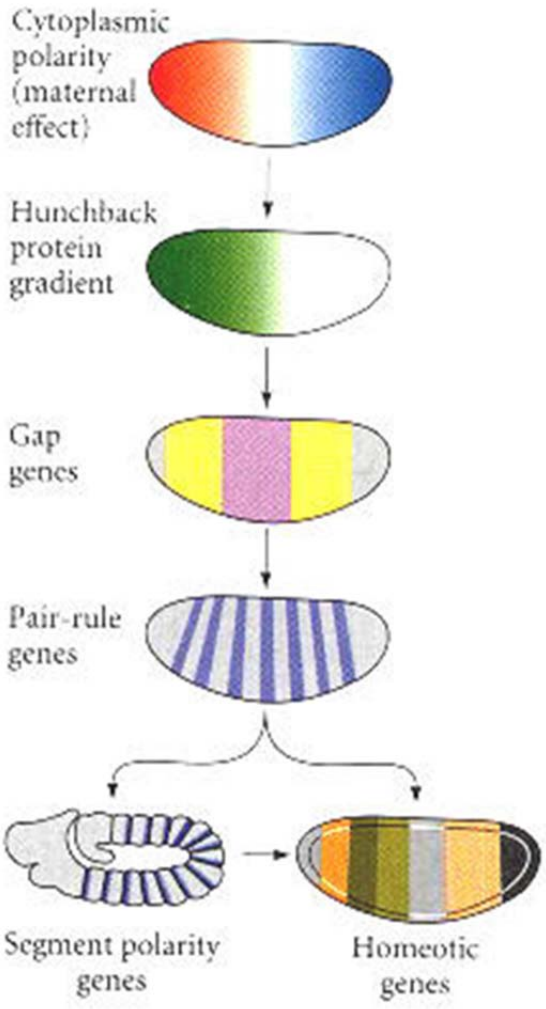

Figure E) The signalling cascade in *Drosophila melanogaster* segmentation. Maternal effect genes specify cytoplasmic polarity in the syncytial blastoderm of *Drosophila melanogaster*. These then activate the graded expression of proteins such as Hunchback across the AP axis. These protein gradients active the zygotic gap genes in different broad overlapping regions of the embryo. The pair-rule genes which mark the embryo in stripes of 2-segments wide are activated by the gap genes. Finally, the segment polarity genes divide the embryo into segment-wide domains and the concerted action of the various segmentation genes determine the localisation of the homeotic genes to define segment morphology along the AP axis. (Taken from **Gilbert, 2006**)

Bicoid and Hunchback have been shown to activate a number of targets present in anterior embryo, such as *Kruppel* and *knirps* (Hulskamp et al, 1990)*,*that are known as zygotic gap genes due to mutations in these genes leading to gaps in the segment pattern of the embryo (Cohen and Jürgens, 1990). Caudal also activates expression of posterior zygotic gap genes such as *giant* (Schulz and Tautz, 1995). The zygotic gap genes are expressed in broad, partially overlapping domains of roughly 3 segments wide which then activate a range of pair-rule genes, including *hairy, even-skipped, and runt*, which are expressed in 7 transverse stripes perpendicular to and across the AP axis thus dividing the embryo into periodic units (Gilbert, 2006). The expression profiles of the pair-rule genes are then stabilised via repressive interactions between their protein products (Levine and Harding, 1989). Finally, the striped pattern of pair-rule genes activates the expression of segment polarity genes belonging mainly to the Wingless and Hedgehog (Hh) pathways in 14 stripes across the AP axis to demarcate the 14 embryonic parasegments (Gilbert, 2006). The 14 embryonic segments of mesoderm in the *Drosophila* embryo are known as parasegments because, much like the somites in vertebrates, these structures will undergo a resegmentation process whereby the posterior portion of one segment and the anterior portion of the next neighbouring posterior segment will later combine to form a segment of the larva and adult (Martinez Arias and Lawrence, 1985). For example, *wingless* expression is present in the anterior compartment of each parasegment, while *engrailed* expression is limited to the posterior compartment of each parasegment (Gilbert, 2006). *Hh* is then expressed by those cells expressing *engrailed* and secreted Hh protein maintains *wingless* expression from the cells in the neighbouring compartment, which in turn secrete Wingless protein to maintain *Hh* expression in the neighbouring cells from which they received the Hh signal (Heemserk et al, 1991, Ingham et al, 1991). These positive feedback loops ensure that the pattern of segment polarity is maintained.

Other insect species such as the Red flour beetle *Tribolium castaneum* form some anterior segments from the blastoderm, while the remaining embryonic segments form sequentially from a 'growth-zone' region with fibroblast growth factor (Fgf) signalling activity more similar to that of the caudal vertebrate embryo (Beerman and Schroder, 2008; Davis and Patel, 2002). The process of segment formation in *Drosophila melanogaster* is more uncommon as the majority of other segmented organisms, including vertebrates, form segments in succession rather than simultaneously (Dequeant and Pouquie, 2008). The *Drosophila* embryo has adapted a long-germ type of development that involves the anterior gradient of Bicoid (Wolff et al, 1998). However, this mode of embryogenesis appears to be a later adaptation of higher dipterans, as the ancestral mode of arthropod development involves short-germ development and no homologue of *Bicoid* has been identified outside of the dipteran order (Wolff et al, 1998). The expression of homeotic selector genes in *Drosophila melanogaster* is activated within each formed segment depending on a specific combination of gap and pair-rule genes in order to determine the anatomical identity of the segments along the AP axis (Levine and Harding, 1989). Again this feature is not shared in vertebrates, as the Homeobox (Hox) genes that define AP spatial identity of the vertebrae and associated tissues in vertebrates are expressed in broader, overlapping domains which encompass multiple segments (Gould et al, 1997).

Indeed, the acquisition of segment identity across the AP axis in higher vertebrates appears to be much more complicated than *Drosophila melanogaster.* As for the fly, vertebrate somite identity along the AP axis relies on a co-linear relationship between the timing and spatial order of Hox gene expression (Izpisúa-Belmonte et al, 1991). However, as each pair of somites bud of in succession from the rostral end, the vertebrate PSM is extended at the caudal end by the influx of migrating progenitors from the node, the PS, and later from the CNH in the tailbud to maintain the length of the PSM. As a result, PSM cells are constantly displaced and acquire an increasingly more anterior spatial position within the PSM until they are incorporated into a segmented somite. This links axial elongation and segmentation in the

vertebrate embryo. Benazeraf et al (2010) reported that a gradient of random cell motility exists across the antero-posterior (AP) axis of the PSM tissue in the chick embryo which is important for the control of axis elongation. PSM cells are present at the lowest density and highest motility in the caudal end of the PSM. As development progresses and they assume a more rostral position, the PSM cells become increasingly less motile and more tightly packed within the PSM (Benazeraf et al, 2010). Gradients of activity from the Fgf and wingless-related integration site (Wnt) signalling pathways also exist across the AP axis of the caudal embryo (Aulehla et al, 2003; Aulehla et al, 2008; Boulet and Capecchi, 2012; Naiche et al, 2011, Stulberg et al, 2012). Cells in the very caudal PSM are exposed to the highest levels of Fgf and Wnt signalling and decreasing levels towards the rostral PSM. The gradients of Fgf and Wnt signalling in the caudal embryo therefore have roles in controlling both axial elongation and the maintenance of the axial progenitor pool within the node/PS and later in the tailbud (Benazeraf et al, 2010; Boulet and Cappechi, 2012; Naiche et al, 2011).

The Vertebrate Segmentation Clock

One of the major questions within the field of vertebrate embryology has been to understand how the embryo is able to produce somites at regular intervals and with specific timing from the PSM. The somites also always form in a rostral to caudal direction in vertebrate species. The strict periodicity with which somites segment away from the rostral PSM led to mathematical models which predicted the existence of an oscillator within the unsegmented PSM to explain how this periodicity is regulated (Cooke and Zeeman, 1976; Murray et al, 2011). The 'clock and wavefront' model first proposed by Cooke and Zeeman (1976) predicted that a molecular oscillator exists in the unsegmented PSM which periodically exposes PSM cells to different phases of the smooth oscillator. Meanwhile, a slower wavefront was proposed to exist across the AP axis of the PSM which could induce a cell change to slow and eventually stop the oscillation in the rostral PSM to allow somite formation (Cooke and Zeeman, 1976; Murray et al, 2011). This model predicts that the size of the somite is determined by the speed of the wavefront, while the periodicity of somite formation depends on the rate of the clock (Cooke and Zeeman, 1976; Gibb et al, 2010).

Stern et al (1988) proposed another model in which the cell cycle is linked to somitogenesis. Heat shock or treatment with cell cycle inhibitor drugs in the chicken embryo results in repeated somite abnormalities every 6-7 somites, with normal somites in between (Primmett et al, 1989; Stern et al, 1988). They hypothesised that this could correspond to the cell cycle, which was measured to be ~10 hours in the chicken PSM, the same time predicted to form 6-7 somites (Stern et al, 1988). The Cell Cycle model of somitogenesis that arose from this study proposed that cells destined to contribute to the somites leave the Hensen's node in the order that they are derived from progenitors and remain in that order as they assume an increasingly more rostral position in the PSM while axial elongation occurs from the caudal end of the embryo. This would mean that PSM cells at the same level would be synchronised regarding their position along the cell cycle, with more rostral cells having progressed further through

the cell cycle than younger cells in the caudal PSM. At a certain point, these synchronised cells would reach a point in the anterior PSM and increase their adhesion to each other via cell adhesion molecules. Finally, one cell cycle after this window this group of cells would segment away from the rostral PSM and enter a new phase of the cell cycle where they are no longer responsive to the signal (Stern et al, 1988).

Another model proposed suggests that somite boundaries are determined in a manner more similar to *Drosophila* segmentation. The metameric (repeated segments) pattern in vertebrates could be generated by opposing groups of cells with different identities (Meinhardt, 1982; Meinhardt, 1986). This model speculated that an AP gradient of positional information could generate such cell states via a reaction-diffusion mechanism. A presumptive somite cell first oscillates between these states before attaining a final, stable identity to contribute either to the anterior or posterior half of a somite (Keynes and Stern, 1988). Meinhardt (1986) suggested that the metameric pattern in vertebrates could be achieved by a two-segment periodicity reminiscent of the pair-rule genes in *Drosophila*. Blocks of cells the size of a somite could oscillate between two states (say Odd and Even), while borders will form between consecutive Odd and Even margins. It has been argued that the AP separation in the middle of the sclerotome which later forms from the somite is evidence for this model (Keynes and Stern, 1988; Meinhardt, 1986). This model, like that of Cooke and Zeeman (1976), suggests that the oscillator must coincide with the period of somite formation (i.e ~90 minutes in the chicken) (Meinhardt, 1986).

The ‘clock and trail’ model proposed that a single entity governs somite formation, while relying on cellular ‘memory’ of when cells exit the ‘progress zone’ of proliferating cells in the caudal end of the PSM (Kerszberg and Wolpert, 2000). This model suggests that the progress zone leaves behind a trail of cells as it regresses. Cells in the progress zone exhibit some form of synchronised oscillation that may be periodic gene transcription. As cells leave the progress zone, they make a permanent ‘record’ of the oscillator state at that moment. These cells then

continue to oscillate for a defined period of time based on their interpretation of the spatial sine wave until somite segmentation occurs once they reach the rostral PSM (Kerszberg and Wolpert, 2000).

The clock and wavefront model is the most widely accepted model for somitogenesis and has received the most experimental evidence over the past two decades (Fig. F) (Dequeant and Pourquie, 2008). Oscillating Notch activity across the PSM is a conserved feature among vertebrates and is likely to constitute a core mechanism of the segmentation clock. Meanwhile, gradients of Fgf and Wnt signalling activity from the posterior opposing retinoic acid (RA) signalling activity from the anterior embryo are shown to establish the wavefront which determines somite boundary position (Aulehla et al, 2003; Aulehla et al, 2008; Diez del Corral and Storey, 2004; Dubrulle et al, 2001).

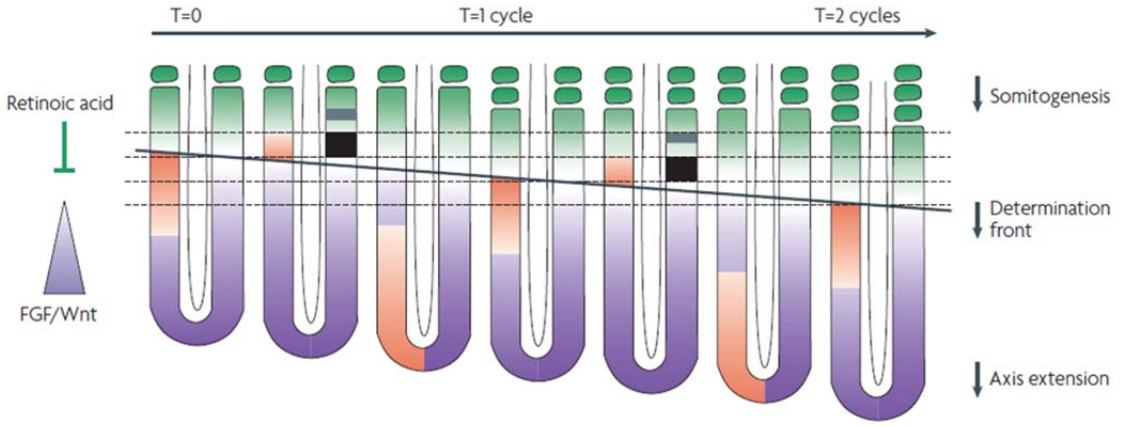

Figure F) A model of somitogenesis integrating molecular evidence for the segmentation clock and the wavefront. Opposing gradients of Fgf and Wnt signalling from the caudal embryo (purple) and Retinoic acid from the rostral embryo (green) are proposed to specify the determination front position (black line) along the AP axis of the PSM. This determines the level at which cells become competent to respond to the segmentation clock. Cycling gene expression controlled by the segmentation clock oscillator sweep through the PSM in a caudal-to-rostral direction (orange). At the end of each clock cycle, competent cells that have passed the determination front receive the segmentation clock signal and active *Mesp2* expression (black) to define the future somite boundary. The size of the prospective somite depends on the distance travelled by the wavefront during one clock oscillation cycle. During the following oscillation cycle, *Mesp2* is restricted to the rostral compartment of the S-1 and the boundary forms exactly anterior to this domain. (Taken from **Dequeant and Pourquie, 2008**)

The Notch pathway

Molecular evidence to date suggests that Notch signalling components constitute the core segmentation clock conserved in a number of vertebrate species studied (Dequeant and Pourquie, 2008; Krol et al, 2011). The Notch signalling pathway in metazoans plays important roles in the regulation of developmental processes and tissue renewal, generally relying on short-range signals between neighbouring cells (Kopan and Ilagan, 2009). One interesting aspect of Notch signalling is that both the Notch receptors and their ligands are transmembrane proteins. The transduction of the Notch signal relies on the Delta/Serrate/LAG-2 (DSL) ligand on the surface of the signalling cell binding to the Notch receptor on the receiving cell (Fig. G). *Drosophila* has just one Notch receptor and only the Delta and Serrate ligands. However, vertebrates have Notch receptors 1-4, as well as multiple DSL ligands including Delta-like 1 (Dll1), Dll3, Dll4, Jagged (known as Serrate in the chicken) 1, and Jagged2 (Bray, 2006; Kopan and Ilagan, 2009). The chicken only has homologues for the Notch1 and Notch2 receptors, and lacks the Dll3 ligand. Of these, it has been shown that Serrate/Jagged expression is restricted to the anteriormost region where somite boundary formation occurs (Mitsiadis et al, 1997) whereas Notch1, Notch2, Dll1, and Dll3 are expressed throughout the mouse paraxial mesoderm, while only Notch1 and Dll1 are expressed throughout the chicken PSM (Dunwoodie et al, 1997; Franco del Amo et al, 1992; Reaume et al, 1992).

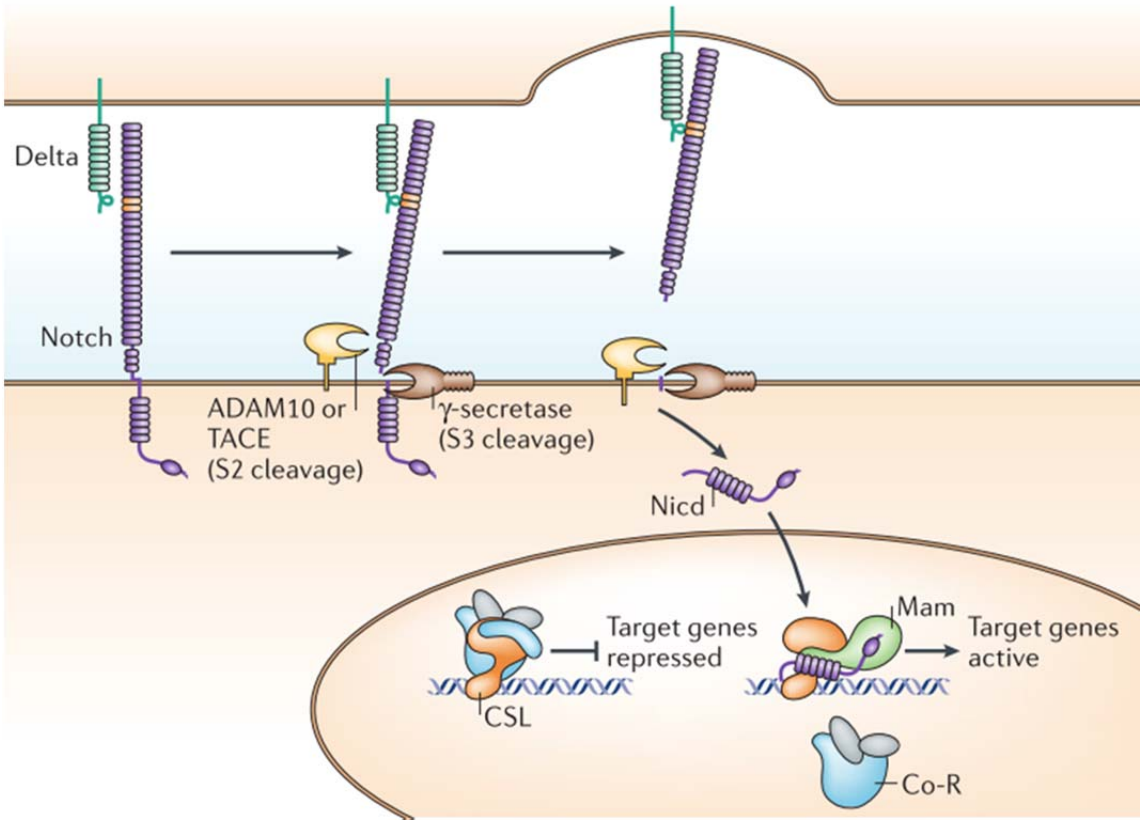

Figure G) The core Notch signalling pathway. Binding of the Delta ligand (green) on the surface of the signalling cell to the Notch receptor (purple) on the surface of a responding cell triggers a series of cleavage events within the Notch receptor protein. The ADAM metalloprotease (yellow) catalyses cleavage at the S2 site of Notch, providing a substrate for the γ-secretase enzyme complex (brown) to catalyse cleavage at the S3 site. This releases the activated Notch intracellular domain (NICD) protein, which translocates to the nucleus to form a complex with CSL (CBF1, Su(H) and LAG-1)/Rbpjκ (orange) and Mastermind (MAM) on the DNA and releases co-repressors (co-R, blue). This allows activation of downstream Notch target transcription. (Taken from **Bray, 2006**)

Receptor-ligand binding triggers successive proteolytic cleavage events within the Notch receptor that allow signal transduction. The first cleavage event is catalysed by the A Disintegrin And Metalloproteinase (ADAM) family enzymes and occurs at the site 2 (S2), which is roughly 12 amino acids upstream of the transmembrane domain (TMD) of Notch and within the negative regulatory region (NRR) (Kopan and Ilagan, 2009). The remaining membrane-bound intermediate is known as Notch extracellular truncation (NEXT) and is a substrate for the γ-secretase complex of enzymes, made up of presenilin, nicastin, PEN2, and APH1 (Bray, 2006). The γ-secretase complex then catalyses the second progressive cleavage event, which starts at site 3 (S3) near the inner plasma membrane leaflet and ends at site 4 (S4) in the middle of the TMD of Notch (Kopan and Ilagan, 2009). The Notch intracellular domain (NICD) is now free to translocate to the nucleus, where it associates with CBF1, Su(H) and LAG-1 (CSL)/ Recombination signal-Binding Protein 1 for J Kappa (RBPJκ) (Fig. G). The association with CSL/RBPJκ first occurs via the RBPJκ association module (RAM) domain of NICD, and then through the Ankyrin repeat (ANK) domain, which in turn allows the recruitment of co-activators Mastermind (MAM) and MED8 to induce the transcription of downstream Notch targets (Kopan and Ilagan, 2009).

Notch signalling & Human Segmentation defects

Molecular studies into somitogenesis have clearly shown that the oscillating expression of clock genes in the PSM is a tightly regulated process that is essential for normal segmentation in vertebrates. Disruption of the segmentation clock by genetic, pharmacological, or environmental means can lead to severe segmentation abnormalities, as has been evidenced in studies utilising model vertebrate species such as the chicken, mouse, and zebrafish embryos (Ferjentsik et al, 2009; Sparrow et al, 2012; Stern et al, 1988; van Eeden et al, 1996). These species have been studied in detail due to their remarkable similarities with human development, as well as the relative ease of access to multiple embryos per litter undergoing rapid development. The ethical implications have also limited the number of studies with human embryos. However, one of the major motives behind studies into vertebrate segmentation has been to understand the genetic regulatory mechanisms of congenital birth defects which disrupt human skeletal patterning.

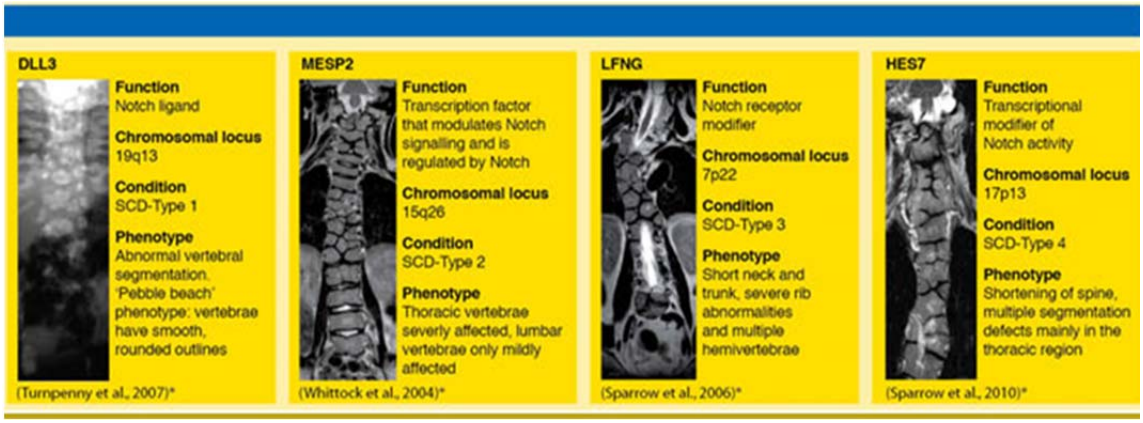

Figure H) Pathologies of Spondylocostal dysostosis in humans. Mutations in four Notch-related genes involved in early patterning of the PSM (DLL3, MESP2, LFNG, HES7) cause the four types of Spondylocostal dysostosis (SCD) in humans. These defects result from disrupted segmentation. The range of phenotypes are briefly described for each mutation. Authors of original images are shown beneath each panel (*). (Taken from **Maroto et al, 2012**)

Congenital vertebral malformations (CVM) defects such as SCD and STD are not usually caused during the formation of the bones themselves, but rather occur much earlier in development during somitogenesis in the PSM (Sparrow et al, 2012). Genetic screens into clinical cases have found that homozygous mutations in either DLL3, MESP2, HES7, or LFNG can cause SCD in humans (Fig. H) (Bulman et al, 2000; Sparrow et al, 2006; Sparrow et al, 2008; Sparrow et al, 2011; Whittock et al, 2004). Similarly, mutated DLL3 has been associated with human spondylocostal dysplasia (Dunwoodie et al, 2002), while mutations in either DLL3, HES7, or MESP2 have been found in patients with congenital scoliosis (Bulman et al, 2000; Sparrow et al, 2012). All of these genes are members of the Notch signalling pathway and are established as regulators of somitogenesis within the PSM of vertebrates. These studies therefore suggest a fundamental role for Notch signalling to direct normal segmentation and axial skeleton formation during human development.

CVM can occur as a single condition, or as an associated symptom of other defects. Indeed, it is estimated that 30-60% of human CVM cases are linked to an underlying syndrome or chromosomal abnormality (Jaskwhich et al, 2000). Alagille syndrome is one such example, with patients exhibiting bile duct defects, pulmonic stenosis, facial feature characteristics, and vertebral irregularities (Giampietro et al, 2009). Mutations in both *JAG1* and *NOTCH2* genes have been found in patients with this autosomal dominant disorder (Giampietro et al, 2009).

The causes of CVM can be genetic, but most do not have a simple etiology and are known as sporadic (Bajard and Oates, 2012). This means that genetic causes alone may not explain the severity of the abnormalities observed. It is likely that a number of environmental factors also contribute to normal vertebral development. Teratogens (environmental factors causing embryonic abnormalities) may interact with underlying genetic defects to cause sporadic CVM cases (Bajard and Oates, 2012). Reports have suggested that during early pregnancy, CVM may be caused in the developing embryo if the mother is exposed to certain dietary insufficiencies such as folic acid deficiency, or to alcohol or certain drugs (Bajard and Oates, 2012; Giampietro

et al, 2009; Sparrow et al, 2012). However, there is a great lack of epidemiological studies to prove these links.

A recent seminal report by Sparrow et al (2012) showed that a gene-environment interaction does exist in the etiology of congenital scoliosis. This study screened cases of congenital scoliosis in human patients and found a heterozygous single-nucleotide polymorphism (SNP) mutation in the gene *HES7* in one family, while a heterozygous SNP mutation in the gene *MESP2* was found in members of another family exhibiting congenital scoliosis (Sparrow et al, 2012). These mutations found in *HES7* and *MESP2* both result in a single amino acid substitution in the respective protein products. *In vitro* assays revealed that this greatly reduces the repressor activity but not the expression level of HES7 protein, while the mutation in *MESP2* completely inactivates the protein (Sparrow et al, 2012). Interestingly, both of these families studied contained family members who carried the heterozygous mutation but did not exhibit any vertebral defects. This suggested that these defects showed only partial penetrance and that another factor may induce the severity of the phenotype in certain individuals (Sparrow et al, 2012). Sparrow et al (2012) then assessed mice embryos heterozygous null for *Hes7* (*Hes7*$^{+/-}$) and *Mesp*$^{+/-}$. Haploinsufficiency of *Hes7* caused vertebral defects in about half of the embryos viewed, while loss of one allele of *Mesp2* had very little effect (Sparrow et al, 2012). However, short-term hypoxia induced during gestation greatly increased both the prevalence and severity of vertebral defects observed by E14.5 in WT mice, but especially in both *Hes7*$^{+/-}$ and *Mesp*$^{+/-}$ mice (Sparrow et al, 2012). Immunohistochemistry analyses of WT mice revealed that embryos exposed to hypoxic conditions no longer had oscillating NICD expression, which was instead stable throughout the PSM resulting in a loss of *Lfng* and *Hes7* negative feedback loops (Sparrow et al, 2012). A number of Fgf and Wnt signalling components were also severely downregulated in the PSM upon temporary hypoxia exposure.

Sparrow et al (2012) concluded that the evidence for Fgf signalling acting upstream of Wnt and Notch signalling (Wahl et al, 2007) suggests that disruption of Fgf signalling specifically by hypoxia causes the temporary failure of somitogenesis as a mechanism in the etiology of congenital scoliosis. While it is clear that these three genetic pathways are all affected in the PSM by hypoxia, the speculation as to the relative hierarchy between Fgf, Wnt, and Notch signalling in the PSM (Gibb et al, 2010) means that the exact genetic mechanism behind this genetic-environment interaction remains to be determined. This report shows some of the first experimental evidence to prove that an environmental factor (atmospheric oxygen level) can increase the penetrance and severity of vertebral abnormalities in genetically compromised organisms and could account for the sporadic nature of CVM in humans (Sparrow et al, 2012).

The Fibroblast Growth Factor pathway

The Fgf signalling pathway targets become activated in response to a signalling cascade that is triggered upon receptor-ligand binding (Fig. I). The FGF ligands bind to certain receptor tyrosine kinases (RTKs), called the fibroblast growth factor receptors (FGFRs) at the cell surface. This promotes the kinase activity of the receptor to phosphorylate other protein including other FGFRs which causes receptor dimerization at the cell surface (Pownall and Isaacs, 2010). The dimerised RTK proteins then autophosphorylate on specific tyrosine residues on the intracellular C-terminal domain, as well as phosphorylating the FGFR substrate 2 (FRS2) protein which then associates with the FGFR dimer (Kouhara et al, 1997). This promotes the recruitment of the growth factor receptor-bound protein 2 (Grb2) adaptor via its SH2 domain and the associated son of sevenless (SOS) then binds Grb2 on its two SH3 domains (Ong et al, 2000). The Grb2 adaptor protein along with SOS then promote the active form of the small GTP binding protein Ras, which in turn associates with and activates the kinase Raf at the cell membrane to initiate the mitogen-activated protein kinase (MAPK)/ extracellular signal-regulated kinase (ERK) signalling cascade (Kyriakis et al, 1992). Activated Raf/mitogen-activated protein kinase kinase kinase (MAP3K) is able to phosphorylate MEK/mitogen-activated protein kinase kinase, which itself then phosphorylates MAPK/ERK (Pownall and Isaacs, 2010). MAPK/ERK is also a kinase itself, and once phosphorylated by MEK is able to translocate to the nucleus in order to phosphorylate certain transcription factors which leads to the expression of downstream FGF targets (Pownall and Isaacs, 2010). Akt is another cytosolic protein kinase that can mediate the intracellular response of Fgf signalling. Phosphatidylinositol-3-OH kinase (PI(3)K) is a lipid kinase that is activated by the SH2 adaptor in response to activation of the FGFR RTK complex (Schlessinger, 2000). The PI(3)K pathway then activates Akt which is another effector of Fgf signalling, but has other roles including the indirect activation of the mTor pathway which functions to regulate cell growth (Schlessinger, 2000).

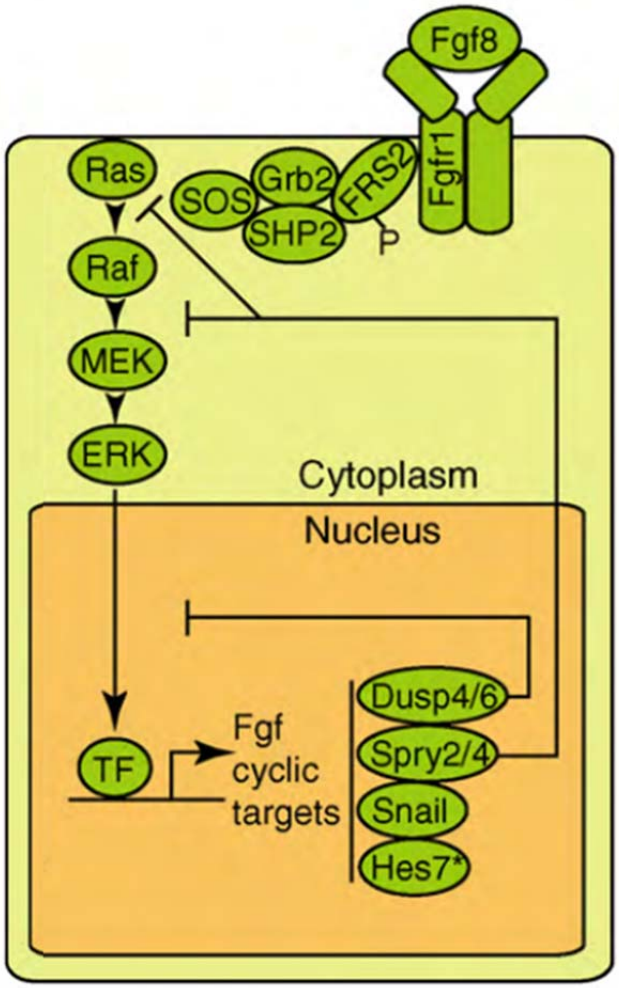

Figure I) Fgf signalling. Binding of the Fgf ligand to the dimerised Fgf receptor (Fgfr) proteins on the cell surface allows the dimerised Fgfr proteins to phosphorylate and recruit the intracellular protein FGFR substrate 2 (FRS2) to the complex. This promotes the recruitment of the growth factor receptor-bound protein 2 (Grb2) adaptor and the associated son of sevenless (SOS). Grb2 and SOS promote the active form of the small GTP binding protein Ras, which then associates with and activates the kinase Raf at the cell membrane to initiate the mitogen-activated protein kinase (MAPK)/ extracellular signal-regulated kinase (ERK) signalling phosphorylation cascade. At the end of the cascade, phosphorylated MAPK/ERK enters the nucleus and is able to phosphorylate transcription factors (TF) that allow the transcription of Fgf target genes. Gene products of the Sprouty (Spry) and dual specificity phosphatase (Dusp) genes exert negative feedback regulation on the pathway. (Taken from **Gibb et al, 2010**)

A range of FGF ligands and FGFR proteins exist in vertebrates, although most notably only FGFR1 is expressed within the PSM along with some FGF ligands including Fgf4 and Fgf8 whose expression is caudally restricted and which act to maintain the caudal pool of axial progenitors (Naiche et al, 2011; Wahl et al, 2007). Opposing the gradient of Fgf signalling is a gradient of RA signalling highest in the anterior embryo and provided by the somitic mesoderm. RA is required to repress signals from the Fgf pathway thereby promoting tissue specification including neuronal and paraxial mesoderm differentiation as cells become displaced more rostrally during axial elongation from the tail end (Diez del Corral and Storey, 2004).

The Wnt pathway

The canonical Wnt signalling pathway comprises the other main group of molecular signals that appear to regulate the clock and wavefront activities within the PSM. In the absence of Wnt pathway activation, the Wnt effector protein β-catenin is held in the cytoplasm by a destruction complex that relies on the scaffold proteins Axin2 and adenomatous polyposis coli (APC) (Muñoz Descalzo and Martinez Arias, 2012). In this complex, β-catenin is phosphorylated by casein kinase 1 and then by Glycogen synthase kinase 3 beta (GSK3β). Phosphorylated β-catenin is recognised and ubiquitinated by the E3 ubiquitin ligase β-TrCP, leading to its rapid proteasomal degradation (Clevers, 2006) (Fig. J). The outcome is that β-catenin is actively degraded in the cytoplasm and is therefore unable to activate downstream targets in the nucleus.

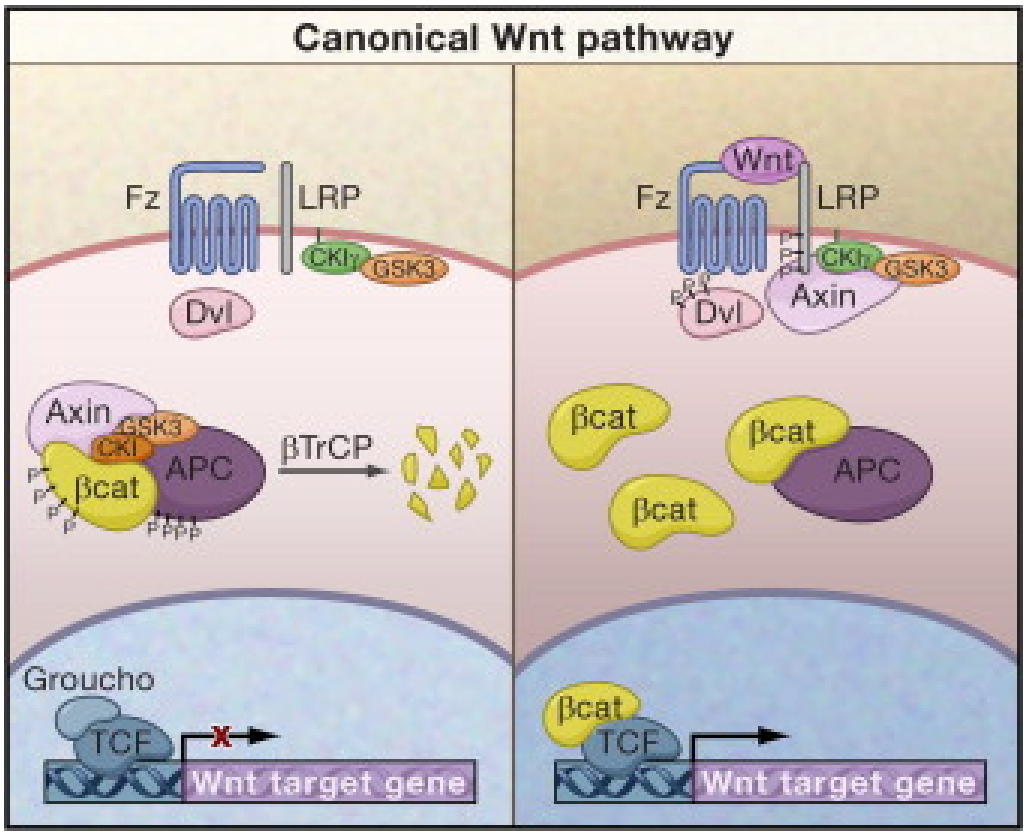

Figure J) The canonical Wnt signalling pathway. Left panel: In the absence of receptor/ligand binding, the Wnt effector protein β-catenin is held in the cytoplasm in a destruction complex by Axin and Adenomatous polyposis coli (APC) proteins, while being phosphorylated by the serine/threonine kinases Casein kinase 1 (CK1) and Glycogen synthase kinase 3 (GSK3). Phosphorylated β-catenin is then targeted for ubiquitination by the F-box/WD repeat E3 ligase component β-TrCP and rapid degradation via the ubiquitin proteasome. In the nucleus, Groucho remains bound to TCF/Lef and represses Wnt target transcription. **Right panel**: Wnt ligand binding to the seven-pass Frizzled(Fz)/LRP co-receptor complex at the cell surface activates the canonical Wnt pathway. Fz interacts with the cytoplasmic protein Disheveled (Dsh), which inhibits the activity of GSK3β and promotes docking of Axin2 protein to the LPR receptor component. As a result, the destruction complex dissociates and β-catenin is released to enter the nucleus and displace Groucho on Tcf/Lef on the DNA to activate transcription of Wnt targets. (Taken from **Clevers, 2006**)

As with Fgf signalling, Wnt ligands also activate the intracellular signal via interaction with specific transmembrane receptors. Wnt protein binding to the seven-pass receptor protein Frizzled at the cell surface promotes heterodimerisation with LPR5/6, a single-pass transmembrane receptor (Clevers, 2006). In this complex, Frizzled is able to interact with and activate the cytoplasmic protein Disheveled (Dsh). In turn, Dsh represses the activity of GSK3β and promotes the docking of Axin2 protein to LPR5/6. As a result, the destruction complex dissociates and now allows free β-catenin to translocate to the nucleus. β-catenin forms a heterodimer with a LEF or TCF deoxyribonucleic acid (DNA)-binding protein in the nucleus, thus becoming a transcription co-factor to activate the transcription of downstream Wnt targets (Clevers, 2006) (Fig. J).

Both the Fgf and Wnt signalling pathways can establish gradients of signalling strength over distances in order to regulate tissue specification and patterning during embryogenesis (Muñoz Descalzo and Martinez Arias, 2012, Stulberg et al, 2012). Fgf and Wnt signalling are known to regulate a range of T-box transcription factors in the embryonic tail including Brachyury and Tbx6, which control paraxial mesoderm specification (Stulberg et al, 2012).

Molecular evidence for the Clock and Wavefront in the PSM

There is now strong molecular evidence for a wavefront of gene expression across the AP axis of the PSM. Dubrulle et al (2001) first noticed that if chicken PSM tissue of a somite in length from the S0 up to the S-4 was inverted with respect to its AP axis, the resulting somite that formed was also inverted in respect to its rostro-caudal (RC) patterning. However, when a similar inversion was performed in any prospective somite region of the PSM posterior to the S-4, the somite which formed exhibited normal AP polarity (Dubrulle et al, 2001). These results highlighted that a determination front exists within the chicken PSM, whereby the caudal two thirds of the PSM (S-4 to S-12) are not determined but once PSM cells are displaced anterior to the prospective S-4 boundary then they become determined with respect to anteroposterior compartmentalisation and boundary position to form the somite. Similarly, the determination front in the E10.5 mouse PSM is at the level of the prospective S-2 posterior boundary, while cells posterior to this and up to the caudal terminus of the PSM at the S-6 are yet to be determined (Oginuma et al, 2008). Fibroblast growth factor 8 (*Fgf8*) was the first gene shown to be present as a gradient in the chicken PSM acting like the predicted wavefront, which is highest caudally and decreases towards the rostral PSM (Dubrulle et al, 2001). Inducing higher expression of *Fgf8* in the anterior PSM by placing *Fgf8* soaked beads next to the PSM or by electroporation of FGF led to the determination front being moved rostrally and resulted in smaller somites forming (Dubrulle et al., 2001). Indeed, the phosphorylated form of the Fgf effector protein Akt also exhibits a graded profile in the mouse PSM, being highest in the caudal-most region and decreasing sharply towards the segmented region (Dubrulle and Pourquie, 2004). This suggests that the *fg8* gradient is translated into a ligand gradient in the mouse PSM (Dubrulle and Pourquie, 2004). Subsequently, strong evidence has been given that both fgf4 and fgf8 expression comprise the wavefront activity in the PSM in concert with Wnt signalling (Aulehla et al, 2003; Boulet and Capecchi, 2012; Naiche et al, 2011; Stulberg et al, 2012). Moreover, the expression of the Wnt target *Brachyury* (*T*) in the tailbud is required to maintain the undifferentiated pool of axial progenitors, as inhibition of *T* expression in the tail

in conditional PSM-specific *Fgf4* and *Fgf8* double knockout mice results in a severely truncated embryo and the disruption or loss of caudal vertebrae (Boulet and Capecchi, 2012; Naiche et al, 2011). This demonstrates that the wavefront activity of Fgf and Wnt signalling in the caudal PSM are required for both axial elongation and somite segmentation.

The first molecular evidence for a segmentation clock oscillator came with the discovery that the Notch target gene c*Hairy1* was transcribed in a dynamic fashion within the PSM of staged-matched chick embryos with a periodicity that matched the rate of somite formation (Palmeirim et al, 1997). *cHairy1* is also known as hairy and enhancer of split 1 (HES1) and is a homologue of the *Drosophila melanogaster* segmentation gene *hairy* (Dequeant and Pourquie, 2008; Nüsslein-Volhard and Wieschaus, 1980). *cHairy1* expression is categorised into three different phases of spatial expression within the chicken PSM (Fig. K). In phase 1, *cHairy1* is expressed as a sharp stripe at the level of the next prospective somite boundary in the rostral PSM, with a broader domain in the caudal PSM and expression absent in between. In phase 2, *cHairy1* expression remains in the rostral band, but the caudal domain now shifts rostrally and expression is no longer present in the very caudal PSM. Finally, between phase 2 and 3, the somite boundary forms at the level of the rostral band posterior to the S0 and *cHairy1* expression remains in the caudal domain of the formed somite. This new somite is now termed the S1 and the more caudal domain of *cHairy1* expression in the phase 2 PSM has now moved more rostrally still and narrowed to form the sharp rostral domain that demarcates where the next somite boundary will form in the new S0 (Palmeirim et al, 1997, Pourquie and Tam, 2001). Expression of *cHairy1* is then activated in the caudal PSM again to begin a new oscillation cycle.

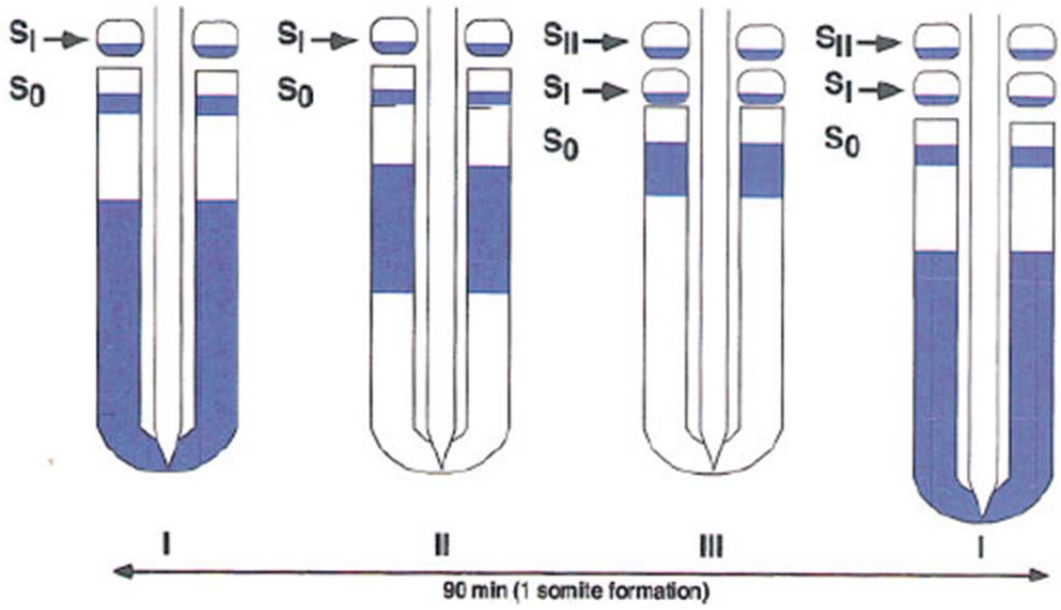

Figure K) Phases of dynamic clock gene transcription in the chicken PSM. The dynamic expression profile of cycling clock gene transcription such as *cHairy1* in the PSM are categorised into phases 1-3 during the oscillation cycle. In phase 1, *cHairy1* (blue) is expressed a sharp domain at the caudal edge of the next prospective somite in the rostral PSM (S0), as well as a broader domain in the very caudal PSM. By phase 2, the caudal domain has moved more rostrally in the PSM and is *cHairy1* is no longer expressed in the very caudal PSM. Between phases 2 and 3 the next somite boundary forms to generate the new S1 somite, which has *cHairy1* expression localised to the caudal compartment. Within the PSM, the broader domain of *cHairy1* expression has moved to the rostral PSM and narrowed to the caudal limit of the next prospective somite (i.e. the new S0 region). This domain narrows further and a new wave of *cHairy1* expression starts from the very caudal PSM to begin phase 1 of a new oscillation cycle. The period of this full oscillation cycle takes approximately 90 minutes, which is the same as the period of somite formation in the chicken embryo. (Taken from **Palmeirim et al, 1997**)

Assays where the PSM was bisected along the midline and culturing the two halves of the PSM for different times revealed that one oscillation cycle of *cHairy1* takes approximately 90 minutes, which matched the periodicity with which each new pair of somites forms in the chick embryo (McGrew et al, 1998; Palmeirim et al, 1997). Subsequently, transcripts of the following genes involved in the Notch signalling pathway have been found to oscillate with the same periodicity within the chicken PSM: *Lunatic fringe* (*Lfng*) (McGrew et al, 1998), *Notch-regulated ankyrin repeat protein* (*Nrarp*) (Wright et al, 2009), *Hairy2,* and *Hairy and enhancer-of-split related with YRPW motif 2* (*Hey2*) (Leimeister et al, 2000). Indeed, all of the cycling genes identified in the zebrafish PSM also belong to Notch signalling pathway. These include: the Notch ligand *DeltaC* (Jiang et al, 2000), as well as *nrarp-a* (Wright et al, 2009), *her1* (Holley et al, 2000)*, her7* (Oates and Ho, 2002)*, Her11* (Sieger et al, 2004)*, her12,* and *her15* (Shankaran et al, 2007). The *her* genes of the zebrafish are all homologous to *cHairy1* in the chicken (Dequeant and Pourquie, 2008). Jiang et al (2000) proposed that Notch signalling synchronises oscillations in neighbouring PSM cells, as clock gene oscillations appear disrupted and desynchronised in zebrafish mutants for the Notch1A receptor, as well as in mutants for the DeltaC and DeltaD ligands (Holley et al, 2000; van Eeden et al, 1996).

The cyclical transcription of Notch signalling components has also been observed in the mouse PSM, including the targets *Lfng* (Forsberg et al, 1998), *nrarp* (Wright et al, 2009), *Hey2* (Leimeister et al, 2000), *Hes1* (Jouve et al, 2000), *Hes7* (Bessho et al, 2001a), *Hes5*, and *Hey1* (Dunwoodie et al, 2002). The fact that many of the cycling clock genes studied in a range of amniote and lower vertebrates are components of the Notch signalling pathway suggest that Notch signalling may be an essential conserved part of the somitogenesis clock mechanism (Dequeant and Pourquie, 2008; Gibb et al, 2010; Krol et al, 2011; Rida et al, 2004). Such short cycles are termed ultradian oscillations, as they occur within the 24-hour circadian period and appear to rely on the rapid production and turnover of gene products to maintain short cycles (Dequeant and Pourquie, 2008). Lewis (2003) suggested that the direct auto-repression of the *her1* and *her7* zebrafish clock genes by their own protein products could generate rapid

intracellular oscillations in the PSM. This model takes into account the proposed role for Notch in synchronising oscillations in neighbouring cells, while also predicting that the oscillations can only be maintained if the mRNA and protein products have short half-lives in comparison to the transcriptional and translational delays in the system (Jiang et al, 2000; Lewis, 2003). These unstable protein products will only exert negative feedback transiently, as transcription can iniate again following their rapid degradation and the period of the clock is largely dependent on the transcriptional delay to synthesise an mRNA molecule (Lewis, 2003). This fundamental model of the segmentation clock therefore predicts that the period of oscillation can be altered by altering either the transcriptional delay of clock gene transcription or altering the half-life of clock gene prodcuts in the PSM (Lewis, 2003). RA also seems to be important to synchronise the clock on the left and right sides of the PSM, as inhibition of RA synthesis in both the mouse and chicken embryos delays clock gene oscillations in the right side of the PSM compared to the left (Vermot et al, 2005; Vermot and Pourquie, 2005).

As described above, the Hes family of basic helix-loop-helix (bHLH) transcription factors have been shown to oscillate in the PSM of a number of different vertebrate species. The protein products of these Notch target genes are transcriptional repressors and family members such as HES7 have been shown to inhibit Notch-mediated transcription of clock genes as evidenced by the fact that *Lfng* and *Hes7* are not transcribed in the domain of the PSM which contains HES7 protein expression (Bessho et al, 2001b; Bessho et al, 2003). The expression of HES7 protein itself is oscillatory in the mouse PSM (Bessho et al, 2003) and HES7 is inherently unstable with a half-life of just 22 minutes in the mouse PSM (Hirata et al, 2004). HES7 protein only periodically represses transcription of Notch target clock genes until it rapidly degrades, allowing renewed transcription of clock genes once more in that domain (Bessho et al, 2003; Hirata et al, 2004). The resulting negative feedback loop is suggested to drive molecular oscillations across the PSM tissue, relying on the instability of clock gene mRNAs and proteins. These studies on Hes7 expression and activity in the mouse PSM were among the first to support models which suggested that the direct auto-repression of the *her1* and *her7* zebrafish

clock genes by their own protein products could generate rapid intracellular oscillations in the PSM (Lewis, 2003).

The *Lfng* gene is among the Notch targets shown to oscillate in the PSM of some amniote species including the chick and the mouse, while localising to the rostral compartment of the somites (Forsberg et al, 1998; McGrew et al, 1998). However, *Lfng* is not expressed in the zebrafish PSM (Holley et al, 2000) and Eckalbar et al (2012) recently discovered that *Lfng* is also not expressed in the PSM of the anole lizard *Anolis carolinensis*, rather it is localised only to the rostral compartment of the few newest somites, even though *Hes6* is expressed as a gradient and *Hes7* displays cyclical transcription in the PSM of the *Anolis* embryo. This suggests either some divergence between avian and reptile species, or a convergent evolution between avian and mammalian species (Eckalbar et al, 2012). *Lfng* encodes a glycosyl-transferase which modifies the extracellular portion of the Notch receptor on the EGF repeats by the addition of O-fucose residues at the Golgi apparatus, thus altering the ability of certain ligands to activate the Notch receptor once presented at the cell surface membrane (Kopan and Ilagan, 2009). Dale et al (2003) proposed that in the context of the PSM, Notch signalling activates cyclic *Lfng* expression. Lfng protein then modifies Notch, thereby inhibiting interactions with the Dll ligand from the signalling cell to prevent Notch signalling. The resulting negative feedback loop is transient due to the evident short half-lives of both NICD and Lfng proteins in the system (Dale et al, 2003). Therefore Lfng activity in the PSM provides another example to support models for a transient negative feedback loop maintaining cyclical expression of clock genes (Morales et al, 2002). Lfng plays a role in the RC patterning of somite compartments, as loss of *Lfng* causes undefined segment boundaries and randomised RC somite patterning (Evrard et al, 1998; Zhang and Gridley, 1998).

Indeed, NICD activity itself is shown to oscillate across the mouse PSM in mutually exclusive domains to Hes7 protein expression, which gives further evidence for the dynamic activation of Notch signalling in the PSM (Huppert et al, 2005; Morimoto et al, 2005; Niwa et al, 2011).

Morimoto et al (2005) found that NICD was activated across the length of the PSM in *Lfng* knockout mice, indicating that the negative feedback loop established between Lfng and Notch has a conserved role in avian and mammalian somitogenesis (Dale et al, 2003; Dequeant and Pourquie, 2008).

The bHLH transcription factor Mesoderm posterior 2 (Mesp2) is a key regulator of somite boundary position, as well as for the establishment of rostro-caudal (RC) patterning within the formed somites (Morimoto et al, 2005; Saga et al, 1997; Takahashi et al, 2000). *Mesp2* is initially expressed as a somite-wide stripe in the anterior PSM at the level of the determination front due to positive input from the Tbx6 transcription factor that is expressed throughout the PSM but inhibition by Fgf signalling in the caudal PSM (Oginuma et al, 2008; Takahashi et al, 2010). The stripe of *Mesp2* then narrows rapidly due to repression of *Tbx6* expression by the Ripply2 transcription factor which is itself Mesp regulated, until becoming restricted to the rostral compartment of the forming somite (Saga et al, 1997; Takahashi et al, 2010). Mesp2 acts to repress activation of Notch1 in the rostral PSM at the interface between Notch1-activated and Notch1 repressed domains (Fig. L.a), thus demarcating the next prospective somite boundary position at the caudal limit of S0 (Morimoto et al, 2005). Subsequently, Mesp2 expression in the rostral somite compartment specifies RC somite pattern by inhibiting NICD through destabilisation of the obligate NICD partner mastermind-like 1 (MAML1), and therefore restricting NICD activity to the caudal somite (Morimoto et al, 2005; Sasaki et al, 2011).

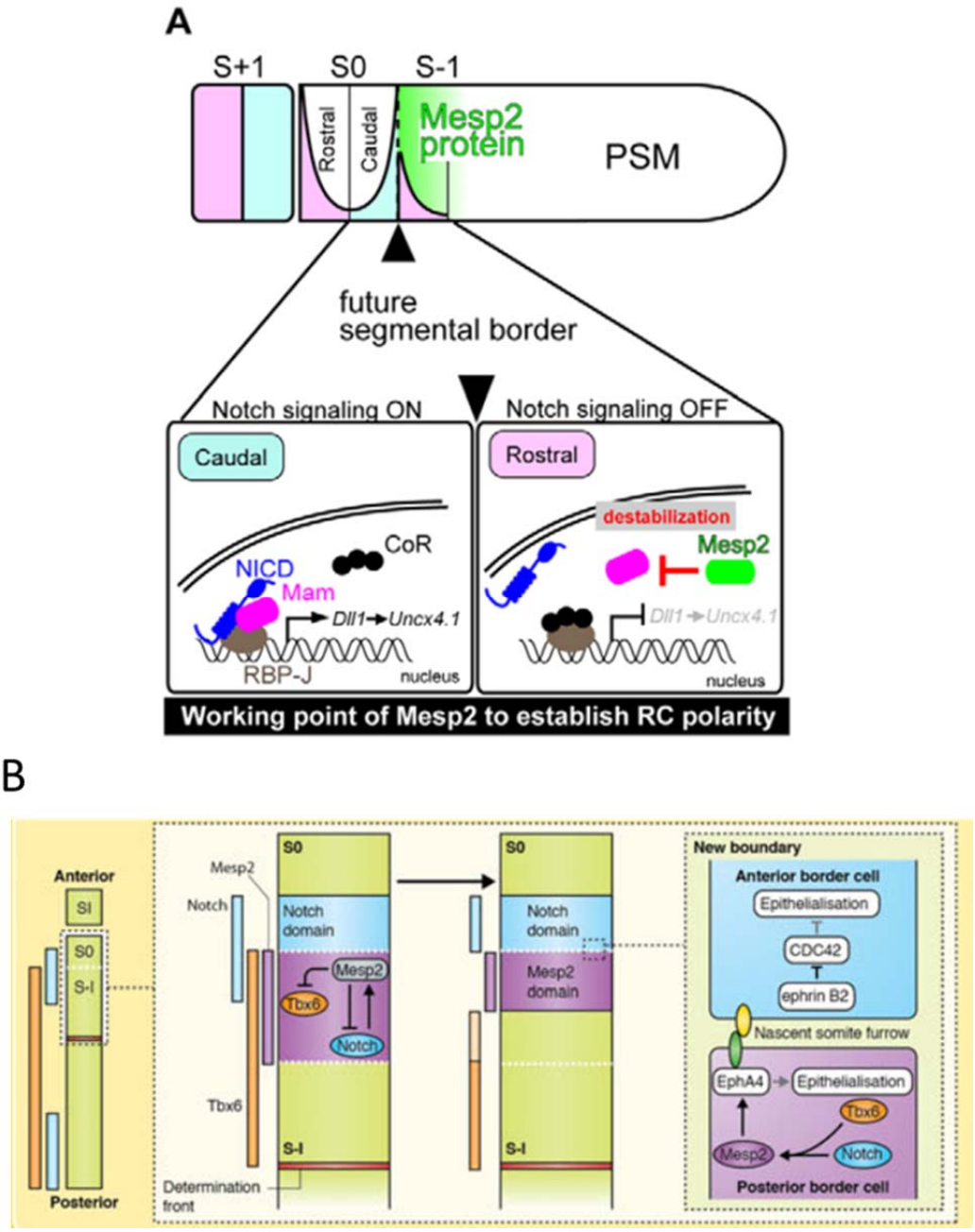

Figure L) Rostro-caudal patterning and boundary formation of the somites. **A**) Mesp2 regulates the rostro-caudal (RC) patterning of the somite. Mesp2 (green) is expressed in the rostral compartment of the S-1 somite, behind the caudal limit of the next presumptive somite boundary. In this region, Mesp2 destabilises Mastermind (Mam, bright pink) and therefore represses NICD from forming an active complex with RBPJκ on the DNA. As a result, Notch targets, including caudal somite markers *Dll1* and subsequently *Uncx4*.1 are repressed in the rostral half of the S0 and S-1 where Mesp2 is active. However, Notch is active in the caudal

somite domain where *Mesp2* falls below threshold level and these caudal somite markers are expressed here. **B**) Mesp2 activation from Notch and Tbx6 in the rostral compartment of the S-1 (i.e. in cells just posterior to the next presumptive somite boundary) induces Eph-ephrin signalling in border cells between the S0 and S-1 which can induce the physical separation that generates the segment boundary and promotes somite epithelialisation (**A** taken from **Sasaki et al, 2011**; **B** taken from **Maroto et al, 2012**)

Somite boundary Formation

While oscillations of *Lfng* in the caudal PSM are regulated by Notch signalling, *Lfng* expression in the rostral PSM is regulated by Mesp2 (Dale et al, 2003; Morimoto et al, 2005). Mesp2 is proposed to restrict *Lfng* expression to the rostral PSM, where it represses Dll-Notch signalling to establish the position of the next presumptive somite boundary (Morimoto et al, 2005). Mesp2 then induces the expression of the tyrosine kinase EphA4, which interacts with its Ephrin B2 ligand on the surface of neighbouring cells to generate a physical cell-cell repulsion which allows the morphological somite boundary to form as the new somite segments away from the rostral PSM (Durbin et al, 1998; Gilbert, 2006) (Fig. L.b). Expression analysis reveals that EphrinB2 is localised to the caudal region of the prospective S0 somite in the rostral PSM, while EphA4 is expressed in the rostral S0, as well as in the rostral S-1 (Durbin et al, 1998). Therefore, the nascent somite furrow forms at the interface between the S0 and the S-1. Once the somite has formed, EphrinB2 marks the caudal somite and EphA4 is expressed in the rostral somite compartment, while disruption of the Eph/Ephrin expression pattern in the zebrafish PSM disrupts both somite boundary formation and myogenic differentiation (Durbin et al, 1998).

A Conserved requirement for Notch signalling in the vertebrate Segmentation Clock

Although there is clear evidence in the PSM for cycling Notch gene expression in the regulation of periodic somite formation and for Wnt and Fgf signalling in the wavefront of maturation, the clock and wavefront mechanism seems to be more complicated. Studies in the mouse in particular revealed that some targets of the Wnt and Fgf pathways also oscillate across the PSM in the manner of a clock gene (Aulehla et al, 2003; Dale et al, 2006; Dequeant et al, 2006; Krol et al, 2011; Niwa et al, 2007; Niwa et al, 2011). The Wnt target *Axin2* was the first clock gene not directly under the control of Notch activity found to oscillate at the transcriptional level in the mouse PSM (Aulehla et al, 2003). *Axin2* transcription was found to oscillate in the PSM out of phase with the Notch target *Lfng* and even when Notch signalling was impaired in *Dll1*-null mice (Aulehla et al, 2003). The *Snail1* and *Snail2* genes also exhibit cyclical expression in the PSM of the chick and mouse embryos independently of Notch signalling, but require Wnt and Fgf signalling (Dale et al, 2006). Subsequently, genome-wide screens have suggested that a range of transcripts from the Fgf and Wnt signalling pathways also oscillate in the PSM of the mouse, chick, and zebrafish (Dequeant et al, 2006; Krol et al, 2011). These studies found that the targets of Notch and Fgf pathways oscillate in phase with each other, while out of phase with Wnt targets (Dequeant et al, 2006; Niwa et al, 2007). Despite the cycling gene networks appearing to range from 40 to 100 genes in these species, cycling of only the *Hes/Her* genes appeared conserved between all three species (Krol et al, 2011). However, these outcomes are often not observed when viewing the spatial localisation of these transcripts by *in situ* hybridisation (ISH). For example, the array study by Krol et al (2011) suggested that *Axin2* transcription is also cyclic in the chick PSM, but ISH analysis of *Axin2* expression both in this study and by Gibb et al (2009) failed to observe dynamic expression profiles in the PSM of different embryos. Krol et al (2011) concluded that ISH is not sensitive enough to detect small changes in gene expression, although the mouse microarray dataset from this study failed to detect oscillatory expression of the well-characterised clock gene *Lfng*. This brings into

question the reliability of such an approach when trying to identify cycling gene transcription within the PSM.

FGF signalling regulates cycling transcription of *Hes7* in the caudal mouse PSM

Niwa et al (2007) observed that the Fgf target Dusp4 exhibits dynamic expression in the mouse PSM at both the mRNA and protein levels, while *Dusp4* transcription in particular is in phase with *Hes7* transcription. They found that *Hes7* expression was only downregulated in the rostral PSM compared to the control treatment when inhibiting Notch activity with the γ-secretase inhibitor DAPT (Niwa et al, 2007). Conversely, treatment with Fgf signalling inhibitors severely downregulated *Hes7* transcription in the caudal PSM only during phases 1 and 2 of expression. They therefore proposed that *Hes7* oscillation in the caudal PSM is controlled by Fgf signalling, while it is Notch regulated in the rostral PSM (Niwa et al, 2007). Niwa et al (2011) further demonstrated that the effector proteins of Notch and Fgf signalling oscillate with different dynamics in the mouse PSM. They suggested that Notch signalling periodically segregates a synchronised group of cells while Fgf signalling simultaneously releases these cells for segmentation from the rostral PSM (Niwa et al, 2011).

Cross-regulation between the Notch, FGF, and Wnt signalling pathways in the PSM

Defining the pacemaker mechanism underlying somitogenesis has been a major unanswered question in the field since the discovery of the first cycling genes in the vertebrate PSM. The study by Niwa et al (2011) proposed that Fgf activity constitutes the pacemaker of somitogenesis, although the relative importance of Notch, Wnt and Fgf signals in controlling the periodicity of clock gene oscillations requires further clarification. The majority of characterised cycling transcripts in the PSM are found to be members of the Notch pathway, but it remains unclear as to whether cycling Notch activity itself determines the periodicity of somitogenesis, or is simply an output of the segmentation clock that synchronises waves of clock gene expression (Dequeant et al, 2008; Jiang et al, 2000). Although mice containing

mutations in Notch signalling components generally have severe segmentation defects, they do still form somewhat disrupted segments (Gibb et al, 2010; Rida et al, 2004). This suggests that Notch signalling may not be essential for somitogenesis. However, a comprehensive study found that blocking Notch activation by either culturing mice embryos in the presence of γ-secretase inhibitors, or by creating double knock-out mice for *Psen1*$^{-/-}$ and *Psen2*$^{-/-}$, abolishes both dynamic clock gene expression of all three pathways and also blocks somite formation from the PSM (Ferjentsik et al, 2009). These outcomes show that Notch signalling is essential for both dynamic clock gene expression and somitogenesis (Gibb et al, 2010).

Different studies on the roles of Notch, Fgf, and Wnt signalling have attempted to establish a hierarchy that may clarify the most significant signalling pathway in somitogenesis. Cross-regulatory links found between these three pathways in the context of the mouse PSM are summarised in Figure M. The Wnt and Notch pathways are shown to have close associations (Muñoz Descalzo and Martinez Arias, 2012). Wnt and Notch targets are shown to oscillate out of synchrony with each other at the mRNA level in the PSM by microarray (Krol et al, 2011), while ISH reveals that the Notch ligand *Dll1* and the Wnt target *Snail1* oscillate in phase in the mouse PSM (Bone et al, manuscript in preparation). Furthermore, it was demonstrated that *Dll1* expression is Wnt dependent (Bone et al, manuscript in preparation). This highlights an important point of cross talk between the two pathways. Furthermore, Notch1 activation in keratinocytes is shown to induce p21-mediated downregulation of *Wnt4* expression to promote stem cell differentiation (Devgan et al, 2005). The cycling expression of *Lfng* is reported to be dependent on *Wnt3a* expression, however *mAxin2* itself is repressed in Notch signalling mutant mice (Aulehla et al, 2003; Ferjentsik et al, 2009). As described above *Hes7* expression is FGF dependent in the caudal PSM but its dynamic expression across the PSM is Notch dependent.

The fact that conditional Fgf signalling mutant mice lack *Lfng* and *Axin2* expression in the PSM suggests that Fgf signalling may act upstream of both Wnt and Notch signalling (Wahl et al,

2007). Fgf signalling is upstream of the cycling Notch targets *Her1* and *Hes6* in the zebrafish PSM (Kawamura et al, 2005), however the oscillations of Notch targets are unaffected in Fgf signalling mutants or upon pharmacological inhibition of Fgf signalling (Delfini et al, 2005; Dubrulle et al, 2001; Gibb et al, 2009). Furthermore, inhibition of Notch signalling alters the expression of the Fgf/Wnt target *Snail1* (Ferjentsik et al, 2009). When comparing the Wnt and Fgf pathways, again there are contrasting reports. *Axin2* expression is abolished in mice following the conditional PSM knock-out of *Fgfr1,* while *Fgf4/Fgf8* double conditional knock-out in the PSM severely reduces Wnt3a expression in the tail (Boulet and Cappechi, 2012; Naiche et al, 2011; Wahl et al, 2007). However, the expression of the Fgf targets *Snail1* and *Sprouty2* also require Wnt signalling (Dale et al, 2006; Gibb et al, 2009). These findings suggest that there is not a simple tiered hierarchy but rather a level of co-regulation between these three signalling pathways in controlling vertebrate segmentation (Gibb et al, 2010).

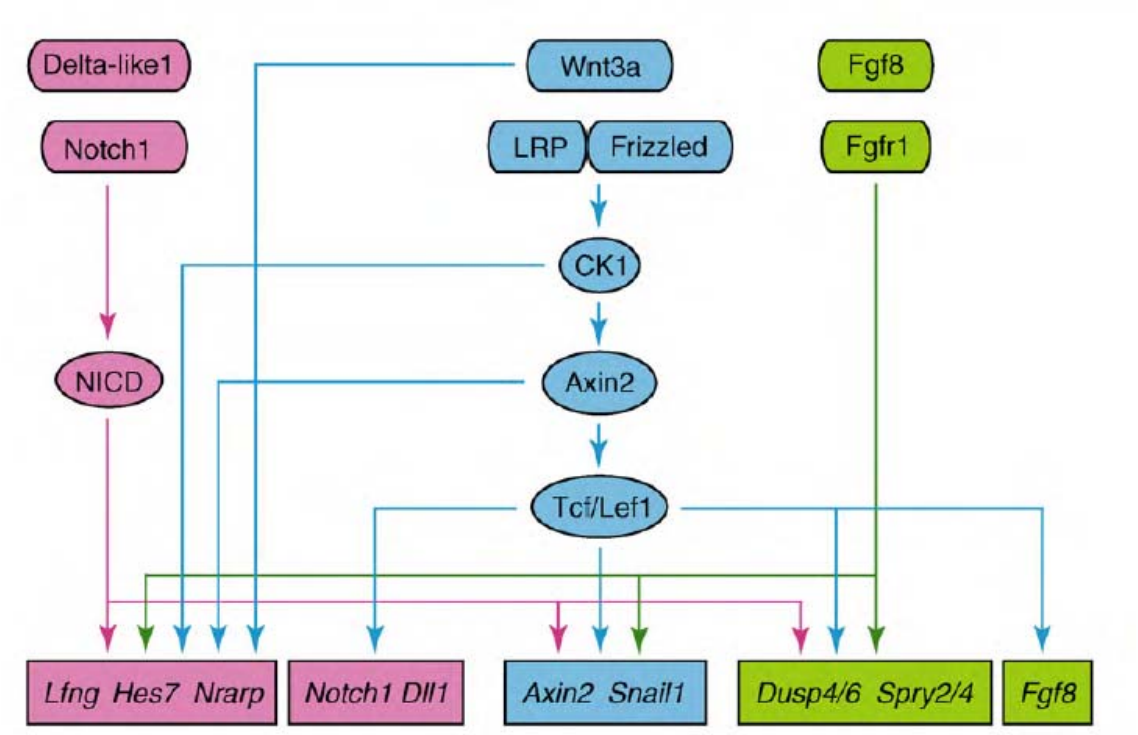

Figure M) Cross-regulation of Notch, Wnt, and Fgf oscillators in the mouse PSM. This figure highlights the levels of cross-talk between the Notch (pink), Wnt (blue), and Fgf (green) pathways observed to date in the mouse PSM and that are referenced in the main text. Components in rounded boxes are components of the core signalling mechanism for each pathway, while those in rectangular boxes represent targets of each pathway involved in the molecular clock or wavefront oscillators. Arrow colour matches the signalling pathway and shows cross-regulation of targets principally associated with one of the other pathways. (Taken from **Gibb et al, 2010**)

Defining the Pacemaker of Somitogenesis

A reduction in Wnt signalling has been suggested to be necessary for slowing and halting clock gene oscillations in the rostral PSM (Aulehla et al, 2008). This conclusion was drawn from the observations that oscillations of clock gene transcription slow down in the rostral PSM where nuclear β-catenin levels are lower (Aulehla et al, 2008; Dale et al, 2003; Palmeirim et al, 1997). This is supported by evidence that at the end of somitogenesis in the chick the period of the clock and somite formation becomes progressively slower for the last 5-8 somite pairs, as *Wnt3a* expression also gets progressively lower (Gibb et al, 2009; Tenin et al, 2010). Gibb et al (2009) also observed an increase in the oscillation period for *Lfng* transcription in both the chick and mouse PSM upon pharmacological inhibition of Wnt signalling using the CK1α inhibitor CKI7.

Evidence that Fgf signalling may be upstream of Wnt and Notch signalling in controlling the segmentation clock (Wahl et al, 2007) prompted Gibb et al (2009) to test whether direct inhibition of Fgf signalling would also slow clock gene oscillations. However, treatment with the Fgf inhibitor SU5402 did not have any effect on clock gene oscillations in either the chick or mouse PSM (Gibb et al, 2009). This outcome therefore suggested that Fgf signalling does not regulate the pace of clock gene oscillations as was speculated by Niwa et al (2011). However, although targeting CK1 as a negative regulator of canonical Wnt signalling was a valid approach to attenuate Wnt signalling, it should be noted that CK1 has important regulatory roles in a range of other cellular processes including transcription and circadian rhythm (Harms et al, 2003). This may explain why CKI7 treatment was found to inhibit a spectrum of targets from signalling pathways other than just Wnt (Gibb et al, unpublished communication). The specific role of Wnt signalling in the pacemaker of somitogenesis therefore requires further verification.

Studies where Wnt signalling has been induced ectopically in the PSM have raised more questions about the role of Wnt signalling in the temporal control of cyclic Notch target

expression. Culturing chick PSM explants in the presence of either Wnt3a-conditioned medium, or with lithium chloride (LiCL) – a direct inhibitor of GSK3β kinase activity – was not found to have any effect on clock gene oscillations in the chicken PSM (Gibb et al, 2009). Similarly, constitutive activation of Wnt signalling in the PSM does not alter the oscillation period in a *Lfng* live reporter mouse (Aulehla et al, 2008). However, in contrast to the study by Gibb et al (2009), Gonzalez et al (2013) reported that inducing Wnt signalling by treating the mouse PSM with LiCl increases the period of the clock in a dose-dependent manner in the *Hes7* reporter mouse (Takashima et al, 2011). It has been suggested that both Tbx6 and Wnt signalling act in co-operation to regulate *Hes7* expression and normal oscillation pace through of a number of Tbx6 and Lef1 binding sites within the *Hes7* promoter (Gonzalez et al, 2013). In the same study it was hypothesised that inhibition of Wnt signalling would therefore increase the pace of clock gene oscillations. XAV939 is a small molecule inhibitor which stabilises Axin protein through the inhibition of Tankyrase enzymes, thereby promoting β-catenin degradation to repress downstream canonical Wnt targets (Huang et al, 2009). As well are their roles in Wnt signalling, Tankyrases are poly(ADP-ribose) polymerase enzymes and are shown to have roles in the regulation of spindle assembly, telomere elongation, and mitosis (Chang et al, 2005; Chiang et al, 2008). Therefore, treatment with XAV939 could potentially affect a range of the aforementioned cellular processes involved in the cell cycle in addition to reducing the activity of canonical Wnt signalling.

Treatment of the *Hes7* reporter mouse with 1μM XAV939 did not have a significant effect on the pace of *Hes7* oscillations, however treatment with 100μM CKI7 (the CK1 inhibitor) did appear to slow oscillations in the *Hes7* reporter (Gonzalez et al, 2013) as was reported previously for *mLfng* expression (Gibb et al, 2009). The conflicting results on the pace of clock gene oscillations following Wnt inhibition by different pharmacological methods query the significance of this study by Gonzalez et al (2013). Another possibility is that clock oscillations are sensitive to either an increase or decrease of Wnt signalling, as is the case for levels of Notch activity (Ferjentsik et al, 2009; Kim et al, 2011).

It has been proposed that induction of Wnt signalling may not be able to shorten the period of the clock because the tissue is already Wnt saturated (Gibb et al, 2010). Alternatively, the limiting dynamics of clock gene mRNA and protein synthesis and subsequent degradation in the wild type PSM may already generate oscillations at the fastest pace possible (Gibb et al, 2009; Gibb et al, 2010; Harima et al, 2013; Hirata et al, 2004; Hoyle and Ish-Horowicz, 2013; Lewis, 2003; Monk, 2003). Hirata et al (2004) first found that generating a point mutation in the mouse *Hes7* gene increased the protein half-life from the Wild-type 22.3 minutes to 30.3 minutes in the mutant. As a result, both *Hes7* oscillations and somitogenesis became severely disrupted after a few oscillation cycles, showing the instability of Hes7 is required to maintain normal oscillation frequency for regular somite production from the PSM (Hirata et al, 2004). Subsequently, Takashima et al (2011) predicted that the processing of introns in the *Hes7* gene leads to a ~19 minute delay in its mature mRNA expression that is essential for Hes7 oscillations. This was proven, as removing all three of the introns from *Hes7* abolished oscillations, leading to stable *Hes7* expression in the PSM and severely disrupted segmentation (Takashima et al, 2011).

Furthermore, mathematical models have predicted that reducing the number of introns in cyclic genes with auto-repressive feedback loops will cause a reduction in the clock period (Harima et al, 2013; Hoyle and Ish-Horowicz, 2013). In line with this prediction, removing introns 1 and 2 from *Hes7* (pH7-Hes7-3) results in oscillations with an average period of ~115 minutes in comparison to ~127 minutes in the WT *Hes7* mouse (Harima et al, 2013). The outcome of these more rapid oscillations in the pH7-Hes7-3 mouse is an increase in number and decrease in the size of anterior somites when viewed at E8.5, while neonates exhibited 1 or 2 extra vertebrae in the cervical/ upper thoracic region compared to WT littermates (Harima et al, 2013). However, more caudal vertebrae were fused in pH7-Hes7-3 mice, suggesting the segmentation clock may have stopped later on during more caudal segmentation (Harima et al, 2013). Hoyle and Ish-Horowicz (2013) also used *in vivo* measurements of the spatial domains of nascent and mature mRNA expression of the clock genes *Lfng*, *Hes7*, and *Nrarp*.

From these values they derived equations and translated them into temporal information to thereby demonstrate that the rates of mRNA splicing and export are much slower than transcript elongation (Hoyle and Ish-Horowicz, 2013). All together these data suggest that mRNA and protein production and destruction are likely to make up for much of the clock period necessary for delayed auto-repressive activity in maintaining oscillations (Lewis et al, 2003).

There is also evidence for the role of Notch signalling in the regulation of the clock period. Mice lacking the Notch target gene *Nrarp* form fewer vertebrae than WT mice, with morphological abnormalities also evident (Kim et al, 2011). In these *Nrarp* null mice, Notch activity is higher in the PSM, with an extended clock period of about 5 minutes longer compared to WT mice which leads to fewer somites and the resultant vertebrae forming (Kim et al, 2011). Herrgen et al (2010) demonstrated that the clock period is also extended on average between 7-23% longer in zebrafish mutants for the Notch signalling components *deltaC, deltaD*, notch1a, or *mib*. These results suggest that intercellular coupling of Notch/Delta signalling is required to maintain the normal clock period in the zebrafish PSM (Herrgen et al, 2010). Another study in the zebrafish embryo found that *Hes6* mutants display an increased clock period of ~6.5% along the entire trunk, even though the total time for somitogenesis was the same as WT fish (Schröter and Oates, 2010). Again, this leads to a reduced number of total somites and resultant vertebrae at the end of somitogenesis, but the position of Hox gene expression and anatomical markers are aligned accordingly with an axis containing fewer somites in the *Hes6* mutant (Schröter and Oates, 2010). Therefore *Hes6* appears to contribute to the regulation of somite periodicity relative to axial elongation in order to confirm the correct number of somites form (Dequeant and Pourquie, 2008; Schröter and Oates, 2010). Hes6 acts as the hub for Her/Hes dimers that comprise a network of negative transcriptional feedback loops, while Her7 strongly associates with He6 as a heterodimer and therefore modulates the network topology by regulating the availability of Hes6 to dimerise with other Her proteins (Schröter et al, 2012; Trofka et al, 2012).

While these studies show clear genetic pathway disruptions linked to increasing the period of clock gene oscillations, it should be noted that neither *Nrarp* nor *Hes6* are essential for segmentation (Kim et al, 2011; Schröter and Oates, 2010; Wright et al, 2009). Harima et al (2013) therefore argued that currently the genes shown to affect the pace of somitogenesis are not crucial for somite formation per se. It is also clear that the zebrafish has evolved to contain a number paralogues in the *Her* gene family which are not present in higher vertebrates such as the mouse or the chicken (Dequeant and Pourquie, 2008). These differences highlight a way in which the network of interacting Notch-regulated clock oscillator components has changed during vertebrate evolution.

Sonic Hedgehog in the temporal regulation of Somitogenesis

Sonic hedgehog (Shh) is a homologue of the *Drosophila* Hh and functions as a signalling morphogen to regulate patterning and differentiation of crucial embryonic tissues including the NT and limb bud digit specification (Briscoe and Novitch, 2008; Towers and Tickle, 2009). The NC is a potent source of the Shh morphogen and lies ventrally to the NT, running along the midline of the embryo and separating the left and right sides of the paraxial mesoderm and somite pairs (Briscoe and Novitch, 2008). Resende et al (2010) reported that bisecting the PSM down the midline to generate left and right half-PSM explant pairs resulted in the side lacking the NC exhibiting slower oscillations of *cHairy2* in the PSM and delayed somite production compared to the PSM side retaining the underlying NC. They postulated that the delayed oscillation of this clock gene in the PSM was due to a loss of the Shh source from the NC, as these effects were recapitulated when half-PSM explants were treated with the Shh inhibitor cyclopamine compared to the control (Resende et al, 2010). However, while the somite phenotype was clear, these effects were observed for culture periods of 9 hours, by which time the remaining unsegmented PSM is short and clock gene oscillation phase difficult to determine accurately. Conversely, Gibb (unpublished communication) found that culturing half-PSM explants in similar -/+ cyclopamine assays for 6 hours at twice the concentration still

had no effect on oscillations of *cLfng* transcription. These conflicting reports bring into question the whether Shh has a role in the temporal control of somitogenesis.

Evidence that Somitogenesis does not require the Segmentation Clock

A recent report has suggested that somites can form in the absence of the molecular oscillator (Dias et al, 2014). Treatment of the posterior PS tissue from a donor stage HH5 embryo with Noggin for 3 hours before grafting to a remote extra-embryonic region results in the simultaneous generation of multiple somites as a 'bunch of grapes' which exhibit normal size and shape, with axial identity as the Hox code appears fixed independently of somite fate (Dias et al, 2014). These somites do not have clear RC patterning however and there is an absence of cycling Notch gene transcription in this mesoderm, suggesting that the segmentation clock is required only to determine somite RC polarity required to segment neural tissue and not for somite size (Dias et al, 2014).

There are however a number of issues with this study. Firstly, the tissue treated in this study was grafted to an extraembryonic region, which is lateral to the native PSM and is likely to receive different levels of key signalling morphogens such as Fgf and Wnt signals which appear to be important regulators of normal somitogenesis. Secondly, as there is currently no live reporter of the segmentation clock in the chicken embryo, it is impossible to determine whether clock gene oscillations had really ceased in this Noggin-induced mesoderm (Dias et al, 2014). Another important aspect to consider is that all the evidence for the somitogenesis clock points to a regulation of the timing of somite formation and not the actual formation of the somites themselves. Models currently suggest that the segmentation clock acts in the caudal PSM, while the wavefront of Fgf activity controls where the oscillation ceases in the rostral PSM and releases a block of PSM cells from the clock to undergo segmentation under the control of *Mesp2* expression and in the domain of RA activity (Delfini et al, 2005; Morimoto et al, 2005; Niwa et al, 2011; Takahashi et al, 2000). Therefore, the fact that these somites formed simultaneously, rather than sequentially, in the absence of the molecular oscillator

may not be altogether surprising. As this study was performed outside the context of the PSM, it is difficult to interpret how significant this result achieved by Dias et al (2014) really is.

miRNAs in the regulation of the Segmentation Clock

In addition to the growing evidence for auto-repressive feedback loops maintaining segmentation clock gene oscillations, more recently a number of studies have indicated that micro-RNAs (miRNAs) also regulate the temporal expression of certain Notch-related clock genes in a variety of contexts (Bonev et al, 2012; Poulton et al, 2011; Riley et al, 2013). *mir-125a-5p* is shown to target the 3' UTR of the *Lfng* gene in the chicken PSM, while blocking this interaction disrupts both clock gene oscillations and somitogenesis (Riley et al, 2013). Ultradian oscillations of *Hes1* in neural progenitors are essential to maintain a proliferative state and rely on the controlled instability of *Hes1* (Bonev et al, 2012). *miR-9* is shown to control the stability of *Hes1* mRNA, as either *miR-9* overexpression or loss of *miR-9* dampens *Hes1* oscillations and leads to premature differentiation (Bonev et al, 2012). Furthermore, mice with a PSM conditional knock-out for the *Dicer* gene, which encodes a protein key for the processing of miRNAs, have irregular and fused vertebrae, as well as an extra thoracic vertebra than WT littermates, suggesting that miRNAs do have functional roles in somitogenesis (Maroto and Bone, unpublished communication). It is therefore possible that miRNAs may provide another level of post-transcriptional regulation to control the pace of clock gene oscillations in the PSM.

It was recently demonstrated that the mRNAs of the cycling Notch targets *Lfng* and *Hes7* exhibit overlapping domains of spatio-temporal expression in the caudal PSM of the mouse embryo (Bessho et al, 2003; Nitanda et al ,2014). However, closer inspection reveals that the *Lfng* domain in the caudal PSM is more distinct than the broader *Hes7* domain, as well as *Lfng* mRNA being less stable than *Hes7* mRNA (Nitanda et al ,2014). Transgenic mice with reporters followed by just the 3' UTR of either the *Lfng* or the *Hes7* gene can recapitulate the endogenous distribution patterns of *Lfng* mRNA or *Hes7* mRNA, respectively (Nitanda et al,

2014). This reveals that 3' UTR-dependent mRNA stability is an important mechanism which determines the differential distribution profiles of *Lfng* and *Hes7* mRNAs within the caudal mouse PSM (Nitanda et al ,2014). Given that stability of clock gene mRNAs is suggested to be important to maintain rapid oscillations of transcription across the PSM, it is likely that the 3' UTR of certain clock genes may regulate their differential stability in controlling the pace of the segmentation clock (Lewis, 2003; Monk, 2003; Nitanda et al, 2014).

Post-translational regulation of NICD Protein Stability

A number of clock products including Hes7, NICD, and Lfng proteins have been shown to exhibit a short half-life in the PSM that is crucial to maintain rapid oscillations of their mRNA and protein expression (Bessho et al, 2003; Dale et al, 2003; Lewis, 2003; Niwa et al, 2011). Hes7 protein is shown to be rapidly degraded by the ubiquitin proteasome to ensure rapid turnover in the mouse PSM (Bessho et al, 2003). In other cellular contexts, NICD protein is also shown to be targeted for post-translation modification to regulate its activity and degradation. In cell culture systems it was demonstrated that when NICD is bound in complex with CSL on the *Hes1* promoter, the co-activator MAM directly associates with CDK8/Cyclin C and thereby recruits it to the complex (Fig. N) (Fryer et al, 2004). CDK8/Cyclin C is then able to phosphorylate NICD on a number of serine residues within the transactivation domain (TAD) and proline/glutamic acid/serine/threonine-rich motifs (PEST) domain at the C-terminal end (Fryer et al, 2004). These specific phosphorylation events greatly enhance PEST-dependent degradation of NICD protein by the ubiquitin ligase F-box and WD repeat domain-containing 7 (Fbw7) (Fryer et al, 2004). This shows that MAM and CDK8/Cyclin C are important regulators of rapid NICD complex turnover at the site of target promoters (Fryer et al, 2004). There are three isoforms of Fbw7 (α,β, and γ), although it was recently shown that FBW7β in particular is essential for NICD turnover (Sancho et al, 2013).

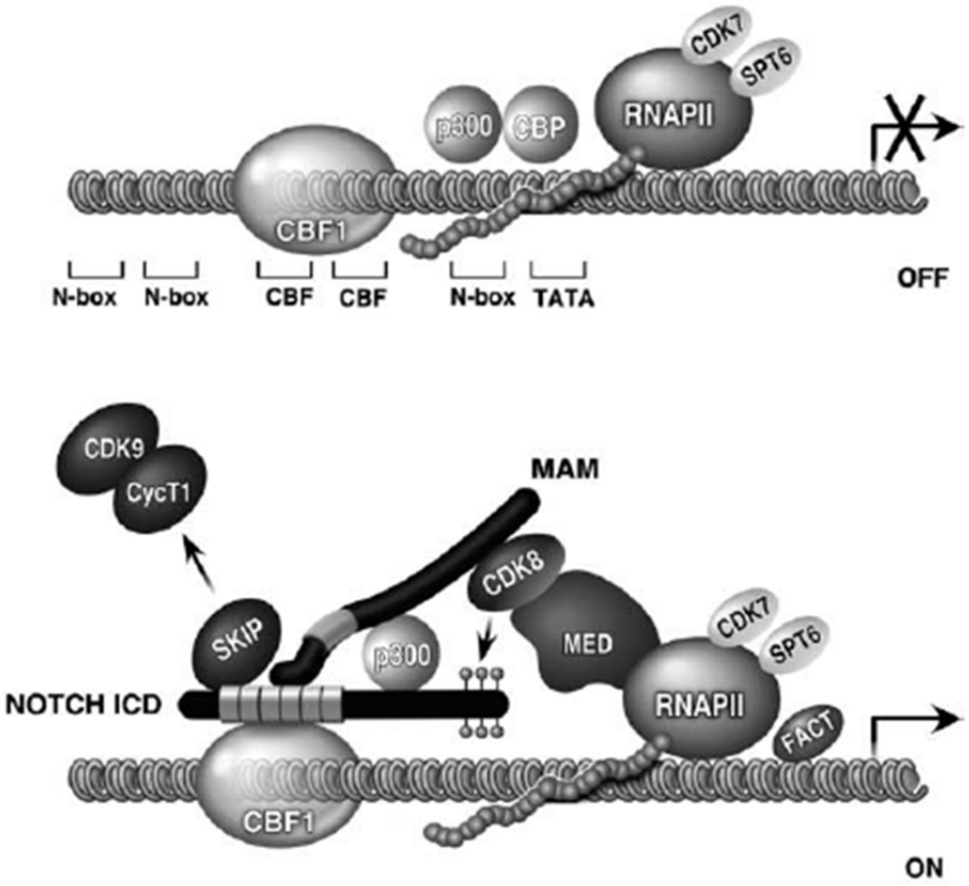

Figure N) The NICD complex on the *Hes1* promoter: target activation and NICD turnover. Proteins that are bound to the promoter prior to activation of *Hes1* transcription are indicated in lighter shades: CBF1 (Rbpjκ), p300, RNA polymerase II (RNAPII), Cdk7, Spt6. In the absence of NICD binding, the gene is repressed (upper panel). Proteins recruited together with NICD are shown in darker shades: MAM, SKIP, MED, CDK8, FACT. NICD binding to CBF1 (Rbpjκ) promotes transcription of the target *Hes1*, while MAM recruitment of Cdk8/cyclin C promotes hyperphosphorylation on the PEST domain of NICD (small circles). Hyperphosphorylated NICD is targeted for ubiquitination by Fbw7 and subsequent degradation to maintain rapid turnover of the Notch enhancer complex. (Taken from **Fryer et al, 2004**)

Another study identified that NICD levels are increased following inactivation of GSK3α and GSK3β by treatment with LiCL or specific siRNA (Jin et al, 2009). Further analysis revealed that GSK3α can bind NICD through phosphorylation of at least three threonine residues, which are necessary for the response to LiCL treatment as LiCL does not increase transcriptional activity of NICD and *Hes1* mRNA levels when these sites are absent (Jin et al, 2009). This suggests that GSK3 represses Notch signalling by phosphorylating NICD, which is similar to its role in targeting β-catenin to inhibit transcription of Wnt signalling targets (Clevers, 2006). NICD is also shown to be acetylated on 14 conserved lysine residues in order to modulate the strength and duration of Notch signalling in endothelial cells (Guarani et al, 2011). Indeed, the presence of the SIRT1 de-acetylase opposes stabilisation of NICD through acetylation, as blocking SIRT1 activity leads to increases NICD levels and a reduces ubiquitination of NICD (Guarani et al, 2011). This suggests that acetylation stabilises NICD protein by repressing its ubiquitin-mediated proteolysis, while the SIRT1 de-acetylase is required to reverse this and promote NICD destabilisation which may be important to regulate cell growth and fate determination (Guarani et al, 2011). These studies show that post-translational modification of NICD protein may be another mechanism by which the stability of NICD and thus the pace of clock gene oscillations are regulated within the PSM.

Cyclin-dependent Kinases and the Segmentation Clock

The potential role for cyclin dependent kinases (cdks) and their cyclin binding partners in setting the pace of the segmentation clock have received little attention to date. Cdks/Cyclins are well established as regulators of fundamental cellular processes, including most-notably cell cycle progression and RNA polymerase II (RNA pol II)-dependent transcription (Malumbres and Barbacid, 2009). Cdks 1-4, and cdk6 primarily regulate cell cycle progression and division, while cdk7/cyclin H, cdk8/cyclinC, and cdk9/cyclinT promote global transcription initiation and elongation via direct phosphorylation of RNA pol II on Serines within the C-terminal domain (CTD) (Fisher, 2005; Malumbres and Barbacid, 2009).

It was previously shown that inhibition of Casein Kinase 1 alpha (CK1α) with the small molecule inhibitor CKI7 delays oscillations of *Lfng* expression in the PSM of both the chicken and mouse (Gibb et al., 2009). CKI has regulatory roles in multiple signalling pathways including Wnt signalling (Clevers, 2006), however it is also known to be involved in many other processes such as the circadian clock rhythm (Harms et al, 2003). Interestingly, the small molecule inhibitor R03306, which targets Cyclin dependent kinase 1 (CDK1) activity, can also delay oscillations of *cLfng* in the chicken PSM (Gibb, unpublished), while the general cdk inhibitors Olomoucine and Roscovitine has been shown to lengthen the circadian clock in the optic nerves of the marine snail *Bulla gouldiana* (Krucher et al, 1997). Stern et al (1988) suggested that a panel of cell cycle inhibitor drug treatments could each cause repeated somite abnormalities similar to those seen upon heat-shock in chicken embryos. Treating the chicken PSM with the cdk1 inhibitor RO-3306 in similar -/+ half-PSM assays as Gibb et al (2009) caused a somewhat inconsistent delay effect on the oscillation phase of *Lfng* expression compared to the corresponding control treated PSM side (Gibb, unpublished communication). These findings suggest that cdks/cyclins may have a role in the temporal control of the segmentation clock and warrants further testing.

Somite specification and their Derivatives

The formed somites have clear RC patterning which is necessary to direct normal development of the vertebrae, as well as the associated nerves and blood vessels later on (Keynes and Stern, 1988). During somite formation Mesp2 stabilises *Lfng* expression at the determination front and therefore represses Notch/Dll signalling here, while inducing EphA4 expression to promote boundary formation (Morimoto et al, 2005; Sasaki et al, 2011). As a result, once the somite fully segments away from the rostral PSM, there are clear markers of somite polarity: *Mesp2*, *Lfng*, and EphA4 mark the rostral compartment, while *Dll1*, NICD, *Uncx4*.1, *Hairy1*/*Hes7*, and EphrinB2 mark the caudal half of the somite (Bessho et al, 2001b; Dale et al, 2003; Durbin et al, 1998; Mansouri et al, 1997; Morimoto et al, 2005; Neidhardt et al, 1997; Niwa et al, 2011; Palmeirim et al, 1997; Saga et al, 1997; Takahashi et al, 2003). The epithelialisation and RC polarity of the somites relies on the expression of *Paraxis*, a marker of somitic tissue which is absent from most of the un-segmented PSM (Johnson et al, 2001). *Paraxis*-null mice display even expression of the caudal somite markers *Dll1* and *Uncx4*.1 throughout the somite tissue and the somites themselves fail to epithelialize (Johnson et al, 2001). Paraxis is suggested to regulate cell-adhesion to maintain the boundary between the rostral and caudal halves within each somite (Johnson et al, 2001). Negative regulation between these markers, such as between Mesp2 and NICD (Sasaki et al, 2011), also ensures their relative RC localisation within the somite.

A recent metabolomics study analysing sections of tissue along the AP axis of the PSM and some of the formed somites in the chick and mouse embryos found that fundamental characteristics of PSM cells change during differentiation towards the anterior PSM (Pourquie, unpublished communication). This report showed that posterior PSM cells exhibit a highly glycolytic status, with rounded mitochondria. However, many glycolysis enzymes become downregulated during PSM differentiation with concomitant up regulation of TCA cycle and anti-oxidant enzymes as cells are displaced towards the anterior PSM, with mitochondrial

shape becoming elongated by the time these cells contribute to the somites (Pourquie, unpublished communication). This study found that the respiratory inhibitor sodium azide could arrest somitogenesis and clock gene oscillations, but not stop axis elongation (Pourquie, unpublished communication). Therefore, the determination front appears to mark a major metabolic transition in segmentation determination and the apparent gradient of metabolic status across the PSM may also be required for normal clock gene oscillations.

The PSM is made up of loosely organised mesenchymal cells, but as the somites form a mesenchymal-epithelial transition (MET) cellular rearrangement occurs to generate somites with an organised outer epithelium surrounding the inner mesenchyme. Clustering of α5β1 integrin at the somite boundary binds to the extracellular matrix (ECM) protein fibronectin and promotes rearrangement of the ECM by cell adhesion molecules to create the epithelial outer layer of the somite (Giros et al, 2011; Maroto et al, 2012). Mesp2 induction of EphA4 signalling also appears to be instrumental in promoting MET in the forming somite tissue (Barrios et al, 2003 Jülich et al, 2009).

The specification of the somites and the derivative vertebrae along the AP axis begins at very early stages, being determined already within the paraxial mesoderm prior to segmentation (Gilbert, 2006). The expression of overlapping domains of *Hox* genes determine the axial identity of the somites and associated tissues (Zakany et al, 2001). Vertebrates have four *Hox* gene clusters (*A-D*) numbered between 1 to 13, which are homologues of the *Drosophila* homeotic selector genes (McGinnis and Krumlauf, 1992). Each *Hox* cluster is arranged in numerical order on a different chromosome, while also being activated temporally in this order in epiblast cells ingressing through the PS during axial elongation (Maroto et al, 2012). Therefore, the *Hoxa13, c13, d13* paralogues are activated last and demarcate the most caudal somites (Zakany et al, 2001). Some *Hox* genes appear to be expressed dynamically in the PSM under the control of Notch signalling, which may be a mechanism by which the embryo links *Hox* gene expression and the segmentation clock to activate Hox genes in the appropriate

somites along the AP axis (Zakany et al, 2001). Moreover, altering somite boundary position by changing the activity of the Fgf8 wavefront in the chicken PSM alters somite size but Hox gene expression is still within the appropriate somites, suggesting that the clock and not the wavefront is involved in regulating somite specific *Hox* gene expression (Dubrulle et al, 2001). *Hox* gene expression within the somites is retained and determines the morphological identity of the tissues which arise from them. The first 5 anterior-most somites contribute to the occipital bone at the base of the skull in vertebrates, while the posterior somites give rise to the vertebral column (Dequeant and Pourquie, 2008). Vertebrate species display a varied number of each set of vertebrae along the body axis. For example, the chicken has 14 cervical (neck) vertebrae, 7 thoracic (rib-bearing), 12 or 13 lumbosacral (strain dependent), and 5 coccygeal (fused tail) (Fig. O.a) (Gilbert, 2006). The mouse (like all other rodents) however, displays only 7 cervical vertebrae, with 13 thoracic, 6 lumbar (abdominal), 4 sacral (hip), and a variable number of at least 20 small caudal vertebrae in the tail (Fig. O.b) (Gilbert, 2006). However, despite the chick and mouse having differing numbers of each type of vertebrae, the domains of *Hox* expression appear to align accordingly within their somite precursors (Fig. O.c).

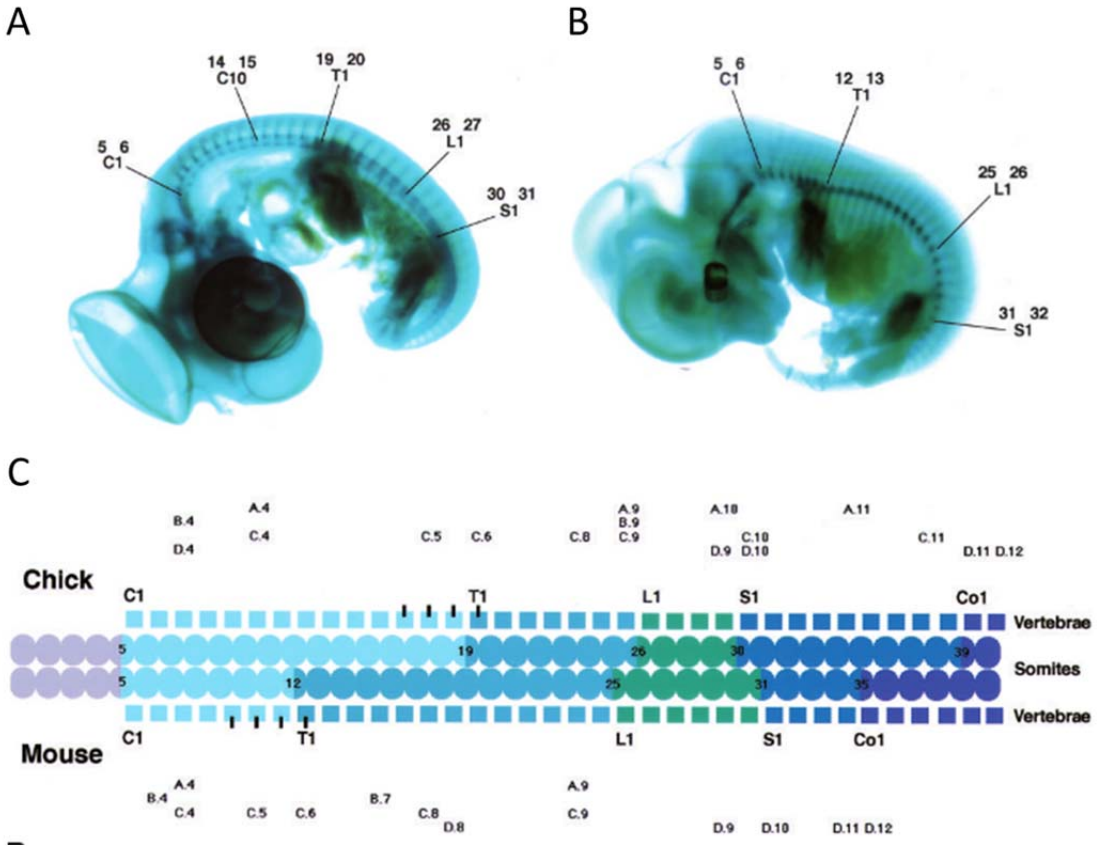

Figure O) Domains of *Hox* gene expression in the somites determine the morphological patterning of the vertebrae in the chicken and mouse embryos. Side on view of a stage HH25-26 chick embryo (**A**) and an E13 mouse embryo (**B**), both have been cleared and stained with alcian green. The position of certain vertebrae are marked by a letter and number (C1 = 1st cervical; T1 = 1st thoracic; L1 = 1st lumbar; S1 = 1st sacral). Above these, the somite numbers shown to give rise to these vertebrae are indicated (e.g ^{5}C1^{6} shows that the 5th and 6th somites give rise to the 1st cervical vertebra). **C**) Schematic view of the somites and their vertebral derivatives in the chicken and mouse embryos. The first 5 somites (grey) give rise to the occipital bone in the base of the skull. Cervical vertebrae/forming somites are shown in lightest blue, thoracic in blue, lumbar in green, sacral in navy blue, coccygeal in darkest blue. The anterior boundary of different *Hox* gene expression domains are identified relative to the level of the somites/vertebrae in both species. (Taken from **Burke et al, 1995**)

The boundary between expression domains of *Hox5/6* paralogues mark the boundary between cervical and thoracic vertebrae forming somites, while the boundary between expression domains of *Hox9/10* paralogues mark the boundary between thoracic and lumbar vertebrae in both species (Fig. O.c) (Burke et al, 1995; Gilbert, 2006). Simultaneous homozygous knock out of all the *Hox10* paralogues in mice causes a loss of all lumbar vertebrae, being replaced instead by more rib-bearing thoracic vertebrae (Wellik and Cappechi, 2003). Such a homeotic transformation is characteristic of those seen in *Drosophila*, but also suggests that there is a posterior prevalence of *Hox* gene expression in vertebrates as this paralogous deletion results in an increase in the number of vertebrae with the next anterior identity (Wellik and Cappechi, 2003). The gradient of RA activity in the embryo also seems to contribute to the regulation of *Hox* gene expression, as increasing the levels of RA activity in the embryo can activate Hox genes in more anterior domains and cause anterior shifts in vertebral morphology along the AP axis (Kessel and Gruss, 1991).

Somite maturation and differentiation into the somitic lineages begins almost immediately upon epithelialisation and segmentation (Yusuf and Brand-Saberi, 2006). The ventral side of the somite nearest the NC forms the sclerotome cells through epithelial-mesenchymal transition (EMT), which will give rise to the vertebrae and the ribs of the axial skeleton, as well as the cartilage cells (chondrocytes) and the syndetome (tendon-forming tissue) (Christ et al, 2000). The dorsal somite forms the dermamyotome, which produces the skeletal muscles and the dermis of the back (Yusuf and Brand-Saberi, 2006). The ventral somite is in closest proximity to the underlying NC and it appears that inductive Shh signalling from the NC promotes expression of the paired box 1 (*Pax1*) and *Pax9* transcription factors in the ventral somite to specify the sclerotome lineage (Fig. P) (Christ et al, 2007; Yusuf and Brand-Saberi, 2006). The ventral-most sclerotome cells expressing *Pax1* invade the perinotochordal space and give rise to the vertebral bodies and intervertebral discs (Christ et al, 2000). The lateral sclerotome contributes to the laminae and pedicles of the vertebral arches and to the ribs. The dorsal sclerotome cells express *Msx1* and *Msx2* induced by BMP4 from the roof plate of the

dorsal NT and migrate dorsally between the roof plate and the dermis (Christ et al, 2007). These cells will contribute to the vertebral arch and the spinous processes of the vertebrae (Yusuf and Brand-Saberi, 2006). Shh also appears to promote chondrogenesis (cartilage formation) from the sclerotome by modulating the cellular response to BMP signalling (Murtaugh et al, 1999).

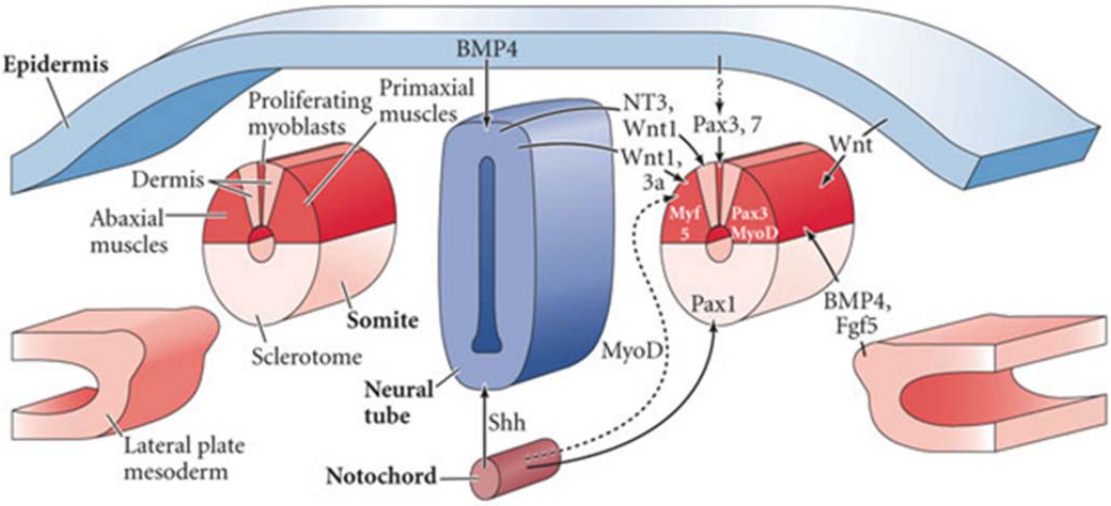

Figure P) Somite patterning and lineage specification. Schematic transverse section through the somite region of a chicken embryo. The somite on the left is labelled to show which regions give rise to the different somite lineages. The somite on the right is labelled regarding the signalling mechanisms from neighbouring tissues which specify these lineages. The ventral somite (pink) is specified to form the sclerotome by expressing *Pax1* in response to the Shh morphogen from the notochord. The roof plate of the neural tube receives BMP4 signals from the overlying epidermis. NTF3 from the neural tube specifies the central-dorsal regions of the somite to form the dermatome, which gives rise to the dermis of the back. Wnt1 and Wnt3a morphogens from the neural tube promote *Pax3* expression in the forming myotome of the dorsal somite. Pax3 then induces the myogenic markers *Myf5* and *MyoD* within the myotome. (Taken from **Gilbert, 2006**)

The RC polarity of the vertebrate somites appears to be crucial to allow the sclerotome somitic lineage to undergo a process known as resegmentation similar to the *Drosophila* embryo, whereby the sclerotome from the posterior half of one somite associates with the sclerotome from the anterior half of the next posterior somite adjacent to it (Christ et al, 1997). This is a vital process to allow correct segmental patterning of the skeletal elements including the vertebrae and ribs, as well as the peripheral nervous system, whose boundaries are shifted half a segment relative to the sclerotome (Maroto et al, 2012; Remak, 1850).

The dorsal cells of the somite remain epithelial and form the two layers of the dermamyotome: the dermatome and the myotome (Christ et al, 2000). The central-dorsal region of the dermamyotome is specified by neurotrophin 3 (NTF3) inductive signalling from the NT to form the dermatome (Fig. P) (Yusuf and Brand-Saberi, 2006). The dermatome in turn forms the dermis; a mesenchymal connective tissue of the back skin (Gilbert, 2006). The primary myotome forms in the two lateral regions of the dermamyotome and produces the myoblast muscle progenitor cells. The region of primary myotome nearest to the NT (i.e. in the medial somite) is termed the epaxial muscle. Inductive signals of Wnt1 and Wnt3a from the neighbouring NT promote *Pax3* expression in the epaxial dermamyotome (Fig.O) (Munsterberg et al, 1995). Pax3 can then induce *Dmrt2* expression, which in turn binds to the early epaxial enhancer of myogenic factor 5 (*Myf5*) to initiate myogenesis (Sato et al, 2010). The epaxial muscles form the intercostal muscles between the ribs and back muscles (Gilbert, 2006). The region of primary myotome furthest from the NT (i.e. in the lateral somite) is termed the hypaxial muscle. In the hypaxial muscle, Pax3 directly activates *Myf5* expression to promote myogenesis to create the musculature of the body wall and the limbs (Bajard et al, 2006; Gilbert, 2006). Another key myogenic regulator called myogenic differentiation 1 (*MyoD*) is also induced by Pax3 to promote myogenesis in the myotome (Fig. P) (Maroto et al, 1997). Some *Pax3* expressing cells from the most central region of the dermamyotome are also able to delaminate and translocate to the myotome (Gros et al, 2005). Most of these cells proliferate rapidly and contribute to muscle tissues, while some remain as progenitors to

maintain a stem cell pool surrounding adult muscles called the satellite cells (Gilbert, 2006; Gros et al, 2005).

The layered specification of the somitic lineages ensures the correct positioning of the adult tissues, so that the intervening tendons formed from the syndetome will connect the skeletal muscles to the vertebrae. Similarly, the resegmentation of the sclerotome enables correct formation of the vertebrae themselves, but also directs segmentation of the nervous system so that the motor neurons elongating laterally from the NT can innervate the skeletal muscles appropriately between the forming vertebrae (Gilbert, 2006). The vertebral column acts as the major structural support for the musculature of the body and to encase the spinal cord, while the rib cage protects vital organs including the heart and lungs. It is clear that the correct patterning and specification of the somitic lineages requires instructive signals from neighbouring axial tissues including the NT and NC. The positioning of the somites relative to these adjacent tissues is therefore vital during embryogenesis and is established in early development during gastrulation.

The Aims of the study

Periodic gene expression of targets from three cross-regulated pathways in the PSM match the rate of somite formation in a number of amniote and anamniote species. However, despite the wealth of information on cycling gene targets and their regulatory networks, the pacemaker mechanism that regulates the period of clock gene oscillations and somite formation remains unclear. This may be in part due to a lack of clear hierarchy among the Notch, Wnt, and Fgf pathways (Gibb et al, 2010). Lewis (2003) utilised mathematical modelling to show that auto-repressive negative feedback loops with delays by clock gene protein products on their own transcription is sufficient to generate stable oscillations of expression in the PSM as long as the half-life of both the mRNA and protein are sufficiently short that the repressive action is only transient until the protein rapidly degrades to permit transcription again. A variety of studies that utilised genetic or pharmacological means to alter the pace of the segmentation clock have attempted to uncover the 'pacemaker' mechanisms of somitogenesis with a degree of conflicting conclusions, and these have established a number of potential candidates including: the Wnt and Shh signalling pathways, Cdks, the level of Notch activity, and stability of Notch-regulated clock proteins such as Hes7 (Gibb et al, 2009; Gibb, unpublished communication; Gonzalez et al, 2013; Harima et al, 2013; Herrgen et al, 2010; Kim et al, 2011; Resende et al, 2009; Schröter and Oates, 2010).

1) This study will aim to clarify: i) Whether Wnt signalling regulates the pace of clock gene transcriptional oscillations in the vertebrate PSM. ii) Whether Shh signalling regulates the pace of clock gene transcriptional oscillations in the vertebrate PSM. iii) Whether Cdks regulate the pace of clock gene transcriptional oscillations in the vertebrate PSM. These candidate regulators will be tested by assessing whether the pace of oscillating clock gene transcription in the PSM is slowed when treated with small molecule inhibitors of Wnt signalling, Shh signalling, or Cdk activity, respectively, in both the chicken and mouse embryos.

2) This project will then aim to test the models which predict that increasing the stability of clock proteins will result in an extended clock period in the PSM (Lewis, 2003; Monk, 2003). The levels of the clock proteins chicken NICD, as well as mouse NICD and Hes7 will be evaluated in the PSM following treatment with small molecule inhibitors of Wnt signalling, Shh signalling, and Cdk activity, respectively, to assess whether any of these inhibitor treatments which slow the segmentation clock will also increase the levels of clock proteins as predicted. Furthermore, the custom-made cNICD antibody will also be used in this study to view the spatial domains of cNICD localisation in the chicken PSM for the first time. This will confirm whether oscillating Notch activity in the PSM and localisation to the caudal compartment of formed somites is a conserved feature of segmentation in amniotes.

3) i) In tissues outside of the PSM, NICD protein has been shown to be targeted for phosphorylation at conserved residues by kinases including Cdk8 and GSK3 to promote rapid NICD degradation (Fryer et al, 2004; Jin et al, 2009). Given that the stability of key Notch protein components of the clock are predicted to be fundamental to maintaining rapid oscillations of clock gene transcription within the PSM (Lewis, 2003), we hypothesise that candidate regulators of the clock pace such as Wnt signalling and Cdks may modify NICD protein post-translationally to promote its rapid degradation in the PSM in order to maintain rapid oscillations of Notch activity. This hypothesis will be tested using mass spectrometry to assess whether NICD protein from chicken PSM tissue displays an altered phosphorylation status when treated with small molecule inhibitors of Wnt signalling, or Cdks, respectively, compared to the control. ii) We hypothesise that the pacemaker of the segmentation clock may be constituted by one or a few key genetic regulators of cycling clock gene expression. Transcriptomic analysis by microarray or Next generation RNA-sequencing (RNA-seq) will allow global

changes in gene expression to be viewed following any drug treatment which delays the molecular oscillator in order to ascertain any targets which appear to be significantly altered in their expression level in a similar manner by all of the delaying agents. These would provide excellent candidates for regulators of the clock period to pursue further in functional assays.

Materials & Methods

Micro-dissection & Culture Conditions

Chicken Embryo dissection

Fertilised chicken eggs from the White Leghorn breed of *Gallus gallus* (Winter Egg Farm, Royston UK) were incubated in a humidified incubator at 38.5^{0}C for 40 hours to generate embryos of Hamburger Hamilton (HH) (Hamburger and Hamilton, 1951) stage 9-11. Blunt forceps were used at a shallow angle to cut a hole of approximately 25mm in diameter in the shell at the very top of the broad end of the egg and care taken to then remove the shell membrane from the top of the yolk surface using pointed forceps. On the surface of the yolk the embryo proper can be seen surrounded by the area pellucida. Surrounding this is the area opaca, which contains the forming blood vessels that start to become visible at this stage of development. Pointed forceps were used to grip the area opaca just to one side of the embryo proper while dissection scissors were used to cut around the embryo to extract it from the egg and placed into a 10cm plate containing phosphate buffered saline (PBS) solution. The vitelline membrane was then carefully removed from the surface of the embryo using pointed forceps. At this point embryos were either prepared for half-PSM dissection, or trimmed down using dissection scissors just to contain the surrounding area pellucida and fixed overnight at 4^{0}C in 4% (v/v) formaldehyde (Sigma)/PBS followed by dehydration in alcohol series.

Mouse embryo dissection

Timed-matings for cd1 laboratory wild type strain *Mus musculus* embryos were set up and embryos were collected at embryonic day 10.5 (E10.5) post-fertilisation stage by the transgenic facility at the University if Dundee, College of Life Sciences. Embryos were then placed in autoclaved PBS and removed from the uterine horns using pointed forceps before isolating the tail from the rest of the embryo at the posterior limit of the hindlimb buds using a sharp tungsten needle. Any attached membranes were also removed using pointed forceps

and tails were placed in a new 6cm dish containing mouse media consisting of Dulbecco's modified Eagle's medium (DMEM)/F12 +GlutaMAX (Life Technologies) supplemented with 10% (v/v) foetal bovine serum (BioSera), 100 U/ml Penicillin-Streptomycin (Life Technologies), 10ng/ml basic human fibroblast growth factor (FGF) protein (Peprotech). Whole tails could then be fixed overnight at 4^0C in 4% (v/v) formaldehyde (Sigma)/PBS followed by dehydration in alcohol series and storage in 100% ethanol at -20^0C, or prepared for half-PSM dissection.

Half-PSM dissection

The methodology was adapted from that used by Palmeirim et al (1997). Chicken embryos were placed dorsal-side up into a dissection dish containing a charcoal agar base in Leibovitz's L-15 medium (Life Technologies). Dissection pins were used to pin the embryo to the surface of the agar. The caudal half of the embryo containing a few somites and the PSM was isolated and bisected along the midline to produce two identical explants each containing half of the neural tube (NT), one side of the PSM and a somite from each pair of the few most recently formed caudal somites, as well as some adjacent lateral plate mesoderm (LPM) tissue (Figure Q).

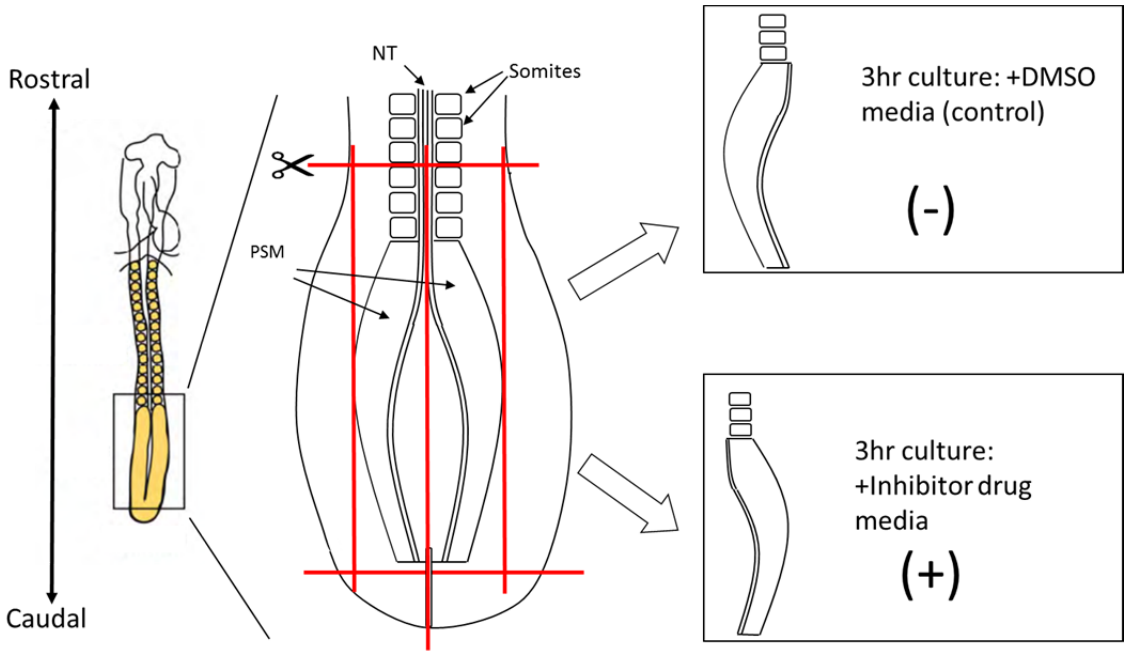

Figure Q) Chicken half-PSM dissection. Schematic of an HH10 chicken embryo, dorsal view. The caudal end of the embryo is isolated several somites anterior to the PSM and bisected down the midline along the neural tube (NT) before removing more lateral tissues to produce identical left and right half-PSM explants (red lines represent cuts). Explants are cultured simultaneously; one side in a control vehicle medium (-) and the other side in the presence of a small molecule inhibitor (+).

Mouse half-PSM explants were generated as for the chicken, with the exception that the isolated tail was pinned to the dish in the two hindlimb buds before bisecting down the midline and removing tissue above the most caudal few somites (Figure R).

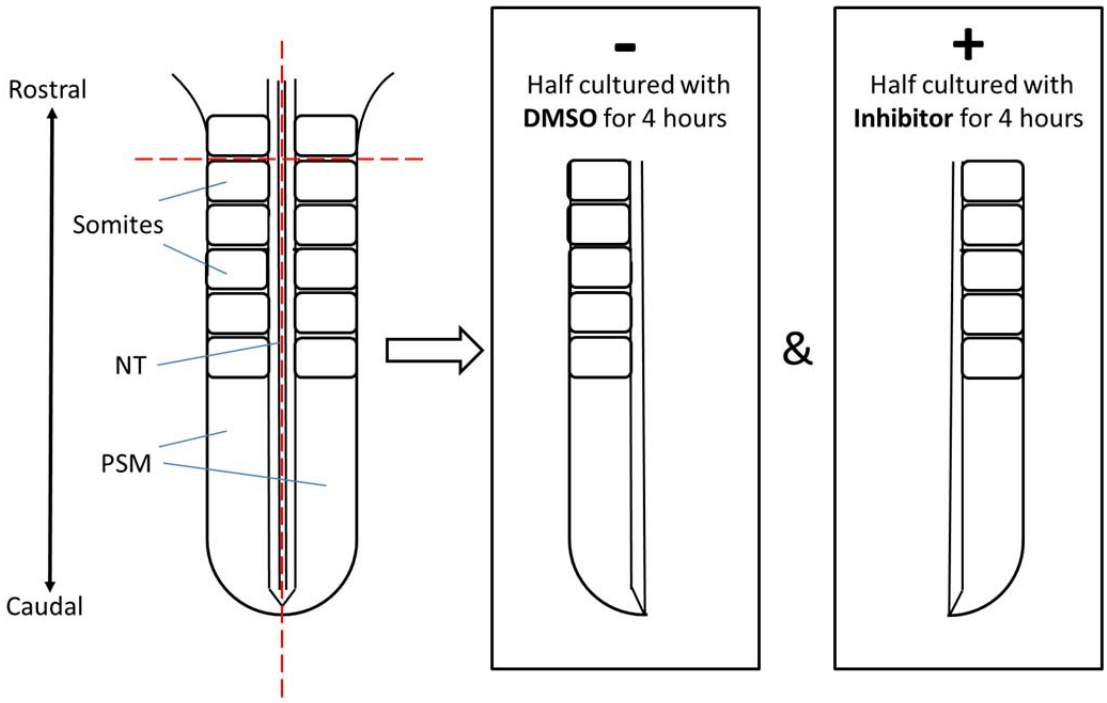

Figure R) **Mouse half-PSM dissection**. Schematic of an E10.5 mouse embryo tail, dorsal view. The caudal end of the embryo is isolated several somites anterior to the PSM and bisected down the midline along the neural tube (NT) to produce identical left and right half-PSM explants (red lines represent cuts). Explants are cultured simultaneously; one side in a control vehicle medium (-) and the other side in the presence of a small molecule inhibitor (+).

Chick explant culture conditions

Explant pairs to be analysed by *in situ* hybridisation (ISH) were each laid flat on a cyclopore track etched membrane filter (Whatman). The filter was then placed on the surface of medium consisting of OptiMEM (Gibco), 5% FBS (BioSera), 20µM Glutamine, 50µg/ml Gentamycin and additionally containing either small molecule inhibitor or control vehicle within a 4-well plate. The following inhibitors/corresponding vehicle control were used: 25µM Cyclopamine (Calbiochem)/DMSO; 10µM 5,6-Dichlorobenzimidazole Riboside (DRB) (Sigma)/DMSO; 150nM LY-411575 (Ly) (University of Dundee)/DMSO; 10µM Roscovitine (Calbiochem)/DMSO; 100µM XAV939 (Tocris Bioscience)/DMSO (see Table 1 also).

Inhibitor	Solvent/ Control	Working Concentration	Solvent dilution in media	Target/ Target Pathway	Supplier
Cycloheximide	Ethanol	20µM	1:2,500	Protein Synthesis	Tocris Bioscience
Cyclopamine	DMSO	25µM	1:400	Shh	Calbiochem
DRB	DMSO	10µM	1:1,000	cdk7, cdk9	Sigma
Ly-411575	DMSO	150nM	1:10,000	Notch	University of Dundee
Roscovitine	DMSO	10µM	1:1,000	cdk2, cdk7, cdk9	Calbiochem
XAV939	DMSO	100µM	1:200	Wnt	Tocris Bioscience

Table 1) Small molecule Inhibitor information summary.

For '-/+' drug assays, one half PSM explant was cultured in the presence of the small molecule inhibitor (+) and the corresponding half cultured in the vehicle control medium (-). Each -/+ pair was cultured for 3 hours in an incubator at 38.5^{0}C and 5% Carbon dioxide before being removed from culture simultaneously and fixed in 4% formaldehyde/PBS overnight at 4^{0}C prior to removal from the filter and dehydration in alcohol series and storage in 100% ethanol at -20^{0}C.

Explant pairs for the 'fix & culture' assay were treated as for -/+ pairs, with the exception that both halves of the corresponding pair were cultured in the presence of the same inhibitor but one half ('fix') was removed from culture after 3 hours for fixation, while the other half ('culture') was left in culture for an additional 45 minutes before fixation.

Samples for the protein stability assay to be analysed by western blotting were dissected as for ISH samples, with the exception that explants were cut to contain just one somite, one side of the PSM only (without any adjacent LPM), and half of the NT. Samples were pooled so that one half PSM explant from each of 9 embryos were cultured as a pool in the control medium and

the corresponding 9 half PSMs from the same 9 embryos were cultured as a pool in the presence of the inhibitor. The corresponding -/+ pools were cultured for 3 hours, followed by the simultaneous addition of 20µM Cycloheximide (Tocris Bioscience) to both pools and briefly mixing gently by slowly agitating the plate before further culture for an additional hour. For each stability assay a control set of 9 pooled explants cultured in 20µM Cycloheximide (+) or corresponding ethanol (-) control were cultured for 3 hours only to confirm the effect of Cycloheximide on protein synthesis.

At the end of culture, each pool of 9 explants was transferred to a 1.5ml eppendorf tube and medium aspirated. Each pool was then lysed in 90µl lysis buffer mixture consisting of protein lysis buffer: 50mM Tris Hydrochloride pH7.5, 150mM Sodium chloride (NaCl), 1mM ethylenediaminetetraacetic acid (EDTA), 1mM ethylene glycol tetraacetic acid (EGTA), 10mM Sodium pyrophosphate, 10mM Sodium glycerophosphate, 50mM Sodium fluoride, 1mM Sodium orthovanadate, 0.3% 3-[(3-cholamidopropyl) dimethylammonio]-1-propanesulfonate (CHAPS), 1mM Benzamidine, 0.1% β-mercaptoEtOH, 0.1mM phenylmethanesulfonylfluoride (PMSF), supplemented with 1x Sample Reducing Agent (Life Technologies) and 1x LDS Sample Buffer (Life Technologies). Even lysis was achieved by pipetting up and down until samples were no longer visible. Samples were then reduced at 95^0C for 5 minutes and allowed to cool briefly before freezing down in liquid nitrogen and storage at -80^0C.

Mouse explant culture conditions

Mouse explants were cultured as for chicken explant tissue, with the exception that -/+ and f/c explants to be analysed by ISH were each cultured in a ‘hanging drop’ of mouse media supplemented with control or drug on the underside of a plate lid (Potter and Morris, 1985). Plates were placed within a humid chamber and samples cultured in an incubator as for chicken samples, but for 4 hour periods instead of 3 hours where-ever stated for chicken previously to account for the longer oscillation period in the mouse embryo. Mouse explants were then fixed and processed for ISH or for generating protein lysates as for chicken samples.

NucView live cell apoptosis assay

+/- explant pairs were cultured for 2 hours (chicken) or 3 hours (mouse) as for culture prior to ISH analysis, before the addition of 5µM NucView 488 Caspase-3 Assay Kit for live cells (Biotium) and cultured for an additional 1 hour. Samples were then fixed for 1 hour at 4^0C in 4% formaldehyde/PBS. Samples were then washed into PBST and explant pairs were mounted on superfrost slides (VWR) in Prolong Gold antifade reagent (Molecular Probes) for imaging on a Zeiss 710 confocal microscope. Quantification of NucView cell staining was performed using Volocity v6.0.1 imaging software (Perkin Elmer) and statistical analyses done using either t-tests or Mann-Whitney tests with Sigmaplot v12.0 software.

Cloning of expression vectors & plasmids for antisense-RNA probe synthesis

Antisense Probe	Linearisation Enzyme	Linearisation Buffer & BSA (if required)	Working concentration in Hyb. Mix	*In Vitro* Transcription enzyme	Lab Source/ Reference
cAxin2	Not I	3 + BSA	10µl/ml	T3	K. Storey lab
mAxin2	Sal I	3 + BSA	20µl/ml	T7	B. Hermann lab
cDcaf13	Xho I	2 + BSA	20µl/ml	T7	Dale lab
cGli1	Hind III	2	10µl/ml	T3	K. Storey lab
cHairy2	Hind III	2	20µl/ml	T3	O. Pourquie lab
cLef1	BamH I	2 + BSA	10µl/ml	T7	Dale lab
cLfng	Cla I	4 + BSA	15µl/ml	T3	D. Ish-Horowitz lab
mLfng	Hind III	2	15µl/ml	T7	Morales et al, 2002
cMib1	Eae I	1	20µl/ml	T3	Dale lab
cMib2	Xho I	2 + BSA	20µl/ml	T7	Dale lab
cSprouty2	EcoR I	1	20µl/ml	T7	Minowada et al, 1999
cT	Xho I	2 + BSA	10µl/ml	T3	S. Mackem lab
cWnt3a	EcoR I	1	20µl/ml	T3	I. Mason lab

Table 2) Summary of Information and Conditions for synthesising antisense-RNA ISH probes.

Plasmids used were either received as kind gifts (see Table 2) or cloned by Elizabeth Farrell (Dundee Cell Products). All plasmid backbone sequences contained the Ampicillin resistance gene for selection.

Plasmids used for synthesising antisense ribonucleic acid (RNA) probes for ISH (Table 2) or for full length expression vectors were transformed into heat-shock inducible XL1 *Escherichia coli* bacteria (Life Technologies) and cultures allowed to grow in 1ml of LB broth for 30 minutes in a 37^0C shaker. The culture was then spread on a 10cm plate containing LB-agar with Ampicillin

(100µg/ml) and incubated overnight at 37^{0}C. A single colony was picked the following day and transferred to 5ml of LB broth with Ampicillin (100µg/ml) to be incubated in a 37^{0}C shaker for 9 hours. The 5ml culture was then added to a 1L conical flask containing 250ml of LB broth with Ampicillin (100µg/ml) and incubated overnight in a 37^{0}C shaker. The culture was then transferred to a Beckman tube and centrifuged at 6000xg for 15 minutes at 4^{0}C. The supernatant was discarded at this point and the remaining cell pellet used to purify the plasmid deoxyribonucleic acid (DNA) using a HiSpeed Plasmid Maxi Kit (Qiagen). Plasmids were each eluted in 1ml H_2O and DNA concentration quantified on a Nanodrop 1000 spectrophotometer (Thermo). The insert sequence was verified using the DNA sequencing facility at the University of Dundee.

The following plasmids detailed below were generated for this project by Elizabeth Farrell (Dundee Cell Products, Dundee UK). To generate plasmids for synthesising intronic antisense RNA probes, insert sequences for the following genes were each cloned into modified pBluescript II SK(-) plasmid:

Chicken Dcaf13 (*cDcaf13*)

tttttttatggttctaatatgaggaacagttacttgcctctcaaaaatctgtatcaatttcactcttcttttgcagtaatggtatcagagggta
ggtgttgaactactgatatcctacaccagtgatcaagctatctgcttctatgagaagggtcaagctccactgaaatacagagttagggca
gtaacatcagaccggtaataaacgattccagggccaattcttacaaccagccaatgcaggcaatgacttgacaaactggaacaagttt
atgcttgtaagaaaagcaacatctctggagcccatatacttgtct

Chicken Mindbomb1 (*cMib1*)

atgagcagctcgaggaacaaccgcgtgatggtggagggcgtcggggcccgcgtggtgcgcggccccgactggaagtggggaaagca
ggacggcggcgagggccacgtgggcaccgtgcgcagcttcgagagccccgaggaggtggtggtggtgtgggacaacggcaccgccgc
caactaccgctgctccggggcctacgacctccgcatcctggacagcgcgcccaccggtatcaagcatgatgggactatgtgtgacacat
gtcgacagcagccaatcattggcatccgatggaaatgt

Chicken Mindbomb2 (*cMib2*)

actccttcatggagggggccttggagatggacagcatcaacagcaacgcacccagcatcctctgctgcatttttagcacacctgacaga
gaggagagacagcaaaatccggagagcccttcagacagccgctgtcctcgatcgacggccgcgttcgtgtccctcccgcattcattctc
ggtgcagaagcctggacgctgacccgccccgccggcccccagggaagcggccgaagagccgtgccgaggcgggacggccccgcggg
tgctgcagcggaggctcccttcgaccccgctccccc

Full length expression vectors for the following genes were generated by cloning the insert sequence (in brackets after each gene) into the pCS2+ plasmid backbone:

cNICD

GGATCCATGGTGCTGGTGTCCCGCAAGCGGCGCAGGGAGCATGGCCAGCTCTGGTTCCCAGAGGGCTT
CAAAGTGACGGAGTCGAGCAAGAAGAAGCGCCGGGAACCACTTGGGGAAGATTCTGTTGGACTGAAA
CCCCTCAAAAATGCTTCTGACGGCACGCTGATGGACGACAACCAAAATGAGTGGGGTGACGAGGAGA
CCCTGGACACCAAGAAGTTCAGGTTCGAGGAGCAGGCGATGCTGCCCGACACGGATGACCAGACGGA
CCACAGGCAGTGGACTCAGCAGCACCTGGATGCTGCCGACCTCCGCATCTCCTCCATGGCCCCTACCCC
ACCACAGGGCGAGATCGATGCAGACTGCATGGATGTCAACGTACGAGGTCCAGACGGCTTCACGCCCC
TCATGATCGCCTCGTGCAGCGGAGGGGGGCTGGAGACTGGCAACAGCGAGGAGGAGGACGATGCCC
CTGCAGTCATCTCAGATTTCATCTACCAAGGCGCCAGTTTGCACAACCAGACTGACCGCACCGGCGAGA
CCGCGCTGCACCTGGCTGCCCGCTACTCGCGCTCCGACGCTGCCAAACGCCTGCTGGAAGCCAGTGCTG
ATGCGAACATTCAGGATAACATGGGCAGGACCCCTCTGCACGCCGCTGTCTCTGCTGATGCCCAAGGA
GTCTTCCAGATCCTGATAAGGAACAGGGCGACTGATCTCGATGCCCGAATGCACGATGGGACGACCCC
ACTGATCCTGGCTGCTCGCTTGGCTGTGGAGGGGATGCTGGAGGACCTCATCAACTGCCACGCAGACG
TCAACGCTGTGGATGATCTGGGCAAGTCAGCACTGCACTGGGCAGCTGCTGTGAACAATGTCGAAGCC
GCTGTCGTCCTCCTGAAGAACGGTGCCAATAAGGATATGCAGAACAATAAGGAGGAGACCCCGCTGTT
CCTCGCCGCCAGAGAAGGGAGCTACGAAACAGCCAAGGTTCTGCTGGACCACTTTGCGAACCGCGACA
TCACGGACCACATGGACCGGCTGCCGCGGGACATCGCGCAGGAGCGCATGCACCACGACATCGTGCG
GCTGCTGGATGAGTACAACCTGGTGCGGAGCCCTCCGCTGCACAGCGGCCCTCTCGGGGCCCCCACGC
TGTCCCCCCCGCTCTGCTCCCCCAGCAGTTACATCGGCAACCTGAAGCCGGCCGTGCAGGGCAAGAAG
GCCAGGAAGCCGAGCACCAAGGGCCTGAGCTGCAACGGCAAGGATTCCAAAGACCTGAAAGCCCGGA
GGAAAAAATCACAAGATGGAAAAGGCTGTCTGCTCGACAACTCCAGCGTGCTGTCCCCAGTGGACTCC
CTGGAGTCACCCCACGGGTACCTGTCCGACGTCGCCTCCCCTCCGCTGATGACTTCTCCGTTCCAGCAGT
CCCCTTCCATGCCTCTGAACCACCTGCCTGGCATGCCCGACGCCCACATGAGCATCAACCACCTCAACAT
GGCAGGGAAGCAGGAGATGGCCCTGGGCGGCTCTGGCAGGATGGCCTTCGAGGCGGTGCCGCCGCG
CCTCTCGCACCTCCCCGTCTCCAGCCCCAGCACGGCGATGAGCAACGCCCCGATGAATTTCTCCGTCGG
CGGAGCTGCCGGCCTGAGCGGGCAGTGCGACTGGCTGAGCCGGCTGCAGAGCGGCATGGTGCAGAA

CCAGTACGGCGCCATGCGGGGCGGCATGCAGCCGGGCACGCACCAGCAAGCACAGAACCTGCAGCAC
GGCATGATGAGCTCCCTGCACAACGGGCTGCCCAGCACCAGCCTGTCGCAGATGATGAGCTACCAGGC
CATGCCCAGCACCCGGCTGGCCTCCCAGCCCCACCTGCTGCAGAACCAGCAGATGCAGCAGATGCAGC
AGCCCGGAATGCAGCCGCAGCCCGGAATGCAGCCGCAGCCCGGCATGCAGCAGCCTCAACAGCAGCC
CCAGCAACAGCCCCAGCCGCAGCAGCACCACAACCCCGGCTCCAACGCCAGCGGCCACATGGGCCAAA
ATTTCCTCGGTACTGAGCTGAGCCAGCCCGACATGCAGCCGGTGAGCAGCAGCGCCATGGCGGTGCAC
ACCATCCTGCCCCAAGATTCGCAGCTGCTACCCACCTCTCTGCCGTCCTCCCTCGCGCAGCCCATGACCA
CCACGCAGTTCCTGACCCCCCCTTCCCAGCACAGCTATTCCTCCCCGTTGGACAACACCCCCAGCCACCA
GCTCCAGGTGCCCGACCACCCCTTCCTCACTCCCTCTCCGGAGTCTCCAGACCAGTGGTCGAGCTCCTCG
CCCCACTCCAACGTGTCCGACTGGTCCGAGGGCATCTCCAGCCCCCCCACCAGCATGCAGTCGCAGATG
GGACACATCCCCGAGGCCTTCAAGTGACTCGAG

mHES7

GGATCCATGGTCACCCGGGAGCGAGCTGAGAATAGGGACGGCCCCAAGATGCTGAAGCCGTTGGTGG
AGAAGCGGCGCCGGGACCGCATCAACCGCAGCCTAGAAGAGCTGAGGCTGCTGCTCCTGGAGAGGAC
CAGGGACCAGAACCTCCGGAACCCGAAGCTGGAGAAAGCGGAGATACTGGAGTTCGCCGTGGGCTAC
TTGAGGGAGCGAAGCCGGGTGGAGCCCCCGGGGGTTCCCCGGTCCCCAGGCCAGGACGCCGAGGCG
CTCGCCAGCTGCTACTTGTCCGGCTTCCGCGAGTGCCTGCTTCGCTTGGCGGCCTTTGCGCACGACGCC
AGCCCGGCCGCACGCTCCCAGCTTTTCTCCGCGCTGCACGGCTACCGGCGCCCCAAACCGCCCCGGCCC
GAGGCCGTAGATCCAGGGCTCCCAGCGCCGCGCCCACCGCTGGACCCCGCTTCACCAATCCTTGGCCCC
GCGCTGCACCAGCGCCCCCCAGTGCACCAGGGCCCTCCTAGTCCCCGCCTCGCTTGGTCCCCATCCCACT
GCTCCTCTCGCGCCGGGGATTCGGGCGCGCCGGCGCCCCTCACCGGACTGCTGCCGCCACCGCCACCG
CCTTACAGACAAGACGGGGCGCCCAAGGCCCCGTCACTCCCACCGCCCGCGTTTTGGAGACCTTGGCCC
TGACTCGAG

In Situ Hybridisation

DNA linearisation

10µg circular plasmid DNA for the given ISH gene probe was first linearised by incubation with the addition of 2µl the appropriate restriction endonuclease, with 4µl of the corresponding buffer (New England Biolabs), as well as 0.4µl Bovine Serum Albumin (BSA, New England Biolabs) if necessary. See Table 2 for details. The reaction was made up to a total volume of 40µl with MilliQ water and incubated at 37^0C (unless otherwise stated, Table 2) for 2 hours. The linearization reaction was then purified using the Qiaquick PCR Purification Kit (Qiagen)

and eluted in 50µl MilliQ water before putting the elutant over the column once more. Successful linearization was confirmed with gel electrophoresis by running the reaction next to the undigested sample on a 1% agarose gel containing 1x GelRed Nucleic Acid stain (Biotium) and visualisation under ultra violet light.

Synthesis of the DIG-labelled Antisense RNA probe

Synthesis of the antisense RNA probe was achieved by preparation of an *in vitro* transcription (IVT) reaction: 3µg linear DNA, 1x transcription buffer (Promega), 10mM DTT (Promega), 1x DIG RNA labelling mix (Roche), ~2U/µl RNA polymerase II (Promega, see Table 2 for details), (Roche). The 60µl reaction was incubated at 37^0C for 3 hours. 10% DNase I recombinant (Roche) and an additional 2U/µl Protector RNase Inhibitor were then added to the reaction before a further 2 hour incubation at 37^0C. The IVT reaction was purified using the Purelink RNA Mini Kit (Life Technologies) and eluted in 100µl RNase-free water from the kit before an additional 100µl RNase-free water added to the column for a further elution into the collection tube and this collective elution was made to 300µl final volume. As for the purified linearization reaction, each IVT was verified by agarose gel electrophoresis.

In situ Hybridisation Procedure

The protocol for ISH was adapted from Henrique et al (1995). Samples for ISH were brought to room temperature and rehydrated by washing for 5 minutes in 50% ethanol in PBS/0.1% Tween 20 (PBST) before two 5 minute washes in PBST. Samples were then incubated in 10µg/ml proteinase K (Roche)/PBST for a period of minutes equivalent to the HH stage number of the embryo from which the tissues were dissected (e.g. 10 minutes for HH10 embryo). Samples were then immediately washed into PBST briefly before fixation in 4% formaldehyde, 0.1% gluteraldehyde (Sigma), in PBST for 30 minutes at room temperature. Samples were then washed twice for 5 minutes in PBST before each being loaded into a medium-sized basket and placed into PBST inside a well of the 96-well sample tray for an Insitu Pro VS (Intavis) ISH robot.

Once fully loaded, the sample tray was screwed into position on a temperature-controlled block within the robot. Antisense RNA probes were loaded into a corresponding 96-well plate which was also placed into position within the robot. All other solutions were prepared prior to beginning the ISH run and placed within the robot. Separate programs were run for exonic and intronic ISH probes due to the lower abundance of intronic mRNA transcripts and greater difficulty to successfully hybridise antisense probes to them.

For the exonic ISH program, samples were heated to 65^0C before being washed for 45 minutes in 1:1 PBST/exonic hybridisation mixture: 50% (v/v) formamide (Acros Organics), 1.3x SSC pH5.0, 5mM EDTA pH8.0, 50µg/ml tRNA (Roche), 0.2% Tween 20 (VWR), 0.1% SDS (National Diagnostics), 100µg/ml Heparin sodium salt (Sigma). Samples were then washed for 30 minutes at 65^0C in exonic hybridisation mixture and then again in fresh hybridisation mixture for 2.5 hours at 65^0C. Samples were then incubated in exonic antisense mRNA probe/exonic hybridisation mixture (see Table 2 for probe concentrations) at 65^0C for 15 hours before 3 further 1 hour washes in exonic hybridisation mixture at 65^0C and then a 45 minute wash in 1:1 exonic hybridisation mixture/Tris-buffered saline, 0.1% Tween 20 (TBST). Samples were then cooled to room temperature and washed a further 3 times for 45 minutes in TBST. Samples were then cooled to 4^0C and washed for 2 hours in blocking buffer: TBST/ 2% Blocking (Roche)/ 20% decomplemented goat serum (Life Technologies). Following an 8 hour incubation at 4^0C in blocking buffer supplemented with 1:1000 anti-digoxigenin AP fab fragments (Roche), samples were brought to room temperature to be washed four times in TBST for 45 minutes and then twice for 45 minutes in 100mM NaCl, 100mM Tris HCl (pH 9.5), 50mM $MgCl_2$, 1% tween 20 (NTMT). At this point samples were removed from the ISH robot and placed into NTMT/ 337.5µg/ml NBT (Promega)/ 175µg/ml BCIP (Promega) colour revelation substrate mixture in darkness for a period ranging from 30 minutes to 4 days depending on the antisense RNA probe. Once staining was judged to have been completed, samples were washed twice in NTMT and then three times in PBST before fixation again in 4% formaldehyde/PBST overnight at 4^0C and washed twice in PBST and stored at 4^0C until imaging. All ISH samples were imaged

on a silicone-based plate in PBST on a Leica MZ16 microscope using Volocity v6.0.1 imaging software (Perkin Elmer).

Primary Antibody Synthesis

For synthesis of the anti-chicken NICD (cNICD) primary antibody, the peptide VLVSRKRRREHGC (corresponding to residues 1792-1803 of the chicken NOTCH1 protein, with the addition of a C-terminal cysteine residue for coupling) was coupled separately with Keyhole Limpet Hemocyanin (KLH) and bovine serum albumin (BSA) using m-maleimidobenzoyl-N-hydroxysuccinimide ester (MBS) and dialysed into PBS. The affinity purification of the cNICD antibody was achieved by putting the 3rd bleed serum from the rabbit which had been immunised with the peptide on an affinity column which had been previously prepared by coupling the cNICD peptide with vinylsulfone activated sepharose. The purified antibody was then dialysed into PBS and stored at -20^{0}C.

Synthesis of the anti-mouse GST-Hairy/enhancer of split (GST-HES7) antibody was achieved by expressing the GST-HES7 fusion protein in bacteria with the following amino acid sequence: MSPILGYWKIKGLVQPTRLLLEYLEEKYEEHLYERDEGDKWRNKKFELGLEFPNLPYYIDGDVKLTQSMAIIRY IADKHNMLGGCPKERAEISMLEGAVLDIRYGVSRIAYSKDFETLKVDFLSKLPEMLKMFEDRLCHKTYLNGD HVTHPDFMLYDALDVVLYMDPMCLDAFPKLVCFKKRIEAIPQIDKYLKSSKYIAWPLQGWQATFGGGDHP PKSDLEVLFQGPLGS-

MVTRERAENRDGPKMLKPLVEKRRRDRINRSLEELRLLLLERTRDQNLRNPKLEKAEILEFAVGYLRERSRVEP PGVPRSPGQDAEALASCYLSGFRECLLRLAAFAHDASPAARSQLFSALHGYRRPKPPRPEAVDPGLPAPRPP LDPASPILGPALHQRPPVHQGPPSPRLAWSPSHCSSRAGDSGAPAPLTGLLPPPPPPYRQDGAPKAPPLPPP AFWRPWP (dash indicates the end of the GST sequence and the start of HES7). This fusion protein was purified from bacteria and used to immunise rabbits. Serum collected from the 3rd

bleed of rabbits immunised with the GST-HES7 fusion protein was depleted against GST to remove any GST-specific antibodies before affinity purification of the GST-HES7 antibody from the serum on an affinity column which had been previously prepared by coupling the GST-HES7 peptide to CH-activated sepharose. The purified antibody was then dialysed into PBS and stored at -20^{0}C. The HES7 protein sequence used to synthesise the GST-HES7 antibody was taken from Y. Bessho (Bessho et al, 2003).

All of the peptide processing involving coupling and purification was performed by James Hastie and Fiona Brown in the Division of Signalling Transduction Therapy (DSTT) at the University of Dundee. The housing and the immunisation of the rabbits, as well as serum collection was performed at the Scottish Blood Transfusion Service (Penicuik, UK). Sera were then sent back to the DSTT for purification of the antibodies.

1^0 Antibody	Species derivation	$[1^0]$ for Western blot	$[2^0]$ for Western blot	TBST for western washes	$[1^0]$ for Immuno-histochemistry	$[2^0]$ for Immuno-histochemistry	1^0 Antibody Source/ Supplier
α-tubulin	Monoclonal	1:5,000	gαm HRP 1:40,000	0.25% TBST	N/A	N/A	Abcam
Total β-catenin	Rabbit polyclonal	1:5,000	gαr HRP 1:10,000	0.25% TBST	N/A	N/A	I. Nathke lab
Phospho S33, S37,T41 β-catenin	Rabbit polyclonal	1:1,000	gαr HRP 1:2,500	TBST	N/A	N/A	Cell Signalling Therapies
De-phospho β-catenin	Mouse monoclonal	1:500	gαm HRP 1:2,000	TBST	N/A	N/A	Millipore
mHES7	Rabbit polyclonal	1:1,000	gαr HRP 1:2,500	0.25% TBST	1:200	gαr HRP	University of Dundee
cNICD	Rabbit polyclonal	1:1,000	gαr HRP 1:2,500	0.25% TBST	1:1,000	gαr HRP 1:500	University of Dundee
mNICD	Rabbit polyclonal	1:500	gαr HRP 1:1,000	TBST	1:50	gαr HRP	Cell Signalling Therapies
Total RNA pol II	Rat Monoclonal	1:200	gαrat HRP 1:5,000	0.25% TBST	N/A	N/A	Chromotek
Phospho S2 RNA pol II	Rat Monoclonal	1:200	gαrat HRP 1:5,000	0.25% TBST	N/A	N/A	Chromotek
Phospho S5 RNA pol II	Rat Monoclonal	1:200	gαrat HRP 1:20,000	0.25% TBST	N/A	N/A	Chromotek

Table 3) Summary of Antibody Information and Conditions for Western Blotting and Immunohistochemistry.

Immunohistochemistry

cNICD Immunohistochemistry on Chicken cryosections

The caudal end containing a few of the most caudal somite pairs, the PSM and the tailbud were isolated from HH9-11 chicken embryos and fixed for 2 hours at 4^0C in 4% paraformaldehyde (PFA)/PBS. These tail tissues were then washed twice in PBS before washing overnight at 4^0C in 30% (w/v) sucrose/PBS. Samples were then embedded in 4.8% sucrose/PBS supplemented with 1.5% (w/v) LB agar and left to equilibrate overnight at 4^0C in 30% (w/v) sucrose/PBS before sucrose agar blocks were frozen down on dry ice and stored at -80^0C. 16µm sagittal cryosections were taken from these using a Leica CM 3050S Cryostat and placed onto Superfrost slides (VWR). Slides were left to dry at room temperature before being stored at -20^0C until used for immunohistochemistry.

Sections were allowed to warm up to room temperature before washing 3 times for 5 minutes in PBST and then 3 times 5 minutes in distilled water. Antigen retrieval was then performed on sections by boiling slides in 0.01M Citrate buffer, pH6.0 (Vector Laboratories) for 15 minutes in a microwave at a low power setting to avoid boiling over. Slides were then left in antigen retrieval buffer for 30 minutes to cool at room temperature before washing twice for 5 minutes in PBST, followed by a 10 minute wash in 3% hydrogen peroxide (Sigma)/methanol and a further 3 washes of 5 minutes each in PBST. Sections were then blocked in PBST supplemented with 10% (v/v) normal goat serum (NGS, Life Technologies) and 2% (w/v) BSA for 1 hour at room temperature before incubation in appropriate primary antibody diluted in the same blocking solution overnight at 4^0C (see table 3 for antibody concentrations). The cNICD antibody was previously ‘pre-blocked’ with chicken embryo tails to reduce non-specific binding.

Following primary antibody incubation, slides were washed 3 times for 5 minutes each in PBST at room temperature before incubation with the appropriate HRP-tagged secondary antibody

diluted in the same blocking solution as for primary antibody for 1 hour at room temperature (see table 3 for antibody concentrations, all secondary antibodies conjugated with HRP were sourced from Millipore). Slides were washed 3 times for 5 minutes each in PBS before incubation in 1:50 TSA Plus Cyanine3 in provided amplification buffer (PerkinElmer) for 10 minutes at room temperature and 3 further washes of 5 minutes each in PBST. Slides were then incubated with 1µg/ml 4',6-diamidino-2-phenylindole (DAPI)/PBS for 30 seconds and washed once more with PBST. Sections were then mounted with Prolong Gold antifade reagent and slides covered with a 24x60mm #1 cover slip (Menzel-Gläser) for imaging on a Leica DM5500 B compound microscope using Volocity v6.0.1 imaging software.

mHES7 & mNICD Immunohistochemistry on Mouse Paraffin sections

E10.5 mouse tails containing the most-caudal few somite pairs and the tail were dissected into cold autoclaved PBS and fixed for 2 hours at 4^0C in 4% PFA/PBS. Tails were then washed twice in PBS for 5 minutes each before dehydration in graded alcohol series and stored at -20^0C in 100% ethanol. Samples were transferred to glass bijous to be washed twice in xylene (VWR) for 1 hour each and then another 1 hour wash in liquid paraffin wax (VWR) at 60^0C. Samples were changed into fresh liquid paraffin wax and left overnight at 60^0C. Samples were then embedded in liquid paraffin wax at 60^0C and blocks then allowed to set on a cold plate at 4^0C. 7µm sagittal sections were taken from the paraffin-embedded mouse tails using a Reichert-Jung 2035 paraffin microtome. Sections were placed on the surface of a 50^0C waterbath and collected onto Superfrost slides before being allowed to dry onto the slides overnight in a 60^0C oven. Slides were stored at room temperature until used for immunohistochemistry.

Slides were washed twice for 5 minutes in Histoclear (VWR) before being rehydrated in graded alcohol series. Antigen retrieval was achieved by placing slides into 0.01M Citrate buffer (pH6.0) inside a 2100 Retriever pressure cooker (PickCell Laboratories) using a standard program at 121^0C. Slides were allowed to cool before washing them 4 times for 3 minutes in de-ionised water and for 3 minutes in PBS followed by a 40 minute wash in 1% hydrogen

peroxide/methanol, 3 washes of 5 minutes in PBS, and 2 washes of 10 minutes with 0.3% Triton X-100 in PBS (PBSX). Sections were then blocked in PBST supplemented with 10% normal goat serum and 2% BSA for 1 hour at room temperature before incubation in appropriate primary antibody diluted in the same blocking solution overnight at 4^0C (see table 3 for antibody concentrations).

The following day, slides were taken back to room temperature and washed twice for 5 minutes in PBS and twice for 5 minutes in PBSX before incubation with the appropriate HRP-tagged secondary antibody diluted in the same blocking solution as for primary antibody for 1 hour at room temperature (see table 3 for antibody concentrations). Slides were then washed as for after primary antibody incubation before incubation in 1:50 TSA Plus Cyanine3 in provided amplification buffer for 10 minutes at room temperature and a further 2 washes of 5 minutes in PBS. Slides were then DAPI stained, mounted and imaged as for cNICD and cLFNG immunohistochemistry.

Phospo-histone H3 whole-mount Immunohistochemistry

+/- explant pairs were cultured, fixed and dehydrated as for prior to ISH. Explants were then rehydrated into PBST before being incubated in proteinase K, washed in PBST, and then post-fixation as for samples being prepared for ISH. Samples were washed twice for 5 minutes in PBST before being blocked in 2% BSA/PBST for 2 hours at room temperature and incubated in 1:100 anti-phospho-Histone-H3 (ser10) primary antibody (Millipore) in blocking solution overnight at 4^0C. Explants were washed 3 times for 3 hours each in PBST before incubation with 1:1000 Alexa-fluor 488 conjugated goat-anti-rabbit secondary antibody (Life Technologies) in PBST overnight at 4^0C. Explants were then washed a further 3 times for 3 hours each in PBST before being mounted and imaged as for NucView stained explants. Images were quantified using Volocity v6.0.1 imaging software (Perkin Elmer) and either t-tests performed using SigmaPlot v12.0 software.

Western blotting

Sample pools for western blotting analysis were thawed out and reduced again by heating at 95^0C for 5 minutes before being allowed to cool. 20µl sample (equivalent to 2 half-PSMs) was loaded per lane on a 12-well NuPAGE Novex 4-12% Bis-Tris polyacrylamide gel (Life Technologies) in 1x MOPS running buffer (Formedium) inside an XCell Surelock tank (Life technologies). Samples were then run by SDS-polyacrylamide gel electrophoresis (SDS-PAGE) at 180V for approximately 1 hour and 15 minutes until the SeeBlue Plus2 pre-stained standard protein ladder (Life Technologies) was resolved fully. Samples were then transferred by placing the resolved PAGE gel onto a protran BA 85 nitrocellulose membrane (Whatman) inside a Mini Trans-blot Cell (Biorad) containing 1x NuPAGE transfer buffer (Life Technologies). An ice pack was inserted into the tank and more ice surrounding the tank to aid cooling while the transfer was run at 300mA for 1 hour at room temperature. The nitrocellulose membrane was then removed and stained with Ponceau S solution (Sigma) to confirm successful transfer of proteins onto the membrane. Membranes were then rinsed with MilliQ water to remove the stain before cutting into strips as necessary and blocked for 1 hour at room temperature in 5% (w/v) milk powder/TBST. At this point the membrane was incubated with the appropriate antibody dissolved in 5% milk/TBST overnight at 4^0C (see table 3 for specific conditions for each primary antibody).

The following day the membrane was washed 6 times for 10 minutes in either TBST, or TBS/ 0.25% tween 20 (0.25% TBST) before incubation in the appropriate HRP-tagged secondary antibody dissolved in 5% milk/TBST for 1 hour at room temperature (see table 3 for specific conditions for each primary antibody). Following a further 6 washes of 10 minutes each in the same TBST solution as prior to secondary antibody incubation, the membrane was incubated in Supersignal west pico chemiluminescent substrate (Thermo) 1:1 mixture for 1 minute. At this point the membrane was placed face-up into a sealed plastic wallet inside a dark room cassette that had been previously exposed to light. Western blots were then developed on X-

ray medical film (Konica Minolta) in a dark room. Changes in cNICD protein levels for different treatments were quantified by densitometry and normalised to α-tubulin loading control using ImageJ software and either one-sample t-tests or one-sample signed-rank tests were performed using SigmaPlot 12.0 statistical analysis software.

Immunoprecipitation

Sample lysates were prepared as for protein lysates for western blotting, with the exception that samples were lysed only in protein lysis buffer before centrifugation at 14,000rpm for 10 minutes at 4^0C and cleared lysate transferred to a fresh tube before freezing down in liquid nitrogen and storage at -80^0C. The full length expression vector for cNICD (insert sequence mentioned previously) was used to synthesise recombinant cNICD protein by adding 0.5µg plasmid DNA to 1x TnT SP6 Quick Coupled Transcription/Translation System Master Mix (Promega) in a final volume of 25µl and incubating at 30^0C for 90 minutes.

Throughout the IP procedure all reagents were kept at 4^0C. Protein A/G PLUS-agarose beads (Santa Cruz Biotechnology) were fully resuspended and 25µl were taken per immunoprecipitation (IP) reaction. Beads were washed in 1ml protein lysis buffer (recipe as for protein lysate preparation) by inversion several times and centrifugation at 4000rpm for 30 seconds at 4^0C before aspirating the supernatant and repeating once more. Beads were then resuspended in 100 µl protein lysis buffer per reaction and added to a 1.5ml eppendorf tube with the addition of the sample lysate (endogenous sample: x60 whole PSM tissues in 390µl protein lysis buffer alone; or recombinant cNICD protein: the entire 25 µl reaction), 1µg cNICD primary antibody, and reaction volume made up to 500µl with protein lysis buffer. This IP reaction was left to rotate overnight at 4^0C. The IP reaction was then centrifuged at 4000rpm for 30 seconds at 4^0C before recovering the first supernatant. The IP reaction was then washed in 1ml protein lysis buffer by inversion several times before centrifugation at 4000rpm for 30 seconds at 4^0C before aspirating the supernatant and repeating the process 4 more times. Following the final wash, the remaining beads with bound material were resuspended with

50µl sample buffer: 1x Sample Reducing Agent (Life Technologies) and 1x LDS Sample Buffer (Life Technologies) before reducing at 95^0C for 5 minutes and centrifugation at 14,000rpm for 2 minutes. The IP could then be analysed immediately by SDS-PAGE and western blotting with the cNICD primary antibody, or frozen down on liquid nitrogen and stored at -80^0C.

For cNICD IPs on endogenous chicken PSM lysates, a small portion of the first supernatant recovered after overnight incubation was kept to be analysed by SDS-PAGE and western blotting, while the remaining majority of the supernatant was used as the input for another round of cNICD IP. This process was repeated once more on the second IP supernatant to generate supernatants from 3 successive rounds of IPs altogether. These successive IPs could then be run in neighbouring lanes by SDS-PAGE and excised as a single gel slice for processing and in-gel digestion as a single pooled sample for mass spectrometry.

Mass Spectrometry

Sample immunoprecipitates for cNICD protein were run in duplicate for each treatment in neighbouring lanes on a 4-12% Bis/Tris gel by SDS-PAGE (run twice as IP volume limiting) just 2cm into the gel before staining the gel with Simplyblue safestain coomassie reagent (Thermo) for 1 hour and excising the entire duplicate samples as a single gel slice. The gel slice was processed by washing for 15 minutes while shaking in 1:1 MilliQ water: Acetonitrile, followed by 15 minutes washing with 100 mM Ammonium bicarbonate and then 15 minutes with 100 mM Ammonium bicarbonate in 1:1 MilliQ water: Acetonitrile. The gel slice was washed for 10 minutes in Acetonitrile before drying out using a speedvac.

The sample was reduced and alkylated by washing for 1 hour at 56^0C with 10mM DTT in 20mM Ammonium bicarbonate, before cooling to room temperature and incubating in 50 mM IAA solution for 30 minutes in darkness. The sample could then be incubated in consecutive 15 minute washes of 100 mM Ambic, followed by 100 mM Ambic/Acetonitrile, and then Acetonitrile before drying down the gel slice with a speedvac. The dried sample could then be

typically digested with 10 µl/ 0.125 µg Chymotrypsin proteolytic enzyme dissolved in Ammonium bicarbonate solution in a 30^0C shaker overnight. The sample was diluted in an equal volume of Acetonitrile and incubated in a shaker at room temperature for 15 minutes before transferring all liquid to a new tube and reducing the volume in a speedvac. An equal volume of 5% formic acid was added to the remaining dry sample and incubated in a shaker for another 15 minutes before addition of an equal volume of Acetonitrile and further washing for 45 minutes in a shaker. This solution mixture was then combined with the previously recovered solution in other tube, and 100% acetonitrile was added to the remaining sample before shaking for 10 minutes. The sample was finally dried down with a speedvac before reconstituting in 10 µl 5% formic acid, vortexing for 1 minute, and addition of 40 µl MilliQ water to make it in a final volume of 50 µl in 1% formic acid.

The amino acid sequences of cNICD and the intracellular domain of human Notch1 protein (May 2004 build) were aligned using the SIM alignment tool from the Expasy bioinformatics website (http://web.expasy.org/sim/) to reveal that phosphorylation sites in human NICD are mainly conserved within cNICD. The amino acid sequence for the intracellular domain of chicken Notch1 protein (NCBI Gene ID 395655, ENSGALT00000003754) was *in silico* digested with chymotrypsin using the MS-Digest software (http://prospector.ucsf.edu/prospector/cgi-bin/msform.cgi?form=msdigest) to generate an inclusion list of peptides within a suitable mass-range to search for. For endogenous samples analysed at the proteomics facility (University of Dundee), the 50 µl sample was transferred to High-performance liquid chromatography (HPLC) tubes before injecting 10 µl for liquid chromatography. Nano liquid chromatography (LC) was performed with an UltiMate 3000 RSLCnano system (Thermo): the injected sample was washed onto a C18 trap with 0.1% formic acid (‘Buffer A’). After a 3 minute wash at 5µl/minute, the sample was introduced onto the column and a gradient formed with ‘Buffer A’ and ‘Buffer B’ (80% acetonitrile in 0.08% formic acid).

Gradient:

Time (mins)	Flow (µl/min)	%B
0	0.3	2
0	0.3	2
4	0.3	2
128	0.3	40
130	0.3	98
150	0.3	98
151	0.3	2
180	0.3	2

Peptides were initially trapped on an Acclaim PepMap 100 (C18, 100 µM x 2cm) and then separated on an EasySpray PepMap RSLC C18 column (75 µM x 50cm) (Thermo). Each sample was transferred to the mass spectrometer via an Easy-Spray source with temperature set at 50C and a source voltage of 1.9 kV. The mass spectrometer used was an LTQ OrbiTrap Velos Pro (Thermo): Top 15 Method: FT-MS plus 15 IT-MS/MS (120 min acquisition) with Multi-Stage Activation (only required for Phosphorylation).

FTMS Full AGC Target: 1000000.00; Ion Trap MSn AGC Target: 5000.00; Fill Time FTMS (ms): 500; Fill Time ITMS (ms): 100; Lock Mass: 445.120024

FT-MS:

Resolution: 60,000; Mass Range (m/z): 335-1800; Scan Type: Full; Polarity: Positive; Data Type: Profile

IT-MS/MS:

Data Type: Centroid; Activation Type: CID; Min. Signal Required: 5000.0; Isolation Width: 2.00; Normalized Coll. Energy: 35.0; Default Charge State: 2; Activation Q: 0.250; Activation Time: 10.000

Orbitrap Velos Pro .raw data files were analysed using a standardized Proteome Discoverer (1.4.0.288) workflow (Thermo). The .raw data files were extracted to mgf (mascot generic file) format and used to search against the IPI-Chick database using the mascot search engine

(version 2.3.2, Matrix Science). The resultant data from the mascot search was parsed back to Proteome Discoverer for reporting in an Excel report. The search parameters used for the database searches with the mascot search engine were as follows:

Type of search: MS/MS Ion Search; Enzyme: Chymotrypsin; Fixed modifications: Carbamidomethyl (C); Variable modifications: Acetyl (N-term),Dioxidation (M),Gln->pyro-Glu (N-term Q), Oxidation (M), Phospho (ST), Phospho (Y); Mass values: Monoisotopic; Protein Mass: Unrestricted; Peptide Mass Tolerance: ± 10 ppm (# 13C = 2); Fragment Mass Tolerance: ± 0.6 Da; Max Missed Cleavages: 2; Instrument type: ESI-TRAP.

The recombinant cNICD protein sample was processed and run by Thermo (Hemel Hempsted) by re-dissolving in 20 µl of 0.1% formic acid before injecting 10 µl for Nano LC as for endogenous samples. Mass spectrometry was performed on an OT Fusion (Thermo): using data dependent TopS, 3s cycle [Full MS (OT) + HCD (IT or OT) with the inclusion list for cNICD protein. Peptide and protein identification was performed using Proteome Discoverer 1.4. Spectra were searched against the protein sequence for cNICD with the Sequest search engine.

Microarray

+/- explant pairs were dissected and cultured as for samples for ISH. The head end of each embryo from which +/- half-PSM pairs were dissected were kept and stored at -80^{0}C for genomic DNA (gDNA) extraction to determine the sex of the samples. +/- samples were removed from culture after 3 hours and transferred to an eppendorf tube each before aspirating excess media and storage at -80^{0}C until RNA extraction. Total RNA was extracted from the samples using the RNeasy Plus Micro Kit (Qiagen). The protocol was modified so that following sample lysis in RLT buffer, lysate was transferred onto a Qiashredder column (Qiagen) and centrifuged at 13,200rpm for 2 minutes. The flow-through was then transferred into a gDNA eliminator column and the standard protocol followed until elution of each

sample in 14µl RNase-free H_2O. RNA was quantified using 1µl of each sample elution on a Nanodrop spectrophotometer. The remainder of each sample elution was stored at -80^{0}C.

Microarray analyses were performed by Dr. David Chambers at King's College London University. Total RNA quality was checked using a 2100 BioAnalizer with an RNA 600 Nano kit (Agilent). The RNA integrity number (RIN) was analysed with 2100 Expert software (Agilent) for 'eukaryote total RNA Nano'. Once satisfactory quality was confirmed, 250 pg of each total RNA sample were labelled and prepared (Ovation Pico, Nugen Inc). Labelled RNA samples were hybridised to Affymetrix whole genome Chicken microarray GeneChips, built largely from the BBSRC chickEST database (http://www.chick.manchester.ac.uk) (method taken from Chambers and Lumsden, 2008). Each -/+ treatment pair was run in quadruplicate.

The microarray data analysis was performed by Pieta Schofield (University of Dundee) using the R-Bioconductor (v2.12) software packages 'Affy' (for processing affymetrix array data) and 'Limma' (Linear Models for Microarrays – differential expression analysis) (Gautier et al, 2004; Gentleman et al, 2004; Smyth, 2005). The suitability of the data sets for further analysis and the relationship between and within the biological replicates was determined using principle components analysis (PCA) and hierarchical clustering. The RMA normalisation method was performed as a standard approach for Affymetrix microarray datasets. The list of significant Gene Ontology (GO) terms was obtained using the 'topGO' and 'chicken' packages also on R-Bioconductor.

RNA Sequencing

RNA from the same samples used for microarray analyses was used as the template for RNA Sequencing (RNA-seq) to be run by Melanie Febrer at the Genomic Sequencing Unit (GSU, University of Dundee). Total RNA samples were checked for quality using the Agilent TapeStation RNA R6K kit and for quantity using the Invitrogen Qubit fluorometer RNA kit.

For library preparation, total RNA samples were diluted to 1-10ng and cDNA synthesis was performed using the SMARTer Ultra Low RNA Kit (Clontech). This kit is designed to produce high quality cDNA synthesis from very small amounts of total RNA. A modified oligo(dT) primer primes the first strand synthesis reaction, When SMARTScribe Reverse Transcriptase reached the 5'end of the mRNA, the enzyme's terminal transferee activity adds a few additional nucleotides to the 3' end of the cDNA. The carefully designed SMARTer oligonucleotide base-pairs with the non-template nucleotide stretch, creating an extended template to enable the SMARTScribe Reverse Transcriptase to continue replicating to the end of the oligonucleotide. The resulting full length, single stranded cDNA contains the complete 5' end of the mRNA as well as sequences that are complementary to the SMARTer oligonucleotide. The SMARTer anchor sequence and the poly A sequence serve as universal priming sites for end-to-end cDNA amplification. 'Illumina ready' libraries were then constructed from the cDNA samples using the NEBNext Ultra DNA Library Prep kit as per manufacturer's instructions. Libraries were checked for quality using the Agilent TapeStation DNA D1K kit and for quantity using the Qubit fluorometer DNA Broad range kit. Libraries were normalised to 10nM and pooled in 3 sets of 8.

Sequencing of each pool of 8 samples was done on an Illumina HiSeq2000 as paired end 100bp reads as per manufacturer's protocol. Each DNA pool sample was diluted to 2nM and then was denatured with 0.1N NaOH to a DNA concentration of 20pM. The denatured molecules were further diluted to 10pM and mixed with 1% PhiX library, which is used as internal control for sequencing. Each template was loaded on the Illumina cBOT and the flow cell was clustered using the Illumina TruSeq PE cluster kit v3. The 3 pools were sequenced for 10 days using the Illumina TruSeq SBS kit v3.

The data analysis was performed by Pieta Schofield at the University of Dundee. The fastq read files were aligned to the Ensembl 75 release of the Galgal4 tanscriptome (http://www.ensembl.org/Gallus_gallus/Info/Index). This release has over 15000 contigs, which were first filtered against the annotation file for the Galgal4 release and the reads were

only aligned against contigs with annotation on them. This reduced the number of contigs to the order of 900. The alignment was performed with Subread software (Liao, Smyth et al. 2013) and the mapping of reads to annotated features was performed with 'featureCounts' in the Subread package. Differential expression analysis was performed in R-bioconductor using the DESeq2 package, which calculated the log2 fold-changes (Anders and Huber 2010, Anders, McCarthy et al. 2013). Gene Ontology analysis was performed using the DAVID Functional Annotation Tool (http://david.abcc.ncifcrf.gov/home.jsp).

Quantitative PCR

Sex Determination qPCR

The W-repeat (sex-linked) and the 18S (housekeeping) primers, as well as the method are adapted from Clinton *et al.,* (2001). The remaining anterior ends of the embryos used for the microarray and RNA-seq analyses were used to extract gDNA for quantitative polymerase chain reaction (qPCR) analysis to determine the sex of the embryos. Each anterior embryo piece was lysed in 200µl 10mM Tris (pH 8.0), 1mM EDTA, 1% SDS, 10µg/ml proteinase K overnight at 45^0C. Samples were then cooled to 4^0C and each mixed with 800µl MilliQ H_2O before being centrifuged at 10,000 x G for 5 minutes. Samples were diluted 100-fold in MilliQ H_2O and 8µl of this sample dilution was used per qPCR reaction to be mixed with 12µl of base mixture consisting of: 1x Precision qPCR Master Mix with SYBR Green (Primer Design), 0.5µM forward primer, 0.5µM reverse primer, diluted in MilliQ H_2O. Each 20µl final sample/primer pair combination was loaded in duplicate into a Thermo-Fast 96, semi-skirted well plate (Thermo) with a Microseal B adhesive sealer (Bio-Rad). Samples were run on a Realplex^2 Mastercycler (Eppendorf) with the following program: 50^0C for 2 minutes, 95^0C for 2 minutes, then 40 cycles of: 95^0C for 15 seconds followed by 60^0C for 30 seconds. Samples were then heated at 95^0C for 1 minute, 60^0C for 30 seconds and 95^0C again for 15 seconds before cooling to 25^0C for 30 seconds. Strong signal for the W-repeat primers indicates that the sample is from a female embryo and a no signal indicates a male sample.

Results

Chapter 1: Inhibition of canonical Wnt signalling or Cdks delays oscillating clock gene transcription in the chicken PSM

The chicken embryo has been and continues to be extensively used as a robust model species for studying the process of somitogenesis and the segmentation clock and moreover this molecular oscillator was first described in chick in the seminal paper by Palmeirim et al., (1997). At early somite stages in particular the chicken embryo has a relatively long PSM tissue along the AP axis compared to other model species, as well as a flat body axis. These factors make the chicken embryo an ideal model system for studying somitogenesis.

1.1) Cycling transcription of *cLfng* in the chicken PSM is dependent on Notch signalling

Cyclical oscillation of Notch target gene transcription across the presomitic mesoderm (PSM) has been found to be a conserved feature of the vertebrate segmentation clock in all model systems studied to date and therefore provides a good identifier of the pace of the segmentation clock within the PSM (Gibb et al, 2010). Chicken *Lunatic fringe* (*cLfng*) mRNA expression was used in this study as a cycling Notch target due to its robust signal and ease of identifying oscillation phase within the chicken PSM following ISH (Fig. 1.1A-C, F). In order to get a better understanding of how the segmentation clock is regulated, the oscillation phase of *cLfng* transcription was viewed in the chicken PSM following treatment with small molecule inhibitors of potential regulatory pathways of the segmentation clock pacemaker. A delay in the oscillation phase of *cLfng* when treated with an inhibitor compared to a control treatment would provide good evidence for a role of the affected signalling pathway in controlling the pace of the segmentation clock. The caudal end of the chicken embryo was isolated to contain just a few of the most caudal somite pairs and the tail tissues (Fig. Q, see methods). The isolated tail could then be bisected down the midline along the neural tube to produce two identical left and right half-PSM explants from the same embryo. This assay allows an internal

control from the same embryo with which to compare the oscillation phase of *cLfng* expression by ISH following culturing of the two halves in various culture conditions or for various time periods (Gibb et al, 2009).

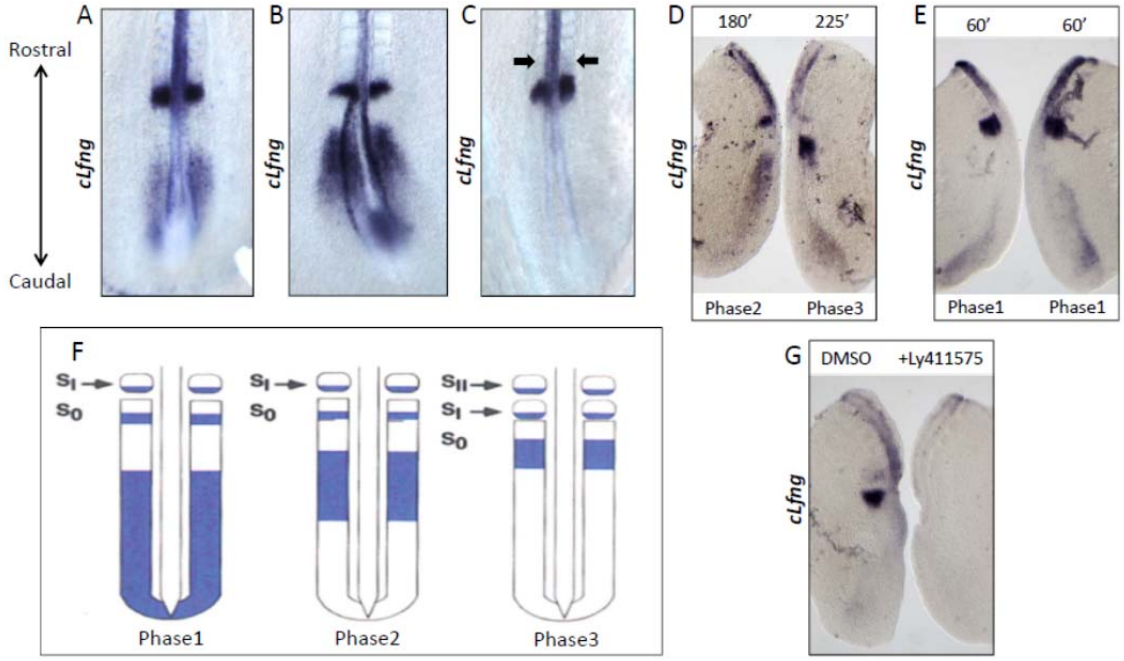

Figure 1.1) *cLfng* mRNA expression is dynamic and cyclical across the chicken PSM. Dorsal view of bisected caudal half explants or caudal region of HH 12-15 chick embryos after in situ hybridisation using the *cLfng* probe. Dynamic *cLfng* can be categorised into 3 phases of expression (summarised in **F**, adapted from Palmeirim et al., 1997): in phase 1 (**A**) *cLfng* is present in a broad domain of the caudal PSM, with a sharp rostral stripe also present at the site of the presumptive next somite boundary (S-1); in phase 2 (**B**) *cLfng* expression is activated more rostrally in the PSM and now absent in the very caudal PSM; in phase 3 (**C**) the caudal domain of *cLfng* expression moves more rostrally still in the PSM and narrows as the new somite pair segment (arrows) at the level of the previous rostral band present in phases 1 and 2. Fix and culture assay shows that the expression phase of *cLfng* advances in the PSM side cultured for longer (**D**, n=5/5), but is unchanged when both sides are cultured for 1 hour (**E**, n=4/4). *cLfng* transcription is abolished in the chicken PSM when treated with the Notch inhibitor Ly411575 (**G**, n=5/6).

To reveal that the half-PSM assay is a valid method of recapitulating active oscillations of Notch transcription in the PSM, the 'fix and culture' assay was performed whereby one half of the pair was cultured for 3 hours in standard chick media before fixation. The corresponding half was cultured for an additional 45 minutes (corresponding to half of an oscillation cycle) before also being fixed. ISH for *cLfng* expression revealed that the oscillation phase advanced in the side cultured for longer as expected (Fig. 1.1D, n=5/5). Conversely, when both halves of the pair were removed from culture at the same time the oscillation phase for *cLfng* was identical (Fig. 1.1E, n=4/4). To show that *cLfng* expression is dependent on Notch signalling, the γ-secretase inhibitor Ly411575 was used in a '-/+' drug assay (Lanz et al, 2004). One half PSM explant was cultured in the presence of the small molecule inhibitor Ly411575 (+) and the corresponding half cultured in the DMSO vehicle control medium (-). The -/+ pair was cultured for 3 hours before simultaneous fixation. *cLfng* expression was abolished in the PSM treated with Ly411575 but unaffected in the PSM of the DMSO control half (Fig. 1.1G, n=5/6).

1.2) XAV939 inhibits β-catenin dependent Wnt signalling

It has previously been shown that the small molecule inhibitor CKI7 can inhibit Wnt signalling and delay transcriptional oscillations of the Notch target gene *Lfng* in both the chicken and mouse embryo PSM (Gibb et al., 2009). However, the exact relevance of Wnt signalling in regulating the pace of the molecular oscillator remains unclear given that the transcripts of targets from several other signalling pathways were also found to be downregulated by CKI7 at the same concentration (Gibb et al., unpublished data). Given that CKI7 targets CK1 which is involved in the regulation of multiple signalling processes including Wnt and the circadian clock (Harms et al, 2003), it is clear that a more specific inhibitor of canonical Wnt signalling is required to address the importance of Wnt signalling in regulating the pace of the molecular oscillator of the segmentation clock.

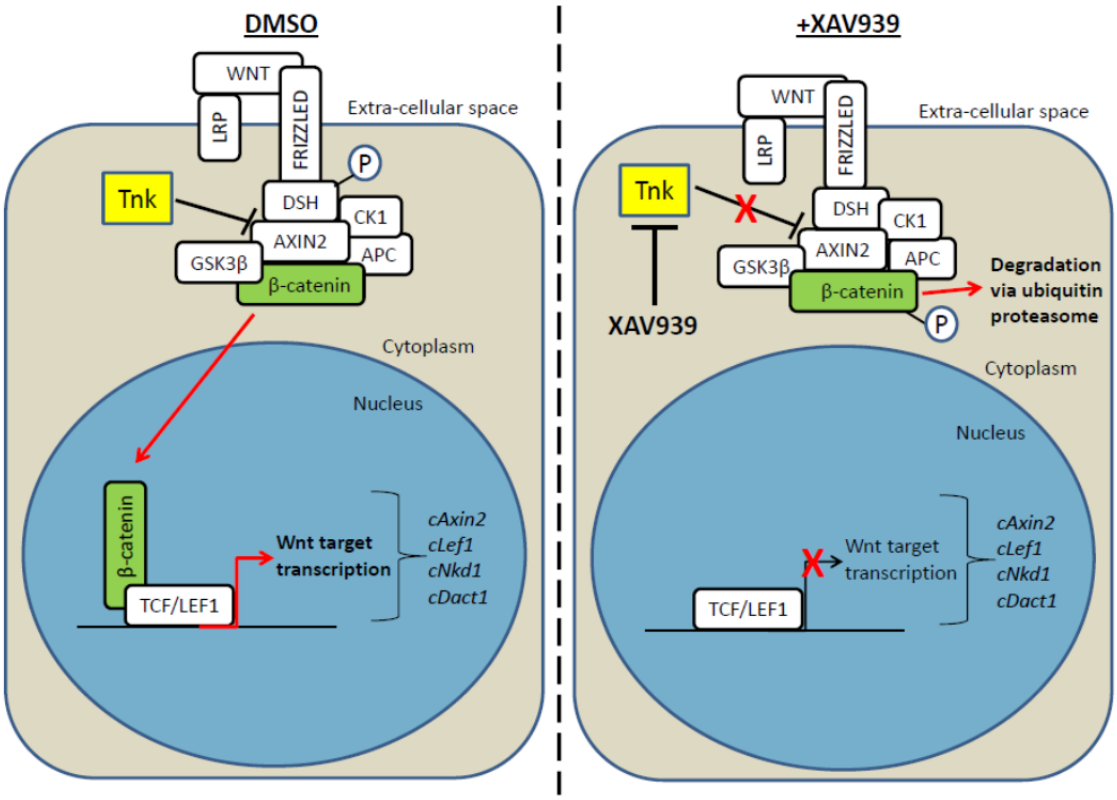

Figure 1.2) Schematic showing the mode of XAV939 inhibition on canonical Wnt signalling. **Left panel**: DMSO has no effect on Wnt signalling, as receptor/ligand binding still promotes β-catenin dependent transcription of Wnt targets. **Right panel**: XAV939 promotes stabilisation of Axin2 protein by inhibiting Tankyrase (Tnk) enzymes which degrade Axin proteins, so that even in the presence of Wnt activation of the Frizzled/LPR receptors, β-catenin is sequestered in the cytoplasm by the intact destruction complex and is targeted for phosphorylation and subsequent degradation. As a result, Wnt target transcription is repressed in the nucleus. Figure adapted from Gibb et al., (2010).

The small molecule inhibitor XAV939 was developed more recently as a specific inhibitor of canonical Wnt signalling (Huang et al, 2009). XAV939 acts by inhibiting Tankyrase1 (TNK1) and TNK2 enzymes which degrade Axin2. As a result, in the presence of XAV939, AXIN2 protein is stabilised even in the presence of receptor-ligand binding and this maintains β-catenin protein in the destruction complex, thereby blocking β-catenin from entering the nucleus to activate downstream Wnt target gene transcription. Instead, XAV939 promotes phosphorylation of β-catenin by CK1 and GSK3β (Huang et al, 2009), leading to its ubiquitination and proteasomal degradation (summarised in Fig. 1.2). It has been previously suggested that treatment of the mouse PSM with XAV939 does not affect oscillations of *Hes7* (Gonzalez et al, 2013). However the concentrations used in this study were low and the outcomes regarding the role of Wnt in the pace regulation of cycling clock gene expression were conflicting from the same report (Gonzalez et al, 2013), meaning that further clarification as to the potential role of Wnt signalling in this process is required.

1.3) Titration of XAV939 treatment in the chicken PSM

Initially I performed a titration assay with XAV939 to determine the optimal concentration for down regulation of Wnt target gene expression in chick explant culture. The Wnt target *cLef1*(i) was viewed by ISH following -/+ treatment with different concentrations of XAV939 dissolved in chick media. *cLef1*(i) exhibits a sharp rostral stripe, with a broader and weaker domain across the chicken PSM which is not dynamic (Fig. 1.3A, Gibb et al, 2009). At 50µM *cLef1*(i) only showed down regulation in the caudal PSM of some explants when compared to normal expression in their corresponding DMSO control halves (Fig. 1.3B, n=2/4). However more consistent down regulation of *cLef1*(i) was seen at 100µM (Fig. 1.3C, n=2/2) and 500 µM (Fig. 1.3D, n=3/3) XAV939 treatment.

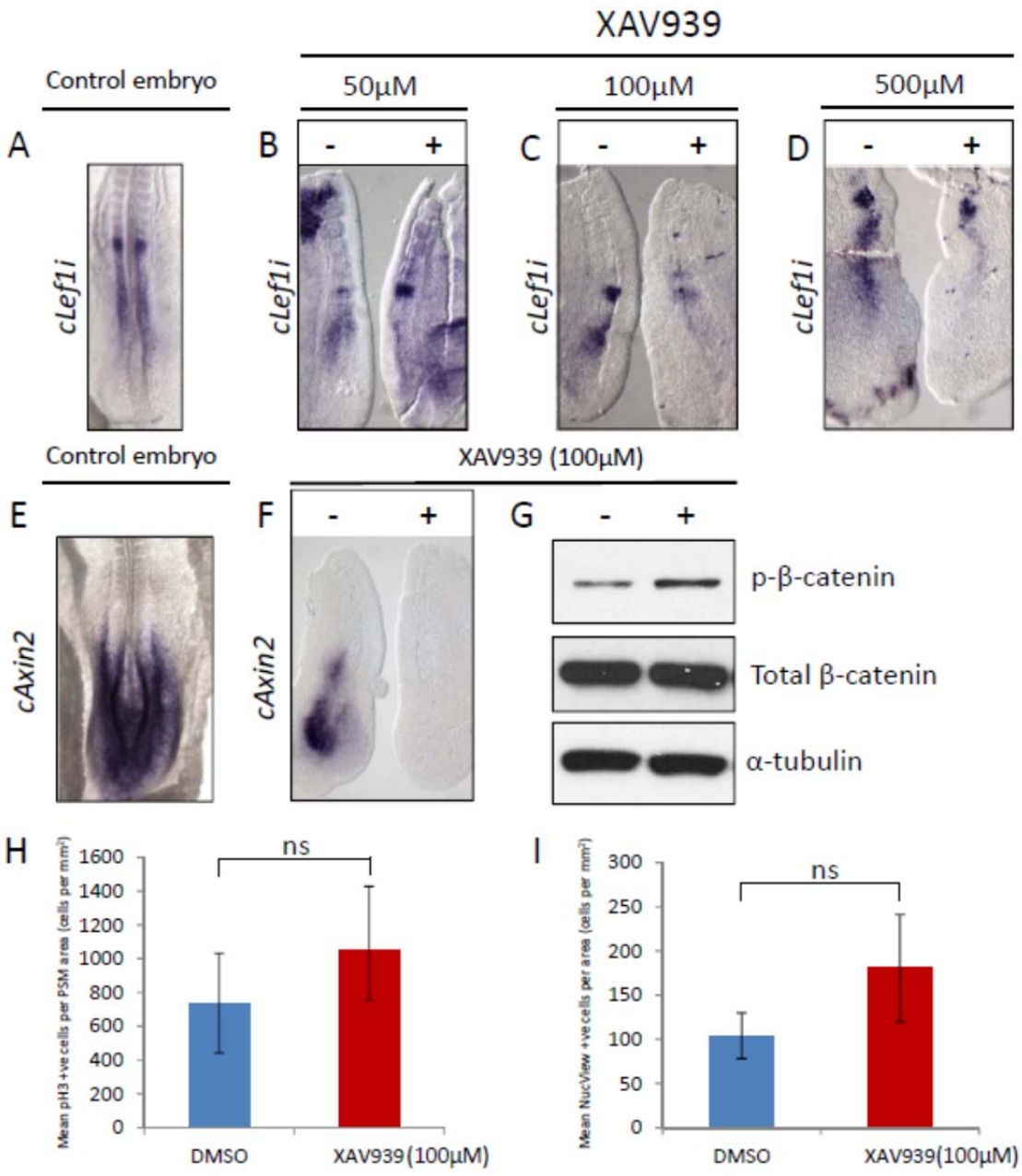

Figure 1.3) XAV939 optimisation titration assay. Dorsal view of bisected caudal half explants after in situ hybridisation using different probes. The Wnt inhibitor XAV939 was titrated for -/+ assays in the chicken PSM. The Wnt target mRNA *cLef1*(i) which normally exhibits a non-oscillatory sharp rostral stripe and broader caudal domain of expression in the chicken PSM (**A**) was not obviously affected by XAV939 at 50µM (**B**,), but appeared visibly downregulated particularly in the caudal PSM when treated with 100 µM (**C**) and 500 µM (**D**) XAV939 compared to the DMSO control side. *cAxin2* expression exhibits a non-dynamic caudal-rostral gradient in the chicken PSM (**E**). -/+ assays show that 100 µM XAV939 downregulates *cAxin2*

(**F**), as well as increasing phosphorylation of β-catenin at S33, S37, T41 (**G,** mean fold-change=2.856, p=0.016). 100 μM XAV939 treatment has no significant effect on either the number of pH3 positive cells (**H,** n=4, p=0.236) or NucView positive cells (**I,** n=4, p=0.292) in the chicken PSM relative to the corresponding DMSO control half-PSM explant.

Following the titration assay, XAV939 was used at 100μM to assess the effects on Wnt signalling using other expression markers as this was the lowest concentration which consistently downregulated transcription of Wnt targets while not having adverse effects on either proliferation nor on apoptosis in the chicken PSM. The Wnt target gene mRNA for *cAxin2* which normally exhibits a non-oscillatory high-low gradient of expression in the tail end of the chicken embryo (Fig. 1.3E; Gibb et al, 2009) was robustly downregulated when treated with 100μM XAV939 compared to the corresponding DMSO control side (Fig. 1.3F, n=59/66). In the absence of receptor-ligand binding or inhibition of canonical Wnt signalling, β-catenin protein is targeted for phosphorylation and subsequent degradation (Clevers, 2006; Huang et al, 2009). As expected, phosphorylation of β-catenin by GSK3β was significantly increased following treatment with XAV939 (Fig. 1.3G, n=8/10, mean fold-change=2.856, p=0.016). These results confirmed that Wnt signalling was inhibited in the caudal chicken embryo by 100μM XAV939 treatment.

To assess whether these effects could be due to changes in cell proliferation within the PSM, +/-XAV939 explant pairs were analysed by immunohistochemistry for the proliferation marker phospho-histone H3 (pH3), which is a marker of G2-M transition during the cell cycle (Hendzel et al, 1997). The number of pH3 cells per PSM area was not significantly different with XAV939 treatment when compared to the corresponding DMSO control (Fig. 1.3H, n=4, p=0.236). Apoptosis was also quantified for +/-XAV939 explant pairs using NucView staining during culture. Nucview stains for Caspase 3 activity as a marker of apoptosis in live cells (Cen et al, 2008). The number of NucView positive cells in the PSM was not significantly different with

XAV939 treatment when compared to the corresponding DMSO control (Fig. 1.3I, n=4, p=0.292).

1.4) XAV939 delays *cLfng* oscillations and inhibits Wnt signalling in the chicken PSM

Having confirmed that XAV939 could efficiently inhibit Wnt signalling at 100µM and above, this inhibitor was used to assess the effects on the segmentation clock. -/+ assays revealed that the oscillation phase of *cLfng* was delayed by XAV939 at both 100 µM (Fig. 1.4A, n=57/64 and 500 µM (Fig. 1.4B, n=7/7). For example, in Figure 1.4A it is clear that *cLfng* exhibits a phase 3 expression profile in the PSM of the DMSO (-) control half and two new somites have formed during culture, whereas in the +XAV939 side PSM *cLfng* still exhibits a more caudal phase 2 profile of expression and the second new somite boundary has yet to form (see Fig 1.1F). *cLfng* oscillation in the +XAV939 PSM is therefore delayed as it is lagging behind relative to the control and has yet to be de-activated in more caudal cells in the PSM that already no longer express *cLfng* in the control PSM.

The -/+ assay gave a good indication that XAV939 affects the oscillation phase of *cLfng* expression in the PSM, however it did not reveal whether oscillations are slowed or simply arrested altogether. To clarify this, the fix and culture assay was performed whereby both half-PSM explants were treated with XAV939, but while one was removed from culture after 3 hours ('fix'), the other side was cultured for an additional 45 minutes ('culture') which corresponds to half of the usual 90 minute cycle for a complete oscillation of *cLfng* in the chicken PSM. Fix and culture assays revealed that *cLfng* expression was still dynamic in the presence of 100µM XAV939 (Fig. 1.4C, n=8/9 dynamic). For example, in Figure 1.4C the side cultured for 3 hours is in a phase 2 of *cLfng* expression, while the side cultured for an additional 45 minutes has advanced to phase 1 of expression of the next oscillation cycle in the PSM and has also formed one more new somite during culture. Conversely, at 500µM XAV939 there was no obvious difference in the expression phase of *cLfng* between the fix and culture sides suggesting that oscillations had halted with 500µM XAV939 (Fig. 1.4D, n=2/3 halted).

These results show that 100 µM XAV939 was the optimal concentration to slow oscillations of *cLfng* in the chicken PSM, suggesting that a reduction in Wnt activity may cause slower clock gene oscillations, while higher concentrations such as 500 µM XAV939 may reduce Wnt activity so much that oscillations of *cLfng* transcription stop altogether.

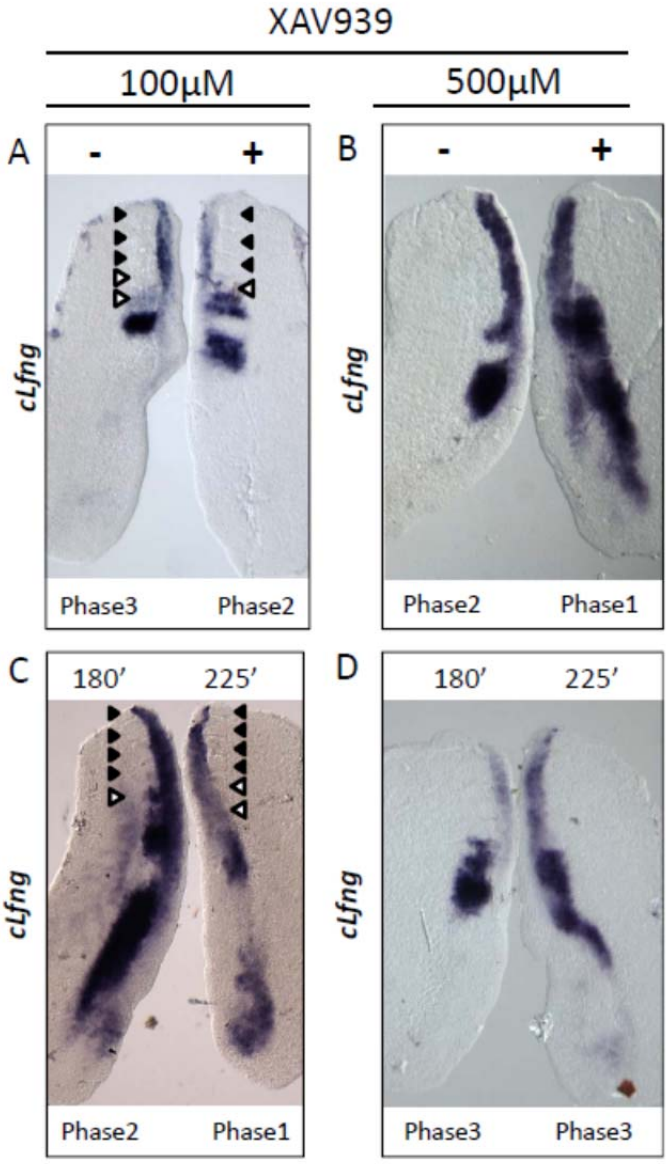

Figure 1.4) XAV939 delays oscillations of *cLfng* expression in the chicken PSM. Dorsal view of bisected caudal half explants after in situ hybridisation using different probes. *cLfng* oscillation phase appears delayed in the PSM by XAV939 at both 100 µM (**A**) and 500µM (**B**). Fix and culture assays for XAV939 reveal that *cLfng* expression is still dynamic at 100 µM (**C**) but no

longer dynamic at 500 µM (**D**). Black arrows indicate somites present at the start of culture and white arrows mark somites formed during culture.

1.5) DRB and Roscovitine: two small molecule Cyclin dependent kinase inhibitors

Cdks and their Cyclin partners are key regulators in fundamental cellular processes including the cell cycle progression and RNA pol II–dependent transcription (Malumbres and Barbacid, 2009). Previous evidence that small molecular inhibitors of cdk activity can slow the segmentation clock and delay somite boundary formation suggests that further investigation into the potential roles of cdks in the molecular oscillator of the segmentation clock is warranted (Gibb et al, 2009; Gibb, unpublished communication; Gonzalez et al, 2013; Stern, 1988). In order to assess the importance of the cell cycle and/or transcriptional regulation in the vertebrate segmentation clock, cdk inhibitors were used in the same assays as described above for XAV939.

Roscovitine (also known as Seliciclib or CYC202) is a 2,6,9-subsituted purine analogue which competes with ATP for the active binding site on CDKs (MacCallum et al., 2005). Roscovitine has highest efficacy against CDK2/CyclinE, CDK7/CyclinH, CDK9/CyclinT (McClue et al., 2002). CDK2/CyclinE functions mainly in the progression of G1-S phases of the cell cycle. CDK7/CyclinH and CDK9/CyclinT phosphorylate the CTD of RNA pol II and therefore promote transcriptional initiation and elongation (Malumbres and Barbacid, 2009). CDK7 is also reported to have roles as an activator of other CDKs involved in the cell cycle (Fisher, 2005). Roscovitine therefore has been used as a general cdk inhibitor to repress both cell cycle progression and RNA pol ii-dependent gene transcription (Fig. 1.5A). 5,6-Dichloro-1-beta-D-ribofuranosylbenzimidazole (DRB) is a nucleoside analogue that inhibits transcription by reducing the kinase activities of CDK7/CyclinH and CDK9/CyclinT towards the C-terminal domain (CTD) of RNA pol II (Fig. 1.5B) (Wada et al, 1998). By using both these inhibitors we aimed to tease out whether inhibiting either class of CDK specifically affected the pace of the segmentation clock in the chick PSM. To that end we titrated the reagents in the +/- chick PSM

culture assay and assayed the effect upon cell proliferation (regulated predominantly by CDKs 1-4, and 6 involved in cell cycle), RNA pol II phosphorylation (regulated by CDKs 7 and 9 involved in transcription predominantly), and the pace of cyclic *Lfng* expression.

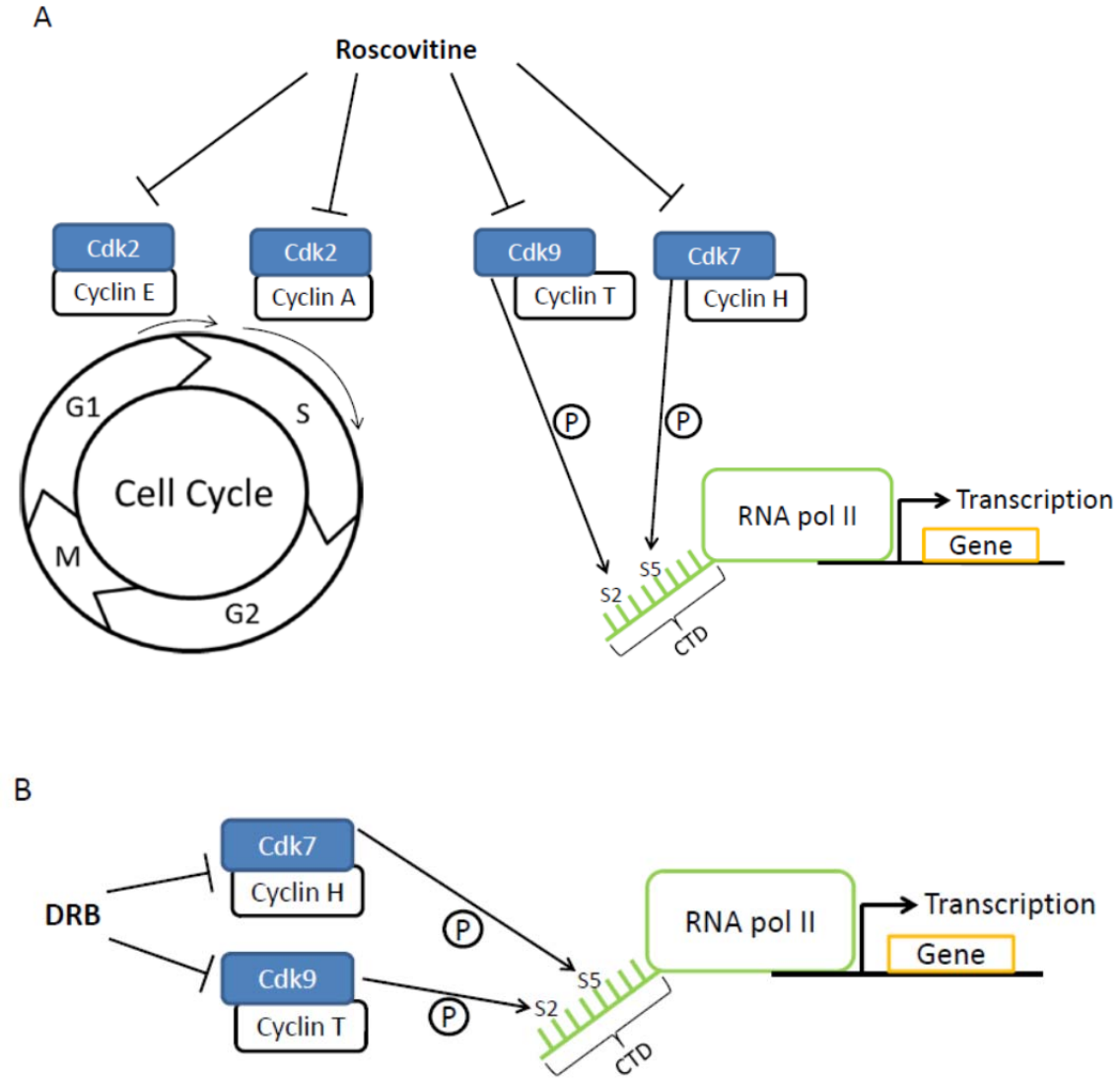

Figure 1.5) Schematic showing the mode of Roscovitine and DRB inhibition on transcription and the cell cycle. **A)** Roscovitine inhibits Cdk2/CyclinE during G1-S transition and Cdk2/CyclinA during S phase of the cell cycle. Roscovitine also inhibits Cdk7- and Cdk9- mediated phosphorylation on the C-terminal domain (CTD) of RNA polymerase protein, therefore blocking transcription elongation. **B**) DRB inhibits transcription elongation in the same manner as Roscovitine.

1.6) Titration of DRB treatment in the chicken PSM

Before Roscovitine and DRB could be used to assess the effects of CDK inhibition on the segmentation clock, the drugs needed to be titrated to find the optimal concentration for use in -/+ assays on chicken PSM tissue. The inhibitor DRB was used to target cdk7 and cdk9 in the chicken PSM, which are more specifically involved in the regulation of transcription (MacCallum et al, 2005; Wada et al, 1998). The expression of *cLfng* was viewed following -/+ treatment with DRB at varying concentrations dissolved in chick culture medium. At 10 µM, DRB delayed *cLfng* oscillation phase compared to the control half-PSM (Fig. 1.6A, 7A n=67/73), but did not have an obvious effect on the number of apoptosing cells in the PSM (Fig. 1.6E). DRB also appeared to delay *cLfng* oscillations at concentrations from 20 µM-100 µM (Figs. 1.6B-D), but apoptosis also appeared noticeably increased compared to respective controls in +DRB explants at these concentrations suggesting that higher concentration of DRB treatment cause significant cell death within the chicken PSM (Figs. 1.6F-H). For these reasons, DRB was used at a concentration of 10 µM in chick culture medium for the rest of the study.

As for XAV939 treatment, quantification confirmed that neither proliferation (Fig. 1.6I, n=5, p=0.884), nor apoptosis (Fig 1.6J, n=3, p=0.844) were significantly affected in the PSM by 10 µM DRB treatment relative to the DMSO control PSM tissue, suggesting that these processes are not important factors in the regulation of the segmentation clock. Western blotting analysis confirmed that phosphorylation of Serine 5 on the CTD of RNA pol II was reduced by 10 µM DRB treatment (n=3/3, mean fold-change=0.789), however Serine 2 phosphorylation appeared unaffected (n=3/3, mean fold-change=0.994) (Fig. 1.6K). These findings reveal that the oscillations of *cLfng* expression in the chicken PSM are slowed by DRB treatment at a concentration that does not affect cell proliferation, but instead suggests that cdks involved in the regulation of RNA pol II – dependent transcription are important in regulating clock gene oscillations in the vertebrate PSM.

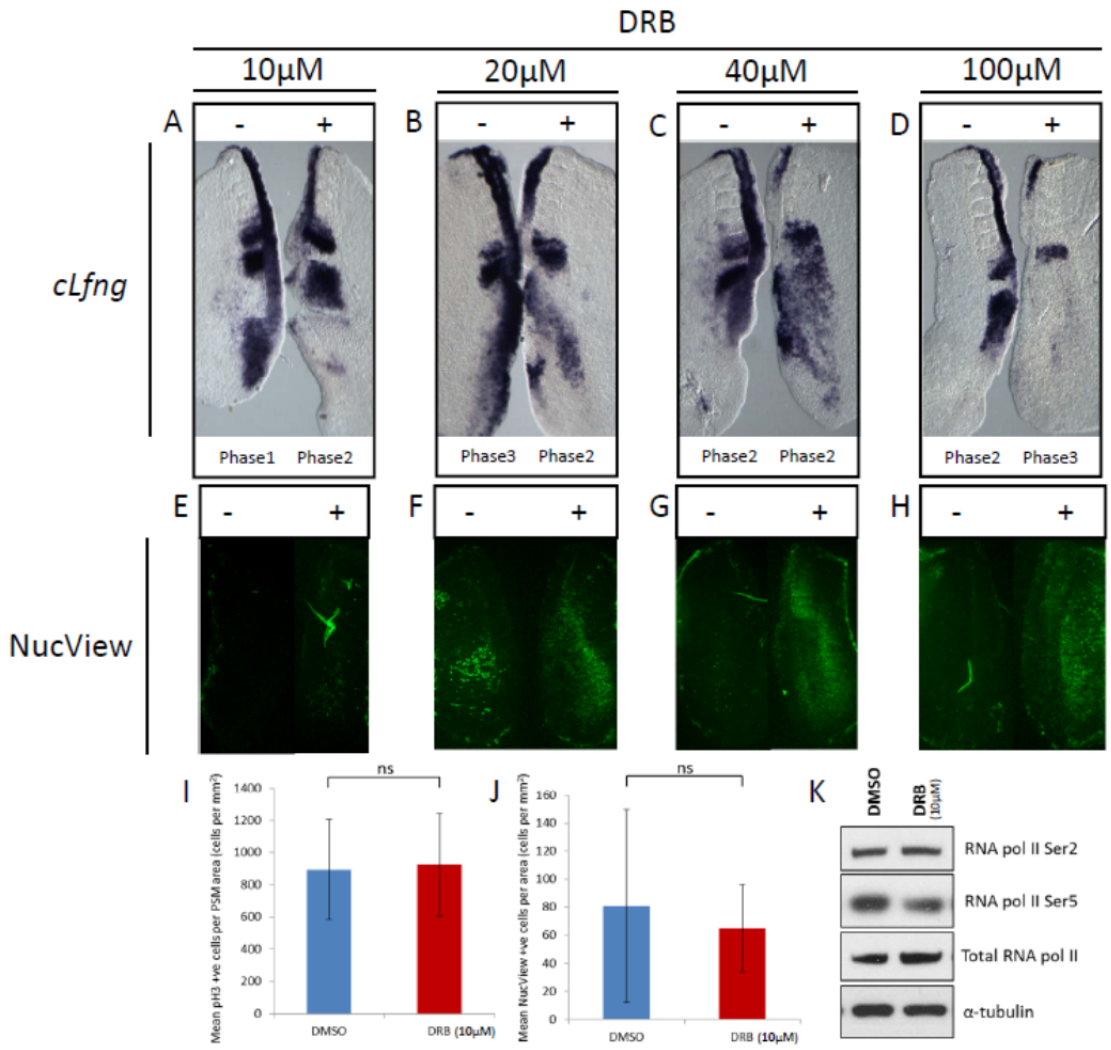

Figure 1.6) DRB titration assay. Dorsal view of bisected caudal half explants after in situ hybridisation using different probes. *cLfng* ISH analysis following -/+ DRB treatment at 10 µM (**A**), 20 µM (**B**), 40 µM (**C**), and 100 µM (**D**). NucView staining following treatment with -/+ DRB at 10µM (**E**), 20µM (**F**), 40µM (**G**), and 100µM (**H**). 10µM DRB has no significant effect on either the number of pH3 positive cells (**I**, n=5, p=0.884) or NucView positive cells (**J,** n=3, p=0.844) in the chicken PSM relative to the corresponding DMSO control half-PSM explant. 10µM DRB has no effect on S2 RNA polymerase II phosphorylation (**K,** mean fold-change=0.994), but decreases S5 RNA pol II phosphorylation (**K,** mean fold-change=0.789).

1.7) DRB slows *cLfng* oscillations and represses RNA pol II phosphorylation in the chicken PSM

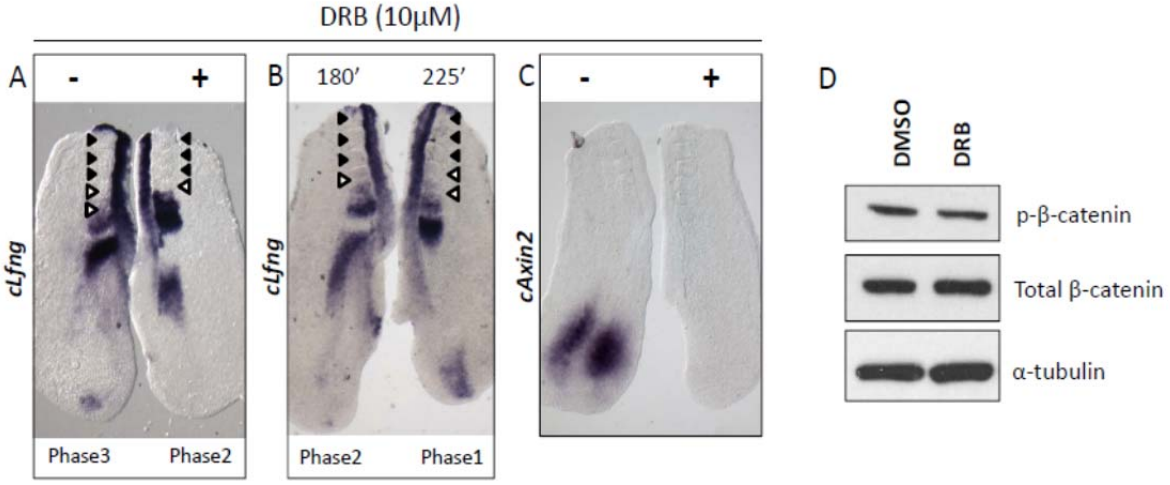

Figure 1.7) 10 µM DRB inhibits *cAxin2* expression and delays oscillations of *cLfng* expression in the chicken PSM. Dorsal view of bisected caudal half explants after in situ hybridisation using different probes. -/+ assays show that 10µM DRB downregulates *cAxin2* (**C**) and delays oscillations of *cLfng* expression in the PSM (**A**). Fix and culture assays reveal that *cLfng* expression is still dynamic in the presence of 10µM DRB (**B**). Black arrows indicate somites present at the start of culture and white arrows mark somites formed during culture. 10µM DRB has no effect on phosphorylation of either β-catenin at S33, S37, T41 (**D,** n=5, p=0.063).

We investigated this hypothesis more closely by performing the fix and culture assay with both explants cultured in the presence of DRB, as described above for XAV939, to ascertain if the dynamic expression of the *lfng* clock gene was stopped or delayed but still moving. These fix and culture assays confirmed that *cLfng* expression was still oscillatory in the PSM treated with 10 µM DRB and had not simply stopped during culture (Fig. 1.7B, n=15/18). The Wnt target *cAxin2* was downregulated by DRB in the PSM compared to the DMSO control half PSM (Fig. 1.7C, n=29/42). However, phosphorylation of β-catenin at Ser33, Ser37, Thr41 was unaffected

following treatment with DRB (Fig. 1.7D, n=5, p=0.063, – each lysate pool is generated from half-PSM explants from 9 separate embryos), suggesting that the mechanism by which DRB inhibits transcription of *cAxin2* may not be through the inhibition of canonical Wnt signalling. This effect on *cAxin2* expression may be a consequence of reduced RNA Pol II activity due to DRB mediated inhibition of cdk7 and 9 phosphorylation of RNA Pol II.

1.8) Titration of Roscovitine treatment in the chicken PSM

To investigate further if the delay effect of DRB treatment on clock gene oscillations was more specifically through inhibition of cdk7 and cdk9 we compared the effect of a different cdk inhibitor in the same assay. Roscovitine is another cdk inhibitor which targets cdks involved in the regulation of both the cell cycle and global transcription (MacCallum et al, 2005; McClue et al, 2002). Roscovitine treatment was titrated on chicken PSM explants in the same manner as DRB, with a view to separate any effects on the cell cycle and the segmentation clock. At 10 µM Roscovitine clearly delayed oscillation of *cLfng* expression relative to the DMSO control (Fig. 1.8A, n=59/62). The result for 100 µM Roscovitine was more severe, with the -/+ assay frequently showing a loss of *clfng* expression in the +Roscovitine NT half (Fig. 1.8B, n=6/7) and sometimes total downregulation (n=1/7) compared to the control half, but fix and culture paired explants exhibited the same profile of *cLfng* expression in both sides of the PSM to reveal that oscillations had ceased (n=3/3, data not shown).

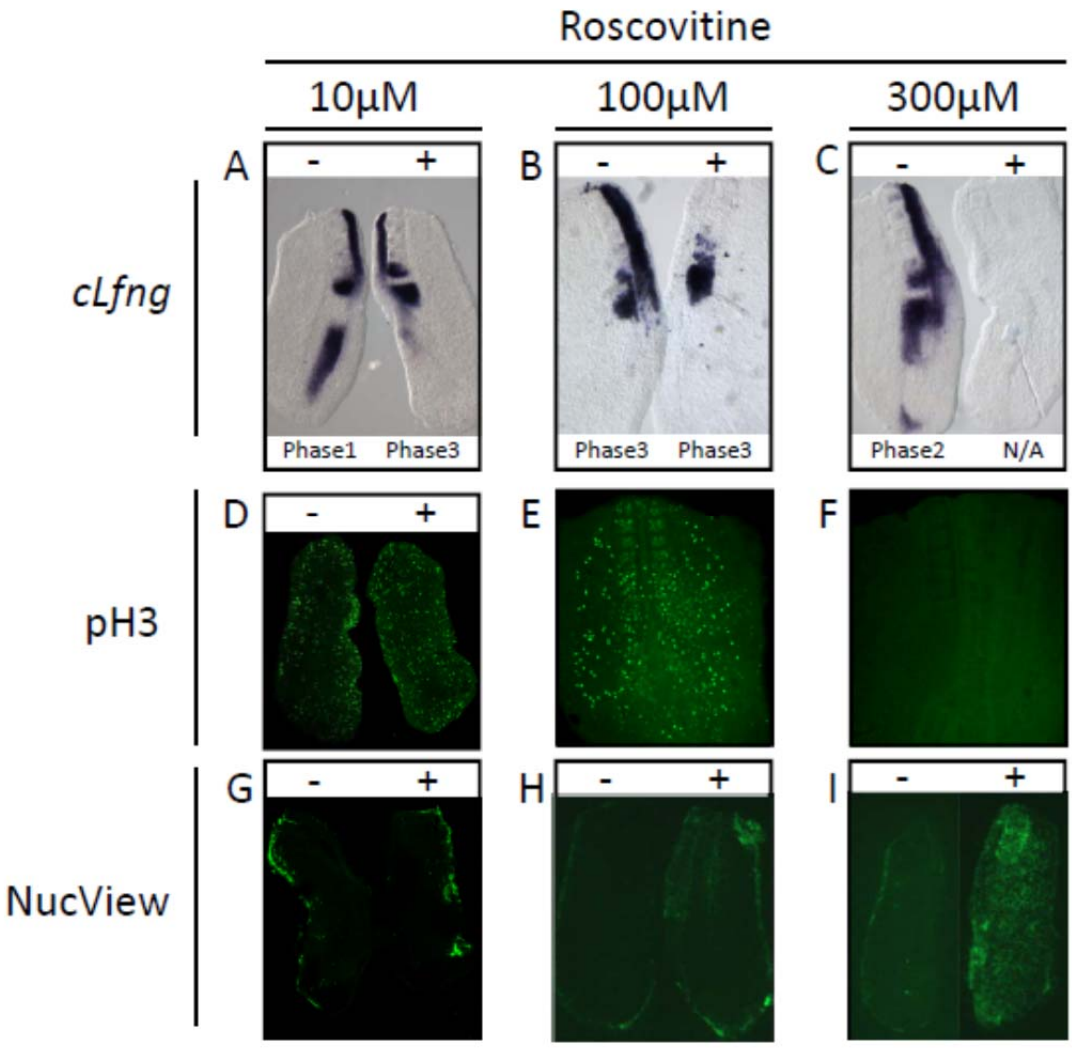

Figure 1.8) Roscovitine titration assay. Dorsal view of bisected caudal half explants after in situ hybridisation using different probes. **A-C**) -/+ Roscovitine titration assay for *cLfng* expression analysis in the PSM. **D**) -/+ 10 µM Roscovitine assay with immunofluorescence staining for phospho-histone H3 (pH3). Caudal chicken embryo explants with immunofluorescence staining for pH3 following 100 µM (**E**) and 300 µM (**F**) Roscovitine treatment. -/+ explant pairs with NucView live cell apoptosis staining for Caspase-3 activity following treatment with -/+ Roscovitine at 10 µM (**G**), 100 µM (**H**), and 300 µM (**I**).

In the presence of 300 µM Roscovitine, *cLfng* expression was completely abolished in both the PSM and NT compared to normal expression in the control side tissues (Fig. 1.8C, n=7/7). This may be explained by both the lack of proliferating cells stained for pH3 (Fig. 1.8F) and noticeable increase in apoptosing cells (Fig. 1.8I) when treated with 300 µM Roscovitine. Interestingly, at 100 µM Roscovitine treatment, there were plenty of proliferating cells still present in all caudal embryonic tissues (Fig. 1.8E), but there was a small increase in the number of apoptosing cells seen compared to the DMSO control (Fig. 1.8H). 10 µM Roscovitine appeared to have no effect on either proliferation (Fig. 1.8D) or apoptosis (Fig. 1.8G) in the chicken PSM. Following the titration assay, 10 µM Roscovitine was used for the rest of the study due the clear delay effect on *cLfng* oscillations, without stopping clock cycling altogether or adversely affecting cell death in treated explants in comparison to their respective controls. Importantly, this segregates the effect of this reagent on clock gene oscillations from its effect upon cdks involved in the cell cycle.

1.9) Roscovitine slows *cLfng* oscillations and represses RNA pol II phosphorylation in the chicken PSM

Roscovitine was used at 10 µM to assess the effects on the segmentation clock and Wnt signalling in particular. The effects of Roscovitine treatment on the chicken PSM were very similar to DRB. -/+ half-PSM assays for Roscovitine revealed that the *cLfng* mRNA oscillation phase was delayed when compared to the PSM of the corresponding DMSO control half (Fig. 1.8A and 1.9A, n=59/62). Fix and culture assay for Roscovitine treated explant pairs confirmed that *cLfng* expression was still oscillatory in the PSM and had not simply arrested during culture (Fig. 1.9B, n=8/10). Longer fix and culture assays suggested that the period of the clock was extended to ~120 minutes in the presence of Roscovitine (Fig. S1, n=2), but further replicates are required to confirm this, as well as for XAV939, and DRB. Interestingly, the Wnt target *cAxin2* was downregulated in the PSM when treated with Roscovitine but unaffected in the DMSO control half PSM (Fig. 1.9C, n=31/41), as seen for -/+ XAV939 treated explant pairs.

However, as for DRB treatment, phosphorylation of β-catenin at Ser33, Ser37, Thr41 was unaffected following treatment with Roscovitine (Fig. 1.9D, n=5/6, mean fold-change=1.134, p=0.617).

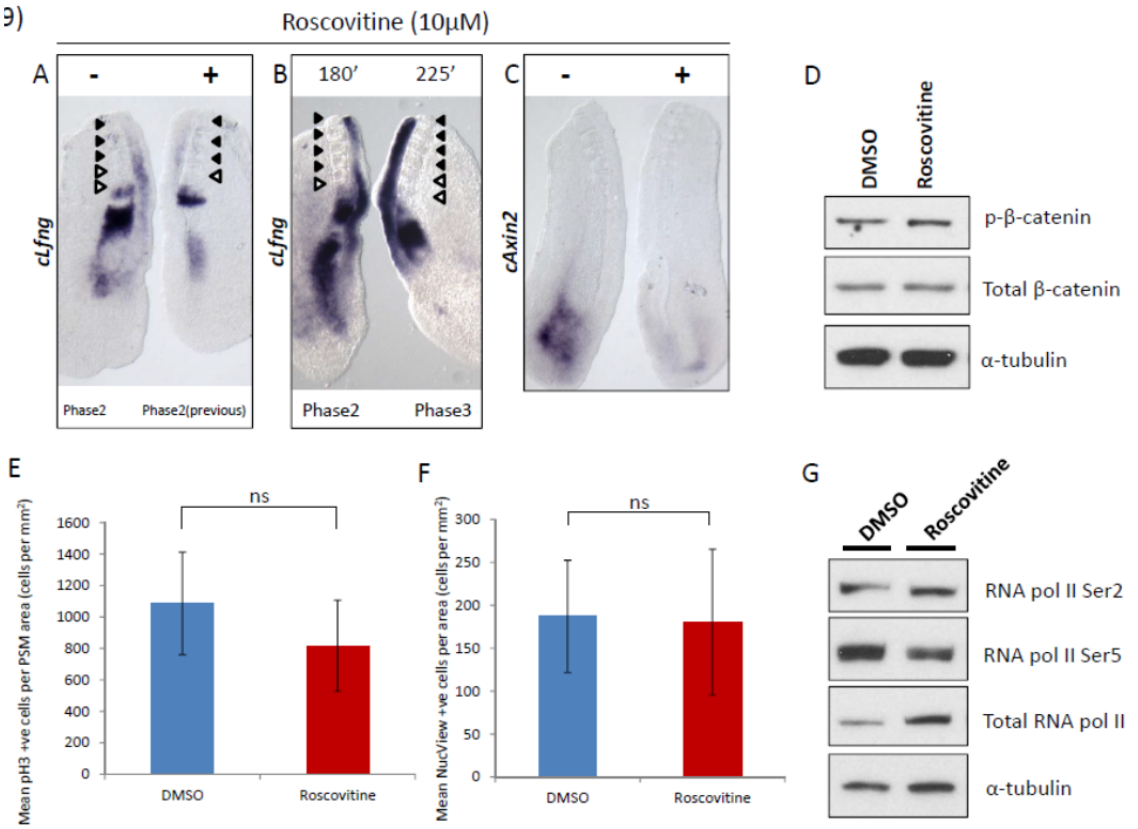

Figure 1.9) 10 µM Roscovitine inhibits *cAxin2* expression and delays oscillations of *cLfng* expression in the chicken PSM. Dorsal view of bisected caudal half explants after in situ hybridisation using different probes. -/+ assays show that 10 µM Roscovitine downregulates *cAxin2* (**C**) and delays oscillations of *cLfng* expression in the PSM (**A**). Fix and culture assays reveal that *cLfng* expression is still dynamic in the presence of 10 µM Roscovitine (**B**). 10 µM Roscovitine has no effect on phosphorylation of either β-catenin at S33, S37, T41 (n=5/6) (**D,** mean fold-change=1.134, p=0.617), or S2 of RNA polymerase II (n=3/3, mean fold-change=1.225) (**G**), but decreases S5 RNA pol II phosphorylation (n=2/3, mean fold-change=0.725) (**G**). 10 µM Roscovitine has no significant effect on either the number of pH3 positive cells (**E,** p=0.204) or NucView positive cells (**F,** p=0.886) in the chicken PSM relative to

the corresponding DMSO control half-PSM explant. Black arrows indicate somites present at the start of culture and white arrows mark somites formed during culture.

Quantification confirmed that neither proliferation (Fig. 1.9E, n=5, p=0.204), nor apoptosis (Fig 1.9F, n=4, p=0.886) were significantly affected in the PSM by 10 μM Roscovitine treatment relative to the DMSO control PSM tissue. Phosphorylation of Serine 5 on the CTD of RNA pol II was reduced with a mean fold change of 0.725 by Roscovitine treatment compared to the DMSO control (n=2/3), however Serine 2 phosphorylation appeared unaffected (n=3/3, mean fold-change=1.225) (Fig. 1.9G). These effects on RNA pol II were remarkably similar to those of DRB treatment. The findings from the assays with Roscovitine reveal that the oscillations of *cLfng* expression in the chicken PSM are slowed by Roscovitine treatment at a concentration that does not affect cell proliferation. These findings therefore suggest that cdks involved in the cell cycle are not important in regulating clock gene oscillations in the vertebrate PSM.

The effects of Roscovitine and DRB on RNA pol II suggest that these inhibitors have a higher efficacy against phosphorylation on Serine 5 rather than phosphorylation of Serine 2 on the CTD of RNA pol II in the chicken PSM at the given concentrations used. Phosphorylation at Serine 5 of RNA pol II in particular is required to promote initiation of transcription as RNA pol II moves away from the gene promoter (Komarnitsky et al, 2000), while Serine 2 phosphorylation is required for transcription elongation (Marshall et al, 1996). It is therefore possible that Roscovitine and DRB treatments have a more specific inhibitory action on initiation of RNA pol II dependent transcription in the chicken PSM. Interestingly, a recent genome-wide study mapping RNA pol II modification in embryonic stem cells identified a large set of genes bound by Polycomb repressor complexes which were not actively transcribed, but were bound by RNA pol II with phosphorylation specifically at Serine 5 and not at Serine 2 (Brookes and Pombo, 2012). These so-called ‘poised’ genes that contain both active and repressive marks of active transcription are mainly developmental genes and RNA pol II is

shown to extend several kilobases into such genes even though their expression is repressed (Brookes and Pombo, 2012). The repressive action of Roscovitine and DRB on RNA pol II serine 5 phosphorylation therefore suggests that these cdk inhibitors may modify such 'poised' developmental genes in the embryo to a more repressed state by reducing this modification required to promote transcriptional initiation. Certainly, the fact that Serine 2 phosphorylation of RNA pol II was unaffected by both Roscovitine and DRB treatments suggest that the effects of these inhibitors may not be global but rather affect such a 'poised' subset of genes as described above.

1.10) XAV939, DRB, and Roscovitine downregulate targets from multiple signalling pathways in the chicken PSM

In order to confirm whether XAV939, Roscovitine, and DRB have a general effect on the segmentation clock or more specifically slow oscillations of *cLfng* transcription, the expression profile of another cycling Notch target *cHairy2* was assessed in -/+ drug assays. *cHairy2* expression in the chicken PSM was consistently delayed in oscillation phase compared to the respective DMSO control when treated with either XAV939 (Fig. 1.10E, n=4/6), Roscovitine (Fig. 1.10J, n=6/7), or DRB (Fig. 1.10O, n=5/6). These results confirmed the delay effects on clock gene oscillations at the transcriptional level seen by all three of the inhibitors.

XAV939, Roscovitine, and DRB all robustly downregulated transcription of the Wnt target *cAxin2* in the caudal chicken PSM. Although this result was expected for the Wnt inhibitor XAV939, Roscovitine and DRB did not increase phosphorylation of β-catenin, suggesting that their effects may not be through Wnt signalling but that rather this may be an output of having inhibited activity of CDKs that regulate transcription. To clarify whether these inhibitors are specifically targeting Wnt signalling or having more general effects on transcription, the expression profile of a number of targets from several signalling pathways that are present in the caudal chicken embryo during somitogenesis stages were viewed by ISH following treatment with each of the three inhibitors (data summarised in Table 1.1).

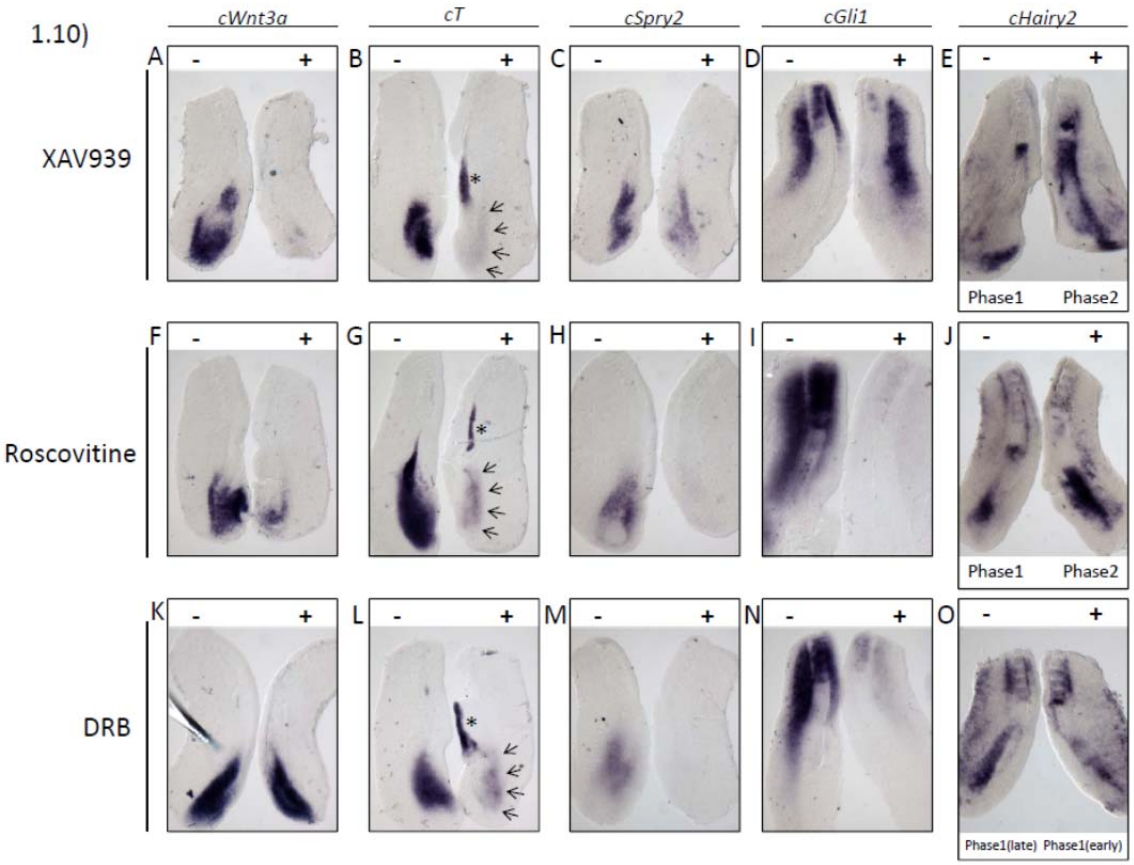

Figure 1.10) Expression of different marker genes following treatment with XAV939, Roscovitine, and DRB. Dorsal view of bisected caudal half explants after in situ hybridisation using different probes. *cWnt3a* expression following -/+ treatment with XAV939 (**A**), Roscovitine (**F**), and DRB (**K**). *cT* expression following -/+ treatment with XAV939 (**B**), Roscovitine (**G**), and DRB (**L**). Asterisk in **B,G,L** indicates notochord expression remaining in + explant half. Arrows in **B,G,L** demarcate the tailbud region of *cT* downregulation in the + explant side. *cSpry2* expression following -/+ treatment with XAV939 (**C**), Roscovitine (**H**), and DRB (**M**). *cGli1* expression following -/+ treatment with XAV939 (**D**), Roscovitine (**I**), and DRB (**N**). *cHairy2* expression following -/+ treatment with XAV939 (**E**), Roscovitine (**J**), and DRB (**O**).

cWnt3a and chicken *Brachyury* (*cT*) are non-cycling Wnt targets that are expressed in the tailbud of early chicken embryos. The effects of the 3 inhibitors on *cWnt3a* was variable, with *cWnt3a* showing some downregulation with XAV939 (Fig. 1.10A, n=2/5 downregulated, 2/5 unaffected, 1/5 upregulated) and more consistent downregulation with Roscovitine (Fig. 1.10F, n=4/5), but no obvious effect with DRB treatment (Fig. 1.10K, n=2/5 unaffected, 2/5 upregulated, 1/5 downregulated). *cT* also showed some inconsistent downregulation in the tailbud of explants treated with XAV939 (Fig. 1.10B, n=2/4), Roscovitine (Fig. 1.10G, n=2/4), and DRB (Fig. 1.10L, n=3/4). It should be noted that *cT* expression also marks the notochord, which was retained randomly in either the control (-) or drug treated (+) explant, or sometimes in both explants due to the fact that the embryo was bisected along the midline. However, even when maintained in the + half, *cT* expression in the notochord appeared unaffected, presumably due to the more stable levels of expression in this tissue compared to the tailbud (Figs. 1.10,G,L, see asterisks). These expression analyses reveal that all three inhibitors downregulate the Wnt targets *cWnt3a* and *cT* in the chicken PSM, albeit with less consistency than the effects on *cAxin2* transcription.

	XAV939			**Roscovitine**			**DRB**		
	↑	No change	↓	↑	No change	↓	↑	No change	↓
cWnt3a	1/5	2/5	2/5	1/5	0/5	4/5	2/5	2/5	1/5
cT	1/4	1/4	2/4	0/4	2/4	2/4	1/4	0/4	3/4
cSpry2	1/5	1/5	3/5	2/5	1/5	2/5	0/4	2/4	2/4
cGli1	0/5	0/5	5/5	0/5	1/5	4/5	0/4	0/4	4/4

Table 1.1) Summary of effects for XAV939, Roscovitine, and DRB on different gene targets in the chicken PSM. Upwards arrow indicated upregulation, downward arrow indicates downregulation.

cSpry2 expression was viewed as a target of the FGF signalling pathway, which is also present as a non-dynamic domain in the chicken tailbud. *cSpry2* also exhibited some inconsistent downregulation with XAV939 (Fig. 1.10C, n=(3/5 downregulated, 1/5 unaffected, 1/5 upregulated), Roscovitine (Fig. 1.10H, n=2/5 downregulated, 2/5 upregulated, 1/5 unaffected), and DRB (Fig. 1.10M, n=2/4 downregulated, 2/4 unaffected). These downregulation effects on *cSpry2* expression could be explained by the fact that the Fgf and Wnt signalling pathways are known to co-regulate each other in the developing tail of the vertebrate embryo (Aulehla et al, 2003; Gibb et al, 2009; Wahl et al, 2007).

The Shh target *cGli1* is expressed in the NT, somites and LPM of the chicken embryo. Interestingly, -/+ assays revealed that *cGli1* was consistently downregulated by XAV939 particularly in the somites and NT (Fig. 1.10D, n=5/5), as well generally downregulated by both Roscovitine (Fig. 1.10I, n=4/5) and DRB (Fig. 1.10N, n=4/4) compared to their respective controls. Cross regulation between the Wnt and Shh pathways exists in the somites, suggesting that the downregulation of *cGli1* by XAV939 in the somites could be indirectly through Wnt inhibition (Munsterberg et al, 1995). However Roscovitine and DRB may not be specifically inhibiting Wnt signalling but are in fact having a more general effect on transcription in the chicken PSM tissue. The effects varied gene to gene but again there is precedent in the literature for some genes being more sensitive to RNA pol II inhibition than others (Wada et al, 1998).

Overall, the expression analyses reveal that XAV939, Roscovitine, and DRB can all inconsistently downregulate transcriptional targets of the Wnt, Fgf, and Shh signalling pathways in the chicken PSM. Given that the cdk inhibitors both appear to reduce Serine 5 phosphorylation of RNA pol II, these results may represent a more general effect on global transcription. XAV939 downregulated the Wnt targets *cWnt3a* and *cT* as expected, while the effects of XAV939 on Fgf and Shh signalling targets may be via indirect inhibition of interactions between these pathways and Wnt signalling that are shown in the caudal embryo

(Aulehla et al, 2003; Gibb et al, 2009; Munsterberg et al, 1995; Wahl et al, 2007). However, the findings were generally inconsistent and more replicates are required to view the level of transcription of these targets with each given treatment to confirm these effects with greater confidence.

1.11) Inhibition of Sonic Hedgehog signalling does not affect clock gene oscillation in the chicken PSM

The Shh target gene *cGli1* mRNA appeared downregulated by all three inhibitors that delayed *cLfng* oscillations. This suggested that Shh signalling could have a role in regulating the segmentation clock as has also been previously suggested by Resende et al (2010), who showed that using the Shh inhibitor Cyclopamine in -/+ assays at 25 µM for a culture period of at least 6 hours could delay oscillations of the clock genes *cHairy2* and *cLfng*. However, Gibb et al., (unpublished) showed that using Cyclopamine at 50 µM in similar assays had no effect on the oscillation phase of *cLfng* expression in the chicken PSM. To test this further, Cyclopamine was used at both 25 µM and 50 µM in -/+ assays. At 25 µM, Cyclopamine already totally downregulated the Shh target gene *cGli1* in the chicken half-PSM explant compared to normal expression present in the DMSO control side in the NT, somites and LPM tissues after 6 hours in culture (Fig. 1.11A, n=5/5). However, *cLfng* expression in the PSM was not delayed in oscillation phase at either 25 µM (Fig. 1.11B, n=6/9 unaffected, 3/9 delayed) or even 50 µM (Fig. 1.11C, n=3/4 unaffected, n=1/4 delayed). This assay suggests that Shh signalling does not play a direct role in the segmentation clock and that the downregulation of the Shh target *cGli1* by XAV939, Roscovitine, and DRB is independent of their slowing effects on *cLfng* oscillations in the chicken PSM.

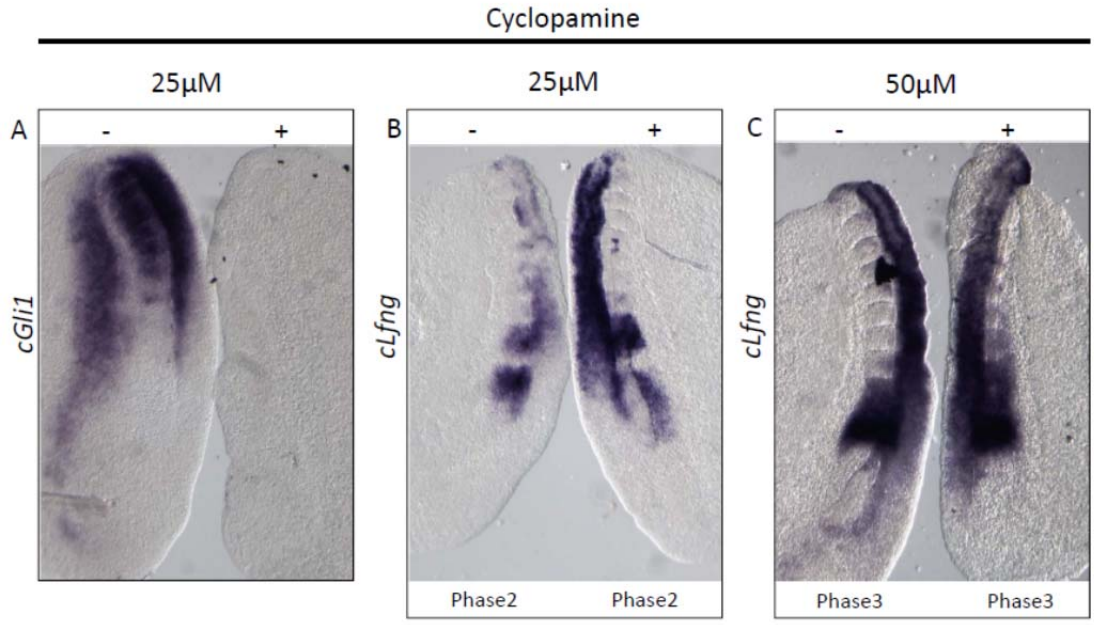

Figure 1.11) Inhibition of Sonic Hedgehog signalling with Cyclopamine does not affect *cLfng* oscillations in the chicken PSM. Dorsal view of bisected caudal half explants after in situ hybridisation using different probes. assays for Cyclopamine show that at 25 µM the Shh target *cGli1* mRNA is already downregulated (**A**), but *cLfng* oscillation phase is unaffected in the PSM compared to the corresponding DMSO control side at both 25 µM (**B**, n=6/9 unaffected, n=3/9 delayed) and 50 µM (**C**, n=3/4 unaffected).

The findings in Chapter 1 reveal that the canonical Wnt inhibitor XAV939 and two Cdk inhibitors can each slow cycling transcription of clock genes within the chicken PSM. These effects were independent of both proliferation and apoptosis. XAV939, promoted β-catenin phosphorylation as expected, but did not appear to affect the action of Cdks on RNA pol II phosphorylation. Conversely, Roscovitine and DRB both specifically reduced phosphorylation on Serine 5 of RNA pol II but did not appear to affect canonical Wnt signalling directly. We find no evidence that Shh has a role in the temporal control of the segmentation clock, as chemical inhibition of Shh signalling had no effect on the oscillation phase of *cLfng* transcription in the PSM. The inhibitors XAV939, Roscovitine, and DRB provide excellent delaying reagents with which to study the mechanism of the segmentation clock pacemaker in further detail.

Chapter 2: cNICD levels are higher in the chicken PSM when treated with inhibitors that slow oscillations of Notch target transcription

2.1) Optimisation of NICD primary antibodies by western blotting analysis

The vertebrate segmentation clock is proposed to rely on unstable clock protein products that are rapidly degraded to maintain timely oscillations of clock gene activity in the PSM (Harima et al, 2004; Lewis, 2003; Monk, 2003). While mathematical models suggest this is necessary (Lewis, 2003), there is currently a lack of experimental evidence to support this. Using the small molecule inhibitors found to delay the segmentation clock (XAV939, Roscovitine, and DRB), we aimed to assess whether the levels of key clock protein components of the Notch signalling pathway are increased under these inhibitor treatment conditions which are shown to slow cycling clock gene transcription in the chicken PSM.

The majority of studies into protein function in the vertebrate segmentation clock have focused on mouse and zebrafish embryos due to their respective genomes having been sequenced with more complete coverage and their greater ease of use for genetic studies and transgenics (Bessho et al, 2003; Morimoto et al, 2005; Herrgen et al, 2010). In addition, there are fewer available reagents to study the role of clock genes at the protein level in the chicken segmentation clock, such as primary antibodies. Indeed, in contrast to the situation in the mouse, there is currently no available antibody against cleaved chicken Notch 1 intracellular domain (cNICD) protein. The commercially available mouse NICD (mNICD) Val#1744 antibody does not cross-react with chicken lysate (data not shown), most probably due to the difference in the amino acid sequence of the S3 cleavage site in chicken and mouse Notch1 proteins. In order to study cNICD protein in the chicken PSM, a polyclonal antibody was generated by immunising rabbits with a peptide corresponding to the first 12 amino acids of cNICD following the cleavage site from full length chicken Notch1, with the addition of a Cysteine residue at the C-terminus to aid coupling during the process of antibody synthesis (Fig. 2.1A, see Methods for

more details). The polyclonal anti-cNICD antibody was affinity purified from the third bleed sera for use in all applications used in this study.

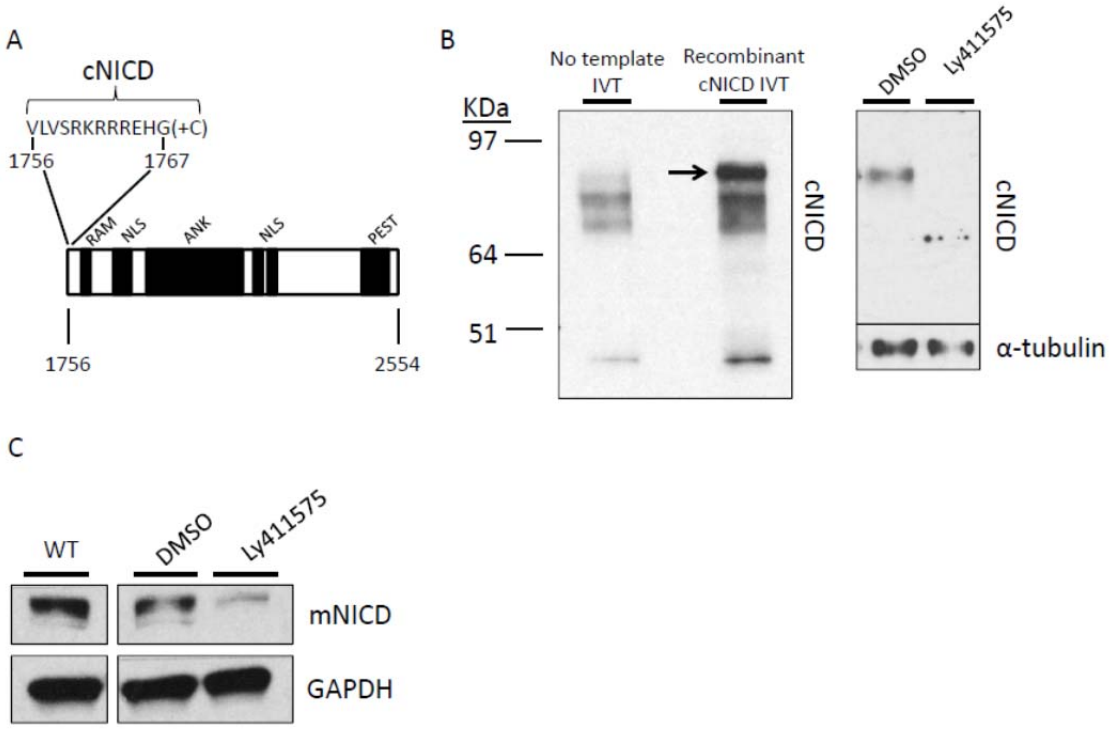

Figure 2.1) Testing of Primary Antibodies. **A**) The cNICD antibody was generated by immunising rabbits with a peptide corresponding to amino acids 1756-1767 at the very N-terminal end of chicken NICD protein following the S3 cleavage site from full length Notch 1. (Note that the cNICD antibody also recognises an additional Cysteine residue at the end of the peptide used for immunisation. This was to aid coupling during antibody synthesis and is not in the endogenous sequence). **B**) Western blotting for cNICD reveals a specific band (see arrow) close to the predicted molecular weight of 85KDa for recombinant cNICD (lane2) and DMSO treated chicken lysate (lane3) which is absent in chicken lysate treated with Ly411575 (lane4). **C**) The mNICD antibody recognises a specific band which is strongly reduced in Ly411575 treated mouse lysate.

The specificity of the antibody to cNICD protein needed to be confirmed before it could be used as a tool to study cNICD protein in the PSM. To test this, the cNICD antibody was used for Western blotting against recombinant cNICD protein synthesised using a full length cNICD expression vector as the template for an *in vitro* transcription/translation reaction. As expected, the cNICD antibody revealed a strong band for the recombinant cNICD protein reaction close to the predicted molecular weight of ~85KDa that was absent in control reaction with no template plasmid (Fig. 2.1B, lanes 1 and 2). To test the antibody on endogenous chicken lysate, pools of corresponding half-PSM explants containing just one somite, the PSM and half of the NT were cultured in the presence of the γ-secretase inhibitor Ly411575 (Lanz et al, 2004) or DMSO vehicle control media for 3 hours before being removed to produce protein lysates. Western blotting against cNICD revealed a specific band in the DMSO control pool at the same predicted size as for recombinant cNICD protein, which was abolished in the +Ly411575 treated pool (Fig. 2.1B, lanes 3 and 4). The cNICD antibody was designed against the peptide sequence close to the S3 cleavage site so that the antibody will not recognise full length Notch 1 protein. The loss of the specific band seen for cNICD by western blotting following inhibition of γ-secretase activity gives a good indication that the cNICD antibody is specific and can be used to view endogenous cNICD protein in the chicken. Similar to cNICD, the Val1744 mNICD antibody recognises a specific band by Western blotting in DMSO treated mouse PSM lysate which is strongly reduced with +Ly411575 treatment (Fig. 2.1C).

2.2) cNICD is present in dynamic domains in the PSM and localised to the caudal somites of the chicken embryo

Activated Notch1 protein in the form of NICD is shown to exhibit dynamic phases of localisation in the mouse PSM that resemble those seen for Notch targets at the mRNA level (Huppert et al, 2005; Morimoto et al, 2005; Niwa et al, 2011). Similarly, the Notch target mHes7 also cycles in the mouse PSM (Bessho et al, 2003). This has been suggested to have functional relevance to the role of Notch in normal segmentation, which is disrupted when the vertebrate embryo is exposed to either a lack of Notch signalling (Dunwoodie et al, 2002; Ferjentsik et al, 2009; Holley et al, 2000; Jiang et al, 2000; Jouve et al, 2000; Morimoto et al, 2005; van Eeden et al, 1996) or a more stable profile of mNICD localisation across the mouse PSM (Feller et al, 2008; Sparrow et al, 2012). These studies have shown that Notch signalling components are expressed in a dynamic manner in the mouse PSM which appears to be important for normal segmentation and these are likely to be conserved features in the PSM of other vertebrates. The cNICD antibody was therefore used for immunohistochemistry on HH10 chicken embryo tails to assess the spatial localisation of cNICD protein in the PSM.

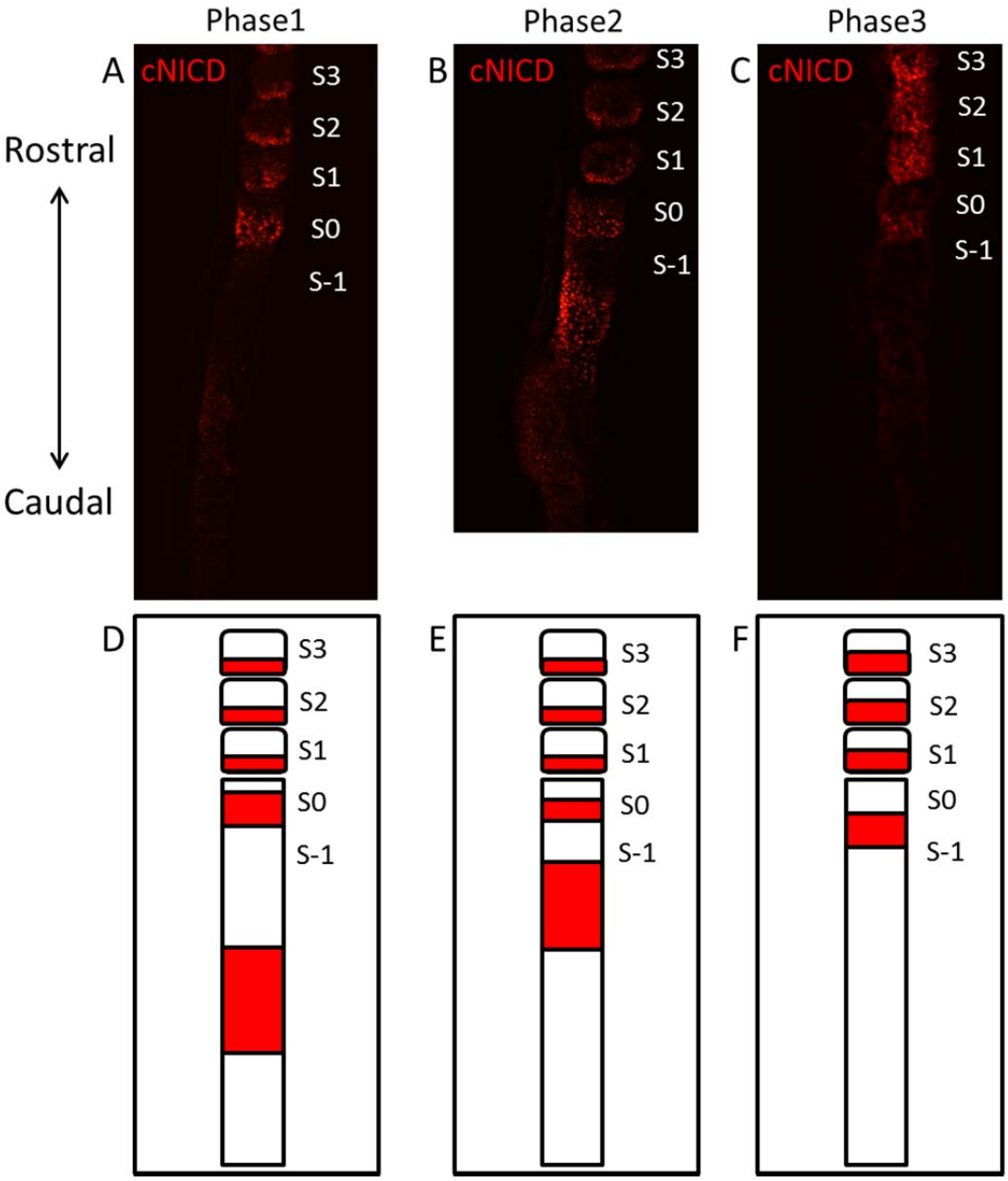

Figure 2.2) cNICD protein is present in dynamic domains in the chicken PSM. A-C) cNICD immunohistochemistry on sagittal cryo-sections of HH10 chicken embryo tails. **D-F**) Schematic diagrams showing distinct phases of dynamic cNICD localisation in the chicken PSM. The formed somites are labelled (S1, S2, S3). The regions of the PSM from which the following two prospective somites will form are labelled (S0 and S-1, respectively).

cNICD immunohistochemistry was first attempted on whole chicken tails with no specific staining achieved (data not shown). Specific immunohistochemistry staining was achieved with the cNICD antibody on sagittal cryo-sections of HH10 chicken tail tissues with the aid of antigen retrieval and secondary antibody signal amplification (see methods for details). The domains of cNICD localisation within the PSM appeared to differ between embryos, but were generally present in the caudal compartment of the formed somites (Fig. 2.2A-C). One cNICD spatial profile observed in the PSM was a sharp, strong domain in the S0, with another weaker and broader domain in the caudal PSM (Fig. 2.2A). In another embryo cNICD was also present in the S0, but the weaker caudal domain was not in the very caudal PSM but present more anteriorly in the PSM with the rostral limit extending to the S-1 region (Fig. 2.2B). Another pattern observed for cNICD in the PSM was just the sharp domain in the S0 and absent from the remaining caudal PSM (Fig. 2.2C). These 3 different cNICD spatial profiles viewed in the chicken PSM can therefore be categorised into the 3 phases of dynamic localisation as viewed for previously characterised clock genes (Fig. 2.2D-F; Pourquie and Tam, 2001).

cNICD therefore exhibited a dynamic spatial profile across the HH10 chicken PSM as seen for mNICD in the mouse embryo. This shows that oscillation of activated Notch 1 protein across the PSM is not only a feature of the mammalian segmentation clock but is in fact conserved in vertebrates, which may highlight a fundamental conserved feature of oscillating Notch signalling in the vertebrate segmentation clock.

2.3) XAV939, Roscovitine, and DRB treatments increase the level of cNICD in the chicken PSM

Mathematical modelling has predicted that a linear increase in the stability of clock gene protein products will lead to a linear increase in the period of a clock gene oscillation cycle (Monk, 2003; Lewis, 2003). Given that we have identified three means by which the period of a clock gene oscillation cycle can be extended, we set out to test these models with empirical data, by performing protein stability assays to assess the effects of XAV939, Roscovitine, and DRB treatments on the level of cNICD protein within the chicken PSM at the same concentration that each inhibitor was found to delay *cLfng* oscillations. Half-PSM explant pairs were dissected from embryos as for the assays in chapter 1, with the exception that each explant was trimmed to remove any LPM tissue and only contained one somite from the most recently formed pair in order to ensure that the entire PSM tissue was included (Fig. 2.3A). Although the cNICD antibody revealed a good signal by western blotting on even a single half-PSM piece of tissue, the band was often not sharp and loading was often uneven between samples most likely due to uneven lysis of the sample tissue (data not shown). Further optimisation revealed that culturing half-PSMs from 9 corresponding embryos for -/+ the inhibitor treatment and lysing in a larger volume gave much cleaner results. This method was used for all the stability assays shown in this study and the equivalent of two half-PSM tissues loaded per lane for each western blotting analysis. It should be noted that all explants contained half of the NT, however pilot assays revealed that removing the NT from half-PSM explants did not make any difference to the outcome and the level of NICD is much lower in the NT compared to the PSM of the mouse (data not shown; Huppert et al, 2005).

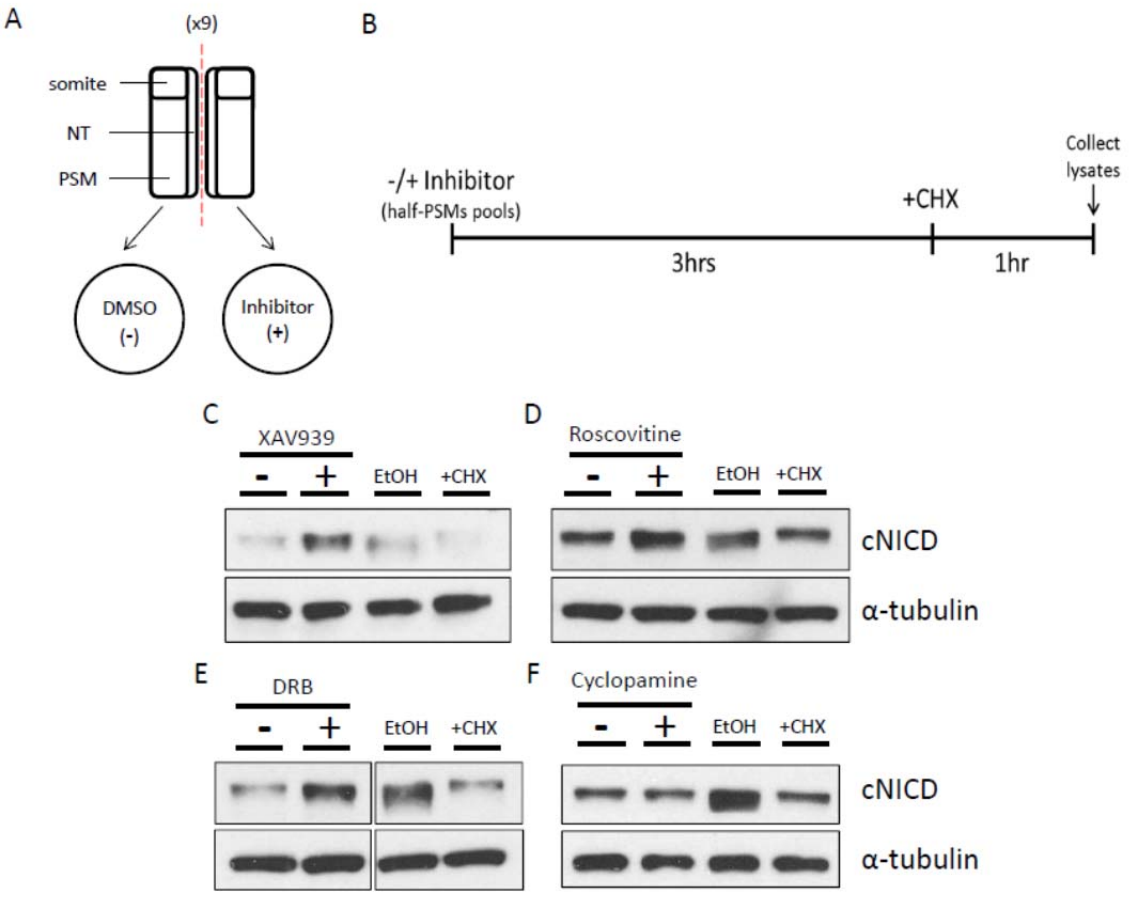

Figure 2.3) XAV939, Roscovitine, and DRB treatments increase cNICD protein levels in the chicken PSM. A) Chicken protein stability assay schematic. **B**) Time-course overview of the chicken stability assay culture period. Western blot results for cNICD protein and α-tubulin protein loading control levels following -/+ stability assay treatment with either XAV939 (**C**), Roscovitine (**D**), DRB (**E**), or Cyclopamine (**F**). Each assay in **C-F** includes a +Cycloheximide(CHX)/Ethanol (EtOH) control to confirm that CHX blocks de novo synthesis of cNotch1 protein in the explant pools.

In order to determine whether the small molecule inhibitor treatments used in Chapter 1 affect cNICD protein levels in the PSM, -/+ inhibitor explant pools for each treatment were cultured simultaneously for 3 hours before 20μM (final concentration) Cycloheximide was added to both the control and + inhibitor pools. Both pools were cultured for an additional hour before protein lysates generated (summarised in Fig. 2.3B). The addition of Cycloheximide for the final part of the culture period was to inhibit any *de novo* Notch1 protein synthesis in order to determine the effects of XAV939, Roscovitine, or DRB on the level of cNICD protein already present in the PSM. It should be noted that 20μM Cycloheximide treatment of the chicken PSM does not affect oscillations of *cHairy1* expression within a short culture period (McGrew et al, 1998; Palmeirim et al., 1997). Western blotting following Cycloheximide treatment revealed that the level of cNICD protein was increased significantly in the chicken PSM with XAV939 treatment compared to the corresponding DMSO control pool where the resident cNICD had degraded (Fig. 2.3C and Table 2.1, n=7/9 increased, p=0.0280). cNICD protein level was also significantly increased in the chicken PSM by both Roscovitine (Fig. 2.3D and Table 2.1, n=9/10 increased, p=0.002) and DRB (Fig. 2.3E and Table 2.1, n=6/8 increased, p=0.008) compared to corresponding control pool lysates. These assays reveal that XAV939, Roscovitine, and DRB treatments all increase the level of cNICD protein in the chicken PSM, just as they all delay oscillations of the Notch target gene *cLfng* transcription thereby supporting the mathematical modelling predictions that these two key parameters of the clock (stability of key components and periodicity) are inextricably linked.

The effectiveness of Cycloheximide was confirmed for each assay by running a separate set of 9 halved sample pools that were both cultured for the first 3 hour period in untreated chick media before the addition of Cycloheximide to one pool and Ethanol vehicle control to the corresponding pool. These pools were then cultured for an additional hour before protein lysates were prepared for western blotting to reveal a reduction in cNICD level compared to the Ethanol control (Fig. 2.3C-F, lanes 3 and 4 in all).

Treatment	Mean Adjusted Relative Fold Change of cNICD protein	± Standard Error of the Mean	Statistical Test	P-value
XAV939	3.078	±0.776	One-sample T-test	0.0280*
XAV939 (no CHX)	2.491	±0.480	One-sample T-test	0.0361*
Roscovitine	1.940	±0.255	One-sample Signed Rank test	0.002*
Roscovitine (no CHX)	1.594	±0.146	One-sample T-test	0.00653*
DRB	2.557	±0.702	One-sample Signed Rank test	0.008*
DRB (no CHX)	1.369	±0.081	One-sample T-test	0.00601*
Cyclopamine	1.263	±0.106	One-sample T-test	0.244

Table 2.1) Summary Table of Densitometry quantifications for cNICD stability assays. Densitometry was performed on western blots for stability assays and the fold-change of cNICD in the + inhibitor treated sample relative to the corresponding DMSO control was adjusted to the relative change in the α-tubulin loading control. The given statistical test was used to compare the average value for each assay to a fixed fold-change value =1 (i.e. no change) and a p-value obtained (* demarcates a statistically significant difference).

A previous study suggested that Shh signalling is involved in the temporal control of clock gene oscillations in the PSM (Resende et al, 2010). However, in Chapter 1 it was shown that exposure to the SHH inhibitor, Cyclopamine, had no effect on the oscillation phase of *cLfng* expression in the PSM. Interestingly, protein stability assays also showed that Cyclopamine had no significant effect on cNICD levels in the chicken PSM (Fig. 2.3F, n=2/2 unaffected, p=0.244). These findings add weight to the evidence that Shh signalling does not have a role in the segmentation clock pacemaker mechanism, but also suggest that the delay of transcriptional Notch gene oscillations and increase of activated Notch1 protein in the PSM treated by XAV939, Roscovitine, and DRB are linked.

2.4) Stability assays without Cycloheximide confirm the increase of cNICD protein by XAV939, Roscovitine, and DRB treatments in the chicken PSM

The stability assay data strongly support the hypothesis that XAV939, Roscovitine and DRB all increase cNICD in the chicken PSM. Nevertheless, there remains the formal possibility that, since NICD protein oscillates in the mouse PSM (Niwa et al, 2011), and this is likely to be conserved in the chick (data in Fig. 2.2), the amount of cNICD may vary simply depending on which phase of the oscillation the tissue is in when removed from culture for lysis. The fact that 2/9 of the assays for XAV939 showed a decrease in cNICD and the other 7/9 showed an increase gave rise to another possible explanation that the stability assay result for cNICD level was in fact more random and actually just depended on the average amount of cNICD in each half-PSM explant within the culture pool. This would make the varying levels of NICD a consequence of the delay rather than a cause.

Protein stability assays were repeated for XAV939, Roscovitine, and DRB, but without the Cycloheximide culture step to assess this possibility, as well as to avoid any potential effects of Cycloheximide on cycling gene expression (McGrew et al, 1998). Instead, -/+ pools for each inhibitor were simply cultured for 3 hours before simultaneous lysis (Fig. 2.4A). Western blotting following stability assays revealed that the level of cNICD is indeed consistently higher in the chicken PSM when treated with XAV939 (Fig. 2.4B and Table 2.1, n=5/5, p=0.0361), Roscovitine (Fig. 2.4C and Table 2.1, n=5/7, p=0.00653), and DRB (Fig. 2.3D and Table 2.1, n=4/6, p=0.00601) compared to respective DMSO control lysates, even in the absence of Cycloheximide, suggesting that the increase in cNICD seen with these treatments may be due to more stable cNICD in the PSM. Interestingly, the mean fold-change increase seen in cNICD level was slightly less for each treatment when the assay lacked the Cycloheximide step during culture. This is most likely due to the fact that in the absence of Cycloheximide, *de novo* cNICD synthesis in the PSM may mask the induction effect seen on existing cNICD to some extent.

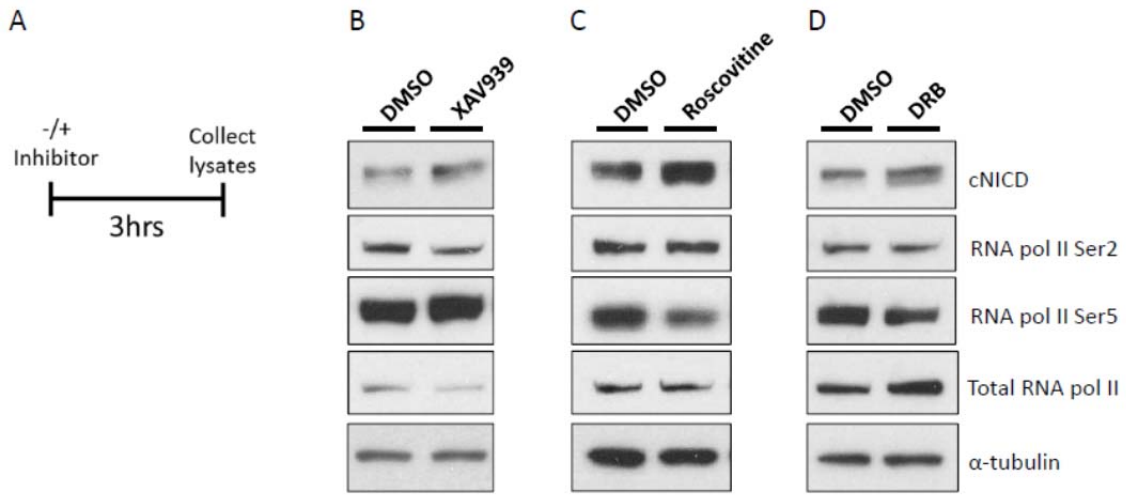

Figure 2.4) cNICD is increased by XAV939, Roscovitine, and DRB in stability assays without Cycloheximide. A) Schematic for the chicken protein stability assay without Cycloheximide. **B-D**) Western blotting results for cNICD, phospho-S2 RNA pol II, phospho-S5 RNA pol II, total RNA pol II, and α-tubulin proteins following stability assays lacking Cycloheximide for -/+ XAV939 (**B**), -/+ Roscovitine (**C**), and -/+ DRB (**D**).

Cdk7 is characterised as a target kinase of S5 on the CTD of RNA pol II (Fisher et al, 2005). However, Cdk8 and Cdk9 can also phosphorylate the S5 site *in vitro* in the regulation of RNA pol II dependent transcription (Galbraith et al, 2010). As reported in chapter 1 both DRB and Roscovitine treatment leads to a reduction in S5 RNA pol II phosphorylation, indicative of inhibition of cdk 7, 8 and 9 activity involved in transcriptional regulation. The levels of modified RNA pol II protein were assessed in the same stability assays with XAV939 as were used to cNICD protein level to ascertain whether XAV939 also affects RNA pol II phosphorylation in a similar manner to Roscovitine and DRB. However as expected, S2 and S5 RNA pol II phosphorylation was unaffected by XAV939 in assays where cNICD was increased (Fig. 2.4B, n=3/3 for both, mean fold-change=1.122 (pSerine2) and =1.171 (pSerine5)), but total RNA pol

II levels did appear slightly decreased (Fig. 2.4B, n=3/3) compared to the DMSO control pool. These results suggest that the effect of XAV939 on *cLfng* oscillations and cNICD level are unlikely to be through Cdk7-, Cdk8- and Cdk9- mediated transcriptional regulation and may therefore be through a different mode of action to the two cdk inhibitors which also affect the segmentation clock.

The data from Chapter 2 has shown that cNICD exhibits dynamic domains of spatial localisation within the chicken PSM, as well as localisation to the caudal compartment of the formed somites. This reveals a conserved spatial profile of dynamic Notch activity with the vertebrate PSM. Stability assays showed that cNICD protein level is increased by the 3 inhibitors (XAV939, Roscovitine, and DRB) also shown to slow transcriptional oscillations of clock genes, while unaffected by the Shh inhibitor Cyclopamine. This increase in cNICD in the PSM when the segmentation clock is slowed may represent an increase in stability of the normally unstable protein product that is proposed to be essential to maintain rapid clock transcriptional oscillations (Lewis, 2003). Further studies into the effects of these inhibitors on cNICD protein half-life will clarify whether the observed increase in cNICD is indeed a stabilisation rather than a general increase in Notch expression.

Chapter 3: Studying the effects of small molecule inhibitors on the segmentation clock in the mouse embryo PSM

3.1) XAV939 delays oscillations of *mLfng* expression and downregulates Wnt signalling in the mouse PSM

The study so far has shown that cNICD protein is increased when *cLfng* mRNA oscillations are slowed in the chicken PSM. This suggests that the level of NICD protein may be important to regulate the pace of clock gene oscillations. Similar results in other vertebrates would strengthen the argument for a conserved mechanism for the segmentation clock pacemaker mechanism. The effects of XAV939, Roscovitine, and DRB on the segmentation clock and NICD level were therefore assessed in the PSM of the mouse embryo using similar assays as for the chicken to test this possibility. The mouse embryo exhibits clock oscillations with a longer periodicity of nearer 120 minutes (Aulehla et al, 2008; Takashima et al, 2011). The periods of culture for assays performed on the mouse PSM were therefore extended accordingly compared to the chicken in order to encompass the same number of clock cycles.

XAV939 was titrated for assays with the mouse embryo as for the chicken and the optimal concentration was found to be 100 µM, as for the chicken (data not shown and Bone et al., manuscript in preparation). XAV939 was used at 100 µM as for the chicken assays to assess the expression profile of mouse *Lfng* (*mLfng)* mRNA and the Wnt target gene mouse *Axin2* (*mAxin2)* mRNA by ISH in the mouse PSM. -/+ assays revealed that *mAxin2* was severely downregulated in the mouse caudal PSM at 100 µM XAV939 as for the chicken (Fig. 3.1A, n=19/26). *mAxin2* expression was less affected in the rostral PSM suggesting that the expression in this domain is not entirely Wnt dependent (Fig. 3.1A).

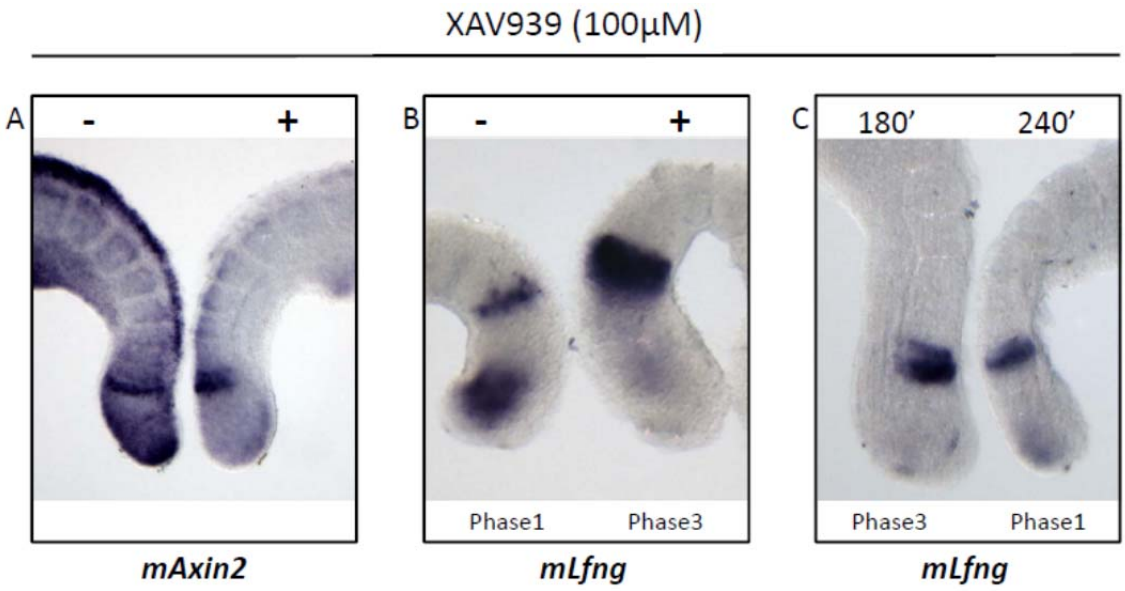

Figure 3.1) XAV939 delays *mLfng* oscillations and downregulates *mAxin2* in the mouse PSM. Lateral view of E10.5 mouse explants after ISH analysis. -/+ assays reveal that 100µM XAV939 downregulates *mAxin2* (**A**, n=19/26) and delays oscillations of *mLfng* expression (**B**, n=18/26) in the mouse PSM. Fix and culture assays reveal that m*Lfng* expression is still dynamic in the presence of 100µM XAV939 (**C**, n=12/20). "+" signifies treated half PSM explant and "-" signifies control contralateral explant half from the same embryo tail.

mLfng mRNA also oscillates as a clock gene in the mouse PSM and was used as a readout of the effects on the clock of modifying Wnt activity in -/+ inhibitor assays for the mouse PSM. As for the chicken, XAV939 delayed the oscillation phase of *mLfng* compared to the DMSO control half (Fig. 3.1B, n=18/26), while fix and culture assays showed that the oscillation phase of *mLfng* was still able to advance in the side cultured for longer (Fig. 3.1C, n=12/20). These results show that XAV939 slows but does not stop oscillations of *mLfng* transcription in the mouse PSM, although these outcomes were less consistent than assays on the chicken PSM.

3.2) Roscovitine delays oscillations of *mLfng* expression in the mouse PSM

Roscovitine was titrated in -/+ mouse culture assays in a similar manner as for the chicken to ascertain the optimal concentration which appeared to delay clock gene oscillations without stopping them altogether (data not shown). Following titrations on the mouse embryo, Roscovitine was used at 10 μM as for assays with the chicken embryo to assess the effects on gene expression in the mouse PSM. Unlike the chicken, -/+ assays showed that *mAxin2* was only sometimes downregulated by Roscovitine in the mouse PSM compared to the control side (Fig. 3.2A, n=7/17). However, the oscillation phase of *mLfng* transcription was consistently delayed in the PSM with Roscovitine treatment compared to the DMSO control (Fig. 3.2B, n=20/22). Fix and culture assays showed that *mLfng* expression was still cycling in the mouse PSM in the presence of 10 μM Roscovitine (Fig. 3.2C, n=8/10). Roscovitine therefore exhibited largely similar effects on the chicken and mouse PSM, although the downregulation of *Axin2* transcription seen in the mouse PSM was less consistent than for the chicken.

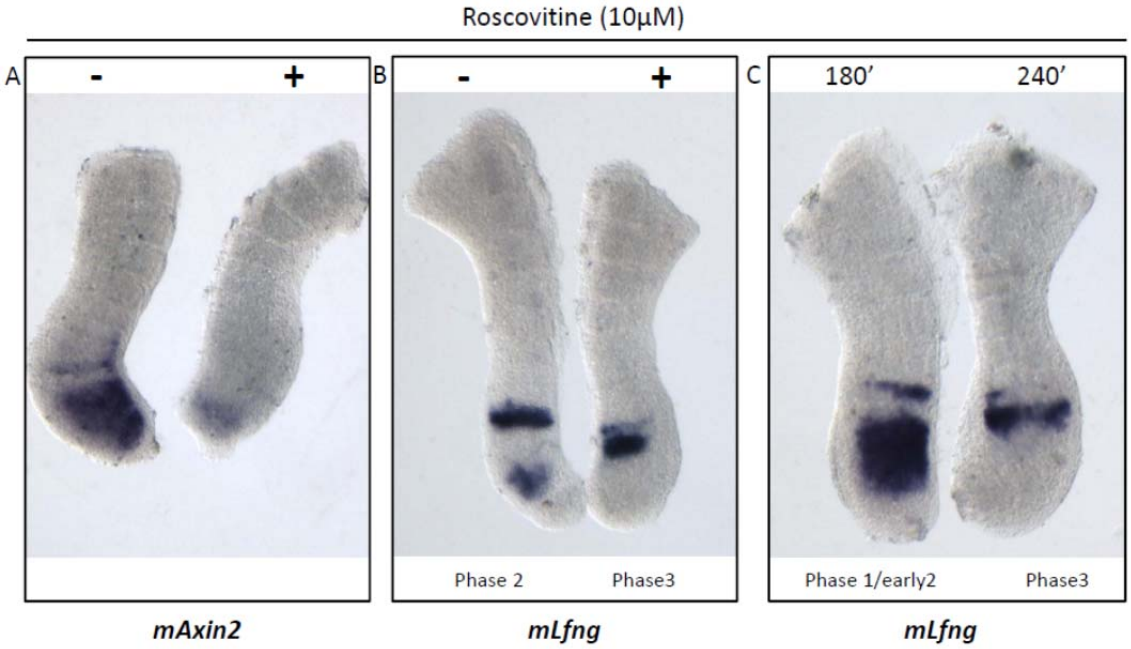

Figure 3.2) Roscovitine delays *mLfng* oscillations in the mouse PSM. Lateral view of E10.5 mouse explants after ISH analysis. -/+ assays reveal that 10µM Roscovitine downregulates *mAxin2* (**A**, n=7/17) and delays oscillations of *mLfng* expression (**B**, n=20/22) in the mouse PSM. Fix and culture assays reveal that m*Lfng* expression is still dynamic in the presence of 10µM Roscovitine (**C**, n=8/10). "+" signifies treated half PSM explant and "-" signifies control contralateral explant half from the same embryo tail.

3.3) DRB treatment affects oscillations of *mLfng* expression in the mouse PSM

DRB was also titrated for assays with the mouse embryo to find the optimal concentration which appeared to slow clock gene oscillations (data not shown), before being used at 5 µM to assess the effects on gene expression in the mouse PSM. Unlike the chicken, -/+ assays showed that *mAxin2* was downregulated only occasionally by DRB in the mouse PSM compared to the control side (Fig. 3.2A, n=2/7). The expression phase of *mLfng* transcription was consistently delayed in the PSM with DRB treatment compared to the DMSO control (Fig. 3.2B, n=10/13). However, fix and culture assays showed that *mLfng* expression was still cycling in the PSM of only half the embryos tested in the presence of 5 µM DRB (Fig. 3.2C, n=8/16). This made it unclear as to whether DRB was delaying or simply halting oscillations of *mlfng* expression. The outcomes from the study with DRB on the mouse PSM therefore suggested that there was not a significant inhibition of Wnt signalling, while the effects on the segmentation clock were too inconsistent to make a clear conclusion.

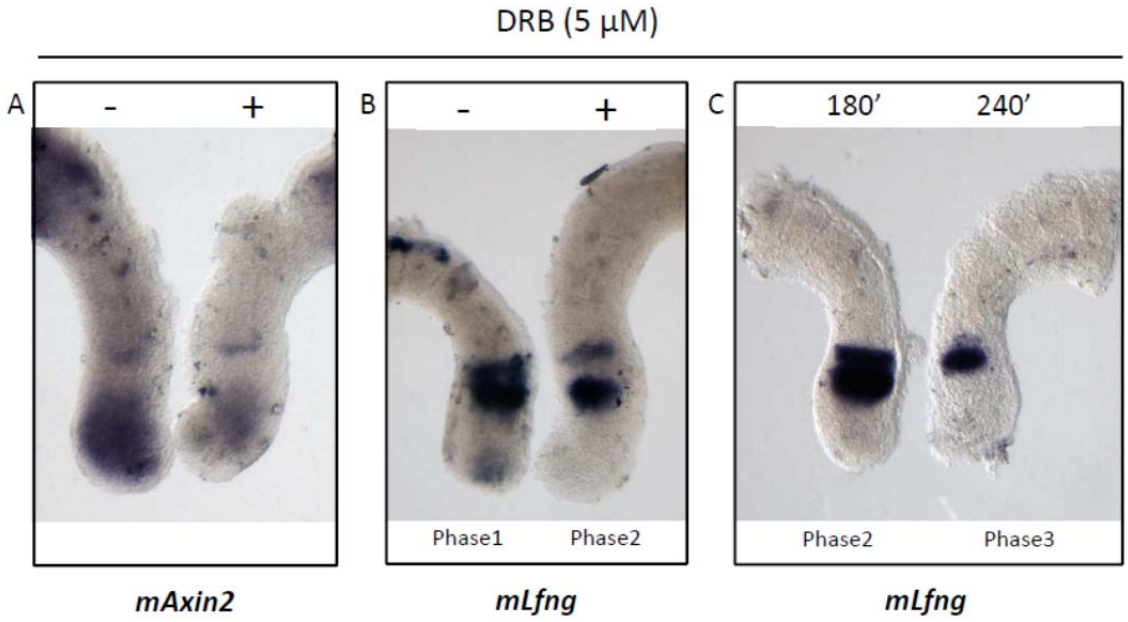

Figure 3.3) DRB delays *mLfng* oscillations in the mouse PSM. Lateral view of E10.5 mouse explants after ISH analysis. -/+ assays reveal that 5µM DRB downregulates *mAxin2* (**A**, n=2/7) and delays oscillations of *mLfng* expression (**B**, n=10/13) in the mouse PSM. Fix and culture assays reveal that m*Lfng* expression is still dynamic in the presence of 5µM DRB (**C**, n=8/16). "+" signifies treated half PSM explant and "-" signifies control contralateral explant half from the same embryo tail.

3.4) XAV939, Roscovitine, and DRB can all increase the levels of clock proteins in the mouse PSM

Evidence of the segmentation clock in mouse embryo has been viewed at both transcriptional and protein expression levels of dynamic clock genes. Indeed, both mNICD and mHES7 proteins have been shown to exhibit dynamic expression in the mouse PSM with a periodicity that is similar to transcriptional waves of expression seen for Notch targets (Bessho et al, 2003; Niwa et al, 2011). These proteins are also inherently unstable, which has been suggested to be important for the rapid turnover of Notch signalling in setting the pace of dynamic waves of Notch activity across the mouse PSM (Bessho et al, 2003; Kim et al, 2011). The effects of XAV939, Roscovitine, and DRB on Hes7 and NICD levels were assessed in the mouse PSM using similar assays as for the chicken. The expression level of these proteins was therefore analysed in the mouse PSM to get a better understanding of these processes.

-/+ assays showed that XAV939, Roscovitine, and DRB all appeared to slow oscillations of the clock gene *mLfng* in the same way that was seen for *cLfng* in the chick PSM. Although these effects were less robust than those seen in the chicken PSM, protein stability assays with -/+ each inhibitor were performed with mouse half-PSM explant pools as described in chapter2 for the chicken, with the exception that the initial culture period was extended to 4 hours to encompass the longer oscillation cycle exhibited in the mouse PSM as compared to the chicken (Fig. 3.4A). Thus, in short we addressed whether the reagents that cause a delay in *mLfng* oscillations across the PSM also lead to increased levels of key clock components, namely mNICD and mHes7. Following the -/+ assay in the presence of each inhibitor, protein lysates were prepared to analyse and compare the levels of the clock proteins mNICD and mHES7 using antibodies that were optimised for western blotting (see Fig. 2.1C, Fig. 3.4B). During the same experiment control samples from the -/+ assay were analysed by ISH for *mLfng* to ensure that the delay effect was observed. Mouse HES7 (mHES7) is another Notch signalling component that is found to cycle at the protein level in the mouse PSM (Bessho et al, 2003). A

mHES7 antibody was raised in the rabbit against the full length protein of mHES7 (as Bessho et al, 2003). The specificity of the mHES7 antibody was confirmed by western blotting, as it recognised a strong band close to the predicted molecular weight of ~25KDa in mHes7$^{+/+}$ lysate and recombinant mHES7 protein (Fig. 3.4B, lanes 1 and 3), which is absent in homozygous null mHes7$^{-/-}$ lysate and in the no template plasmid control *in vitro* transcription/translation reaction as expected (Fig. 3.4B, lanes 2 and 4).

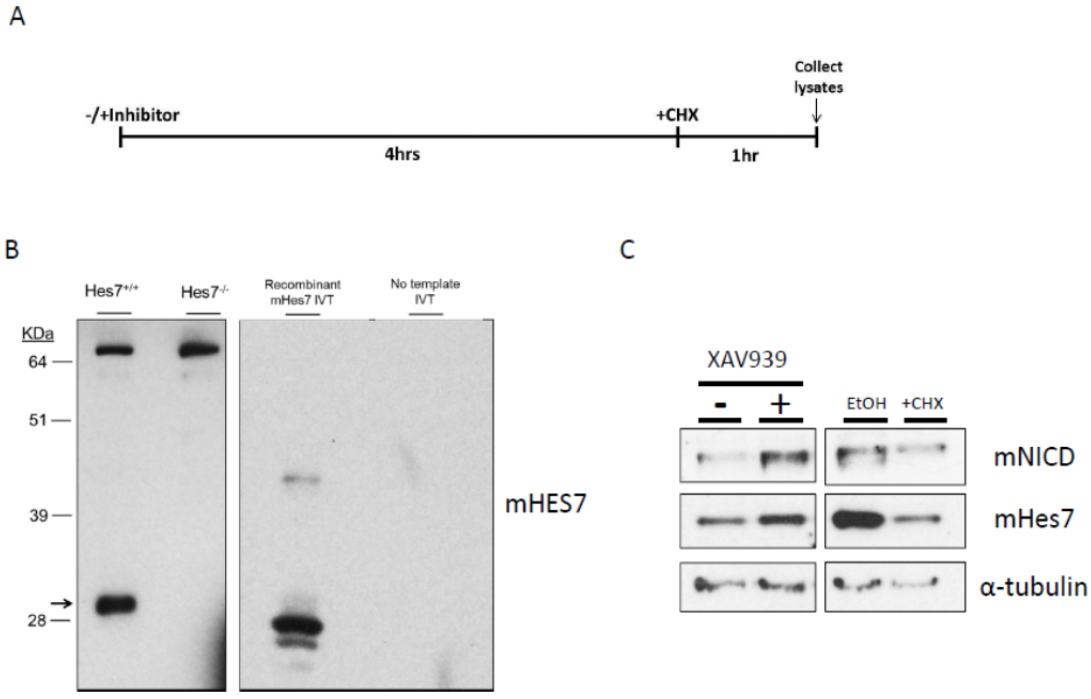

Figure 3.4) XAV939 increases the levels of clock gene proteins in the mouse PSM. A) Schematic of the mouse protein stability assay culture time-course. **B**) Western blotting with the mHes7 antibody recognises a specific band close to the 28KDa ladder marker (see arrow) in Hes7+/+ mouse lysate (lane1) and recombinant mHES7 protein (lane3) which is abolished in Hes7-/- mouse lysate (lane2). **C**) Western blot results for mNICD protein, mHES7 protein, and α-tubulin protein loading control levels following -/+ stability assay treatment with XAV939. The +Cycloheximide(CHX)/Ethanol (EtOH) control for the XAV939 assay confirms that CHX blocks *de novo* synthesis of mNICD and mHES7 proteins in the explant pools. Each "-" explant pool contained half PSM explants from 9 separate embryos, with the corresponding "+" pool containing the corresponding remaining 9 halves.

Western blotting revealed that both the levels of both mNICD (n=7/7) and mHes7 (n=5/6) were higher in pooled PSM lysates cultured in the presence of XAV939 when compared to the corresponding contralateral pooled PSM lysates cultured in the presence of DMSO (Fig. 3.4B, lanes 1 and 2) with α-tubulin serving as the loading control. Pooled PSM lysates cultured in the presence of Cycloheximide as compared to EtOH confirmed that the levels of both of these proteins were reduced in the absence of *de novo* protein synthesis (Fig. 3.4B, lanes 3 and 4). Roscovitine treatment also stabilised mHes7 protein level compared to the DMSO control pool (n=1/1), however mNICD appeared unaffected (n=0/2) (Supplementary Fig. S.2B). As for XAV939, mNICD (n=1/1) and mHes7 (n=1/1) protein levels were both increased with DRB treatment (Supplementary Fig. S.2C).

These outcomes show that, with the exception of mNICD with Roscovitine treatment, clock gene proteins are generally more abundant in the PSM of both the chicken and mouse embryos that have been treated with small molecule inhibitors which cause an extended period of clock gene oscillations. These novel findings are the first empirical data to support the *in silico* models which suggested that the clock period would be increased in the PSM where clock gene proteins were more stable (Lewis, 2003; Monk, 2003).

3.5) mNICD and mHes7 are present in dynamic and mutually exclusive domains in the mouse PSM

We next wanted to ascertain whether XAV939, Roscovitine, and DRB treatments cause a change in the spatial domain of mNICD and mHes7 proteins in addition to the observed effects on the levels of these proteins within the mouse PSM. mNICD and mHes7 have been shown to exhibit dynamic and largely mutually exclusive spatial domains within the mouse PSM (Niwa et al, 2011). However, it is currently not known whether these proteins will exhibit slowed oscillations in the PSM with inhibitor treatments which slow clock oscillations at the transcriptional level. Immunohistochemistry for mNICD using a commercially available antibody, as well as for mHes7 using a custom-made antibody (see Fig. 2.1 for optimisations and Bessho et al, 2003) was performed on E10.5 mouse tails. Initial attempts to achieve specific staining for expression of these proteins on whole embryos were not successful (data not shown). Specific staining was achieved on sagittal paraffin sections with the aid of antigen retrieval and signal amplification (see methods for details). In one embryo, mHes7 exhibited a broad domain of expression with a sharp boundary at the level of the S0 and extending caudally most of the way down the PSM (Fig. 3.5B). In the same embryo, mNICD was present most strongly as a sharp domain in the rostral PSM in the S0, as well as more weakly in the very caudal PSM and caudal somites (Fig. 3.5C). In another embryo the strong domain of mHes7 expression was present in a narrower domain in the S-1 and very weakly in the caudal-most tip of the PSM (Fig. 3.5F). In the same embryo, mNICD was present in the caudal somites and as a strong band of expression in the S0, but the caudal domain of weak expression was extended more rostrally in the PSM (Fig,. 3.5G). The only region containing simultaneous localisation of mNICD and mHes7 was in the very caudal tip of the PSM for the second embryo tested (Fig. 3.5H). This embryo exhibits a late phase 1 of mNICD localisation in the PSM while the first embryo (Fig. 3.5D) exhibited a late phase 3 – early 1 profile of mNICD (as termed by Niwa et al, 2011).

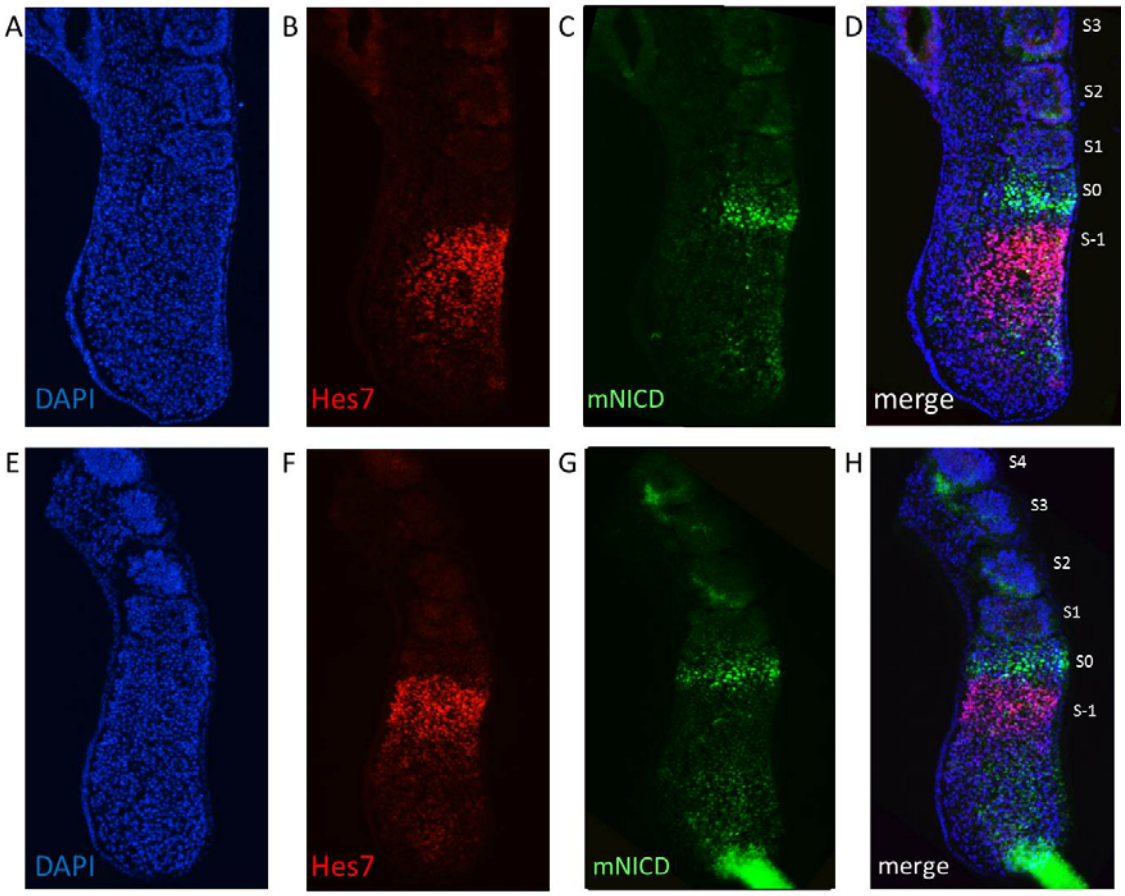

Figure 3.5) mNICD and mHES7 proteins exhibit dynamic and mutually exclusive domains of localisation in the mouse PSM. E10.5 embryonic mouse tails with DAPI stained nuclei (**A, E**) and immunohistochemistry staining on sequential 7uM paraffin sections for mHES7 (**B, F**), and mNICD (**C, G**). The merge images (**D, H**) reveal mutually exclusive domains of mNICD and mHes7 proteins in the mouse PSM. The most recent somite (S1) and previous somites (S2, S3 …) are labelled. The rostral stripe of mNICD is present at the next prospective somite boundary (S0) and mHes7 domain more caudally in the S-1 domain.

mNICD and mHES7 therefore exhibited dynamic and mainly mutually exclusive domains of localisation in the mouse PSM (Fig. 3.5D, H) as has been previously reported by Niwa et al (2011). Immunohistochemistry for mNICD and mHES7 will allow the spatial profile of these clock proteins to be compared between the mouse PSM treated with each inhibitor which slowed oscillations of clock gene transcription and the corresponding DMSO treated control PSM. This will determine whether the oscillation phase of these cycling effectors of Notch signalling are delayed in a similar manner as for oscillating transcripts when treated with XAV939, Roscovitine, and DRB.

The data from Chapter 3 has shown that the effects of Wnt inhibition by XAV939, and the Cdk inhibitors Roscovitine and DRB on slowing transcriptional oscillations of the segmentation clock in the chicken embryo are conserved in the mouse embryo. Similarly, these three inhibitors also showed evidence of increasing the levels of clock proteins related to the Notch signalling pathway in the mouse embryo as for the chick. These outcomes suggest that these inhibitors may target conserved regulatory mechanisms underlying the pacemaker of somitogenesis in the vertebrate PSM. Further assays are required in the mouse embryo to confirm these effects, while parallel studies with the chicken and other vertebrate species will aid the elucidation of the pacemaker mechanisms controlling the period of the segmentation clock.

Chapter 4: Proteomic and Transcriptomic analyses of the chicken PSM following treatment with XAV939, Roscovitine, and DRB

4.1) Analysis of phosphorylation status of NICD in XAV939, Roscovitine, and DRB, treated samples by mass spectrometry analysis

XAV939, Roscovitine, and DRB treatments all consistently increased the level of cNICD protein in the chicken PSM require assessment. Instability of Notch signalling components is important for maintaining oscillations of signalling in different systems including the PSM and in neural stem cell maintenance and differentiation (Bessho et al, 2003; Bonev et al, 2012; Kim et al, 2011; Takashima et al, 2011). Therefore, we predict that the increase in cNICD observed for each of these treatments may represent a stabilisation of cNICD protein which may in turn cause an increase in the period of clock gene oscillations also observed with these inhibitor treatments. A possible mechanism by which XAV939, Roscovitine, and DRB may be able to cause an increase of cNICD protein in the chicken PSM is through the alteration of post-translational modifications that may normally be essential for the turnover of NICD protein. Post-translational modifications such as phosphorylation are common mechanisms used by eukaryotes to mark many proteins for degradation during normal cellular processes (Cohen, 2002). Indeed, it has been reported that NICD is post-translationally modified by various proteins. The two modifications that had been described to affect NICD stability at the time of this work are phosphorylation by CDK8 and GSK3β. CDK8-mediated phosphorylation of NICD in human HeLa cells is required for this protein to be degraded by the ubiquitin ligase FBW7 for normal protein turnover, while expression of kinase-active Cdk8 causes destabilisation of NICD *in vivo* (Fryer et al, 2004). Given that two of the inhibitors found to increase cNICD are cdk inhibitors makes these modifications good candidates to investigate. GSK3β also phosphorylates NICD protein as a negative regulator of Notch activity and stability (Jin et al, 2008; Espinosa et al, 2003).

Closer inspection of the western blots following stability assays sometimes exposed a shift down to generate an additional protein band for cNICD in the lysate treated with the stabilising drug (see Fig. 2.4C,D, top panels). This extra protein band was at a slightly smaller molecular weight than the common cNICD band and not present in the DMSO control. Because the level of cNICD was found to be higher in XAV939, Roscovitine or DRB treated lysates, this shift downwards to a lower molecular weight seen by western blotting could potentially highlight an increase in the portion of unmodified cNICD protein.

Given these findings, we set out to assess the post-translational modification status of cNICD protein in PSM lysates treated with XAV939, Roscovitine, DRB, or the DMSO control vehicle. Although some modifications have already been described for NICD protein (Fryer et al, 2004; Jin et al, 2008; Guarani et al, 2011), there is a lack of antibodies specific to phosphorylated or other variants of NICD. These studies were also performed in other model species, meaning that looking directly at modified levels of cNICD by western blotting or similar techniques was not an option. For these reasons, the proteomic approach chosen for this task was mass spectrometry. Due to the lack of studies with the chicken, there was no peptide ion information available from mass spectrometry for chicken NICD protein. Therefore, the full length amino acid sequence of cNICD was *in silico* digested to generate an inclusion list of peptides for the mass spectrometer to search for in order to identify cNICD protein from the sample lysate (Supplementary Table 1).

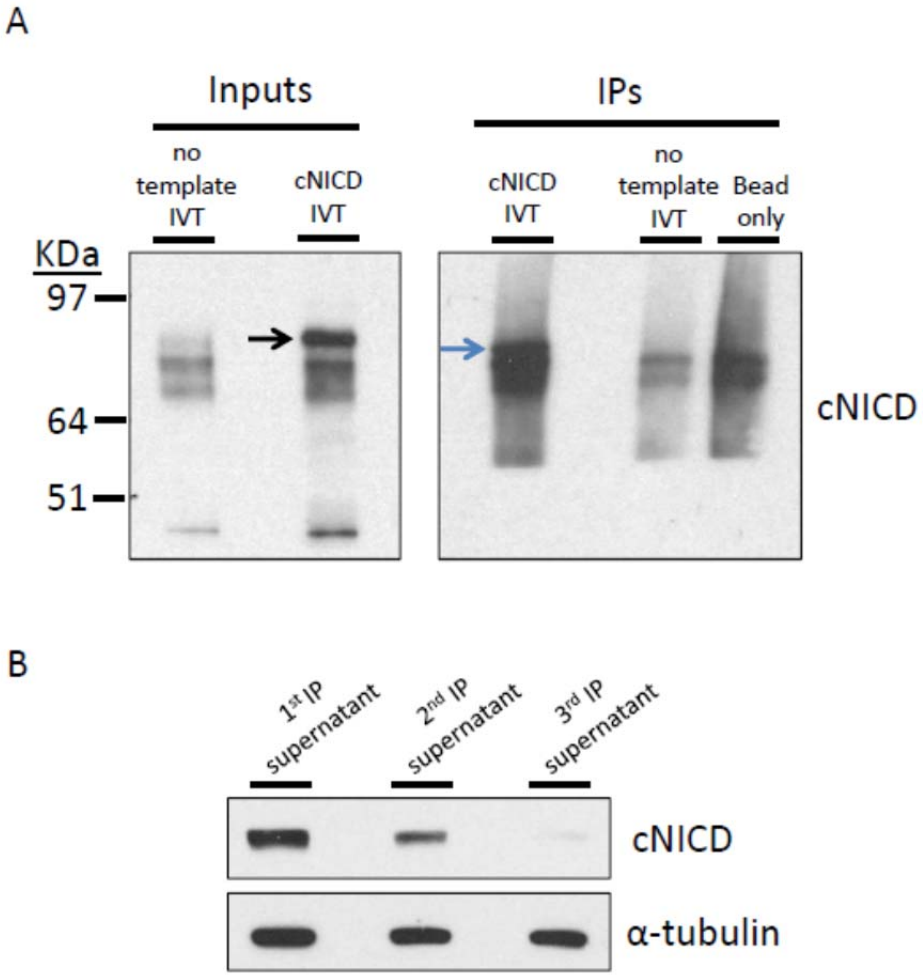

Figure 4.1) Testing the cNICD antibody for Immunoprecipitation of cNICD protein. A) Western blotting with the cNICD antibody confirms the presence of cNICD protein in the cNICD in vitro transcription/translation (IVT) input reaction (lane 2, see black arrow), which is absent in the 'no template' control input reaction (lane 1). cNICD is present following cNICD Immunoprecipitation (IP) on the cNICD IVT reaction (lane 3, see blue arrow), which is absent following IP for cNICD on the 'no template' control IVT (lane 4) or the 'bead only' control IP (lane 5). **B**) Western blotting reveals that cNICD is depleted from the supernatant following each consecutive round of cNICD IP on endogenous chicken lysate.

4.2) Mass spectrometry analysis of recombinant cNICD protein and the Immunoprecipitation enrichment strategy for endogenous cNICD protein prior to mass spectrometry analysis

In silico digestion of cNICD predicted that chymotrypsin would be the most optimal enzyme for digestion in order to create peptides covering the sequence length that were of an amenable size for detection by mass spectrometry. Only the glutamine(Q)-rich region (Fig. 4.2A) was predicted not to digest well with any available enzyme. Sequence alignment revealed that the serine and threonine residues that are phosphorylated by CDK8 and GSK3β respectively in human NICD (Fryer et al, 2004, Jin et al, 2009) are mostly conserved in cNICD and were predicted to be present in viable peptides following chymotrypsin digestion (Fig. 4.2A). For this reason chymotrypsin was chosen as the enzyme to digest samples prior to mass spectrometry analysis.

In order to first confirm that cNICD could be identified by mass spectrometry, the cNICD antibody generated for this study was used for immunoprecipitation (IP) of cNICD from the recombinant cNICD IVT reaction. The cNICD antibody was tested for IP on recombinant cNICD protein which was synthesised with an *in vitro* transcription/translation reaction using full length cNICD expression plasmid DNA (see methods for details). The cNICD antibody was able to identify a specific band for recombinant cNICD at the predicted molecular weight by western blot (Fig. 4.1A, lane 2) which was not present in an IVT reaction with no template DNA (Fig. 4.1A, lane 1). Following cNICD IP on the recombinant cNICD IVT mixture, the cNICD antibody was able to pull down cNICD (Fig. 4.1A, lane 3), which was not present following IPs on either the no-template reaction (Fig. 4.1A, lane 4) or the 'bead only' control (Fig. 2.6A, lane 5).

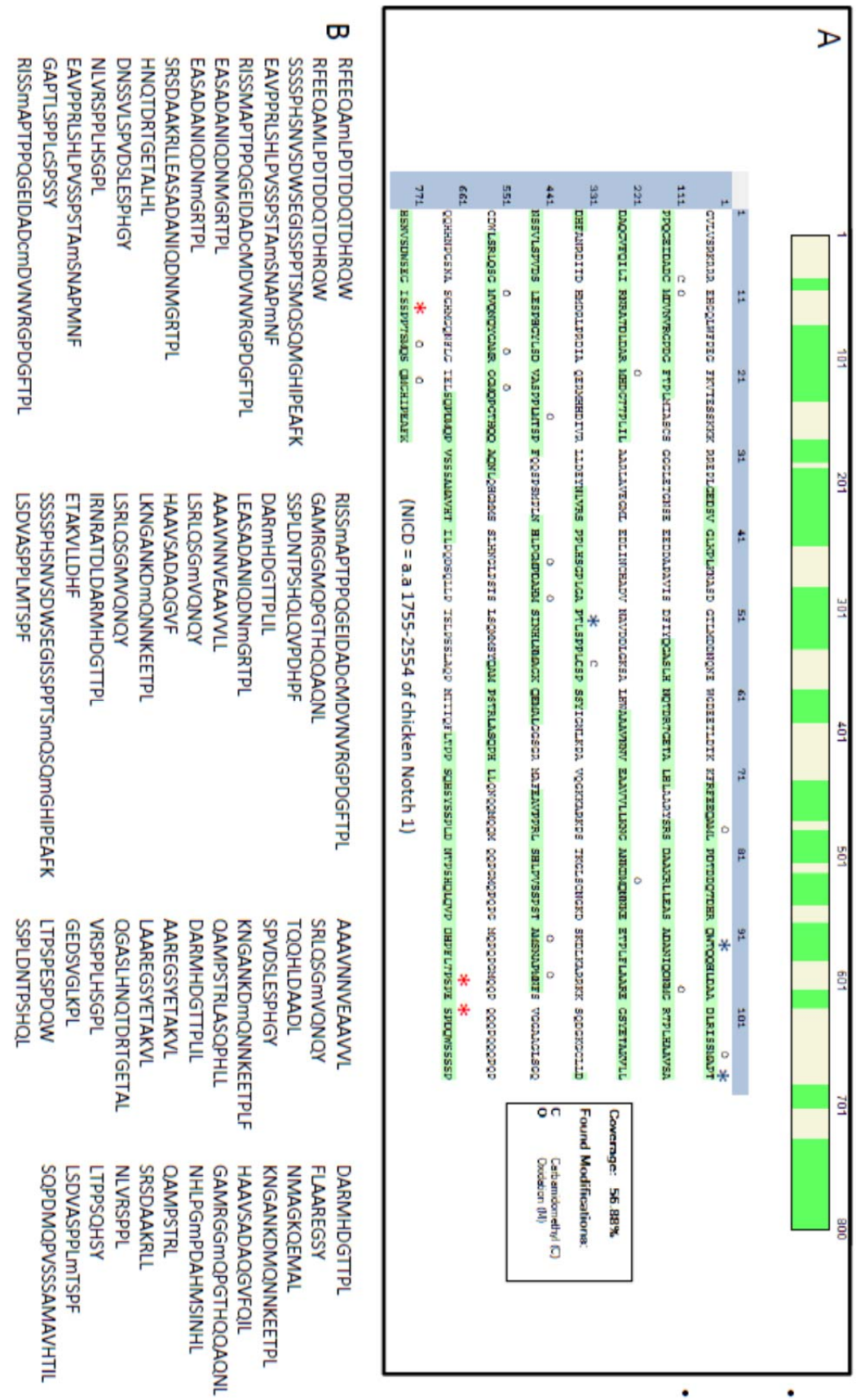

Figure 4.2) Mass spectrometry analysis of cNICD protein. A) Mass spectrometry analysis of chicken NICD protein following chymotrypsin digestion identifies 56.88% of the amino acid

sequence with high confidence. Conserved Threonine (T) residues known to be phosphorylated by GSK3β (Jin et al, 2009, marked with blue asterisk) and Serine (S) residues known to be phosphorylated by CDK8 (Fryer et al, 2004, marked with red asterisk) in human cell lines are labelled on the amino acid sequence of cNICD. Carbamidomethyl (C) and Oxidation (O) modifications found in the cNICD sequence are marked above the corresponding amino acid in the sequence. **B**) The 45 unique peptides identified from cNICD protein, including modified variants.

Subsequently, the sample was chymotrypsin digested following gel processing before analysis by mass spectrometry to search for positive hits from the inclusion list of predicted peptides generated for cNICD (see Supplementary Table 1). Mass spectrometry analysis was able to identify 45 predicted peptides for cNICD protein, giving sequence coverage of 56.88% (Fig. 4.2A,B). This gave a good indication that mass spectrometry could successfully identify cNICD protein and gave physical rather than *in silico* data on peptides to identify from endogenous samples in the future.

Initial attempts to identify cNICD from chicken tail lysate proved unsuccessful, most probably because the levels of cNICD were very low and the lysate contained a complex mixture of many other highly expressed proteins (data not shown). Enrichment for cNICD from the lysate was therefore required before mass spectrometry analysis could be performed. The IP was repeated with the cNICD antibody used to IP the recombinant protein as described above. Mass spectrometry analysis of a pool of 50 half-PSMs following cNICD IP identified only a few peptides specific to cNICD (from the inclusion list built as described above), but not with a sufficient coverage of the full amino acid sequence required to facilitate the later identification and quantification of phosphorylated peptides from cNICD across the amino acid sequence (data not shown).

The PSM tissue pools for mass spectrometry analysis were therefore increased to contain 120 whole PSMs per treatment which is the equivalent of 240 half PSMS (i.e. almost 5 times the amount of starting material). This sample was split into two pools due to the limiting volume of an IP reaction. Western blotting analysis with the cNICD antibody on the recovered IP supernatant revealed that there was still a lot of unbound cNICD left after one round of IP (Fig. 4.1B, first lane). Therefore, the efficiency of the IP was increased by a further two successive rounds of IP on the supernatant run offs, showing that cNICD was almost completely depleted from the unbound supernatant after 3 rounds of IP (Fig. 4.1B). This strategy of 3 successive rounds of cNICD IP was performed on protein lysates from 120 whole chick PSMs for all three inhibitor treatments (XAV939, Roscovitine, DRB) and the DMSO control vehicle treatment. For each sample, the successive IPs have been gel-extracted following SDS-PAGE as a single pooled sample. Each sample has been in-gel digested with chymotrypsin and then treated with titanium dioxide (TiO_2) to enrich for phosphorylated peptides. By pouring the sample over TiO_2-coated beads, the TiO_2 ligand binds to peptides phosphorylated at Serines, Tyrosines, or Threonines and therefore allows enrichment of phosphopeptides while the unmodified peptides in the mixture will flow through the column. These samples have been sent to Thermo (Hemel Hempsted, UK) to be run by mass spectrometry to quantify the levels of any phospho-peptides from cNICD protein within each treated sample, along with TiO_2 column flow through which will allow normalisation of starting amounts of NICD and thereby allowing quantification of phospho-species by comparing these relative to unmodified peptides from each sample treatment.

Mass spectrometry will be performed to assess the phosphorylation status of cNICD in the chicken PSM and whether this is altered by the 3 inhibitors (XAV939, Roscovitine, and DRB) which increase the level of cNICD and slow oscillating clock gene transcription in the chicken PSM. Any residues in cNICD protein found to be significantly altered in the level of phosphorylation by these drugs may reveal key sites of post-translational modification and their kinases that may be required to regulate rapid NICD turnover in the PSM. Future

experimental assays whereby these sites are changed by amino acid substitution will reveal whether this can cause an increase the level of cNICD and the period of somitogenesis as for XAV939, Roscovitine, and DRB treatments. This would categorically link the stability of activated Notch protein to the period of the segmentation clock as we predict.

4.3) Transcriptomic analyses of chicken PSMs treated with XAV939, Roscovitine, or DRB

The data to this point has shown that XAV939, Roscovitine, and DRB all delay *cLfng* oscillations and increase cNICD protein in the chicken PSM. Although the two CDK inhibitors appeared to have the same effects on phosphorylation of RNA pol II and β-catenin, these effects were not shared by XAV939 treatment. There was therefore some discrepancy between the inhibitors, making it unclear as to whether the 3 inhibitors were affecting the pace of clock gene oscillations through a common target mechanism, or through different targets. To elucidate whether common gene targets or pathways were affected by all three inhibitors, transcriptomic analyses were performed for each -/+ drug treatment using both custom chicken microarrays and Next generation RNA sequencing (RNA-seq). Corroboration between the two techniques gives a greater confidence that changes in gene expression with different treatments are reliable.

Single -/+ half-PSM explant paired samples were prepared and cultured as for stability assay samples before total RNA was extracted from each individual sample to be run by RNA-seq analysis, and to prepare cDNA to be run by microarray analysis. Each drug treatment assay was performed in quadruplicate. The sex of the samples was confirmed by quantitative PCR (qPCR), which revealed that both sexes were represented in replicates from each drug treatment to reduce the potential bias in the representation of certain genes which show variable expression between sexes (Supplementary Table 2).

RNA-seq data reads for transcripts were aligned to the latest *Gallus gallus* rel 75 transcriptome annotations from Ensemble as this generally improved the alignment of reads using these latest annotations when compared to the chicken genome annotations (data not shown). RNA-seq analysis revealed that 669 transcripts were differentially expressed with XAV939 treatment, with 44.5% of these showing an increase and 55.5% showing a decrease (Table 4.1). Gene Ontology (GO) terms analysis found that the Wnt signalling pathway was significantly enriched within the list of differentially expressed genes to confirm that XAV939 does target Wnt signalling (Supplementary Table 3). This revealed that while a few Wnt signalling components were upregulated (*Dkk1, Fzd1, Frzb1*), the majority were downregulated as expected (*Snail2, Wnt11, Tbx6, Lins, Nkd1, Spry2*). The increase in *Dkk1* expression was not surprising given that it is also a Wnt signalling inhibitor itself. *Axin2* also appeared downregulated by XAV939 as was shown by ISH, however the log2 fold-change was not great enough to be statistically significant ($p<0.05$ cut-off). Interestingly, transcription of *Snail2* is shown to oscillate in the chicken PSM under the control of Wnt and Fgf signalling (Dale et al, 2006). *Snail2* was the only characterised clock gene found to be differentially expressed by any of the three drug treatments by RNA-seq, being downregulated only by XAV939 to confirm the requirement for Wnt signalling for its expression.

During the study, the newer *Galgal*4 build of the chicken genome was released by Ensemble 74. Therefore, the reads from the microarray were aligned to the new annotations before analysing differential gene expression for the three drug treatments. Microarray analysis revealed that 46 probe sets (45 annotated) were differentially expressed with XAV939 treatment, with 17.8% upregulated and 82.2% downregulated (Table1). However, GO terms analysis did not return any significantly enriched GO terms, presumably due to the number of targets being much smaller than found by RNA-seq.

	Number of Upregulated Annotated Genes/Probe-sets	Number of Downregulated Annotated Genes/Probe-sets	Total Number of Significantly Differentially Expressed Targets
XAV9393 – RNA-seq	298 (44.5%)	371 (55.5%)	669
XAV939 – Microarray	8 (17.8%)	37 (82.2%)	45
Roscovitine– RNA-seq	920 (40.6%)	1347 (59.4%)	2267
Roscovitine-Microarray	604 (23.0%)	2027 (77.0%)	2631
DRB – RNA-seq	114 (36.7%)	197 (63.3%)	311
DRB - Microarray	97 (13.6%)	616 (86.4%)	713

Table 4.1) Summary of Differentially Expressed Targets revealed by RNA-sequencing and Microarray analyses for XAV939, Roscovitine, and DRB treatments.

RNA-seq analysis found that 2267 transcripts were significantly differentially expressed under Roscovitine treatment, with 40.6% showing an increase and 59.4% showing a decrease. 311 transcripts were found to be differentially expressed by DRB using RNA-seq analysis, with 36.7% upregulated and 63.3% downregulated (Table 4.1). The fact that DRB appeared to affect far fewer targets than Roscovitine is perhaps not surprising given that Roscovitine is shown to target the activity of more Cdks than DRB does. Among the most significantly enriched GO terms for the Roscovitine differentially transcripts were genes involved in cell cycle regulation as well as transcription, as expected (Supplementary Table 4). GO terms for chromatin modification and chromosome organisation were both also significantly enriched for the set of differentially expressed transcripts by each of the cdk inhibitors (Supplementary Tables 4, 5, 8). Microarray analyses suggested that 3670 probe-sets, matching to 2631 annotated probes, showed differential expression with Roscovitine treatment. Of these, the majority were downregulated (77.0%) and the rest upregulated (23.0%). Microarray analyses suggested that 999 probe-sets, matching to 713 annotated probes, showed differential expression with Roscovitine treatment. Of these, the majority were downregulated (86.4%) and the rest upregulated (13.6%) (Table 4.1). GO terms analyses of the Microarray data for Roscovitine and DRB treatments confirmed the findings of the RNA-seq data, as genes involved in processes

including cell cycle progression, chromatin modification, and transcription regulation were significantly enriched for these treatments (Supplementary Tables 6 & 7).

A greater percentage of the differentially expressed targets showed a downregulation for the Cdk inhibitors when compared to the Wnt inhibitor XAV939. This is most probably because Roscovitine and DRB both act to inhibit RNA pol II dependent transcription and are therefore likely to repress transcription more globally than the Wnt inhibitor XAV939. This is supported by the finding that the Cdk inhibitors, and not XAV939, were able to reduce Cdk-mediated phosphorylation of RNA pol II in the chicken PSM. Indeed, the GO terms analysis of both the RNA-seq and Microarray datasets did not suggest that Wnt signalling was affected by either of the cdk inhibitors (Supplementary Figs. 4-7), just as neither of these inhibitors affected phosphorylation of β-catenin. In addition, both the RNA-seq and Microarray data suggested that the amount of overlap in terms of targets affected by both cdk inhibitors was much greater than when comparing XAV939 to either of Roscovitine or DRB (Fig.4.3A,B). These findings point to a different mode of action when comparing XAV939 to the cdk inhibitors.

When assessing the common targets found to be differentially expressed for both Roscovitine and DRB treatments, again the majority of targets were downregulated with RNA-seq revealing that 377/572 (65.9%) transcripts were downregulated (Fig. 4.3A). GO terms analysis of the datasets from both RNA-seq and Microarray confirmed that targets commonly affected by both cdk inhibitors included genes involved in chromatin modification and organisation, as well as regulators of transcription and the cell cycle (Supplementary Tables 8 & 9). Indeed, the genes *ccnt2* (*Cyclin T2*) and *cdk7* showed downregulation by both Roscovitine and DRB treatments by RNA-seq, while Roscovitine in particular affected the expression of a larger range of global transcriptional and cell cycle regulators which were mostly downregulated including *cdk17*, *ccnd3 (Cyclin D3), ccnb2 (Cyclin B2), ccny (Cyclin Y), ccnf (Cylin F), ccnl1 (Cyclin L1), ccna2 (Cyclin A2),* and *ccne2 (Cyclin E2*). Both RNA-seq and Microarray suggested that transcription of cdk9 itself was upregulated by Roscovitine, while Microarray suggested that

both Roscovitine and DRB downregulated the cyclin genes *ccny*, *ccnb2*, and *ccna2*. Overall the cdk inhibitors showed very similar effects, largely repressing expression of regulators involved in global transcription and cell cycle as expected.

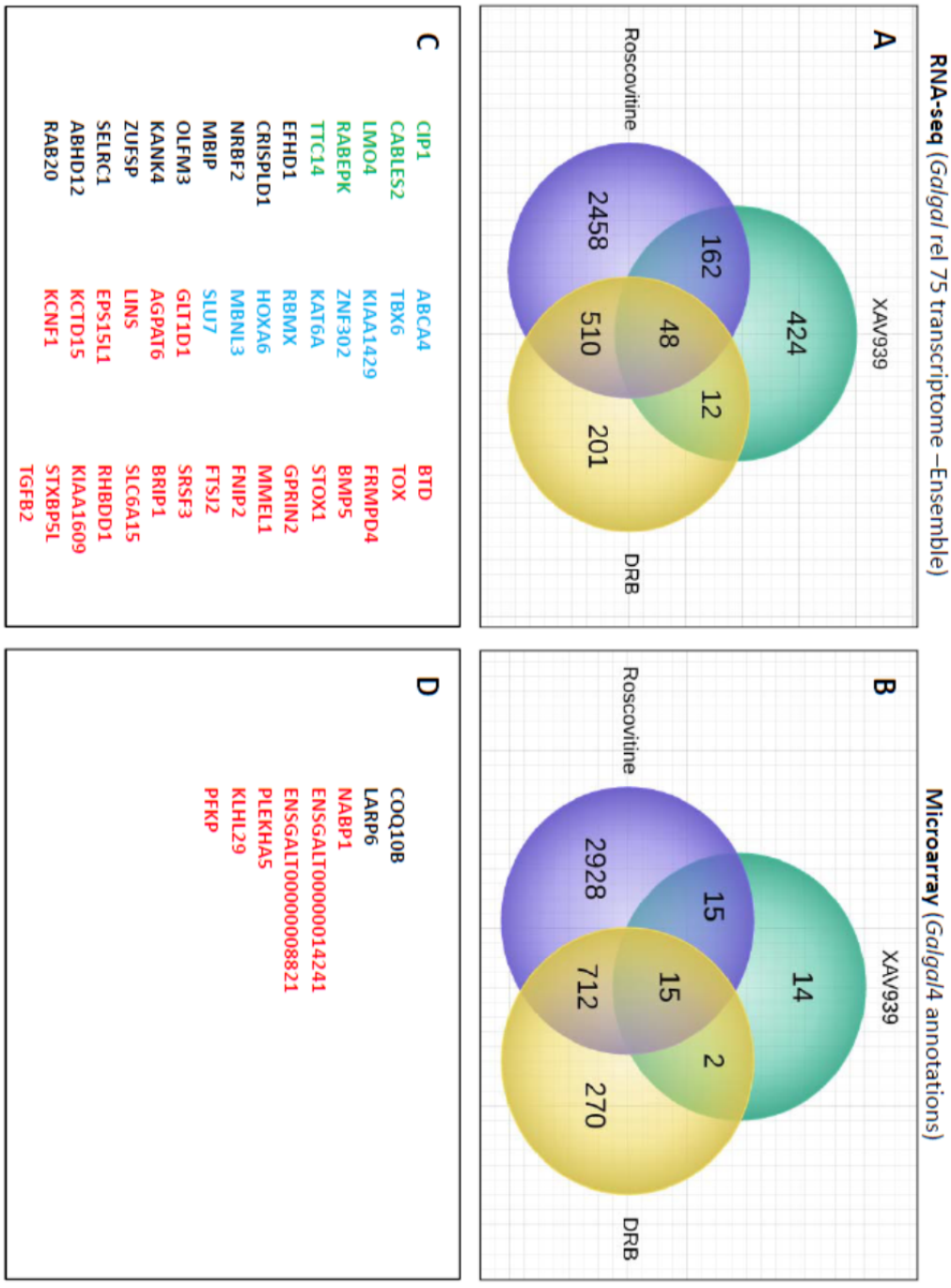

Figure 4.3) Genomic analyses of gene expression changes in the chicken PSM following XAV939, Roscovitine, and DRB treatments. Venn diagrams showing the number of genes with significantly altered expression in the PSM relative to the control for XAV939, Roscovitine, and

DRB treatments by RNA-seq analyses (**A**) and Microarray analyses (**B**) (cut-off of p=0.05 significance for $\log_2$ fold-change relative to DMSO). RNA-seq analysis using the *Gallus gallus* rel 75 Ensemble transcriptome annotations (**A**). Microarray analysis using the *Galgal*4 genome annotations (**B**). **C**) The 46 annotated genes significantly affected by all three drug treatments from the RNA-seq datasets. **D**) The 8 annotated genes significantly affected by all three drug treatments from the Microarray datasets. (Targets in **C** and **D** in Green = upregulated by all three inhibitors, Black = upregulated by XAV939, while downregulated by Roscovitine and DRB, Blue = Upregulated by Roscovitine and DRB, while downregulated by XAV939, Red = downregulated by all three inhibitors.)

Although the much greater overlap between the two cdk inhibitors suggests that they act through a different mechanism to the Wnt inhibitor XAV939 to slow clock gene oscillations in the PSM, the remaining possibility that they affect a common mechanism to XAV939 required assessment by viewing targets commonly affected by all three inhibitors in the PSM. RNA-seq uncovered 48 transcripts differentially expressed for all three inhibitor treatments. 46 of these transcripts mapped to annotated genes (Fig. 4.3C), of which 5 showed upregulation in all three treatments. The gene *CIP1* (encoding the p21 protein) shown the highest fold-change increase of the genes significantly affected by all three drug treatments. p21 is a cdk inhibitor and a key regulator of cell growth and apoptosis and has previously been shown to be a target of Roscovitine (Chang et al, 2000; He et al, 2005; Zhang et al, 2010). This makes p21 an excellent candidate to study further as a regulator in the pace control of the segmentation clock.

The direction of change for all of the targets in this list of 46 genes was the same for the two cdk inhibitors, supporting evidence that they affect similar processes in the PSM. 10 genes showed upregulation by XAV939, but downregulation with Roscovitine and DRB. Conversely, 9 targets were downregulated by XAV939, but upregulated by the cdk inhibitors. This included *Tbx6*, which is a marker of PSM identity as well as regulated by Wnt signalling, making the

downregulation by XAV939 an expected outcome. However, the fact that the cdk inhibitors had the opposite effect on the level of *Tbx6* transcription brings into question whether the effects of these drugs on *Tbx6* expression has any significance to the effects on the segmentation clock or if they are simply incidental. The remaining 22 targets were downregulated by all three inhibitors, including *Transforming growth factor beta 2* (TGFβ2) and *Bone morphogenic protein 5* (*BMP5*). BMPs are members of the transforming growth factor beta (TGFβ) family and are known to be antagonised by Noggin in the development of the somites and chondrocyte differentiation (McMahon et al, 1998; Murtaugh et al, 1999). *LINS* (Lines *Drosophila* homologue) was another gene significantly downregulated by all three inhibitors by RNA-seq analysis. LINS is a Wnt signalling target, as well as a modulator of Wnt signalling and a known segment polarity gene in *Drosophila* (Katoh, 2002). Gene ontology (GO) terms analysis of the 46 targets affected by all three treatments with RNA-seq analysis identified only 'Regulation of cell division' as a particular functional pathway that was significantly affected by all three drugs compared to the background list of all genes. However, proliferation did not appear affected by these inhibitors and this group contained just 2 targets; with *Cdk5 and Abl enzyme substrate 2 (Cables2*) showing upregulation by all inhibitors, while *TGFβ2* was downregulated by all three treatments. Overall, these data did not suggest a key functional pathway was affected by all three inhibitors, suggesting that XAV939 affects the segmentation clock via a different mode of action to the cdk inhibitors.

Microarray found 15 probe-sets whose expression was significantly affected by all three drugs, mapping to 6 annotated genes and two unannotated gene IDs (Fig. 4.3D). 6 of these targets showed downregulation by all three inhibitors, with only two targets upregulated for XAV939, but downregulated by the cdk inhibitors (Fig. 4.3D). However, none of these targets were common to the list of 46 common targets to all three inhibitors found by RNA-seq and as expected, GO terms analysis failed to identify any functional pathway enriched from such a small number of genes. The differences in targets and the lower number of targets found to be differentially expressed by each treatment with Microarray when compared to RNA-seq may

highlight the limitations of Microarray as a genomic approach due to the limited number of pre-defined probes to annotated genes.

Given that these inhibitors affect the expression Notch-regulated components of the segmentation clock, the effects on expression of Notch signalling components were assessed by each inhibitor from the transcriptomic data. RNA-seq suggested that XAV939 in particular downregulated transcription of *Maml2*. Maml is a co-factor of NICD binding to target promoters and additionally has been shown to be required for the recruitment of Cdk8/CyclinC to phosphorylate NICD in promoting rapid turnover of active Notch (Fryer et al, 2004). This suggests that XAV939 may be able to promote NICD stability by inhibition of Maml2 expression in the PSM and subsequently repress Cdk8-mediated degradation of NICD. Roscovitine and DRB treatments both upregulated *Notch1,* while Roscovitine upregulated *Nrarp* transcription when viewed by RNA-seq analysis. The increase in *Notch1* transcription by Roscovitine and DRB seen by RNA-seq supports the hypothesis that the increase in the level of activated Notch1 protein by these treatments seen by Western blotting is due to an induction of Notch1 expression in the PSM. However, Roscovitine treatment also downregulated transcription of *Sirt1*, which encodes a de-acetylase that is shown to destabilise NICD in endothelial cells by counteracting acetylation-mediated stabilisation of active Notch protein (Guarani et al, 2011). Thus the possibility that Roscovitine increases cNICD levels in the PSM by altering the levels of its post-translational modifications cannot be ruled out. Certainly, the enrichment for GO terms of genes involved in protein catabolic process and protein acetylation amongst GO terms enriched by Roscovitine and DRB treatments support this as a potential mechanism.

Microarray suggested that only Roscovitine promoted *Lfng* transcription, while both Roscovitine and DRB inhibited transcription of *Hey2*. However, neither the RNA-seq data, nor ISH staining suggested that *Lfng* expression was increased significantly in the PSM with any of the inhibitors and further analysis of *Hey2* expression in the PSM by ISH staining is required. The transcriptomic data therefore revealed that, with the exception of XAV939 treatment on

Snail2 and the exceptions mentioned above, clock genes were generally not affected in the level of their transcription by any of the three inhibitors. This confirms what was seen by ISH staining, as XAV939, Roscovitine, and DRB all delay the oscillation phase of clock genes but did not obviously affect the level of their expression in the chicken PSM. The transcriptomic data on -/+ drug treated half-PSM pairs does however provide another source of information. Rather than looking at differentially expressed targets, it is also possible to find transcripts whose levels are most variable by comparing individual replicates. This can first be validated by confirming that previously characterised clock genes such as *Lfng* and *Hairy1/2* are among such targets before analysing other targets exhibiting variable expression that may reveal currently unknown clock genes in the PSM.

Overall, the transcriptomic data suggest that XAV939 affects the expression of a different set of targets to the cdk inhibitors. This supports the findings from Chapter 1 which show that XAV939 represses canonical Wnt signalling while the cdk inhibitors repress RNA pol II dependent transcription regulated by the activity of cdks 7-9. RNA-seq and microarray have revealed a set of targets differentially expressed with each inhibitor treatments that provide a short-list of candidate regulators of the segmentation clock pacemaker mechanism to pursue further with functional studies.

4.4) Data mining screen for potential cycling regulators of cNICD turnover in the PSM

The transcriptomic data in this study revealed a number of targets whose expression was affected by XAV939, Roscovitine, and DRB which may include transcriptional regulators of the segmentation clock. Previous genome-wide studies from Dequeant et al. (2006) and Krol et al. (2011) attempted to elucidate genes present in the PSM of the mouse, chicken and zebrafish that may be oscillating at the transcriptional level in the manner of previously characterised 'clock' genes. These studies used one side of the PSM from different embryos of the same species to stain by ISH for a clock gene in order to create a 'time-series' encompassing more than a complete oscillation cycle. Nucleic acid from the other side of the PSM in each of the

corresponding embryos was then used to perform microarray analyses to identify other genes that appeared to oscillate significantly in their expression level during the cycle. These studies therefore provided useful resources from which to search for potential regulators of the segmentation clock mechanism that have not been characterised.

The data from this study so far has suggested that cNICD localisation is oscillatory in the chicken PSM, as well as increased when oscillations of clock gene transcription are slowed. It is possible that cNICD is actively degraded by one or more proteolytic enzymes which may themselves be expressed in an oscillatory manner in the PSM. These could be targets of the inhibitors shown to both delay *cLfng* oscillations and increase cNICD in this study. E3 ligases are common regulators of protein degradation and ubiquitinate their targets for degradation by the ubiquitin proteasome (Desterro et al, 2000). These are therefore good candidates to search for potential cycling regulators of cNICD protein degradation within the PSM.

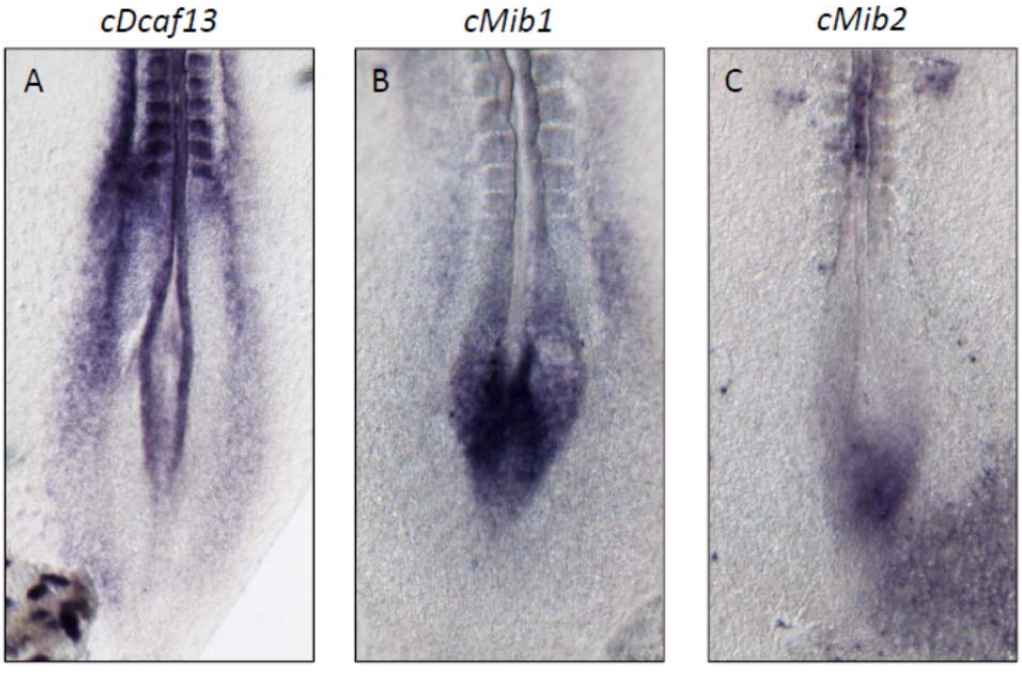

Figure 4.4) Expression analysis of cDcaf13, cMib1, cMib2 in the chicken embryo tail. Dorsal views of *In Situ* Hybridisation analysis of *cDcaf13* (**A**), *cMib1* (**B**), and *cMib2* (**C**) in HH10 chicken embryo tails.

The mouse and chicken datasets by Dequeant et al. (2006) and Krol et al. (2011) were first searched in collaboration with Amit Garg (University of Dundee) for the presence of any E3 ligases. Once identified, the expression profiles of the E3 ligases from each dataset were analysed to find those genes that appeared to oscillate in the PSM (methods previously described by Dequeant et al, 2006 and Krol et al, 2011). The data from Krol et al, (2011) suggested that *DDB1 And CUL4 Associated Factor 13 (Dcaf13)* expression was significantly oscillatory in both the chicken and mouse PSM, while *Mindbomb 2 (Mib2)* was significantly oscillatory in the chicken PSM. *Mindbomb 1 (Mib1)* expression was not shown to be significantly dynamic. However, the p-value obtained for *Mib1* in the chicken PSM was very low and given that *Mib1* and *Mib2* are already shown to regulate Notch activity made these excellent targets to assess further (Itoh et al, 2003). These three genes were chosen to make plasmids for the synthesis of antisense-RNA probes to visualise the transcripts by ISH within the tails of chicken embryos. This would confirm whether these transcripts do indeed display dynamic domains of expression in the PSM in the manner of clock genes (plasmid insert sequences shown in methods).

cDaf13 expression was clear in the formed somites, NT and LPM flanking the PSM (n=4), as well as one embryo exhibiting a diffuse band of expression in the very rostral PSM in the S0 region which is characteristic of many clock genes (Fig. 2.8A). However, staining of more embryos is required to confirm whether *cDcaf13* is indeed expressed in the PSM and whether this expression is oscillatory in the manner of a clock gene. *cMib1* (Fig. 2.8B, n=2/3) and *cMib2* (Fig. 2.8C, n=4/4) exhibited expression clearly in the very caudal open neural tube but no obvious expression in the PSM. ISH analysis may not be sensitive enough to observe dynamic transcription of certain genes seen by microarray as suggested by Krol et al (2011). Alternatively, these genes may oscillate in other tissues that were not efficiently removed from the embryo tail prior to microarray analyses by Dequeant et al. (2006) and Krol et al. (2011). Lastly it may be that higher numbers of embryos is required and Fix and culture analysis performed to confirm oscillating expression in the PSM. Any transcripts of ubiquitin ligases

found to oscillate within the PSM could then be viewed following treatment with XAV939, Roscovitine, or DRB to assess whether such cycling regulators of protein degradation are targeted by these inhibitors. These assays may reveal the potential mode of action by which these inhibitors are able to slow the segmentation clock and increase the level of cNICD.

The data from Chapter 4 has shown that we have successfully identified peptides from recombinant cNICD protein by mass spectrometry. This provides real spectral data from which to identify cNICD from endogenous samples with the aim of assessing whether inhibitors which increase the level of cNICD in the PSM do so by altering post-translational modifications and thereby stabilise active Notch protein as a mechanism that causes an increased period of the segmentation clock. Transcriptomic analyses of the chicken PSM also revealed targets showing differential expression with each of these inhibitor treatments that slow the segmentation clock, which indicates a set of candidates to test as potential regulators of the pacemaker of oscillating transcription in the PSM.

Discussion

Slowing oscillations of clock gene transcription in the Chicken PSM

This study aimed to elucidate the molecular mechanism regulating the pace of the somitogenesis clock. It has previously been suggested that inhibition of Wnt signalling with the drug CKI7 in the PSM of both chick and mouse causes an increased period of clock gene oscillation (Gibb et al, 2009, Gibb et al, 2010; Gonzalez et al, 2013). However another report has in fact given evidence that induction of Wnt signalling also slows the segmentation clock in the mouse PSM (Gonzalez et al, 2013). It should be noted that CKI7 treatment caused downregulation of targets from several other signalling pathways in the caudal embryo, leading to speculation as to the importance of Wnt signalling in the regulation of clock gene oscillations (Gibb et al, 2010, unpublished communication).

XAV939 was used in this study as a specific inhibitor of Wnt signalling, consistently downregulating transcription of the Wnt target *Axin2* in both the chicken and mouse PSM. XAV939 treatment also increased GSK3β-mediated phosphorylation of β-catenin protein in the chicken PSM, which is an active mark for degradation of β-catenin and therefore Wnt inhibition. I have shown that cycling transcription of Notch target genes is delayed in the PSM of both chicken and mouse embryos when treated with the canonical Wnt inhibitor XAV939. However, the transcription of genes from other signalling pathways including Fgf and Shh was also generally found to be downregulated in the posterior chicken embryo. However, these data do not put in doubt the specificity of XAV since the downregulation of the Fgf target *cSpry2* by XAV939 could be an indirect effect as the Fgf and Wnt signalling pathways have been shown to co-regulate each other in the embryo tail during embryonic development (Aulehla et al, 2003; Boulet and Capecchi, 2012; Gibb et al, 2009; Naiche et al, 2011; Stulberg et al, 2012; Wahl et al, 2007). Similarly, cross regulation between Shh and Wnt pathways has previously been reported in somites (Munsterberg et al, 1995), which is the tissue where the downregulation of the Shh target *Gli1* was seen in the presence of XAV939. No effect was seen

in the LPM by XAV939, which is the other site of *Gli1* expression in these explants. Interestingly, aside from being delayed in their oscillation phase in the PSM, the cycling Notch target transcripts *cLfng* and *cHairy2* did not generally appear downregulated by XAV939 treatment by either ISH or transcriptomic analyses.

The Effect of XAV939 to delay oscillations of *cLfng* and *cHairy2* transcription in the chicken PSM was an effect shared by the cdk inhibitors DRB and Roscovitine. Both of these drugs act to inhibit the kinase activity of Cdk7, 8 and Cdk9 on the CTD of RNA pol II (Chodosh et al, 1989; MacCallum et al, 2005, Malumbres and Barbacid, 2009). This was confirmed by the reduction of Serine 5 phosphorylation seen on RNA pol II in the chicken PSM treated with either inhibitor. This particular modification is known to be mediated by Cdk7, Cdk8, and Cdk9 (Galbraith et al, 2010), suggesting that DRB and Roscovitine both inhibit the activity of Cdks involved in regulating global transcription at the same concentrations at which they delay oscillations of clock genes in the PSM. At the same concentrations, these drugs appeared to have no significant effect on cell proliferation in the PSM. Importantly, this separates their effects on the segmentation clock from their effects on the cell cycle. It also supports evidence that the cell cycle is not important in regulating the pace of clock gene oscillations. These outcomes are in contrast to studies which suggested that heat-shock induced periodic somite abnormalities are due to effects on the cell cycle (Stern et al, 1988). The ‘clock and wavefront’ model of somitogenesis is now widely favoured over the ‘cell cycle model’ (Cooke and Zeeman, 1976; Stern et al, 1988), as live reporters reveal that the oscillation period of clock gene expression in the PSM matches the period of somite formation (Aulehla et al, 2008; Takashima et al, 2011).

When the expression of Wnt signalling components was viewed in the chicken PSM, it was clear that *cAxin2* transcription was downregulated by both cdk inhibitors. However, phosphorylation of the Wnt effector protein β-catenin was unaffected by both of these drugs. Given that both Roscovitine and DRB were shown to inhibit phosphorylation of RNA pol II, it is

more likely that *cAxin2* downregulation by these inhibitors was due to a more general effect on global transcription rather than specific inhibition of Wnt signalling in the caudal chicken embryo. This was supported by the downregulation of transcripts from other signalling pathways seen for both DRB and Roscovitine treatments in the chicken tail. Interestingly, the cycling Notch targets *cLfng* and *cHairy2* were only delayed in the PSM and not generally downregulated, similar to what was seen for XAV939 treatment. It has been reported that certain gene transcripts are more susceptible to downregulation by DRB treatment than others (Chodosh et al, 1989; Wada et al, 1998; Zandomeni et al, 1982).

XAV939, DRB, and Roscovitine treatments all consistently downregulated the Shh target *cGli1* in the chicken (XAV939 only in somites tissue but not in lateral plate mesoderm, whereas DRB, and Roscovitine affected both sites of expression). It has previously been reported that Shh signalling may be important in the regulation of oscillatory transcription of Notch targets in the PSM, through use of the small molecule inhibitor Cyclopamine which was reported to cause a delay in the oscillation phase of *cHairy2* within the chicken PSM (Resende et al, 2010). However, this effect was only evidenced for culture periods of more than 6 hours. It is generally considered unadvisable to culture PSM explants for periods longer than 6 hours because the explants lack the tail bud and therefore do not extend their AP axis during culture. The length of the remaining un-segmented PSM tissue becomes progressively shorter until it is too short along the AP axis to accurately identify the oscillation phase of cycling gene expression. It was also shown by Gibb (unpublished) that using Cyclopamine at twice the concentration as used by Resende et al (2010) had no effect on oscillations of *cLfng* transcription, despite *cGli1* being consistently down regulated.

My findings in this study also gave no evidence for a role of Shh signalling in the regulation of the segmentation clock, as *cLfng* oscillations were unaffected by Cyclopamine at both 25 µM and 50 µM. It is therefore most likely that the downregulation of the Shh target *cGli1* by XAV939, Roscovitine, and DRB was independent of their effects on delaying clock gene

oscillation. *cGli1* may just have been one of multiple targets whose transcription was downregulated by these inhibitors, rather than a specific effect on Shh signalling. Alternatively, evidence that Wnt and Shh signalling pathways interact during somite maturation (Munsterberg et al, 1995) suggest that XAV939 may indirectly affect Shh signalling targets through inhibition of Wnt signalling. It should be noted that the NC, a potent source of the Shh morphogen, will generally have been localised to either the right or left half-PSM explant upon bisecting the PSM down the midline for these studies. This provided a potential source of bias in the results. However, care was taken to choose the explant side at random for the drug treatment and its control. In summary, the observations in this report suggest that Shh does not have a role in the pace of clock gene oscillations.

Oscillating cNICD protein expression is increased in the Chicken PSM when the clock is slowed

We successfully generated a custom made antibody to the intracellular portion of the chick Notch1 receptor (cNICD). This serves as a read-out of active Notch signalling. Immunohistochemistry revealed that cNICD is present in the caudal domain of the formed somites, while exhibiting different localisation patterns within the PSM of different chick embryos. These localisation profiles were characteristic of the 3 oscillation phases seen for NICD protein in the mouse PSM and therefore suggested that cycling Notch activation is a conserved feature within the vertebrate PSM (Niwa et al, 2011).

Expression of Mesp2 in the rostral somite compartment inhibits NICD production here, thus restricting NICD to the caudal domain of formed somites in the mouse embryo (Sasaki et al, 2011). This has been shown to be important for establishing the rostral-caudal (RC) patterning of somites (Saga et al., 1997; Takahashi et al., 2000). Conversely, transcription of the chicken *Mesp2* homologue *cMeso2* is present in the caudal compartment of formed somites in the chicken embryo (Buchberger et al, 2002). Given that NICD localisation does appear conserved in the caudal somite compartment in the chicken makes it unclear whether the relationship between Notch activity and Meso2 expression is conserved in the chicken tail for the establishment of RC somite patterning. Double immunohistochemistry for NICD and Meso2 on chicken tail sections would uncover the spatial profiles of these two proteins within the same embryo and aid clarification on whether this mechanism is a conserved feature of somitogenesis.

The technical difficulties during optimisation of the novel cNICD antibody for immunohistochemistry meant that specific staining was achieved on sections from only a few different embryo tails. Although the differing domains of NICD within the PSM are good evidence for dynamic Notch activation, cNICD immunohistochemistry on more embryos is required to be confident that this phenomenon is real. Fix and culture assays as depicted in

Figure 1.1D will strengthen the evidence for Notch activation cycling in the chicken PSM, as an advance in the observed domain of oscillating cNICD within the PSM side cultured for longer would confirm that the domain of cNICD production is indeed dynamic in the chicken PSM. cNICD immunohistochemistry on similar assays for -/+ XAV939, Roscovitine, and DRB would uncover whether the spatial profile of NICD is affected in the PSM by inhibitors which delay cycling clock gene mRNA expression. NICD protein is shown to be inherently unstable in the mouse PSM as well as oscillatory (Huppert et al, 2005; Niwa et al, 2011), while studies in cell culture reveal that NICD is rapidly degraded by the E3 ligase Fbw7 to maintain rapid turnover of active Notch at the target promoter (Fryer et al, 2004). Therefore, it is possible that XAV939, Roscovitine, and DRB will delay the domain of Notch activation in the PSM in a similar manner as for the cycling Notch target gene transcripts *cLfng* and *cHairy2*. However, another possible outcome would be that cNICD protein would be stabilised across the PSM, with less defined spatial phases of oscillation as seen in the mouse embryo when subjected to hypoxic conditions during early development (Sparrow et al, 2012).

As a complementary approach the cNICD antibody generated for this study was used for Western Blotting analysis to compare the levels of NICD protein in chicken half-PSM lysates treated with -/+ XAV939, Roscovitine, and DRB. cNICD was found to be significantly higher in the PSM treated with all three of these inhibitors relative to their respective DMSO controls. Mathematical models had previously predicted this outcome, as an increase in the stability of clock gene protein products within the PSM was shown to result in an extended period of the clock (Lewis, 2003; Monk, 2003). These inhibitor assays give the first experimental evidence that the level of cNICD protein is higher in the PSM where cycling gene transcription is slowed, suggesting that the increase in clock period results from an increase in the level of active Notch. This result is similar to *Nrarp*-null mice, which display an extended period of somite formation and increased NICD levels in the PSM (Kim et al, 2011). In the same study, dynamic phases of clock genes were still observed in the PSM of *Nrarp*-null mice, although the pace of clock gene oscillations was not assessed (Kim et al, 2011). It would be interesting to confirm

whether similar delays to clock gene oscillations such as *Lfng* would be observed in Nrarp-null mice as seen in the chicken PSM when treated with XAV939, Roscovitine, or DRB.

All explants used for stability assays still contained the remainder of the bisected NT tissue. It is likely that the NT contained NICD protein which may have contributed to the overall signal of this protein obtained by western blotting. However, pilot assays where the NT tissue was carefully removed did not appear to affect the stability assay result (data not shown). In addition it is clear in mouse that levels of NICD protein are significantly lower in the neural tube than in the PSM (Huppert et al, 2005). The NT was subsequently maintained within half-PSM explants for all protein stability assays as this facilitated the dissection process.

Interestingly, XAV939 treatment caused the greatest fold change in cNICD protein of just over a 3-fold increase compared to the DMSO control, but this was the lowest of the statistically significant differences. With a larger standard error also, it is possible that the propensity of XAV939 to precipitate in the culture medium may have led to more variable results than for the other inhibitors. Although 7/9 of the assays for XAV939 treatment showed increased cNICD, the other 2/9 assays showed reduced cNICD. These outcomes meant that it was formally possible that the changes in cNICD level by XAV939 could in fact be more random and due to changes in the phase of dynamic cNICD localisation rather than a general stabilisation effect. For example, if cNICD exhibited a phase 3 pattern of localisation in the DMSO control side of the PSM, but a phase 1 spatial profile in the corresponding +XAV939 side at the end of culture, the level of cNICD would be expected to be higher in the +XAV939 explant overall due to more overall NICD protein in the caudal PSM rather than stabilised NICD. Indeed, the amount of Lfng protein in the caudal PSM of the chick embryo has been shown to oscillate rapidly (Dale et al, 2003). Therefore, the overall level of cNICD observed at the end of culture may have simply been higher in the explant pool which happened to contain more half-PSMs exhibiting cNICD phases with higher levels of cNICD protein. However, this is unlikely given that the increase in average cNICD protein level was consistently reproducible with all three

drug treatments, as well as the fact that the phase 1 of oscillating gene expression in the PSM is the shortest and therefore should be the least represented within the sample pools (Dale et al, 2003). It was impossible to determine this from these stability assays as both halves of the PSM from an embryo were required to generate protein lysates for western blotting. The possibility that cNICD protein levels vary within the chicken PSM could be tested using similar assays to those by Dale et al (2003), whereby one half of the untreated PSM is used for ISH to determine the oscillation phase of a clock gene transcript and the corresponding side used to determine the level of cNICD in the caudal PSM by western blotting.

Furthermore, inhibitor assays lacking Cycloheximide showed consistent and significant increase of cNICD protein with XAV939, as well as Roscovitine and DRB. A lower mean fold increase in cNICD level was seen for all three drugs in assays lacking Cycloheximide, most probably due to *de novo* synthesis of Notch1 and subsequent production of cNICD partially masking the stabilisation effect. The increase in cNICD seen by XAV939, Roscovitine, and DRB treatments in the chicken PSM could be explained if proteolytic enzymes which normally target cNICD for degradation are inhibited by these three drugs. This would result in more stable cNICD and alter oscillations of Notch activity in the PSM which may underlie the delay effect observed for cycling Notch target transcription. These two effects were always observed together, as inhibition of Shh signalling with Cyclopamine had no significant effect on either oscillations of *cLfng* transcription or the level of cNICD within the chicken PSM. This provided further evidence that Shh signalling is not a regulator in determining the pace of the segmentation clock. Similar effects in the mouse PSM with Cyclopamine would strengthen the evidence from this study and by Gibb (unpublished communication) that Shh does not have a significant regulatory role in the temporal control of the segmentation clock.

The molecular evidence so far supports a fundamental requirement of unstable Notch clock components to maintain rapid transcriptional oscillations and timely somite formation (Harima et al, 2013; Hirata et al, 2004; Kim et al, 2011; Lewis, 2003; Monk, 2003; Takashima et al,

2011). It is therefore most likely that the observed increase in cNICD level seen in the PSM when treated by inhibitors shown to delay cycling transcription of clock genes can be explained by these inhibitors promoting stabilisation of the activated Notch receptor. This may be achieved through inhibition of enzymes normally required to rapidly degrade NICD in the PSM to maintain its short half-life and therefore stabilise cNICD protein and subsequently delay the negative feedback loops on target activation, leading to slower oscillations (Lewis, 2003). However, although the effects of XAV939, Roscovitine, and DRB on cNICD protein level in the chicken PSM were consistent, it cannot be ruled out that the increase observed may be simply through either promotion of Notch1 transcription itself or stimulation of the γ-secretase enzymatic complex which catalyses the cleavage of NICD from Notch1 protein. Western blotting with an antibody for full length Notch1 protein will confirm whether these treatments promote Notch1 expression in the PSM, or more specifically the level of NICD itself. Categorical confirmation that cNICD is indeed more stable in the presence of these inhibitors can be achieved by performing pulse-chase assays whereby the level of S^{35} methionine labelled cNICD protein can be measured to determine its rate of decay over a time-course and ascertain the half-life of cNICD under control conditions. This can then be compared to labelled cNICD protein in equivalent assays in the presence of XAV939, Roscovitine, and DRB to confirm whether these drugs do indeed increase the half-life of cNICD as expected.

Assessing the effects of small molecule inhibitors in the mouse PSM

The effects of XAV939, DRB, and Roscovitine on the segmentation clock were assessed within the PSM of the mouse embryo using similar half-PSM assays as for the chick embryo to confirm whether these effects would be conserved as expected. The effects on gene expression within the PSM by XAV939 were generally less consistent for the mouse embryo when compared to the chicken assays. Downregulation of *mAxin2* mRNA expression was observed following exposure to XAV939 in the PSM, but clear oscillation phases of *mAxin2* mRNA expression were not detected in the PSM as has been previously reported (Aulehla et al, 2003). Nevertheless, *mLfng* transcription was consistently delayed in oscillation phase when exposed to XAV939.

Gonzalez et al (2013) observed that treatment with 1µM XAV939 did not alter the period of *Hes7* oscillation in the *Hes7* reporter mouse, while 5µM XAV939 was sufficient to downregulate Hes7 promoter activity. In this study, we found that 100µM XAV939 was required to downregulate the Wnt target *Axin2* and consistently delay *Lfng* oscillations in the chicken and mouse PSM. Therefore it is perhaps not surprising that Gonzalez et al (2013) did not observe any effect on clock gene oscillations with only 1µM XAV939. In that study they did not look at any expression of Wnt target gene expression. However, although Gonzalez et al (2013) saw reduced *Hes7* promoter activity with 5µM XAV939 treatment, neither *Lfng* transcription in the chick and the mouse, nor *Hairy2* transcription in the chick PSM appeared visibly reduced following even 100µM XAV939 treatment when compared to the DMSO control. This may highlight a discrepancy between an *in vitro* reporter assay system and endogenous expression in the PSM.

The effects of the cdk inhibitors on Wnt signalling were less clear in the mouse embryo. *mAxin2* was downregulated by Roscovitine in less than half of the mouse explants compared to their respective DMSO controls. At 5 µM, DRB only appeared to downregulate *mAxin2* expression in 2 out of 7 explant pairs tested. It should be noted that DRB was used at half the concentration as assays with the chicken embryo because the effects on the segmentation

clock were very inconsistent at 10 μM (data not shown). These data were therefore not consistent enough to suggest that either Roscovitine or DRB treatments downregulate Wnt signalling in the mouse PSM. The inhibition of Wnt signalling has been previously linked to a delay in clock gene oscillations in the chicken and mouse PSM (Gibb et al, 2009). However, this study involved the use of the small molecule inhibitor CKI7, which on further inspection was found to downregulate targets from multiple different signalling pathways other than just Wnt (Gibb et al, 2009; Gibb et al, unpublished communication). These findings along with the data from this study suggest that Wnt signalling may not play a direct role in the regulation of clock gene oscillations within the vertebrate PSM, or alternatively that the cdk inhibitors affect the segmentation clock via a different mechanism to the Wnt inhibitor XAV939.

Roscovitine caused a robust delay on *mLfng* oscillations, whereas at 5 μM DRB, *mLfng* oscillations did appear delayed in the mouse PSM, however the fix and culture assays revealed that the expression phase of *mLfng* was no longer advancing in half of the embryos tested. The fact that the two cdk inhibitors appear to delay clock gene oscillations in the mouse PSM, but fail to consistently down regulate the Wnt target *mAxin2* adds weight to the evidence that Wnt signalling may not be directly involved in the regulation of the segmentation clock. However, another possible explanation may be that XAV939 represses a certain Wnt signalling component which functions to regulate another factor required in the regulation of the period of the clock. Roscovitine and DRB inhibit the activity of Cdks involved in transcription and have a more general inhibitory effect on transcription in the PSM, which could also include the same Wnt-regulated target which controls the temporal expression of clock genes. Further functional studies into the targets found to be affected by all three treatments in the chick PSM by the genomic studies may elucidate the regulator which remains unknown.

Further testing of the effects on Wnt signalling in the mouse embryo is required to confirm whether this pathway is or is not significantly affected by the cdk inhibitors. Other read-outs such as phosphorylation of β-catenin protein and transcription of other canonical Wnt targets

within the mouse embryonic tail will clarify this issue, although it is likely that any effects on Wnt signalling targets by Roscovitine or DRB are most probably downstream of β-catenin at the level of gene transcription (as seen in the chicken). Additionally, read-outs of processes such as the cell cycle, general transcription, and apoptosis need to be performed with the mouse studies as has been done for chick. Immunohistochemistry for phospho-histone H3 protein in E10.5 mouse tail explants treated with -/+ XAV939, Roscovitine, and DRB will allow quantification of proliferation within the mouse PSM as for the chicken. This will confirm whether the cell cycle is unaffected by these inhibitors as was the case for the chicken assays. Similarly, western blotting with the phospho-specific antibodies for RNA pol II protein will confirm whether Roscovitine and DRB inhibit Cdk7, Cdk8, and Cdk9 activity in the mouse PSM at the concentrations used. As with all small inhibitor studies, it is important to check that XAV939, Roscovitine, and DRB are not significantly affecting apoptosis in mouse tail explants.

XAV939, Roscovitine, and DRB increase the levels of clock proteins in the mouse PSM

The half-life of clock gene products such as Hes7 and Lfng proteins are shown to be relatively short within the PSM of the segmentation stage embryo (Bessho et al, 2003; Dale et al, 2003; Takashima et al, 2011). This is fundamental to ensure the rapid progression of clock gene transcription through the PSM (Harima et al, 2013; Hirata et al, 2004; Takashima et al, 2011). Stability assays for the mouse embryo showed that the levels of both mHes7 and mNICD proteins were higher in the PSM when treated with either XAV939 and DRB compared to their respective DMSO controls. Roscovitine also appeared to increase mHes7 protein, but did not appear to affect the level of mNICD. Therefore, with the exception of Roscovitine, NICD protein level was higher in the PSM of both the chicken and mouse embryos when treated by inhibitors which also slow oscillations of clock gene transcription. It is unclear why mNICD level

was not affected by Roscovitine, but a low number of replicates mean that this assay must be repeated before any conclusions can be drawn. The fact that mHes7 also appeared increased by all three inhibitors in the mouse PSM leads to the possibility that other clock gene protein products may be more stable in the vertebrate PSM when the segmentation clock is slowed. Production of more novel antibodies against other clock genes will allow these to be visualised. The shared findings from the chicken and mouse embryo studies suggest that the level of Notch-related clock proteins in the PSM may be critical in determining the period of clock gene oscillations as a conserved mechanism to control the pace of segmentation in vertebrate embryos.

As for the chicken assays, we have optimised the Immunohistochemistry assay on sequential paraffin sections of E10.5 mouse tails and shown that spatial profiles of both mHes7 and mNICD proteins vary within the PSM of different mouse embryos in mutually exclusive domains as previously reported by Niwa et al (2011). Future studies will be performed for Immunohistochemistry following -/+ XAV939, Roscovitine, and DRB treatments on mouse PSM explants to confirm whether the spatial domains of mHES7 and mNICD proteins are altered. These drugs gave some evidence of slowing *mLfng* oscillations at the transcriptional level, as well as stabilising clock protein levels in the PSM. Therefore it is predicted that the oscillation phase of mHes7 and mNICD will also be delayed within the mouse PMS by these inhibitors. The oscillation phases for these proteins may be less well-defined in the presence of these inhibitors, as evidence suggested that they may be more stable under these conditions and therefore degraded more slowly within the PSM.

Studies with the mouse embryo created more technical issues than for the chicken due to the mouse embryo being more sensitive to culturing. The E10.5 mouse embryo tail exhibits a more 3-dimensional structure compared to the relatively flat appearance of the HH10 chicken tail. This makes the mouse embryo harder to bisect along the midline. The half-PSM explants generated from the mouse were generally less robust to culturing, as explants would

sometimes exhibit a less solid appearance after fixation which suggested some cell death may have occurred and meant they were not suitable for ISH analysis. The E10.5 mouse PSM also contains only 5-6 prospective somites compared to the chicken PSM which contains 10-12 prospective somites (Stern et al, 1988). This means that accurately defining phases of clock gene transcription from ISH staining in the relatively shorter mouse PSM is considerably harder than for the chicken. Achieving even lysis when creating protein lysates from mouse tissues was also more difficult than for the chicken, which explains why the western blots for mouse stability assays were often less sharp and were sometimes difficult to load evenly. This resulted in much fewer replicates for the mouse stability assays.

The mouse is generally considered a better model for human development than the chicken, as well as providing a powerful genetic tool to generate transgenic and knock-out lines for certain interesting gene targets in the future. This would enable functional studies into the role of potential regulators of the vertebrate segmentation clock which are not currently feasible with the chicken embryo. Indeed, the *Lfng* reporter mouse (LuVeLu) generated by Aulehla et al (2008) and the *Hes7* reporter mouse developed by Takashima et al (2011) have been used to measure the period of real-time *mLfng* and *mHes7* oscillations respectively within the mouse PSM. These reporters therefore provide powerful genetic models from which to quantify the increase in clock period within mouse PSM explants when treated with XAV939, Roscovitine, or DRB in comparison with the corresponding DMSO control vehicle treatment. *Ex vivo* primary cell culture analysis of real-time oscillations of *Lfng* expression in a monolayer of LuVeLu mouse PSM cells has recently been described as another powerful technique for measuring dynamics of the molecular oscillator in studying the segmentation clock (Lauschke et al, 2013). This could potentially allow the dynamics of the segmentation clock to be observed with drug treatments with much greater ease than *in vivo* assays. The overall findings from the inhibitor studies in the mouse PSM largely corroborate the effects seen in the chicken and therefore suggest that these drugs may target conserved mechanisms which maintain the normal period of somitogenesis in the vertebrate embryo. While the different period of the clock and

somitogenesis observed in different vertebrate species is likely due to the differential stability of clock gene products and delays within the system, it is possible that the pacemaker mechanism of somitogenesis may be conserved through vertebrate evolution. Parallel studies in different model species will elucidate whether this is the case.

Genomic Studies

Genomic approaches were performed on chicken PSM tissues from -/+ assays for XAV939, Roscovitine, and DRB treatments with the view to discover effects on genes which were common and those which differ between these inhibitors. The data from both custom chicken microarray and RNA-seq suggested that replicates from -/+ Roscovitine or DRB treatments showed consistency within treatment groups, as well as exhibiting similar effects across these two treatment groups on the expression of many genes. However, there was much less overlap of affected genes between these treatments and XAV939. This was most probably due to the two cdk inhibitors both targeting RNA pol II CTD phosphorylation (Fisher, 2005; MacCallum et al, 2005; Wada et al, 1998), while XAV939 directly inhibited β-catenin dependent Wnt signalling. The transcriptomic data supported this, as Wnt signalling was significantly enriched amongst the GO terms enriched for XAV939 treatment but was not present in the list of GO terms for either of the cdk inhibitors when assessing the differentially expressed genes for each treatment.

Roscovitine and DRB both appeared to repress the transcription of the majority of their targets and with a generally greater proportion of differentially expressed targets showing downregulation with these cdk inhibitors compared to XAV939. GO terms analyses showed that genes involved in processes related to transcriptional regulation, cell cycle progression, as well as chromatin organisation and modification were affected by both cdk inhibitors, as well as within the list of targets affected commonly to both inhibitors. Indeed, a number of genes

encoding cyclins and cdks were affected by Roscovitine and DRB, being mostly downregulated to confirm the repressive actions of the cdk inhibitors on global transcription in the PSM. Overall these findings support the hypothesis that the cdk inhibitors have a repressive action on RNA pol II dependent transcription, while XAV939 appears to affect a largely non-overlapping range of targets that are most likely to be regulated by Wnt signalling.

Despite the apparent differences between the effects of XAV939 and the cdk inhibitors, the targets differentially expressed by all three treatments were viewed to assess the remaining possibility that a common genetic regulatory mechanism may be affected by all three drugs to slow clock gene oscillations. Looking for overlap in the affected genes revealed that the expression of 46 annotated genes was significantly affected by XAV939, Roscovitine, and DRB with RNA-seq.

Of the 46 genes, 22 were downregulated by all three inhibitor treatments, including the LINS gene. Although LINS is a Wnt target and modulator of Wnt signalling, the genomic studies did not generally identify Wnt signalling molecules as downregulated by all three inhibitors which delayed clock gene oscillations. The TGFβ family members TGFB2 and BMP5 were also downregulated by all three inhibitors. BMPs are known regulators of paraxial mesoderm development, as well as later specification of dorsal fates including chondrocyte differentiation from the dorsal somite tissue (Gilbert, 2006, Murtaugh et al, 1999). The maturation of somites was not assessed in this study, but it is possible that XAV939, Roscovitine, and DRB may also impair the differentiation of later somite lineages directed by the TGFB signalling pathway. Interestingly, the PSM marker and Wnt target *Tbx6* was differentially expressed with all three inhibitors treatments by RNA-seq, however it appeared downregulated by XAV939, while upregulated by the cdk inhibitors. Downregulation of *Tbx6* upon Wnt inhibition is expected in the case of XAV939 treatment. However, the opposite effect on *Tbx6* expression by Roscovitine and DRB to XAV939 would suggest that this may not have relevance to the slowing of oscillating clock gene transcription in the PSM.

CIP1 (encoding the p21 protein) was one of only 5 genes found to be upregulated in the chick PSM by XAV939, Roscovitine, and DRB by RNA-seq and showed the highest $\log_2$ fold-change of these targets. The p21 protein encoded by the *CIP1* gene is a universal CDK inhibitor and plays important roles in the regulation of the cell cycle progression and cell senescence (Chang et al, 2000; Sherr and Roberts, 1999). A genome wide study following induction of p21 expression found global changes in the expression of genes involved in cell cycle regulation were downregulated, indicating a mechanism by which p21 induces cell growth arrest (Chang et al, 2000). The upregulation of *CIP1* transcription by XAV939, Roscovitine, and DRB may therefore explain the changes in transcription seen for many targets by these three inhibitors. This result was expected for Roscovitine and DRB, which are themselves CDK inhibitors. Indeed, Roscovitine was shown to induce p21 expression and cleavage in lung cancer cells as a mechanism to arrest the cell cycle and induce apoptosis (Zhang et al, 2010). Interestingly, despite the induction of *CIP1* expression, neither proliferation nor apoptosis appeared to be significantly affected by any of the inhibitors at the given concentrations, suggesting that the concentrations used may not have been sufficient to arrest cell growth in the PSM.

An *in vitro* study using primary mouse keratinocytes identified that p21 acts downstream of Notch1 activation to negatively regulate the expression of Wnt4 at the promoter and promote stem cell differentiation (Devgan et al, 2005). Importantly, this effect was independent of p21's effects on the cell cycle, as the p21 C-terminal fragment which lacks the ability to bind CDKs/cyclins was still able to directly repress *Wnt3* and *Wnt4* transcription (Devgan et al, 2005). This may explain why Roscovitine and DRB were able to induce some down regulation of Wnt targets in addition to the conventional Wnt inhibitor XAV939, at concentrations where proliferation was not affected in the PSM.

Although *Notch1* mRNA did not appear significantly affected by any of the treatments by microarray, the RNA-seq data showed that it was significantly upregulated by Roscovitine and DRB. This outcome was of interest as activated Notch1 protein (NICD) was also found to be

present at a higher level in the PSM when treated with each of these inhibitors. These outcomes suggest that the increase of NICD protein by these inhibitors may be simply due to the up regulation of *Notch1* transcription in the PSM. This would be confirmed by the analysis of full length Notch1 protein expression level following each treatment by either western blotting or immunohistochemistry for Notch1 protein. An increase in full length Notch1 protein level compared to each respective DMSO control treated PSM would support this proposed mechanism. Similarly, qPCR and ISH analyses in the chicken PSM following each of the -/+ treatments would confirm whether *Notch1* transcription is increased. Unfortunately, as both halves of the PSM were required for the treatment and respective control, it was not possible to determine which phase of the clock cycle each sample was in at the end of culture. This would have provided useful information as to the relative levels of targets at different points of the clock oscillation cycle.

Given the data from the genomic assays for the three inhibitors, it is possible that an increase in *Notch1* transcription by XAV939, Roscovitine, and DRB may lead to a greater level of Notch activity in the chick PSM. Consequently, induction of p21 expression downstream of Notch1 activation would potentially block the transcription of targets within chick PSM tissue, including Wnt targets. The reduced wave-front activity of Wnt signalling molecules would reduce the caudal region of the PSM within which rapid clock gene oscillations could be propagated. This would cause the slowing of clock gene oscillations observed by these three inhibitor treatments and result in a delay in physical somite boundary separation from the rostral PSM as was also sometimes observed within the 3 hour culture periods. It should be noted that in the *in vitro* study linking p21, notch and Wnt, the suppression of Wnt signalling by Notch1 is regulated in part by the down regulation of Wnt gene expression itself, as Notch1 fails to induce p21 expression in *Wnt3* overexpressing keratinocytes (Devgan et al, 2005). This suggests that a fine balance between the levels of Notch and Wnt signals in the PSM may be critical to maintain the correct pace of clock gene oscillations.

In order to test the hypothesised role for p21 in regulating the pace of clock gene oscillations, the pace of the segmentation clock must be measured using similar assays to this study following either direct pharmacological induction or mis-expression of p21 in the chicken PSM. Either of these approaches causing similar delays to the molecular oscillator as observed for XAV939, Roscovitine, and DRB would provide strong evidence to support the role of p21 in the somitogenesis clock pacemaker mechanism. Assessing the expression profile of other wave front markers such as *fgf4* and *fgf8*, as well as determination front markers such as *meso2* will also shed light on the mechanism of delay exerted by XAV939, Roscovitine, and DRB.

However, there remains the possibility that the increase in cNICD seen for the three inhibitors in the chicken PSM is due to alteration of post-translational modifications. Indeed, RNA-seq suggested that Roscovitine significantly upregulates expression of *Sirt1*, encoding a de-acetylase known to counteract acetylation-mediated stabilisation of NICD in endothelial cells and therefore promote NICD turnover (Guarani et al, 2011). XAV939 also appeared to downregulate *Maml2* by RNA-seq. Given that Maml is required to recruit the NICD kinase Cdk8/CyclinC to promote subsequent ubiquitin-mediated proteolysis of NICD, another possibility is that NICD can become more stable when this interaction with maml and Cdk8 is repressed (Fryer et al, 2004). Both RNA-seq and Microarray analyses suggested that Roscovitine and DRB affected targets involved in processes including protein acetylation, as well as regulation of phosphorylation and dephosphorylation. This suggests that the effects of XAV939, Roscovitine, and DRB on post-translation modifications of NICD protein warrants further investigation.

The outcomes from the transcriptomic analyses must be assessed with caution as these techniques have potential drawbacks. The microarray chip may contain one or multiple probes for any given gene, however even with several probes only a small part of the coding sequence would have been covered by the array. This means that the data received on the expression of a given gene will only be from a fraction of the coding sequence and could potentially lead to

bias or miss important information regarding the expression levels in each sample. For example, ISH analysis suggested that *cAxin2* expression was downregulated by all three inhibitors in the chick PSM, but this gene was not significantly affected by all three inhibitors when assessed by the genomic approaches. This may highlight a lack of sensitivity for these techniques. The other major disadvantage of microarrays is that the chip has a set array of probes for the annotated genome at the time of creation. This means that the coverage of the genome is likely to be lower when compared to RNA-seq analysis as it will almost certainly miss out some coding genes or currently unannotated coding sequences and is the most likely explanation as to why fewer targets were generally found as differentially expressed for these treatments compared to RNA-seq.

RNA-seq is likely to give a better genomic coverage than the microarray, however this technique also has its own shortcomings. The data reads for each given gene were aligned to the annotation of the chick genome. However, closer inspection of a number of genes revealed that some reads from the RNA-seq data were positioned very close to the perceived annotation of a coding gene, but were in fact outside of the annotated gene sequence. This is most likely because the current annotations for many coding genes across the chicken genome are not quite correct at present. Such reads would have been classed as inter-genic during the data analysis and therefore not counted when they may in fact be real transcripts associated with the adjacent gene with incorrect annotation. This highlights a weakness of genomic studies with the chicken, which is generally regarded as having a more poorly annotated genome than other common model vertebrate species such as the mouse. For example, the chicken clock gene paralogues *Hairy1* and *Hairy2* are both labelled as *Hes1* when searching via chicken genome browsers, even though they are separate genes residing on different chromosomes. A more comprehensive coverage of the chicken genome will facilitate genomic studies such as this report. Indeed, during this study the newer Galgal rel 75 transcriptome build of the chicken genome was released by Ensemble (http://www.ensembl.org/Gallus_gallus/Info/Index). This prompted us to re-align the

annotations before repeating the data analyses for the RNA-seq studies to increase confidence in the accuracy of the genome annotations. As with most transcriptomic techniques, the financial and time costs meant that only a limited number of replicates were run for each treatment in this study. Ideally, more replicates should be assessed to give greater confidence in the changes of gene expression observed.

The other apparent issue with the RNA-seq data was that the vast majority of the reads obtained for some genes were present only at the end of the gene in the three prime untranslated region (3'-UTR). This was true of some genes such as *Lfng*, while very few reads were obtained from coding exons. This bias towards signal from the 3'-UTR could be explained by previous reports that mapping the polyadenylation (polyA) sites at the 3' end of genes is as accurate as RNA-seq in determining gene expression globally (Derti et al, 2012), or that the mRNA from the samples may have been slightly degraded. The latter could result in some transcripts being fragmented and therefore not being completely sequenced once bound to the RNA-seq chip from the poly-A tail. A genome-wide study of RNA-seq data from human and mouse tissue and cell lines also identified that the mean length of the 3' UTR of genes involved in development, morphogenesis, and signal transduction was greater than the genome average (Ramsköld et al, 2009). This suggests that these classes of genes have a more complex level of 3' UTR regulation, which is supported by recent evidence from the genes *Lfng* and *Hes7* in the mouse PSM (Nitanda et al, 2014). Nonetheless, the list of genes obtained in this study from two separate techniques on the same samples gave higher confidence that these changes in expression were significant. Quantitative PCR (qPCR) is another technique that can be used to more accurately quantify the changes in gene expression seen in the chicken PSM by drug treatments compared to the respective DMSO control treatment. This will provide a method by which to validate the changes in expression level of certain genes by XAV939, Roscovitine, and DRB seen by microarray, RNA-seq, or ISH analyses.

Proteomic Studies

Proteomics provided another approach from which to uncover the mechanisms by which cNICD protein becomes more stable in the presence of the inhibitors which concomitantly slow oscillations of clock gene transcription. NICD has been shown to contain multiple post-translational modifications that are required for Notch activity, as well as NICD degradation (Fryer et al, 2004; Jin et al, 2009; Guarani et al, 2011). Indeed, CDK8-mediated phosphorylation in the PEST domain of NICD is required to target this protein for ubiquitination and subsequent degradation by the E3 ligase FBW7 (Fryer et al, 2004). GSK3 is also shown to phosphorylate NICD protein at several Threonine sites to repress Notch1 expression and stability (Espinosa et al, 2003; Jin et al, 2009). Both of these studies were performed on human cell lines, however sequence alignment revealed that all but one of these amino acid sites were conserved within the sequence of chicken NICD protein. These post-translational modifications were therefore of particular interest as they have been shown to regulate the stability of NICD protein, while two of the inhibitors shown to increase cNICD protein level in this study were cdk inhibitors.

For all three reagents, western blotting sometimes suggested a slight shift for cNICD in the + inhibitor treated sample to create what appeared as an additional band at a slightly smaller molecular weight for cNICD protein. This sort of shift could represent an increase in a variant of a protein which lacks small post-translational modifications such as phosphate groups and consequently runs at a slightly lower molecular weight when separated by SDS-PAGE. This shift seen for cNICD by western blotting in samples that also have a higher level cNICD protein may represent the loss of phosphorylation marks which have been shown to be important for NICD regulation and degradation (Fryer et al, 2004; Jin et al, 2009). NICD protein levels would therefore generally be expected to be more stable when there is a reduction in the proportion of NICD which is phosphorylated at these target sites. XAV939, Roscovitine, and DRB may all promote cNICD stability in the PSM by targeting enzymatic post-translational regulators of cNICD protein such as kinases and alter modifications such as phosphorylation, which are

predicted to be essential for rapid NICD turnover in the PSM as they are shown in other contexts (Espinosa et al, 2003; Fryer et al, 2004; Guarani et al, 2011; Jin et al, 2009).

The ultimate aim of this approach was to identify if XAV939, Roscovitine, and DRB treatments lead to changes in the ratio of phosphorylated NICD compared to non-phosphorylated NICD. Initial identification studies using recombinant cNICD protein proved successful. Recombinant cNICD protein was used to enrich for cNICD by IP before analysis by mass spectrometry. This approach successfully identified 45 of the predicted peptides for cNICD protein with high confidence. This gave an overall sequence coverage of 56.88%; including peptides containing all of the conserved residues which are known to be phosphorylated by either CDK8 or GSK3 in human cells (Fryer et al, 2004; Jin et al, 2009). This was a valid strategy as it allowed the positive identification of predicted peptides within cNICD from the *in silico* Chymotrypsin digestion of recombinant cNICD and therefore provided real spectral data to then use for the identification of peptides from endogenous chicken PSM tissue. However, recombinant cNICD protein synthesised from an expression vector is a much less complex sample with much higher levels of cNICD to detect by mass spectrometry when compared to endogenous PSM tissue. NICD is likely to be present at a very low abundance relative to many other proteins within the complex array of proteins expressed within the PSM since it is inherently unstable within the PSM and is known to be actively targeted for degradation to aid rapid turnover in order to maintain oscillations of Notch activity (Dale et al, 2003; Fryer et al, 2004; Jin et al 2009; Morimoto et al, 2005). Indeed, just to have enough starting material to identify cNICD in endogenous tissue required combining the PSM tissues from 120 chicken embryos and then enriching for cNICD from this pooled lysate using the specific antibody to pull down cNICD with 3 successive rounds of IP.

The level of different phosphorylation marks identified will be measured from the titanium dioxide enriched samples from each treatment to compare with the DMSO control after normalisation to unmodified peptides from the 'flow-throughs' of each sample. For the drug

treated samples, a decrease in any of the marks shown to be targeted by Cdk8 or GSK3 in human cell lines will give a good indication that these kinases are inhibited by the drugs as a mechanism to promote cNICD stability compared to the DMSO control. This would also suggest that these kinases play a role in determining the pace of clock gene oscillations in the PSM at the transcriptional level, as the instability of NICD protein appears to be tightly regulated to maintain rapid oscillations of Notch target clock gene mRNA expression within the PSM.

A number of E3 ligases have been identified as regulators of cNICD protein degradation in other cellular contexts but none identified so far specifically in the PSM (Bray, 2006; Fryer et al, 2004; Kopan and Ilagan, 2009; McGill and McGlade, 2003). Several good candidate E3 ligase genes were found after mining the microarray data from Dequeant et al (2006) and Krol et al (2011) on the PSM of mouse, chicken, and zebrafish embryos including the *Mib1* and *Mib2* genes, which are known regulators of Notch activity (Itoh et al, 2003). However, ISH analysis of these transcripts in chicken embryos using antisense-RNA probes failed to reveal even clear expression in the PSM, let alone oscillatory expression. Although *cDcaf13* did appear to exhibit diffuse expression in the S-1 domain of one embryo, ISH analysis of *cDcaf13* expression in more embryos is required to confirm whether this gene is expressed in the PSM and if this transcription is oscillatory.

In several embryos, *cMib1* and *cMib2* were expressed caudal to the PSM in an area nearer to the stem zone of the NT and the node. Interestingly, some clock genes are shown to oscillate in the PS and the node prior to the formation of the first somite pair in the embryo before stage HH7 (Jouve et al, 2002). Expression analysis of these genes in the caudal tail of more stage-matched embryos will determine whether their expression is oscillatory within the node. Careful dissection is required to eliminate neighbouring tissues from the PSM and it is therefore possible that the genes found to oscillate by Dequeant et al (2006) and Krol et al (2011) may have been dynamic in neighbouring tissues rather than within the PSM. Indeed,

cDcaf13 expression was seen in the neighbouring LPM tissue in several embryos. Alternatively, microarray may be a much more sensitive technique than ISH for identifying the transcription of certain genes within the PSM, as has been suggested previously (Dequeant et al, 2006; Krol et al, 2011). However, care should also be taken when interpreting the data from transcriptomic studies such as these. For example, the transcription of some well-characterised clock genes such as *Lfng* was not found to be significantly oscillatory in the mouse PSM by Krol et al (2011). The results from the E3 ligase expression analysis did not suggest that these regulators of protein degradation are cycling within the chicken PSM, but this cannot be ruled out from the limited number of genes and embryos analysed to this point. Further analysis will elucidate whether any E3 ligases exhibit oscillatory expression within the PSM which could highlight a potential mechanism by which oscillating regulators of NICD protein degradation can maintain rapid oscillations of Notch activity across the PSM.

Major findings

This study has shown that inhibition of Wnt signalling with XAV939, and reducing the activity of Cdks with Roscovitine, and DRB all slow the segmentation clock in the chicken PSM. Preliminary studies suggest that these inhibitors may also be able to delay oscillations within the mouse PSM. These three inhibitors also consistently downregulated the Wnt target mRNA *cAxin2* in the chicken PSM. A significant delay in the pace of clock gene oscillations, if biologically significant, will impact on the segmentation process in a number of ways: in particular the overall effects will be to alter both somite size and final number of somites produced (Dequeant and Pourquie, 2008; Schröter and Oates, 2010).

XAV939 was able to slow the segmentation clock and inhibit canonical Wnt signalling via induction of β-catenin phosphorylation. The transcriptomic data confirmed this effect, as the Wnt signalling pathway was found to be significantly enriched amongst Gene Ontology terms affected by XAV939, with a number of Wnt targets downregulated. These outcomes therefore give strong evidence for the hypothesis that Wnt signalling is required to maintain rapid clock gene oscillations in the PSM. Further analysis will uncover whether a downstream Wnt regulated factor is required to control the period of somitogenesis.

The Cdk inhibitors Roscovitine and DRB were also both able to slow oscillations of clock genes in the PSM, however their mode of action is unlikely to be the same as for XAV939. Although both inhibitors downregulated the Wnt target *cAxin2* in the chicken PSM, Roscovitine and DRB did not affect phosphorylation of β-catenin, therefore suggesting that they do not affect canonical Wnt signalling at the concentrations found to slow the segmentation clock. The fact that both of the cdk inhibitors reduced phosphorylation of Serine 5 on RNA pol II normally targeted by cdks 7-9 suggests that these inhibitors were indeed repressing the activity of transcriptional cdks and that the reduction of *cAxin2* expression was most likely at the level of RNA pol II dependent transcription at the promoter. The evidence from assays with Roscovitine and DRB suggest that cdks do have a role in temporal regulation of clock gene

oscillations. However, it remains unclear whether these inhibitors affect a common target to XAV939 that may be Wnt regulated, or if there are multiple mechanisms in the temporal control of the segmentation clock.

Using a novel antibody, we found that XAV939, Roscovitine, and DRB treatments all consistently increased cNICD protein in the chick PSM relative to the DMSO control. Immunohistochemistry for cNICD revealed a dynamic profile within the chicken PSM, while cNICD was localised to the caudal compartment of the formed somites. This uncovered a conserved profile for NICD in the PSM of the mouse and chick embryos as hypothesised, although further assessment is required to confirm whether cNICD oscillates with the same periodicity as somite formation. Preliminary studies in the mouse PSM also suggested that the levels of the clock proteins mNICD and mHES7 were higher when treated with the same three inhibitors. This supports evidence that the level of Notch activity must be tightly regulated to maintain timely oscillations of clock gene transcription within the vertebrate PSM. The balance of Notch activity in the PSM and the rate of axial elongation at the caudal PSM may be a mechanism by which the segmental body plan has been adapted during vertebrate evolution (Benazeraf and Pourquie, 2013). It is likely that instability of Notch activity in the PSM is critical to regulate transient negative feedback loops applied by targets such as Hes/Her genes in order to maintain rapid oscillations of clock gene activity which determine the period of somite formation. Stabilisation and subsequent slowed turnover of NICD by XAV939, Roscovitine, and DRB may therefore be the mechanism by which these drugs are able to slow clock gene oscillations in the PSM. Slowing of the segmentation clock may only be possible through transient and/or partial stabilisation of Notch activity, as overexpression or loss of Notch signalling components is shown to abolish clock gene oscillations and causes severe segmentation defects (Feller et al, 2008; Ferjentsik et al, 2009; Niwa et al, 2007). However, other possible mechanisms by which these inhibitor treatments can increase the level of cNICD must also be assessed, such as whether these treatments cause an increase in the

transcription of Notch1, or alternatively whether they promote the activity of the enzymes required to catalyse the cleavage of NICD from full length Notch.

A previous report suggested that Shh signalling is involved in the temporal control of somite formation (Resende et al, 2010) and to this end we set out to confirm whether Shh regulates the period of the clock. However, we found no evidence to support this, as inhibition of Shh signalling using the small molecule inhibitor cyclopamine had no effect on either oscillating *cLfng* transcription, nor the level of cNICD protein within the chick PSM.

Genomic studies on half-PSM tissue pairs treated with -/+ XAV939, Roscovitine, or DRB found a set of genes whose transcription was significantly affected by all three inhibitors relative to each respective DMSO treated control PSM. While the majority of these targets were downregulated, targets including *CIP1* (encoding the p21 protein) appeared upregulated by all three inhibitors. It is possible that the increase of NICD seen by these inhibitors may be due to induction of *Notch1* mRNA levels within the PSM. Notch activation has been shown to induce p21 expression (Devgan et al, 2005), which may be a mechanism by which global transcription is repressed and leads to slowed clock gene oscillations within the chicken PSM. Direct induction of p21 in the chick PSM using similar assays to this study will reveal whether p21 is a key regulator in the segmentation clock pacemaker mechanism.

Another possible mechanism for the increase of NICD observed in the PSM by XAV939, Roscovitine, and DRB may be through altering post-translational modification of NICD. Although Cdk8/cyclinC is a known regulator of RNA pol II-dependent transcription along with Cdk7/cyclinH and Cdk9/cyclinT (Malumbres and Barbacid, 2009), it is possible that the general effects on transcription exerted by these three inhibitors was in fact unrelated to or in addition to the increase of NICD levels. Cdk8-mediated phosphorylation of NICD has been shown to be necessary to target its degradation by the ubiquitin proteasome in cell culture (Fryer et al, 2004). Therefore, the three inhibitors may cause a delay in clock gene oscillations through specifically inhibiting Cdk8 kinase activity on NICD protein. However, reports that DRB has

intermediary and Roscovitine only weak effects on Cdk8 activity make it unclear whether this is possible (Pinhero et al, 2004) and more specific Cdk8 inhibitors are required to test this.

Future Directions

In order to assess whether the effects of XAV939, Roscovitine, and DRB on the segmentation clock are sufficient to reduce the number of somites formed, embryos must be cultured for longer periods in the presence of each inhibitor. This can be achieved with chicken embryos utilising EC culture in the presence of either drug or control treatment (Chapman et al, 2001) for periods of at least 12 hours. This will enable the longer term effects on segmentation caused by slower clock oscillations to be assessed with each inhibitor, including whether fewer somites form and whether these somites are larger as is predicted when the period of the segmentation clock is increased. Preliminary assays suggest that longer culture periods are viable, as ISH staining in half-PSM explants reveals that *cLfng* expression is still dynamic after 10 hours in culture (data not shown).

Pulse-chase assays using labelled protein will allow the rate of decay for cNICD to be measured to ascertain whether the increase in cNICD level seen by XAV939, Roscovitine, and DRB treatments are indeed due to promoting a longer half-life of cNICD as we predict. However, the possibility that these drugs simply induce Notch1 expression can be tested by viewing the level of full length Notch1 protein following each inhibitor treatment with Western blotting analyses similar to those performed for cNICD protein in the current study. An induction in the level of full length Notch1 protein by these treatments would be good evidence that the increase in cNICD is due an induction of Notch1 expression and subsequently the presence of more full length receptor from which to generate more cleaved Notch protein.

As hypothesised, we found that NICD protein is localised in dynamic domains within the chicken PSM, similar to that of the mouse NICD. However, immunohistochemistry on half-PSM

chick explants from the same embryo cultured for 90 minutes apart are required to elucidate whether cNICD oscillations match the periodicity of somite formation as expected.

The transcriptomic data revealed that transcription of the p21 gene *CIP1* was one of the very few genes induced by XAV939, Roscovitine, and DRB, making p21 a strong candidate regulator of the segmentation clock pacemaker. Direct induction of CIP1/p21 in the PSM is required to ascertain whether this is sufficient to slow oscillations of clock gene transcription and reveal whether p21 regulates the pace of the segmentation clock. During myogenesis, p21 is shown to be induced under the control of MyoD in co-operation with p300 to promote skeletal muscle cell differentiation (Halevy et al, 1995; Puri et al, 1997). Another bHLH transcription factor protein BETA2 (also known as NeuroD) interacts with p300 to induce p21 expression and coordinate differentiation of secretin-expressing enteroendocrine cells (Mutoh et al, 1998). p21 can also be induced by pharmacological methods: p53 upstream of p21 is a well-established pathway in the regulation of arresting cell growth and apoptosis, while the inhibitor Diaminocyclohexane (transdiacetato) (dichloro) platinum(IV) (DAP) has been shown to induce p53-p21 and cause reduced activity of cdk2 and cdk4 (He et al, 2005). Similarly, treatment of embryonal rhabdomyosarcoma cells with the MAPK/ERK inhibitor U0216 causes upregulation of p21 and induced myogenic differentiation (Ciccarelli et al, 2005). These studies therefore provide candidate pharmacological and genetic approaches to induce p21 in the chick PSM in the future to test the role of p21 in the segmentation clock.

In order to obtain the data on differential gene expression from microarray and RNA-seq analyses, the fold-change in gene expression between + inhibitor and DMSO control was averaged for each set of -/+ pair replicates for each given drug treatment in the chick PSM. However, the raw data can also be used in another way to compare the level of gene expression within each treatment group: by comparing the fold-change for any given gene between each -/+ pair replicate. In doing these comparisons, it will be possible to identify the genes whose expression is most variable within each treatment group and therefore find

previously uncharacterised oscillating transcripts within the chick PSM. These data can be verified by confirming that previously characterised clock genes such as *cLfng* and *cHairy1*/2 also fall into this category. The absolute expression values will allow comparisons between different cycling genes to be made in order to assess whether these targets are in phase with each other or not. Similarly, the levels of these targets can be compared between replicates to other potentially interesting candidate regulators such as *CIP1* to assess whether these targets exhibit a greater fold-change reduction in expression when there is a greater fold-change increase in *CIP1* (p21) induction by XAV939, Roscovitine, and DRB.

The potential role of Cdk8 kinase activity on NICD to regulate the pace of the molecular clock in the PSM can be assessed by performing similar half-PSM assays to this study in the chicken embryo with more specific Cdk8 small molecule inhibitors. A number of Cdk8 inhibitors exist, including dihydrocortistatin (Cee et al, 2009). If inhibitors such as dihydrocortistatin are able to delay oscillation of clock gene transcription and increase the level of cNICD in a similar manner to the drugs used in this study, it will provide good evidence that Cdk8 is involved in the pacemaker mechanism of somitogenesis.

Currently, the hypothesis that the inhibitors shown to delay clock gene oscillations can increase the level of cNICD through alteration of post-translational modifications remains unclear. In depth mass spectrometry analysis of endogenous cNICD protein from the chick PSM will elucidate the post-translational modifications present and assess the levels of these modifications following treatment with XAV939, Roscovitine, DRB, or Cdk8 inhibitors compared to the controls. Any significant alterations in post-translational modifications on NICD such as phosphorylation on conserved Cdk8 target sites may uncover key kinases involved in the regulation of NICD instability that could be fundamental to the molecular oscillator mechanism. This may link the effects on the level of cNICD protein and the slowed oscillations of the Notch target *cLfng* caused by the three inhibitors, which currently remain incidental. It would then be possible to generate a conditional PSM mutant mouse line

whereby key phosphorylation residues within the NICD portion of Notch1 are substituted to code for other amino acids, or alternatively for an inactive form of the key NICD kinase itself. This would block the phosphorylation at these sites within NICD in the PSM of this conditional mutant mouse, thereby increasing the stability of NICD protein. The pace of clock gene mRNA oscillations could then be viewed within the mutant PSM to assess whether more stable NICD results in slower oscillations as seen for the drug treatments in this study. However, care must be taken with this approach, as generating a mutant mouse line with NICD which is too stable may significantly dampen and then rapidly arrest clock oscillations altogether in the PSM if Notch activity is too high. On the other hand, the fact that at least two kinases target NICD protein to regulate its rapid turnover - Cdk8 and GSK3 (Espinosa et al, 2003; Fryer et al, 2004; Jin et al, 2009) - suggest that there may be a level of redundancy in the system that would facilitate this approach.

Supplementary Information

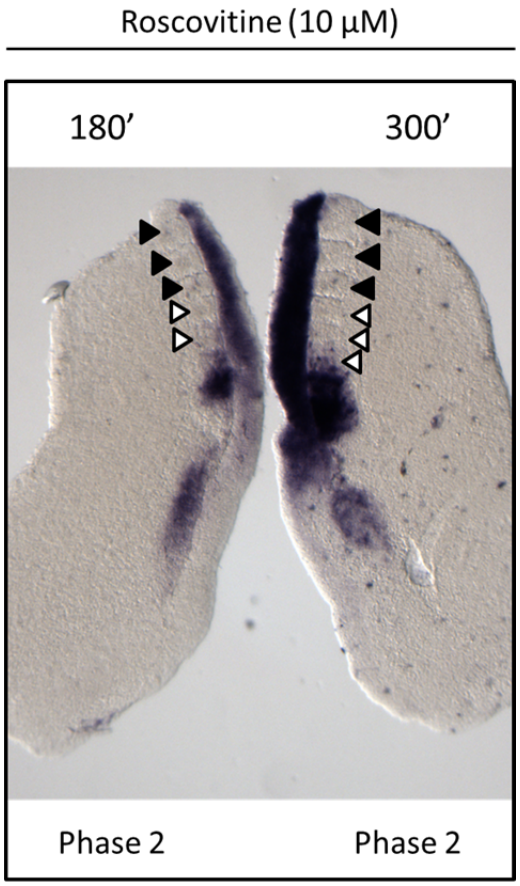

Supplementary Figure S1) Roscovitine treatment extends the period of *cLfng* transcriptional oscillations to 120 minutes in the chicken PSM. In situ hybridisation staining shows that *cLfng* transcriptional oscillations take approximately 120 minutes to complete a full oscillation cycle in the chicken PSM when treated with 10 µM Roscovitine**.** Black arrowheads indicate somites present at the start of culture and white arrowheads show somites formed during the given culture periods.

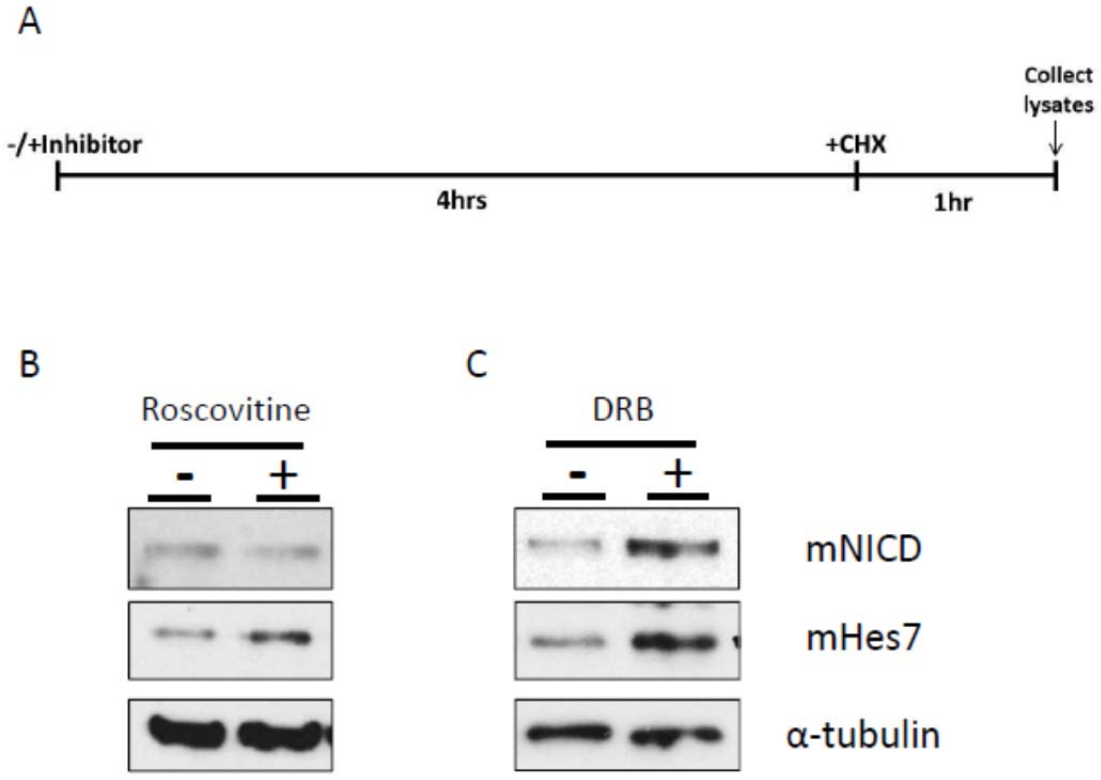

Supplementary Figure S2) Roscovitine and DRB increase the levels of clock gene proteins in the mouse PSM. A) Schematic of the mouse protein stability assay culture time-course. **B-C**) Western blot results for mNICD protein, mHES7 protein, and α-tubulin protein loading control levels following -/+ stability assay treatment with Roscovitine (**B**) and DRB (**C**).

Supplementary Table 1) Inclusion list of predicted peptides from which to identify cNICD protein by mass spectrometry following digestion with Chymotrypsin. (see below)

Sequence
(L)C(Carbamidomethyl)SPSSY(I)
(L)GEDSVGL(K)
(L)ESPHGY(L)
(L)C(Carbamidomethyl)SPSSY(I)
(L)SGQC(Carbamidomethyl)DW(L)
(L)HLAARY(S)
(L)SQMMSY(Q)
(L)LDNSSVL(S)
(F)IYQGASL(H)
(L)SGQC(Carbamidomethyl)DW(L)
(L)AAREGSY(E)
(L)SQMMSY(Q)
(L)ASQPHLL(Q)
(L)LDEYNL(V)
(Y)ETAKVLL(D)
(L)SQMMSY(Q)
(F)EAVPPRL(S)
(L)WFPEGF(K)
(L)GGSGRMAF(E)
(L)SDVASPPL(M)
(L)GGSGRMAF(E)
(L)GKSALHW(A)
(L)ESPHGYL(S)
(L)KNASDGTL(M)
(L)QVPDHPF(L)
(L)QVPDHPF(L)
(L)SGQC(Carbamidomethyl)DWL(S)
(L)GAPTLSPPL(C)
(L)SGQC(Carbamidomethyl)DWL(S)
(F)LAAREGSY(E)
(F)QQSPSMPL(N)
(L)QHGMMSSL(H)
(F)QQSPSMPL(N)
(Y)QAMPSTRL(A)
(F)QQSPSMPL(N)
(L)QHGMMSSL(H)
(L)QHGMMSSL(H)
(Y)NLVRSPPL(H)
(Y)LSDVASPPL(M)
(Y)QAMPSTRL(A)
(F)QQSPSMPL(N)
(Y)QAMPSTRL(A)
(L)QHGMMSSL(H)
(L)QHGMMSSL(H)
(L)DNTPSHQL(Q)
(L)LPTSLPSSL(A)
(L)TPPSQHSY(S)
(Y)QAMPSTRL(A)
(L)QHGMMSSL(H)
(L)HNGLPSTSL(S)
(L)MIASC(Carbamidomethyl)SGGGL(E)
(L)QVPDHPFL(T)
(L)DTKKFRF(E)
(L)MIASC(Carbamidomethyl)SGGGL(E)
(L)HSGPLGAPTL(S)
(L)MIASC(Carbamidomethyl)SGGGL(E)
(L)QVPDHPFL(T)
(L)IRNRATDL(D)
(L)MIASC(Carbamidomethyl)SGGGL(E)
(L)AVEGMLEDL(I)
(L)AVEGMLEDL(I)
(Y)SRSDAAKRL(L)
(L)FLAAREGSY(E)
(L)GEDSVGLKPL(K)
(L)AQPMTTTQF(L)
(F)LTPPSQHSY(S)
(L)AARLAVEGML(E)
(L)QSGMVQNQY(G)
(L)AQPMTTTQF(L)
(L)AARLAVEGML(E)
(L)MDDNQNEW(G)
(L)QSGMVQNQY(G)
(L)QSGMVQNQY(G)
(L)MDDNQNEW(G)
(L)SPPLC(Carbamidomethyl)SPSSY(I)
(L)QSGMVQNQY(G)
(L)C(Carbamidomethyl)SPSSYIGNL(K)
(L)NMAGKQEMAL(G)
(L)SPPLC(Carbamidomethyl)SPSSY(I)
(L)C(Carbamidomethyl)SPSSYIGNL(K)
(L)SC(Carbamidomethyl)NGKDSKDL(K)
(L)NMAGKQEMAL(G)
(W)TQQHLDAADL(R)
(Y)SRSDAAKRLL(E)
(L)SC(Carbamidomethyl)NGKDSKDL(K)
(L)NMAGKQEMAL(G)
(L)AQPMTTTQFL(T)
(L)TPSPESPDQW(S)
(L)KPLKNASDGTL(M)
(L)AQPMTTTQFL(T)
(L)VRSPPLHSGPL(G)
(L)HAAVSADAQGVF(Q)
(Y)ETAKVLLDHF(A)
(L)SGQC(Carbamidomethyl)DWLSRL(Q)
(L)DARMHDGTTPL(I)
(L)SGQC(Carbamidomethyl)DWLSRL(Q)
(L)DARMHDGTTPL(I)
(L)DNSSVLSPVDSL(E)
(F)TPLMIASC(Carbamidomethyl)SGGGL(E)
(W)AAAVNNVEAAVVL(L)
(F)TPLMIASC(Carbamidomethyl)SGGGL(E)
(F)LTPSPESPDQW(S)
(L)ILAARLAVEGML(E)
(F)TPLMIASC(Carbamidomethyl)SGGGL(E)
(L)ILAARLAVEGML(E)
(F)TPLMIASC(Carbamidomethyl)SGGGL(E)
(W)GDEETLDTKKF(R)
(L)SPVDSLESPHGY(L)
(W)SSSSPHSNVSDW(S)
(Y)SSPLDNTPSHQL(Q)
(F)QILIRNRATDL(D)
(L)TPPSQHSYSSPL(D)
(L)DEYNLVRSPPL(H)
(F)QILIRNRATDL(D)
(F)SVGGAAGLSGQC(Carbamidomethyl)DW(L)
(L)HNQTDRTGETAL(H)
(L)HSGPLGAPTLSPPL(C)
(L)LDNSSVLSPVDSL(E)
(L)SDVASPPLMTSPF(Q)
(W)AAAVNNVEAAVVLL(K)
(F)SVGGAAGLSGQC(Carbamidomethyl)DW(L)
(L)SDVASPPLMTSPF(Q)
(Y)NLVRSPPLHSGPL(G)
(L)AARLAVEGMLEDL(I)
(L)AAREGSYETAKVL(L)

(L)SPVDSLESPHGYL(S)

(L)AARLAVEGMLEDL(I)

(L)SRLQSGMVQNQY(G)

(F)LTPPSQHSYSSPL(D)

(L)SRLQSGMVQNQY(G)

(L)INC(Carbamidomethyl)HADVNAVDDL(G)

(L)DARMHDGTTPLIL(A)

(L)MTSPFQQSPSMPL(N)

(F)SVGGAAGLSGQC(Carbamidomethyl)DWL(S)

(L)INC(Carbamidomethyl)HADVNAVDDL(G)

(L)DARMHDGTTPLIL(A)

(Y)LSDVASPPLMTSPF(Q)

(L)AARYSRSDAAKRL(L)

(L)MTSPFQQSPSMPL(N)

(L)SPPLC(Carbamidomethyl)SPSSYIGNL(K)

(F)SVGGAAGLSGQC(Carbamidomethyl)DWL(S)

(Y)LSDVASPPLMTSPF(Q)

(L)MTSPFQQSPSMPL(N)

(L)SPPLC(Carbamidomethyl)SPSSYIGNL(K)

(F)LAAREGSYETAKVL(L)

(L)AAREGSYETAKVLL(D)

(L)GAPTLSPPLC(Carbamidomethyl)SPSSY(I)

(Y)QAMPSTRLASQPHL(L)

(L)VSRKRRREHGQL(W)

(W)LSRLQSGMVQNQY(G)

(L)HAAVSADAQGVFQIL(I)

(L)GAPTLSPPLC(Carbamidomethyl)SPSSY(I)

(Y)QAMPSTRLASQPHL(L)

(Y)QAMPSTRLASQPHL(L)

(W)LSRLQSGMVQNQY(G)

(L)GGSGRMAFEAVPPRL(S)

(Y)QAMPSTRLASQPHL(L)

(L)GGSGRMAFEAVPPRL(S)

(L)HWAAAVNNVEAAVVL(L)

(L)ESPHGYLSDVASPPL(M)

(L)AARYSRSDAAKRLL(E)

(W)GDEETLDTKKFRF(E)

(L)HNQTDRTGETALHL(A)

(L)VRSPPLHSGPLGAPTL(S)

(L)KARRKKSQDGKGC(Carbamidomethyl)L(L)

(L)SQMMSYQAMPSTRL(A)

(L)KARRKKSQDGKGC(Carbamidomethyl)L(L)

(Y)QAMPSTRLASQPHLL(Q)

(L)SQMMSYQAMPSTRL(A)

(Y)QAMPSTRLASQPHLL(Q)

(Y)QAMPSTRLASQPHLL(Q)

(L)HNGLPSTSLSQMMSY(Q)

(L)SQMMSYQAMPSTRL(A)

(Y)QAMPSTRLASQPHLL(Q)

(L)HNGLPSTSLSQMMSY(Q)

(L)HWAAAVNNVEAAVVL(K)

(L)SQMMSYQAMPSTRL(A)

(L)HNGLPSTSLSQMMSY(Q)

(F)KVTESSKKKRREPL(G)

(L)MDDNQNEWGDEETL(D)

(L)VSRKRRREHGQLW(F)

(L)MDDNQNEWGDEETL(D)

(L)HLAARYSRSDAAKRL(L)

(L)KARRKKSQDGKGC(Carbamidomethyl)LL(D)

(L)DNTPSHQLQVPDHPF(L)

(L)KARRKKSQDGKGC(Carbamidomethyl)LL(D)

(L)QHGMMSSLHNGLPSTSL(S)

(Y)QGASLHNQTDRTGETAL(H)

(L)NHLPGMPDAHMSINHL(N)

(L)EDLINC(Carbamidomethyl)HADVNAVDDL(G)

(-)GVLVSRKRRREHGQL(W)

(L)KPAVQGKKARKPSTKGL(S)

(L)QHGMMSSLHNGLPSTSL(S)

(L)QHGMMSSLHNGLPSTSL(S)

(Y)QGASLHNQTDRTGETAL(H)

(L)NHLPGMPDAHMSINHL(N)

(L)GEDSVGLKPLKNASDGTL(M)

(L)EASADANIQDNMGRTPL(H)

(L)QHGMMSSLHNGLPSTSL(S)

(L)EDLINC(Carbamidomethyl)HADVNAVDDL(G)

(L)QHGMMSSLHNGLPSTSL(S)

(L)NHLPGMPDAHMSINHL(N)

(L)EASADANIQDNMGRTPL(H)

(L)QHGMMSSLHNGLPSTSL(S)

(-)GVLVSRKRRREHGQL(W)

(L)KNASDGTLMDDNQNEW(G)

(L)DNTPSHQLQVPDHPFL(T)

(L)DARMHDGTTPLILAARL(A)

(L)KNASDGTLMDDNQNEW(G)

(L)NMAGKQEMALGGSGRMAF(E)

(L)DARMHDGTTPLILAARL(A)

(L)NMAGKQEMALGGSGRMAF(E)

(Y)GAMRGGMQPGTHQQAQNL(Q)

(L)INC(Carbamidomethyl)HADVNAVDDLGKSAL(H)

(L)NMAGKQEMALGGSGRMAF(E)

(Y)GAMRGGMQPGTHQQAQNL(Q)

(L)DNSSVLSPVDSLESPHGY(L)

(L)NMAGKQEMALGGSGRMAF(E)

(L)INC(Carbamidomethyl)HADVNAVDDLGKSAL(H)

(Y)GAMRGGMQPGTHQQAQNL(Q)

(L)LEASADANIQDNMGRTPL(H)

(L)LPTSLPSSLAQPMTTTQF(L)

(L)ETGNSEEEDDAPAVISDF(I)

(L)KNGANKDMQNNKEETPL(F)

(L)LEASADANIQDNMGRTPL(H)

(L)LPTSLPSSLAQPMTTTQF(L)

(L)KNGANKDMQNNKEETPL(F)

(L)SHLPVSSPSTAMSNAPMNF(S)

(-)GVLVSRKRRREHGQLW(F)

(L)SHLPVSSPSTAMSNAPMNF(S)

(L)SHLPVSSPSTAMSNAPMNF(S)

(-)GVLVSRKRRREHGQLW(F)

(L)GKSALHWAAAVNNVEAAVVL(L)

(Y)QGASLHNQTDRTGETALHL(A)

(L)LPTSLPSSLAQPMTTTQFL(T)

(L)AQPMTTTQFLTPPSQHSY(S)

(L)LKNGANKDMQNNKEETPL(F)

(Y)QGASLHNQTDRTGETALHL(A)

(L)LPTSLPSSLAQPMTTTQFL(T)

(L)AQPMTTTQFLTPPSQHSY(S)

(L)HNQTDRTGETALHLAARY(S)

(L)QVPDHPFLTPSPESPDQW(S)

(L)LKNGANKDMQNNKEETPL(F)

(F)IYQGASLHNQTDRTGETAL(H)

(L)QVPDHPFLTPSPESPDQW(S)

(L)KNGANKDMQNNKEETPLF(L)

(L)KNGANKDMQNNKEETPLF(L)

(Y)SSPLDNTPSHQLQVPDHPF(L)

(L)IRNRATDLDARMHDGTTPL(I)

(L)IRNRATDLDARMHDGTTPL(I)

(L)KPLKNASDGTLMDDNQNEW(G)

(L)LKNGANKDMQNNKEETPLF(L)

(L)KNGANKDMQNNKEETPLFL(A)

(Y)IGNLKPAVQGKKARKPSTKGL(S)

(L)KPLKNASDGTLMDDNQNEW(G)

(L)TPPSQHSYSSPLDNTPSHQL(Q)

(L)ETGNSEEEDDAPAVISDFIY(Q)

(L)LKNGANKDMQNNKEETPLF(L)

(L)KNGANKDMQNNKEETPLFL(A)

(L)INC(Carbamidomethyl)HADVNAVDDLGKSALHW(A)

(F)EEQAMLPDTDDQTDHRQW(T)

(L)SDVASPPLMTSPFQQSPSMPL(N)

(F)EEQAMLPDTDDQTDHRQW(T)

(L)SDVASPPLMTSPFQQSPSMPL(N)

(L)INC(Carbamidomethyl)HADVNAVDDLGKSALHW(A)

(L)EDLINC(Carbamidomethyl)HADVNAVDDLGKSAL(H)

(L)SDVASPPLMTSPFQQSPSMPL(N)

(W)FPEGFKVTESSKKKRREPL(G)

(L)SQMMSYQAMPSTRLASQPHL(L)

(L)EDLINC(Carbamidomethyl)HADVNAVDDLGKSAL(H)

(L)SQMMSYQAMPSTRLASQPHL(L)

(L)VSRKRRREHGQLWFPEGF(K)

(L)SQMMSYQAMPSTRLASQPHL(L)

(L)SQMMSYQAMPSTRLASQPHL(L)

(L)MDDNQNEWGDEETLDTKKF(R)

(W)SEGISSPPTSMQSQMGHIPEAF(K)

(L)MDDNQNEWGDEETLDTKKF(R)

(W)SEGISSPPTSMQSQMGHIPEAF(K)

(L)KARRKKSQDGKGC(Carbamidomethyl)LLDNSSVL(S)

(F)KVTESSKKKRREPLGEDSVGL(K)

(W)SEGISSPPTSMQSQMGHIPEAF(K)

(L)KARRKKSQDGKGC(Carbamidomethyl)LLDNSSVL(S)

(L)IRNRATDLDARMHDGTTPLIL(A)

(L)AVEGMLEDLINC(Carbamidomethyl)HADVNAVDDL(G)

(L)IRNRATDLDARMHDGTTPLIL(A)

(L)AVEGMLEDLINC(Carbamidomethyl)HADVNAVDDL(G)

(L)AVEGMLEDLINC(Carbamidomethyl)HADVNAVDDL(G)

(L)TPSPESPDQWSSSSPHSNVSDW(S)

(L)AVEGMLEDLINC(Carbamidomethyl)HADVNAVDDL(G)

(W)SEGISSPPTSMQSQMGHIPEAFK(-)

(L)WFPEGFKVTESSKKKRREPL(G)

(W)SEGISSPPTSMQSQMGHIPEAFK(-)

(L)HAAVSADAQGVFQILIRNRATDL(D)

(W)SEGISSPPTSMQSQMGHIPEAFK(-)

(L)KNASDGTLMDDNQNEWGDEETL(D)

(F)QILIRNRATDLDARMHDGTTPL(I)

(L)KNASDGTLMDDNQNEWGDEETL(D)

(F)QILIRNRATDLDARMHDGTTPL(I)

(L)QHGMMSSLHNGLPSTSLSQMMSY(Q)

(F)QILIRNRATDLDARMHDGTTPL(I)

(F)RFEEQAMLPDTDDQTDHRQW(T)

(L)QHGMMSSLHNGLPSTSLSQMMSY(Q)

(F)QILIRNRATDLDARMHDGTTPL(I)

(L)QHGMMSSLHNGLPSTSLSQMMSY(Q)

(F)LTPSPESPDQWSSSSPHSNVSDW(S)

(F)RFEEQAMLPDTDDQTDHRQW(T)

(L)HNGLPSTSLSQMMSYQAMPSTRL(A)

(L)QHGMMSSLHNGLPSTSLSQMMSY(Q)

(L)QHGMMSSLHNGLPSTSLSQMMSY(Q)

(L)HNGLPSTSLSQMMSYQAMPSTRL(A)

(L)QHGMMSSLHNGLPSTSLSQMMSY(Q)

(L)QHGMMSSLHNGLPSTSLSQMMSY(Q)

(L)HNGLPSTSLSQMMSYQAMPSTRL(A)

(L)QHGMMSSLHNGLPSTSLSQMMSY(Q)

(L)QHGMMSSLHNGLPSTSLSQMMSY(Q)

(L)HNGLPSTSLSQMMSYQAMPSTRL(A)

(L)SHLPVSSPSTAMSNAPMNFSVGGAAGL(S)

(L)QHGMMSSLHNGLPSTSLSQMMSY(Q)

(L)SHLPVSSPSTAMSNAPMNFSVGGAAGL(S)

(L)NMAGKQEMALGGSGRMAFEAVPPRL(S)

(L)SHLPVSSPSTAMSNAPMNFSVGGAAGL(S)

(L)NMAGKQEMALGGSGRMAFEAVPPRL(S)

(F)QQSPSMPLNHLPGMPDAHMSINHL(N)

(L)NMAGKQEMALGGSGRMAFEAVPPRL(S)

(F)QQSPSMPLNHLPGMPDAHMSINHL(N)

(F)QQSPSMPLNHLPGMPDAHMSINHL(N)

(L)ETGNSEEEDDAPAVISDFIYQGASL(H)

(L)NMAGKQEMALGGSGRMAFEAVPPRL(S)

(F)QQSPSMPLNHLPGMPDAHMSINHL(N)

(L)SQPDMQPVSSSAMAVHTILPQDSQL(L)

(F)QQSPSMPLNHLPGMPDAHMSINHL(N)

(F)KVTESSKKKRREPLGEDSVGLKPL(K)

(F)QQSPSMPLNHLPGMPDAHMSINHL(N)

(L)C(Carbamidomethyl)SPSSY(I)

(L)GEDSVGL(K)

(L)ESPHGY(L)

(L)C(Carbamidomethyl)SPSSY(I)

(L)SGQC(Carbamidomethyl)DW(L)

(L)HLAARY(S)

(L)SQMMSY(Q)

(L)LDNSSVL(S)

(F)IYQGASL(H)

(L)SGQC(Carbamidomethyl)DW(L)

(L)AAREGSY(E)

(L)SQMMSY(Q)

(L)ASQPHLL(Q)

(L)LDEYNL(V)

(Y)ETAKVLL(D)

(L)SQMMSY(Q)

(F)EAVPPRL(S)

(L)WFPEGF(K)

(L)GGSGRMAF(E)

(L)SDVASPPL(M)

(L)GGSGRMAF(E)

(L)GKSALHW(A)

(L)ESPHGYL(S)

(L)KNASDGTL(M)

(L)QVPDHPF(L)

(L)QVPDHPF(L)

(L)SGQC(Carbamidomethyl)DWL(S)

(L)GAPTLSPPL(C)

(L)SGQC(Carbamidomethyl)DWL(S)

(F)LAAREGSY(E)

(F)QQSPSMPL(N)

(L)QHGMMSSL(H)

(F)QQSPSMPL(N)

(Y)QAMPSTRL(A)

(F)QQSPSMPL(N)

(L)QHGMMSSL(H)

(L)QHGMMSSL(H)

(Y)NLVRSPPL(H)

(Y)LSDVASPPL(M)

(Y)QAMPSTRL(A)

(F)QQSPSMPL(N)

(Y)QAMPSTRL(A)

(L)QHGMMSSL(H)

(L)QHGMMSSL(H)

(L)DNTPSHQL(Q)

(L)LPTSLPSSL(A)

(L)TPPSQHSY(S)

(Y)QAMPSTRL(A)

(L)QHGMMSSL(H)

(L)HNGLPSTSL(S)

(L)MIASC(Carbamidomethyl)SGGGL(E)

(L)QVPDHPFL(T)

(L)DTKKFRF(E)

(L)MIASC(Carbamidomethyl)SGGGL(E)

(L)HSGPLGAPTL(S)

(L)MIASC(Carbamidomethyl)SGGGL(E)

(L)QVPDHPFL(T)

(L)IRNRATDL(D)

(L)MIASC(Carbamidomethyl)SGGGL(E)

(L)AVEGMLEDL(I)

(L)AVEGMLEDL(I)

(Y)SRSDAAKRL(L)

(L)FLAAREGSY(E)

(L)GEDSVGLKPL(K)

(L)AQPMTTTQF(L)

(F)LTPPSQHSY(S)

(L)AARLAVEGML(E)

(L)QSGMVQNQY(G)

(L)AQPMTTTQF(L)

(L)AARLAVEGML(E)

(L)MDDNQNEW(G)

(L)QSGMVQNQY(G)

(L)QSGMVQNQY(G)

(L)MDDNQNEW(G)

(L)SPPLC(Carbamidomethyl)SPSSY(I)

(L)QSGMVQNQY(G)

(L)C(Carbamidomethyl)SPSSYIGNL(K)

(L)NMAGKQEMAL(G)

(L)SPPLC(Carbamidomethyl)SPSSY(I)

(L)C(Carbamidomethyl)SPSSYIGNL(K)

(L)SC(Carbamidomethyl)NGKDSKDL(K)

(L)NMAGKQEMAL(G)

(W)TQQHLDAADL(R)

(Y)SRSDAAKRLL(E)

(L)SC(Carbamidomethyl)NGKDSKDL(K)

(L)NMAGKQEMAL(G)

(L)AQPMTTTQFL(T)

(L)TPSPESPDQW(S)

(L)KPLKNASDGTL(M)

(L)AQPMTTTQFL(T)

(L)VRSPPLHSGPL(G)

(L)HAAVSADAQGVF(Q)

(Y)ETAKVLLDHF(A)

(L)SGQC(Carbamidomethyl)DWLSRL(Q)

(L)DARMHDGTTPL(I)

(L)SGQC(Carbamidomethyl)DWLSRL(Q)

(L)DARMHDGTTPL(I)

(L)DNSSVLSPVDSL(E)

(F)TPLMIASC(Carbamidomethyl)SGGGL(E)

(W)AAAVNNVEAAVVL(L)

(F)TPLMIASC(Carbamidomethyl)SGGGL(E)

(F)LTPSPESPDQW(S)

(L)ILAARLAVEGML(E)

(F)TPLMIASC(Carbamidomethyl)SGGGL(E)

(L)ILAARLAVEGML(E)

(F)TPLMIASC(Carbamidomethyl)SGGGL(E)

(W)GDEETLDTKKF(R)

(L)SPVDSLESPHGY(L)

(W)SSSSPHSNVSDW(S)

(Y)SSPLDNTPSHQL(Q)

(F)QILIRNRATDL(D)

(L)TPPSQHSYSSPL(D)

(L)DEYNLVRSPPL(H)

(F)QILIRNRATDL(D)

(F)SVGGAAGLSGQC(Carbamidomethyl)DW(L)

(L)HNQTDRTGETAL(H)

(L)HSGPLGAPTLSPPL(C)

(L)LDNSSVLSPVDSL(E)

(L)SDVASPPLMTSPF(Q)

(W)AAAVNNVEAAVVLL(K)

(F)SVGGAAGLSGQC(Carbamidomethyl)DW(L)

(L)SDVASPPLMTSPF(Q)

(Y)NLVRSPPLHSGPL(G)

(L)AARLAVEGMLEDL(I)

(L)AAREGSYETAKVL(L)

(L)SPVDSLESPHGYL(S)

(L)AARLAVEGMLEDL(I)

(L)SRLQSGMVQNQY(G)

(F)LTPPSQHSYSSPL(D)

(L)SRLQSGMVQNQY(G)

(L)INC(Carbamidomethyl)HADVNAVDDL(G)

(L)DARMHDGTTPLIL(A)

(L)MTSPFQQSPSMPL(N)

(F)SVGGAAGLSGQC(Carbamidomethyl)DWL(S)

(L)INC(Carbamidomethyl)HADVNAVDDL(G)

(L)DARMHDGTTPLIL(A)

(Y)LSDVASPPLMTSPF(Q)

(L)AARYSRSDAAKRL(L)

(L)MTSPFQQSPSMPL(N)

(L)SPPLC(Carbamidomethyl)SPSSYIGNL(K)

(F)SVGGAAGLSGQC(Carbamidomethyl)DWL(S)

(Y)LSDVASPPLMTSPF(Q)

(L)MTSPFQQSPSMPL(N)

(L)SPPLC(Carbamidomethyl)SPSSYIGNL(K)

(F)LAAREGSYETAKVL(L)

(L)AAREGSYETAKVLL(D)

(L)GAPTLSPPLC(Carbamidomethyl)SPSSY(I)

(Y)QAMPSTRLASQPHL(L)

(L)VSRKRRREHGQL(W)

(W)LSRLQSGMVQNQY(G)

(L)HAAVSADAQGVFQIL(I)

(L)GAPTLSPPLC(Carbamidomethyl)SPSSY(I)

(Y)QAMPSTRLASQPHL(L)

(Y)QAMPSTRLASQPHL(L)

(W)LSRLQSGMVQNQY(G)

(L)GGSGRMAFEAVPPRL(S)

(Y)QAMPSTRLASQPHL(L)

(L)GGSGRMAFEAVPPRL(S)

(L)HWAAAVNNVEAAVVL(L)

(L)ESPHGYLSDVASPPL(M)

(L)AARYSRSDAAKRLL(E)

(W)GDEETLDTKKFRF(E)

(L)HNQTDRTGETALHL(A)

(L)VRSPPLHSGPLGAPTL(S)

(L)KARRKKSQDGKGC(Carbamidomethyl)L(L)

(L)SQMMSYQAMPSTRL(A)

(L)KARRKKSQDGKGC(Carbamidomethyl)L(L)

(Y)QAMPSTRLASQPHLL(Q)

(L)SQMMSYQAMPSTRL(A)

(Y)QAMPSTRLASQPHLL(Q)

(Y)QAMPSTRLASQPHLL(Q)

(L)HNGLPSTSLSQMMSY(Q)

(L)SQMMSYQAMPSTRL(A)

(Y)QAMPSTRLASQPHLL(Q)

(L)HNGLPSTSLSQMMSY(Q)

(L)HWAAAVNNVEAAVVLL(K)

(L)SQMMSYQAMPSTRL(A)

(L)HNGLPSTSLSQMMSY(Q)

(F)KVTESSKKKRREPL(G)

(L)MDDNQNEWGDEETL(D)

(L)VSRKRRREHGQLW(F)

(L)MDDNQNEWGDEETL(D)

(L)HLAARYSRSDAAKRL(L)

(L)KARRKKSQDGKGC(Carbamidomethyl)LL(D)

(L)DNTPSHQLQVPDHPF(L)

(L)KARRKKSQDGKGC(Carbamidomethyl)LL(D)

(L)QHGMMSSLHNGLPSTSL(S)

(Y)QGASLHNQTDRTGETAL(H)

(L)NHLPGMPDAHMSINHL(N)

(L)EDLINC(Carbamidomethyl)HADVNAVDDL(G)

(-)GVLVSRKRRREHGQL(W)

(L)KPAVQGKKARKPSTKGL(S)

(L)QHGMMSSLHNGLPSTSL(S)

(L)QHGMMSSLHNGLPSTSL(S)

(Y)QGASLHNQTDRTGETAL(H)

(L)NHLPGMPDAHMSINHL(N)

(L)GEDSVGLKPLKNASDGTL(M)

(L)EASADANIQDNMGRTPL(H)

(L)QHGMMSSLHNGLPSTSL(S)

(L)EDLINC(Carbamidomethyl)HADVNAVDDL(G)

(L)QHGMMSSLHNGLPSTSL(S)

(L)NHLPGMPDAHMSINHL(N)

(L)EASADANIQDNMGRTPL(H)

(L)QHGMMSSLHNGLPSTSL(S)

(-)GVLVSRKRRREHGQL(W)

(L)KNASDGTLMDDNQNEW(G)

(L)DNTPSHQLQVPDHPFL(T)

(L)DARMHDGTTPLILAARL(A)

(L)KNASDGTLMDDNQNEW(G)

(L)NMAGKQEMALGGSGRMAF(E)

(L)DARMHDGTTPLILAARL(A)

(L)NMAGKQEMALGGSGRMAF(E)

(Y)GAMRGGMQPGTHQQAQNL(Q)

(L)INC(Carbamidomethyl)HADVNAVDDLGKSAL(H)

(L)NMAGKQEMALGGSGRMAF(E)

(Y)GAMRGGMQPGTHQQAQNL(Q)

(L)DNSSVLSPVDSLESPHGY(L)

(L)NMAGKQEMALGGSGRMAF(E)

(L)INC(Carbamidomethyl)HADVNAVDDLGKSAL(H)

(Y)GAMRGGMQPGTHQQAQNL(Q)

(L)LEASADANIQDNMGRTPL(H)

(L)LPTSLPSSLAQPMTTTQF(L)

(L)ETGNSEEEDDAPAVISDF(I)

(L)KNGANKDMQNNKEETPL(F)
(L)LEASADANIQDNMGRTPL(H)
(L)LPTSLPSSLAQPMTTTQF(L)
(L)KNGANKDMQNNKEETPL(F)
(L)SHLPVSSPSTAMSNAPMNF(S)
(-)GVLVSRKRRREHGQLW(F)
(L)SHLPVSSPSTAMSNAPMNF(S)
(L)SHLPVSSPSTAMSNAPMNF(S)
(-)GVLVSRKRRREHGQLW(F)
(L)GKSALHWAAAVNNVEAAVVL(L)
(Y)QGASLHNQTDRTGETALHL(A)
(L)LPTSLPSSLAQPMTTTQFL(T)
(L)AQPMTTTQFLTPPSQHSY(S)
(L)LKNGANKDMQNNKEETPL(F)
(Y)QGASLHNQTDRTGETALHL(A)

(L)LPTSLPSSLAQPMTTTQFL(T)
(L)AQPMTTTQFLTPPSQHSY(S)
(L)HNQTDRTGETALHLAARY(S)
(L)QVPDHPFLTPSPESPDQW(S)
(L)LKNGANKDMQNNKEETPL(F)
(F)IYQGASLHNQTDRTGETAL(H)
(L)QVPDHPFLTPSPESPDQW(S)
(L)KNGANKDMQNNKEETPLF(L)
(L)KNGANKDMQNNKEETPL(L)
(Y)SSPLDNTPSHQLQVPDHPF(L)
(L)IRNRATDLDARMHDGTTPL(I)
(L)IRNRATDLDARMHDGTTPL(I)
(L)KPLKNASDGTLMDDNQNEW(G)
(L)LKNGANKDMQNNKEETPLF(L)
(L)KNGANKDMQNNKEETPLFL(A)

(Y)IGNLKPAVQGKKARKPSTKGL(S)
(L)KPLKNASDGTLMDDNQNEW(G)
(L)TPPSQHSYSSPLDNTPSHQL(Q)
(L)ETGNSEEEDDAPAVISDFIY(Q)
(L)LKNGANKDMQNNKEETPLF(L)
(L)KNGANKDMQNNKEETPLFL(A)
(L)INC(Carbamidomethyl)HADVNAVDDLGKSALHW(A)
(F)EEQAMLPDTDDQTDHRQW(T)
(L)SDVASPPLMTSPFQQSPSMPL(N)
(F)EEQAMLPDTDDQTDHRQW(T)
(L)SDVASPPLMTSPFQQSPSMPL(N)
(L)INC(Carbamidomethyl)HADVNAVDDLGKSALHW(A)
(L)EDLINC(Carbamidomethyl)HADVNAVDDLGKSAL(H)
(L)SDVASPPLMTSPFQQSPSMPL(N)

Sample	Mean Ct score 18S primers	Mean Ct score W repeat primers	Sex
XAV1	36.595	N/A	Male
XAV2	36.78	35.785	Female
XAV3	37.89	N/A	Male
XAV4	36.535	34.46	Female
Rosc1	38.535	N/A	Male
Rosc2	34.995	N/A	Male
Rosc3	37.71	35.31	Female
Rosc4	35.03	N/A	Male
DRB1	37.1	N/A	Male
DRB2	38.675	N/A	Male
DRB3	38.175	35.2	Female
DRB4	35.91	N/A	Male

Supplementary Table 2) Summary of Sex determination quantitative PCR results from samples used for genomics analyses. Each -/+ drug treatment for the genomics analyses were performed in quadruplicate (i.e. from 4 different embryos). Quantitative PCR (qPCR) performed on genomic DNA from these samples reveal a consistent Ct score for the housekeeping gene 18S rRNA subunit. A strong Ct score for the sex-chromosome W repeat primer set indicates that the sample comes from a female embryo, while no score (N/A) indicates a male sample.

Supplementary Table 3) List of Significantly enriched GO terms for XAV939 treatment following RNA-seq analysis.

Term	Count	%	P-Value
negative regulation of nucleobase, nucleoside, nucleotide and nucleic acid metabolic pr	16	2.7	2.00E-04
skeletal system development	15	2.5	2.10E-04
negative regulation of nitrogen compound metabolic process	16	2.7	2.30E-04
odontogenesis of dentine-containing tooth	7	1.2	2.30E-04
odontogenesis	7	1.2	2.30E-04
regulation of transcription	53	9	3.70E-04
positive regulation of biomineral formation	5	0.8	3.80E-04
positive regulation of bone mineralization	5	0.8	3.80E-04
positive regulation of ossification	5	0.8	5.80E-04
negative regulation of cellular biosynthetic process	16	2.7	5.80E-04
tube development	13	2.2	6.70E-04
negative regulation of biosynthetic process	16	2.7	7.20E-04
regulation of biomineral formation	5	0.8	1.20E-03
regulation of bone mineralization	5	0.8	1.20E-03
regulation of RNA metabolic process	41	7	1.20E-03
negative regulation of macromolecule biosynthetic process	15	2.5	1.20E-03
regulation of transcription, DNA-dependent	40	6.8	1.60E-03
negative regulation of transcription	13	2.2	1.70E-03
negative regulation of macromolecule metabolic process	17	2.9	1.90E-03
respiratory system development	8	1.4	3.20E-03
negative regulation of cell proliferation	10	1.7	4.50E-03
negative regulation of gene expression	13	2.2	4.50E-03
skeletal system morphogenesis	8	1.4	4.90E-03
cell fate commitment	9	1.5	5.70E-03
lung development	7	1.2	7.20E-03
respiratory tube development	7	1.2	8.00E-03
urogenital system development	7	1.2	8.90E-03
tube morphogenesis	8	1.4	1.10E-02
regulation of transcription from RNA polymerase II promoter	16	2.7	1.30E-02
regulation of neurogenesis	7	1.2	1.30E-02
growth	8	1.4	1.30E-02
cartilage development	6	1	1.50E-02
digestive tract morphogenesis	4	0.7	1.50E-02
digestive system development	4	0.7	1.50E-02
regulation of cell proliferation	17	2.9	1.60E-02
positive regulation of osteoblast differentiation	4	0.7	1.80E-02
branching morphogenesis of a tube	6	1	2.00E-02
nitrogen compound biosynthetic process	15	2.5	2.10E-02
kidney development	6	1	2.20E-02
cardiac cell differentiation	4	0.7	2.20E-02
negative regulation of RNA metabolic process	9	1.5	2.20E-02
morphogenesis of a branching structure	6	1	2.40E-02
BMP signaling pathway	4	0.7	2.60E-02
pattern specification process	11	1.9	2.70E-02
nucleobase, nucleoside and nucleotide biosynthetic process	11	1.9	2.70E-02
nucleobase, nucleoside, nucleotide and nucleic acid biosynthetic process	11	1.9	2.70E-02
epithelium development	8	1.4	2.80E-02
regulation of cell size	6	1	2.90E-02
gland development	7	1.2	2.90E-02
regulation of nervous system development	7	1.2	2.90E-02
cell death	10	1.7	3.00E-02
regulation of ossification	5	0.8	3.00E-02
gut development	4	0.7	3.00E-02

cell death		10	1.7	3.00E-02
regulation of ossification		5	0.8	3.00E-02
gut development		4	0.7	3.00E-02
death		10	1.7	3.30E-02
keratinocyte proliferation		3	0.5	3.60E-02
regulation of cell development		7	1.2	3.60E-02
tissue morphogenesis		8	1.4	4.00E-02
apoptosis		9	1.5	4.10E-02
nucleoside monophosphate metabolic process		5	0.8	4.40E-02
ectodermal gut morphogenesis		3	0.5	4.50E-02
ectodermal gut development		3	0.5	4.50E-02
regulation of cell projection organization		4	0.7	4.50E-02
programmed cell death		9	1.5	4.70E-02
cell redox homeostasis		5	0.8	4.90E-02
negative regulation of transcription, DNA-dependent		8	1.4	5.00E-02
ureteric bud development		4	0.7	5.10E-02
embryonic morphogenesis		11	1.9	5.50E-02
limb morphogenesis		6	1	5.60E-02
appendage morphogenesis		6	1	5.60E-02
nucleotide biosynthetic process		10	1.7	5.60E-02
regulation of osteoblast differentiation		4	0.7	5.70E-02
intracellular transport		13	2.2	5.90E-02
gut morphogenesis		3	0.5	6.50E-02
neuron differentiation		10	1.7	6.60E-02
transmembrane receptor protein serine/threonine kinase signaling pathway		5	0.8	6.70E-02
appendage development		6	1	6.80E-02
limb development		6	1	6.80E-02
metanephros development		4	0.7	7.00E-02
regulation of neuron differentiation		5	0.8	7.20E-02
positive regulation of nucleobase, nucleoside, nucleotide and nucleic acid metabolic pro		14	2.4	7.40E-02
smoothened signaling pathway involved in ventral spinal cord interneuron specification		2	0.3	7.60E-02
ureteric bud morphogenesis		3	0.5	7.60E-02
branching involved in ureteric bud morphogenesis		3	0.5	7.60E-02
negative regulation of transcription from RNA polymerase II promoter		6	1	7.60E-02
heart development		8	1.4	7.70E-02
Wnt receptor signaling pathway		6	1	8.10E-02
positive regulation of nitrogen compound metabolic process		14	2.4	8.70E-02
spinal cord development		3	0.5	8.80E-02
ectoderm development		5	0.8	8.90E-02
sensory organ development		8	1.4	9.90E-02
nucleoside monophosphate biosynthetic process		4	0.7	1.00E-01
regulation of Wnt receptor signaling pathway		3	0.5	1.00E-01
palate development		3	0.5	1.00E-01

Supplementary Table 4) List of Significantly enriched GO terms for Roscovitine treatment following RNA-seq analysis.

Term	Count	%	P-Value
translation	45	2.3	1.30E-05
regulation of cellular response to stress	12	0.6	1.80E-05
chromosome organization	38	1.9	7.70E-05
cell cycle	36	1.8	2.50E-04
electron transport chain	14	0.7	2.60E-04
chromatin modification	22	1.1	2.80E-04
cell cycle process	28	1.4	3.60E-04
M phase	18	0.9	6.60E-04
response to DNA damage stimulus	31	1.6	9.20E-04
ATP synthesis coupled electron transport	8	0.4	9.30E-04
DNA metabolic process	46	2.4	1.10E-03
cell cycle phase	21	1.1	1.30E-03
oxidative phosphorylation	16	0.8	1.60E-03
regulation of GTPase activity	16	0.8	1.60E-03
respiratory electron transport chain	9	0.5	1.60E-03
histone modification	13	0.7	1.80E-03
transcription	67	3.4	2.00E-03
chromatin organization	28	1.4	2.40E-03
double-strand break repair	11	0.6	2.60E-03
cellular respiration	12	0.6	2.90E-03
regulation of hydrolase activity	23	1.2	3.00E-03
covalent chromatin modification	13	0.7	3.00E-03
generation of precursor metabolites and energy	29	1.5	3.10E-03
lymphocyte mediated immunity	7	0.4	3.70E-03
B cell activation	10	0.5	4.10E-03
ncRNA metabolic process	21	1.1	4.70E-03
positive regulation of I-kappaB kinase/NF-kappaB cascade	9	0.5	4.80E-03
mitochondrial ATP synthesis coupled electron transport	6	0.3	5.30E-03
regulation of I-kappaB kinase/NF-kappaB cascade	9	0.5	6.50E-03
immunoglobulin mediated immune response	6	0.3	8.70E-03
ncRNA processing	15	0.8	9.20E-03
cellular response to stress	33	1.7	1.10E-02
regulation of Rab protein signal transduction	10	0.5	1.20E-02
regulation of Rab GTPase activity	10	0.5	1.20E-02
adaptive immune response	7	0.4	1.20E-02
adaptive immune response based on somatic recombination of immune receptors built from immunoglobulin superfamily domains	7	0.4	1.20E-02
leukocyte mediated immunity	7	0.4	1.20E-02
phosphate metabolic process	87	4.4	1.20E-02
phosphorus metabolic process	87	4.4	1.20E-02
ribonucleoprotein complex biogenesis	13	0.7	1.30E-02
leukocyte activation	18	0.9	1.30E-02
regulation of DNA repair	5	0.3	1.30E-02
regulation of interleukin-12 production	5	0.3	1.30E-02
B cell mediated immunity	6	0.3	1.30E-02
DNA repair	23	1.2	1.30E-02
regulation of DNA binding	9	0.5	1.50E-02
response to ionizing radiation	7	0.4	1.70E-02
macromolecule catabolic process	36	1.8	1.70E-02
microtubule cytoskeleton organization	11	0.6	1.70E-02
energy derivation by oxidation of organic compounds	13	0.7	1.80E-02
lymphocyte activation	16	0.8	1.80E-02
blastocyst growth	4	0.2	1.80E-02

blastocyst growth	4	0.2	1.80E-02
mitotic sister chromatid segregation	4	0.2	1.80E-02
sister chromatid segregation	4	0.2	1.80E-02
negative regulation of molecular function	14	0.7	1.90E-02
M phase of mitotic cell cycle	11	0.6	2.10E-02
regulation of DNA metabolic process	11	0.6	2.10E-02
regulation of stress-activated protein kinase signaling pathway	5	0.3	2.10E-02
regulation of JNK cascade	5	0.3	2.10E-02
DNA replication	20	1	2.40E-02
cell activation	19	1	2.40E-02
cellular macromolecule catabolic process	32	1.6	2.50E-02
regulation of binding	10	0.5	2.60E-02
negative regulation of binding	6	0.3	2.70E-02
regulation of transcription factor activity	7	0.4	2.90E-02
positive regulation of programmed cell death	19	1	3.00E-02
positive regulation of apoptosis	19	1	3.00E-02
positive regulation of cellular component organization	12	0.6	3.10E-02
regulation of Ras GTPase activity	12	0.6	3.10E-02
ribosome biogenesis	10	0.5	3.20E-02
positive regulation of DNA repair	4	0.2	3.30E-02
positive regulation of cell death	19	1	3.30E-02
mitotic cell cycle	14	0.7	3.30E-02
negative regulation of macromolecule metabolic process	34	1.7	3.30E-02
positive regulation of protein kinase cascade	11	0.6	3.40E-02
negative regulation of immune system process	6	0.3	3.60E-02
immune effector process	8	0.4	4.40E-02
negative regulation of DNA binding	5	0.3	4.50E-02
phosphorylation	71	3.6	4.50E-02
RNA biosynthetic process	11	0.6	4.60E-02
regulation of macrophage activation	3	0.2	4.70E-02
cytokine production	6	0.3	4.70E-02
cell division	13	0.7	4.80E-02
DNA recombination	9	0.5	4.80E-02
positive regulation of stress-activated protein kinase signaling pathway	4	0.2	5.20E-02
positive regulation of JNK cascade	4	0.2	5.20E-02
regulation of gene expression, epigenetic	8	0.4	5.30E-02
regulation of protein kinase cascade	12	0.6	5.40E-02
regulation of cell cycle	17	0.9	5.60E-02
sexual reproduction	17	0.9	5.60E-02
RNA processing	26	1.3	5.70E-02
biopolymer methylation	7	0.4	5.70E-02
regulation of transcription	127	6.5	5.90E-02
proteolysis involved in cellular protein catabolic process	25	1.3	5.90E-02
immune system development	21	1.1	5.90E-02
organelle fission	10	0.5	5.90E-02
transcription, DNA-dependent	10	0.5	5.90E-02
M phase of meiotic cell cycle	5	0.3	6.00E-02
meiosis	5	0.3	6.00E-02
meiotic cell cycle	5	0.3	6.00E-02
protein amino acid acylation	6	0.3	6.00E-02
chromosome segregation	6	0.3	6.00E-02
protein catabolic process	27	1.4	6.20E-02
cellular protein catabolic process	25	1.3	6.80E-02
tRNA metabolic process	12	0.6	6.80E-02

tRNA metabolic process	12	0.6	6.80E-02
tRNA processing	7	0.4	6.90E-02
methylation	8	0.4	7.40E-02
negative regulation of transcription factor activity	4	0.2	7.50E-02
homeostasis of number of cells	10	0.5	7.80E-02
membrane organization	15	0.8	7.90E-02
genetic imprinting	3	0.2	8.50E-02
histone methylation	3	0.2	8.50E-02
iron-sulfur cluster assembly	3	0.2	8.50E-02
G2/M transition DNA damage checkpoint	3	0.2	8.50E-02
metallo-sulfur cluster assembly	3	0.2	8.50E-02
prostaglandin biosynthetic process	3	0.2	8.50E-02
G2/M transition checkpoint	3	0.2	8.50E-02
prostanoid biosynthetic process	3	0.2	8.50E-02
inner cell mass cell proliferation	3	0.2	8.50E-02
regulation of interleukin-12 biosynthetic process	3	0.2	8.50E-02
nuclear division	9	0.5	8.80E-02
mitosis	9	0.5	8.80E-02
gamete generation	14	0.7	8.90E-02
regulation of cytokine production	11	0.6	9.70E-02
establishment of organelle localization	5	0.3	9.90E-02
dephosphorylation	16	0.8	9.90E-02

Supplementary Table 5) List of Significantly enriched GO terms for DRB treatment following RNA-seq analysis.

Term	Genes	%	P-Value	B
chromatin organization	9	3.3	5.10E-04	
chromosome organization	10	3.6	5.50E-04	
chromatin modification	7	2.6	9.30E-04	
histone modification	5	1.8	2.50E-03	
covalent chromatin modification	5	1.8	3.10E-03	
positive regulation of programmed cell death	6	2.2	1.10E-02	
positive regulation of apoptosis	6	2.2	1.10E-02	
positive regulation of cell death	6	2.2	1.20E-02	
mRNA metabolic process	5	1.8	2.00E-02	
protein amino acid acetylation	3	1.1	2.20E-02	
histone acetylation	3	1.1	2.20E-02	
positive regulation of protein kinase cascade	4	1.5	2.60E-02	
protein amino acid acylation	3	1.1	2.80E-02	
induction of apoptosis	4	1.5	3.50E-02	
induction of programmed cell death	4	1.5	3.50E-02	
regulation of protein kinase cascade	4	1.5	4.30E-02	
mRNA processing	4	1.5	5.20E-02	
positive regulation of response to stimulus	4	1.5	8.40E-02	

Supplementary Table 6) List of Significantly enriched GO terms for Roscovitine treatment following Microarray analysis.

Term	Count	%	P-Value
M phase	22	1.1	2.40E-06
transcription	75	3.9	7.60E-06
cell cycle phase	24	1.2	3.50E-05
ncRNA metabolic process	25	1.3	6.80E-05
RNA processing	35	1.8	7.90E-05
cell cycle process	29	1.5	8.10E-05
microtubule cytoskeleton organization	15	0.8	8.40E-05
chromosome organization	37	1.9	8.70E-05
M phase of mitotic cell cycle	15	0.8	1.20E-04
negative regulation of nitrogen compound metabolic process	34	1.8	1.40E-04
negative regulation of cellular biosynthetic process	36	1.9	1.50E-04
cellular macromolecule catabolic process	39	2	1.60E-04
negative regulation of biosynthetic process	36	1.9	2.30E-04
negative regulation of nucleobase, nucleoside, nucleotide and nucleic acid metabolic pr	33	1.7	2.40E-04
nuclear division	14	0.7	2.60E-04
mitosis	14	0.7	2.60E-04
macromolecule catabolic process	41	2.1	4.90E-04
cellular response to stress	37	1.9	5.00E-04
mitotic cell cycle	18	0.9	5.50E-04
negative regulation of macromolecule metabolic process	40	2.1	6.20E-04
organelle fission	14	0.7	6.40E-04
negative regulation of macromolecule biosynthetic process	33	1.7	8.10E-04
response to DNA damage stimulus	30	1.6	1.20E-03
cell cycle	33	1.7	1.30E-03
tRNA metabolic process	16	0.8	1.40E-03
negative regulation of gene expression	30	1.6	1.50E-03
meiosis	7	0.4	1.90E-03
M phase of meiotic cell cycle	7	0.4	1.90E-03
meiotic cell cycle	7	0.4	1.90E-03
multicellular organism reproduction	23	1.2	2.20E-03
reproductive process in a multicellular organism	23	1.2	2.20E-03
cellular protein catabolic process	30	1.6	2.40E-03
negative regulation of transcription	27	1.4	2.40E-03
ncRNA processing	16	0.8	2.60E-03
mRNA metabolic process	18	0.9	2.70E-03
regulation of transcription from RNA polymerase II promoter	41	2.1	3.00E-03
gamete generation	18	0.9	3.20E-03
DNA metabolic process	43	2.2	3.30E-03
ubiquitin-dependent protein catabolic process	19	1	3.40E-03
ribonucleoprotein complex biogenesis	14	0.7	3.50E-03
male gamete generation	13	0.7	3.60E-03
spermatogenesis	13	0.7	3.60E-03
proteolysis involved in cellular protein catabolic process	29	1.5	3.90E-03
regulation of transcription	133	6.9	4.30E-03
protein catabolic process	31	1.6	4.60E-03
sexual reproduction	20	1	4.80E-03
negative regulation of transcription, DNA-dependent	21	1.1	4.90E-03
mRNA processing	15	0.8	5.80E-03
mitochondrion organization	11	0.6	5.80E-03
modification-dependent macromolecule catabolic process	26	1.4	6.30E-03
modification-dependent protein catabolic process	26	1.4	6.30E-03
negative regulation of RNA metabolic process	21	1.1	7.30E-03
RNA modification	8	0.4	8.60E-03
ribosome biogenesis	11	0.6	9.10E-03
DNA repair	23	1.2	9.20E-03
microtubule-based process	21	1.1	1.10E-02
centrosome cycle	5	0.3	1.20E-02
DNA catabolic process, endonucleolytic	6	0.3	1.20E-02

chromosome segregation	7	0.4	1.40E-02
negative regulation of molecular function	14	0.7	1.50E-02
amino acid activation	10	0.5	1.50E-02
tRNA aminoacylation	10	0.5	1.50E-02
RNA biosynthetic process	12	0.6	1.50E-02
biopolymer methylation	8	0.4	1.50E-02
blastocyst growth	4	0.2	1.60E-02
negative regulation of catalytic activity	11	0.6	1.70E-02
regulation of DNA metabolic process	11	0.6	1.70E-02
cell division	14	0.7	1.70E-02
gonad development	10	0.5	1.80E-02
tRNA processing	8	0.4	2.00E-02
transcription, DNA-dependent	11	0.6	2.00E-02
positive regulation of macromolecule biosynthetic process	40	2.1	2.20E-02
chromatin organization	24	1.2	2.30E-02
reproductive structure development	11	0.6	2.40E-02
positive regulation of macromolecule metabolic process	47	2.4	2.40E-02
negative regulation of DNA metabolic process	6	0.3	2.40E-02
transcription initiation	7	0.4	2.50E-02
blood vessel morphogenesis	17	0.9	2.50E-02
reproductive cellular process	13	0.7	2.60E-02
centrosome organization	5	0.3	2.80E-02
telomere organization	5	0.3	2.80E-02
telomere maintenance	5	0.3	2.80E-02
intracellular transport	34	1.8	2.90E-02
negative regulation of transcription from RNA polymerase II promoter	14	0.7	2.90E-02
rRNA processing	8	0.4	3.10E-02
rRNA metabolic process	8	0.4	3.10E-02
reproductive developmental process	19	1	3.30E-02
tRNA aminoacylation for protein translation	9	0.5	3.40E-02
germ cell development	9	0.5	3.40E-02
positive regulation of cellular biosynthetic process	40	2.1	3.50E-02
chromatin modification	16	0.8	3.60E-02
translation	32	1.7	3.60E-02
regulation of hydrolase activity	19	1	3.60E-02
histone modification	10	0.5	3.70E-02
positive regulation of biosynthetic process	40	2.1	3.70E-02
positive regulation of transcription, DNA-dependent	29	1.5	3.70E-02
B cell activation	8	0.4	3.80E-02
development of primary sexual characteristics	11	0.6	3.80E-02
angiogenesis	12	0.6	3.80E-02
positive regulation of transcription	34	1.8	4.00E-02
positive regulation of RNA metabolic process	29	1.5	4.30E-02
cell proliferation	17	0.9	4.30E-02
regulation of cell cycle	17	0.9	4.30E-02
cytoskeleton organization	23	1.2	4.30E-02
centrosome duplication	3	0.2	4.40E-02
female sex differentiation	8	0.4	4.50E-02
positive regulation of nucleobase, nucleoside, nucleotide and nucleic acid metabolic pro	37	1.9	4.60E-02
vesicle-mediated transport	26	1.4	4.70E-02
protein amino acid alkylation	4	0.2	4.70E-02
protein amino acid methylation	4	0.2	4.70E-02
RNA 3'-end processing	4	0.2	4.70E-02
covalent chromatin modification	10	0.5	5.00E-02
negative regulation of cell proliferation	17	0.9	5.30E-02
vasculature development	19	1	5.30E-02
spermatid development	5	0.3	5.40E-02
microtubule organizing center organization	5	0.3	5.40E-02
induction of programmed cell death	11	0.6	5.70E-02
induction of apoptosis	11	0.6	5.70E-02
positive regulation of gene expression	34	1.8	5.70E-02
DNA replication	18	0.9	6.00E-02
negative regulation of transferase activity	7	0.4	6.00E-02

DNA replication	18	0.9	6.00E-02
negative regulation of transferase activity	7	0.4	6.00E-02
transcription from RNA polymerase II promoter	7	0.4	6.00E-02
regulation of transferase activity	17	0.9	6.30E-02
methylation	8	0.4	6.40E-02
positive regulation of nitrogen compound metabolic process	37	1.9	6.40E-02
blood vessel development	18	0.9	6.60E-02
ovulation cycle	6	0.3	6.60E-02
DNA catabolic process	6	0.3	6.60E-02
ovulation cycle process	6	0.3	6.60E-02
DNA fragmentation involved in apoptosis	4	0.2	6.90E-02
negative regulation of DNA replication	4	0.2	6.90E-02
apoptotic nuclear changes	4	0.2	6.90E-02
aspartate family amino acid metabolic process	4	0.2	6.90E-02
aspartate family amino acid biosynthetic process	4	0.2	6.90E-02
mitochondrial transport	5	0.3	7.10E-02
sex differentiation	12	0.6	7.10E-02
glycoprotein metabolic process	14	0.7	7.30E-02
regulation of translation	8	0.4	7.50E-02
immune system development	20	1	7.50E-02
organic acid transport	9	0.5	7.50E-02
carboxylic acid transport	9	0.5	7.50E-02
positive regulation of programmed cell death	17	0.9	7.50E-02
positive regulation of apoptosis	17	0.9	7.50E-02
leukocyte differentiation	12	0.6	7.90E-02
histone methylation	3	0.2	8.00E-02
inner cell mass cell proliferation	3	0.2	8.00E-02
positive regulation of cell death	17	0.9	8.20E-02
regulation of phosphorylation	22	1.1	8.30E-02
posttranscriptional regulation of gene expression	10	0.5	8.40E-02
development of primary female sexual characteristics	7	0.4	8.50E-02
hemopoietic or lymphoid organ development	19	1	8.50E-02
anatomical structure homeostasis	9	0.5	8.60E-02
organic anion transport	5	0.3	8.90E-02
spermatid differentiation	5	0.3	8.90E-02
regulation of protein kinase cascade	11	0.6	9.10E-02
regulation of microtubule polymerization or depolymerization	4	0.2	9.40E-02
mitochondrial membrane organization	4	0.2	9.40E-02
nucleus organization	4	0.2	9.40E-02
cell structure disassembly during apoptosis	4	0.2	9.40E-02
regulation of cellular protein metabolic process	21	1.1	9.40E-02
macromolecular complex assembly	24	1.2	9.60E-02
DNA packaging	9	0.5	9.70E-02
regulation of DNA replication	6	0.3	9.70E-02
aging	6	0.3	9.70E-02
female gonad development	6	0.3	9.70E-02
rhythmic process	8	0.4	9.90E-02
amino acid transport	7	0.4	1.00E-01

Supplementary Table 7) List of Significantly enriched GO terms for DRB treatment following Microarray analysis.

Term	Count	%	P-Value
histone modification	6	1.1	9.30E-03
ncRNA metabolic process	9	1.6	9.50E-03
tRNA metabolic process	7	1.2	9.70E-03
covalent chromatin modification	6	1.1	1.20E-02
histone acetylation	4	0.7	1.50E-02
protein amino acid acetylation	4	0.7	1.50E-02
glucose metabolic process	7	1.2	1.90E-02
protein amino acid acylation	4	0.7	2.10E-02
tRNA aminoacylation for protein translation	5	0.9	2.30E-02
tRNA aminoacylation	5	0.9	2.60E-02
amino acid activation	5	0.9	2.60E-02
negative regulation of transcription factor activity	3	0.5	3.10E-02
microtubule-based movement	6	1.1	3.90E-02
negative regulation of molecular function	6	1.1	4.20E-02
chromatin modification	7	1.2	4.40E-02
M phase	6	1.1	5.10E-02
cell cycle phase	7	1.2	5.20E-02
hexose metabolic process	7	1.2	5.20E-02
negative regulation of DNA binding	3	0.5	5.60E-02
homeostasis of number of cells	5	0.9	5.60E-02
lymphocyte homeostasis	3	0.5	6.60E-02
tyrosyl-tRNA aminoacylation	2	0.4	7.00E-02
protein import	4	0.7	7.60E-02
monosaccharide metabolic process	7	1.2	8.10E-02
positive regulation of response to stimulus	6	1.1	8.40E-02
negative regulation of binding	3	0.5	8.60E-02
chromosome organization	10	1.8	8.80E-02

Supplementary Table 8) List of Significantly enriched GO terms for targets affected by both Roscovitine & DRB treatments following RNA-seq analysis.

Term	Count	%	P-Value
chromosome organization	15	3	1.10E-04
chromatin organization	12	2.4	6.10E-04
transcription	21	4.2	3.50E-03
chromatin modification	8	1.6	4.90E-03
response to DNA damage stimulus	10	2	1.20E-02
positive regulation of programmed cell death	8	1.6	1.30E-02
positive regulation of apoptosis	8	1.6	1.30E-02
positive regulation of cell death	8	1.6	1.30E-02
immune response	10	2	1.70E-02
regulation of transcription	35	7	3.00E-02
homeostasis of number of cells	5	1	3.00E-02
protein import into nucleus, translocation	3	0.6	3.20E-02
mRNA metabolic process	6	1.2	4.20E-02
positive regulation of response to stimulus	6	1.2	4.20E-02
induction of programmed cell death	5	1	4.30E-02
induction of apoptosis	5	1	4.30E-02
fatty acid biosynthetic process	4	0.8	4.60E-02
cellular response to stress	10	2	4.80E-02
DNA metabolic process	12	2.4	5.40E-02
ATP synthesis coupled electron transport	3	0.6	6.00E-02
histone acetylation	3	0.6	6.80E-02
negative regulation of immune system process	3	0.6	6.80E-02
protein amino acid acetylation	3	0.6	6.80E-02
positive regulation of cellular protein metabolic pro	5	1	7.00E-02
positive regulation of protein metabolic process	5	1	7.40E-02
cellular respiration	4	0.8	7.40E-02
electron transport chain	4	0.8	8.00E-02
myeloid cell differentiation	4	0.8	8.00E-02
DNA repair	7	1.4	8.00E-02
somatic stem cell division	2	0.4	8.40E-02
regulation of cell cycle	6	1.2	8.50E-02
protein amino acid acylation	3	0.6	8.50E-02
histone modification	4	0.8	9.10E-02
erythrocyte differentiation	3	0.6	9.40E-02
regulation of DNA metabolic process	4	0.8	9.60E-02

Supplementary Table 9) List of Significantly enriched GO terms for targets affected by both Roscovitine & DRB treatments following Microarray analysis.

Term	Count	%	P-Value
histone modification	6	1.4	2.50E-03
covalent chromatin modification	6	1.4	3.20E-03
protein amino acid acetylation	4	1	6.30E-03
histone acetylation	4	1	6.30E-03
protein amino acid acylation	4	1	9.00E-03
chromatin modification	7	1.7	1.10E-02
M phase	6	1.4	1.60E-02
chromosome organization	10	2.4	1.70E-02
ncRNA metabolic process	7	1.7	2.20E-02
transcription	17	4.1	2.40E-02
chromatin organization	8	1.9	3.50E-02
tRNA metabolic process	5	1.2	4.60E-02
cell cycle phase	6	1.4	4.70E-02
ncRNA processing	5	1.2	5.40E-02
mitosis	4	1	6.60E-02
nuclear division	4	1	6.60E-02
M phase of mitotic cell cycle	4	1	7.50E-02
organelle fission	4	1	8.00E-02
transcription initiation	3	0.7	8.60E-02
homeostasis of number of cells	4	1	9.00E-02
cell cycle	8	1.9	9.10E-02

References

Anders, S., D. J., McCarthy, Y. S. Chen, M. Okoniewski, G. K. Smyth, W. Huber, Robinson, M.D., 2013. Count-based differential expression analysis of RNA sequencing data using R and Bioconductor. *Nature Protocols* 8(9): 1765-1786.

Anders, S., Huber, W., 2010. Differential expression analysis for sequence count data. *Genome* Biol 11(10): R106.

Aulehla A., Wiegraebe W., Baubet V., Wahl M.B., Deng C., Taketo M., Lewandoski M., Pourquié O., 2008. A beta-catenin gradient links the clock and wavefront systems in mouse embryo segmentation. *Nat Cell Biol* 10(2):186-93.

Aulehla, A., Wehrle, C., Brand-Saberi, B., Kemler, R., Gossler, A., Kanzler, B., Herrmann, B. G., 2003. Wnt3a plays a major role in the segmentation clock controlling somitogenesis. *Dev. Cell* 4, 395-406.

Bajard, L., Oates, A.C., 2012. Breathe in and straighten your back: hypoxia, Notch, and scoliosis. *Cell* 149: 255-256.

Bajard, L., Relaix, F., Lagha, M., Rocancourt, D., Daubas, P., Buckingham, M.E., 2006. A novel genetic hierarchy functions during hypaxial myogenesis: Pax3 directly activates Myf5 in muscle progenitor cells in the limb. *Genes Dev*. 20(17):2450-64.

Barrios, A., Poole, R. J., Durbin, L., Brennan, C., Holder, N. and Wilson, S. W., 2003. Eph/Ephrin signaling regulates the mesenchymal-to-epithelial transition of the paraxial mesoderm during somite morphogenesis. *Curr. Biol*. 13, 1571- 1582.

Beermann, A., Schröder, R., 2008. Sites of Fgf signalling and perception during embryogenesis of the beetle Tribolium castaneum. *Dev Genes Evol*. 218(3-4):153-67.

Bellairs, R., F. W. Lorenz, F.W., Dunlap, T., 1978. Cleavage in the chick embryo. *J. Embryol. Exp. Morphol.* 43: 55–69.

Bénazéraf B., Francois P., Baker R.E., Denans N., Little C.D., Pourquié O., 2010. A random cell motility gradient downstream of FGF controls elongation of an amniote embryo. *Nature* 466(7303):248-52.

Bénazéraf, B., Pourquié, O., 2013. Formation and segmentation of the vertebrate body axis. *Annu Rev Cell Dev Biol*. 29:1-26.

Bessho, Y., Hirata, H., Masamizu, Y., Kageyama, R., 2003. Periodic repression by the bHLH factor Hes7 is an essential mechanism for the somite segmentation clock. *Genes Dev*. 17, 1451–1456.

Bessho, Y., Miyoshi, G., Sakata, R., Kageyama, R., 2001a. Hes7: a bHLH- type repressor gene regulated by Notch and expressed in the presomitic mesoderm. *Genes Cells* 6, 175–185.

Bessho, Y., Sakata, R., Komatsu, S., Shiota, K., Yamada, S., Kageyama, R., 2001b. Dynamic expression and essential functions of Hes7 in somite segmentation. Genes Dev. 15, 2642–2647.

Bone, R.A., Bailey, C., Wiedermann, G.E., Ferjentsik, Z., Appleton, P.L., Murray, P.J., Maroto, M., Dale, J.K., 2014. Spatio-temporal oscillations of the Notch1 receptor, Delta1 ligand and NICD are co-ordinated across the mouse PSM. *Manuscript* in preparation.

Bonev, B., Stanley, P., Papalopulu, N., 2012. MicroRNA-9 Modulates Hes1 ultradian oscillations by forming a double-negative feedback loop. *Cell Rep*. 2(1):10-8.

Boulet, A.M., Capecchi, M.R., 2012. Signaling by FGF4 and FGF8 is required for axial elongation of the mouse embryo. *Dev. Biol*. 371, 235-245.

Bray, S.J., 2006. Notch signalling: a simple pathway becomes complex. *Nat. Rev. Mol. Cell. Biol.* 7(9): 678-89.

Briscoe, J., Novitch B.G., 2008. Regulatory pathways linking progenitor patterning, cell fates and neurogenesis in the ventral neural tube. *Phil. Trans. R. Soc. B* 363, 57-70.

Brookes, E., Pombo A., 2012. Code breaking: the RNAPII modification code in pluripotency. *Cell Cycle* 11(7):1267-8.

Buchberger A., Bonneick S., Klein C., Arnold H.H., 2002. Dynamic expression of chicken cMeso2 in segmental plate and somites. *Dev Dyn* 223: 108 – 118.

Bulman, M.P., Kusumi, K., Frayling, T.M., McKeown, C., Garrett, C., Lander, E.S., Krumlauf, R., Hattersley, A.T., Ellard, S., and Turnpenny, P.D., 2000. Mutations in the human delta homologue, DLL3, cause axial skeletal defects in spondylocostal dysostosis. *Nat. Genet*. 24, 438–441.

Burke, A.C., Nelson, C.E., Morgan, B.A., Tabin, C., 1995. Hox genes and the evolution of vertebrate axial morphology. *Development* 121(2):333-46.

Cambray, N. and Wilson, V., 2002. Axial progenitors with extensive potency are localised to the mouse chordoneural hinge. *Development* 129, 4855-4866.

Cambray, N. and Wilson, V., 2007. Two distinct sources for a population of maturing axial progenitors. *Development* 134, 2829-2840.

Cee VJ, Chen DY, Lee MR, Nicolaou KC., 2009. Cortistatin A is a high-affinity ligand of protein kinases ROCK, CDK8, and CDK11. *Angew Chem Int Ed Engl*. 48:8952–8957.

Cen, H., Mao, F., Aronchik, I., Fuentes, R.J., Firestone, G.L., 2008. DEVD-NucView488: a novel class of enzyme substrates for real-time detection of caspase-3 activity in live cells. *FASEB J*. 22(7):2243-52.

Chambers, D., Lumsden, A., 2008. Profiling gene transcription in the developing embryo: microarray analysis on gene chips. *Methods Mol Biol* 2008, 461:631-55.

Chang, B.D., Watanabe, K., Broude, E.V., Fang, J., Poole, J.C., Kalinichenko, T.V., and Roninson, I.B., 2000. Effects of p21Waf1/Cip1/Sdi1 on cellular gene expression: Implications for carcinogenesis, senescence, and age-related diseases. *PNAS*. 97: 4291–4296.

Chang, P., Coughlin, M., Mitchison, T.J., 2005. Tankyrase-1 polymerization of poly(ADP-ribose) is required for spindle structure and function. *Nat Cell Biol*. 7(11):1133-9.

Chapman, S.C., Collignon, J., Schoenwolf, G.C., Lumsden, A., 2001. Improved method for chick whole-embryo culture using a filter paper carrier. *Dev Dyn*. 220(3):284-9.

Charrier, J. B., Teillet, M. A., Lapointe, F. and Le Douarin, N. M., 1999. Defining subregions of Hensen's node essential for caudalward movement, midline development and cell survival. *Development* 126, 4771-4783.

Chiang, Y.J., Hsiao, S.J., Yver, D., Cushman, S.W., Tessarollo, L., Smith, S., Hodes, R.J., 2008. Tankyrase 1 and tankyrase 2 are essential but redundant for mouse embryonic development. *PLoS One* 3(7):e2639.

Chodosh, L.A., Fire, A., Samuels, M., Sharp, P.A., 1989. 5,6-Dichloro-1-β-D-ribofuranosylbenzimidazole inhibits transcription elongation by RNA polymerase II *in vitro. J. Biol. Chem.* 264, 2250–2257.

Christ, B., Huang, R. and Scaal, M., 2007. Amniote somite derivatives. *Dev. Dyn*. 236, 2382-2396.

Christ, B., Huang, R., Wilting, J., 2000. The development of the avian vertebral column. *Anat Embryol* 202:179-194.

Ciccarelli, C., Marampon, F., Scoglio, A., Mauro, A., Giacinti, C., De Cesaris, P., Zani, B.M., 2005. p21WAF1 expression induced by MEK/ERK pathway activation or inhibition correlates with growth arrest, myogenic differentiation and onco-phenotype reversal in rhabdomyosarcoma cells. *Mol Cancer*. 4:41.

Clevers, H., 2006. Wnt/beta-catenin signaling in development and disease. *Cell*, 127, 469–480.

Clinton, M., Haines, L., Belloir, B., McBride, D., 2001. Sexing chick embryos: a rapid and simple protocol. *Br Poult Sci*. 42(1):134-8.

Cohen, P., 2002. The origins of protein phosphorylation. *Nat Cell Biol*. 4(5):E127-30.

Cohen, S.M., Jürgens, G., 1990. Mediation of Drosophila head development by gap-like segmentation genes. *Nature* 346(6283):482-5.

Cooke, J. & Zeeman, E. C., 1976. A clock and wavefront model for control of the number of repeated structures during animal morphogenesis. *J.Theor. Biol.* 58, 455–476.

Criley, B. B., 1969. Analysis of the embryonic sources and mechanisms of development of the posterior levels of chick neural tubes. *J. Morphol.* 128, 465-502.

Dale, J.K., Malapert, P., Chal, J., Vilhais-Neto, G., Maroto, M., Johnson, T., Jayasinghe, S., Trainor, P., Herrmann, B., Pourquie, O., 2006. Oscillations of the snail genes in the presomitic mesoderm coordinate segmental patterning and morphogenesis in vertebrate somitogenesis. *Dev. Cell* 10, 355–366.

Dale, J.K., Maroto, M., Dequeant, M.L., Malapert, P., McGrew, M., Pourquie, O., 2003. Periodic Notch inhibition by Lunatic fringe underlies the chick segmentation clock. *Nature* 421, 275–278.

Davis, G.K., Patel, N.H., 2002. Short, long, and beyond: molecular and embryological approaches to insect segmentation. *Annu Rev Entomol*. 47:669-99.

Delfini, M. C., Dubrulle, J., Malapert, P., Chal, J. & Pourquié, O., 2005. Control of the segmentation process by graded MAPK/ERK activation in the chick embryo. *PNAS* 102, 11343–11348.

Delfino-Machín M1, Lunn JS, Breitkreuz DN, Akai J, Storey KG., 2005. Specification and maintenance of the spinal cord stem zone. *Development* 132(19):4273-83.

Dequeant, M.-L., Glynn, E., Gaudenz, K., Wahl, M., Chen, J., Mushegian, A., Pourquie, O., 2006. A complex oscillating network of signalling genes underlies the mouse segmentation clock. *Science* 314, 1595–1598.

Dequeant, M.L., Pourquie, O., 2008. Segmental patterning of the vertebrate embryonic axis. *Nat. Rev., Genet.* 9, 370–382.

Derti, A., Garrett-Engele, P., Macisaac, K.D., Stevens, R.C., Sriram, S., Chen, R., Rohl, C.A., Johnson, J.M., Babak, T., 2012. A quantitative atlas of polyadenylation in five mammals. *Genome Res*. 22(6):1173-83.

Desterro, J.M., Rodriguez, M.S., Hay, R.T., 2000. Regulation of transcription factors by protein degradation. *Cell Mol Life Sci*. 57(8-9):1207-19.

Devgan, V., Mammucari, C., Millar, S.E., Brisken, C., Dotto, G.P., 2005. p21WAF1/Cip1 is a negative transcriptional regulator of Wnt4 expression downstream of Notch1 activation. *Genes Dev*. 19(12):1485-95.

Dias, A.S., de Almeida, I., Belmonte, J.M., Glazier, J.A., Stern, C.D., 2014. Somites Without a Clock. *Science* [Epub ahead of print]

Diez del Corral, R., Storey, K. G., 2004. Opposing FGF and retinoid pathways: a signalling switch that controls differentiation and patterning onset in the extending vertebrate body axis. *BioEssays* 26, 857-869.

Driever, W., Nüsslein-Volhard, C., 1988. The bicoid protein determines position in the Drosophila embryo in a concentration-dependent manner. *Cell* 54(1):95-104.

Dubrulle, J., McGrew, M.J., Pourquie, O., 2001. FGF Signaling Controls Somite Boundary Position and Regulates Segmentation Clock Control of Spatiotemporal Hox Gene Activation. *Cell* 106, 219–232.

Dubrulle, J., Pourquié, O., 2004. fgf8 mRNA decay establishes a gradient that couples axial elongation to patterning in the vertebrate embryo. *Nature* 427(6973):419-22

Dunwoodie, S. L., Clements, M., Sparrow, D.B., Sa, X., Conlon, R.A., Beddington, R.S.P., 2002. Axial skeletal defects caused by mutation in the spondylocostal dysplasia/pudgy gene Dll3 are associated with disruption of the segmentation clock within the presomitic mesoderm. *Development* 129, 1795–1806.

Dunwoodie, S.L., Henrique, D., Harrison, S.M., Beddington, R.S., 1997. Mouse Dll3: a novel divergent Delta gene which may complement the function of other Delta homologues during early pattern formation in the mouse embryo. *Development* 124(16):3065-76.

Durbin, L., Brennan, C., Shiomi, K., Cooke, J., Barrios, A., Shanmuga- lingam, S., Guthrie, B., Lindberg, R., Holder, N., 1998. Eph signaling is required for segmentation and differentiation of the somites. *Genes Dev*. 12, 3096–3109.

Eckalbar, W.L., Lasku, E., Infante, C.R., Elsey, R.M., Markov, G.J., Allen, A.N., Corneveaux, J.J., Losos, J.B., DeNardo, D.F., Huentelman, M.J., Wilson-Rawls, J., Rawls, A., Kusumi, K., 2012. Somitogenesis in the anole lizard and alligator reveals evolutionary convergence and divergence in the amniote segmentation clock. *Dev Biol.* 363(1):308-19.

Espinosa, L., Inglés-Esteve, J., Aguilera, C., Bigas, A., 2003. Phosphorylation by glycogen synthase kinase-3 beta down-regulates Notch activity, a link for Notch and Wnt pathways. *J Biol Chem.* 278(34):32227-35.

Evrard, Y. A., Lun, Y., Aulehla, A., Gan, L. and Johnson, R. L., 1998. lunatic fringe is an essential mediator of somite segmentation and patterning. *Nature* 394, 377-381.

Feller, J., Schneider, A., Schuster-Gossler, K., Gossler, A., 2008. Noncyclic Notch activity in the presomitic mesoderm demonstrates uncoupling of somite compartmentalization and boundary formation. *Genes Dev*. 22(16):2166-71**.**

Ferjentsik, Z., Hayashi, S., Dale, J.K., Bessho, Y., Herreman, A., De Strooper, B., del Monte, G., de la Pompa, J.L., and Maroto, M., 2009. Notch is a critical component of the mouse somitogenesis oscillator and is essential for the formation of the somites. *PLoS Genet*. 5, e1000662.

Fisher, R. P., 2005. Secrets of a double agent: CDK7 in cell- cycle control and transcription. *J. Cell Sci*. 118, 5171–5180.

Forsberg, H., Crozet, F., Brown, N.A., 1998. Waves of mouse Lunatic fringe expression, in four-hour cycles at two-hour intervals, precede somite boundary formation*. Curr. Biol*. 8, 1027–1030.

Franco Del Amo, F., Smith, D.E., Swiatek, P.J., Gendron-Maguire, M., Greenspan, R.J., McMahon, A.P., Gridley, T., 1992. Expression pattern of Motch, a mouse homolog of Drosophila Notch, suggests an important role in early postimplantation mouse development. *Development* 115(3):737-44.

Fryer, C.J., White, J.B., and Jones, K.A., 2004. Mastermind recruits CycC:CDK8 to phosphorylate the Notch ICD and coordinate activation with turnover. *Mol. Cell* 16, 509–520.

Galbraith, M.D., Donner, A.J., Espinosa J.M., 2010. CDK8: a positive regulator of transcription. *Transcription* 1(1):4-12.

Gautier, L., L. Cope, B. M. Bolstad and R. A. Irizarry, 2004. affy - analysis of Affymetrix GeneChip data at the probe level. *Bioinformatics* 20(3): 307-315.

Gentleman, R. C., V. J. Carey, D. M. Bates, B. Bolstad, M. Dettling, S. Dudoit, B. Ellis, L. Gautier, Y. Ge, J. Gentry, K. Hornik, T. Hothorn, W. Huber, S. Iacus, R. Irizarry, F. Leisch, C. Li, M. Maechler, A. J. Rossini, G. Sawitzki, C. Smith, G. Smyth, L. Tierney, J. Y. Yang and J. Zhang, 2004. Bioconductor: open software development for computational biology and bioinformatics. *Genome Biol* 5(10): R80.

Giampietro, P.F., Dunwoodie, S.L., Kusumi, K., Pourquie´ , O., Tassy, O., Offiah, A.C., Cornier, A.S., Alman, B.A., Blank, R.D., Raggio, C.L., Glurich, I., Turnpenny, P.D., 2009. Progress in the understanding of the genetic etiology of vertebral segmentation disorders in humans. *Ann. N Y Acad. Sci*. 1151, 38–67.

Gibb, S., Maroto, M, Dale, J.K., 2010. The segmentation clock mechanism moves up a notch. *Trends Cell Biol* 20: 10, 593-600.

Gibb, S., Zagorska, A., Melton, K., Tenin, G., Vacca, I., Trainor, P., Maroto, M., Dale, J.K., 2009. Interfering with Wnt signalling alters the periodicity of the segmentation clock. *Dev. Biol*. 330, 21–31.

Gilbert, S.F., 2006. *Developmental Biology* (8th ed.). Sinauer Associates, Inc. Sunderland, MA.

Girós, A., Grgur, K., Gossler, A. and Costell, M., 2011. α5β1 integrin-mediated adhesion to fibronectin is required for axis elongation and somitogenesis in mice. *PLoS ONE* 6, 1-12.

Gomez, C., Ozbudak, E.M., Wunderlich, J., Baumann, D., Lewis, J., Pourquié, O., 2008. Control of segment number in vertebrate embryos. *Nature* 454(7202):335-9.

González, A., Manosalva, I., Liu, T., Kageyama, R., 2013. Control of Hes7 expression by Tbx6, the Wnt pathway and the chemical Gsk3 inhibitor LiCl in the mouse segmentation clock. *PLoS One* 8(1):e53323.

Gould A., Morrison A., Sproat G., White R.A., Krumlauf R., 1997. Positive cross-regulation and enhancer sharing: two mechanisms for specifying overlapping Hox expression patterns. *Genes Dev.* 11(7):900-13.

Gros, J., Manceau, M., Thomé, V., Marcelle, C., 2005. A common somitic origin for embryonic muscle progenitors and satellite cells. *Nature* 435(7044):954-8.

Guarani, V., Deflorian, G., Franco, C.A., Krüger, M., Phng, L.K., Bentley, K., Toussaint, L., Dequiedt, F., Mostoslavsky, R., Schmidt, M.H., Zimmermann, B., Brandes, R.P., Mione, M., Westphal, C.H., Braun, T., Zeiher, A.M., Gerhardt, H., Dimmeler, S., Potente, M., 2011. Acetylation-dependent regulation of endothelial Notch signalling by the SIRT1 deacetylase. *Nature* 473(7346):234-8.

Halevy, O., Novitch, B. G., Spicer, D. B., Skapek, S. X., Rhee, J., Hannon, G. J., Beach, D., and Lassar, A. B., 1995. Correlation of terminal cell cycle arrest of skeletal muscle with induction of p21 by MyoD. *Science* 267, 1018–1021.

Hamburger V., Hamilton H.L., 1992. A series of normal stages in the development of the chick embryo. 1951. *Dev Dyn* 195:231–272.

Harima, Y., Takashima, Y., Ueda, Y., Ohtsuka, T., Kageyama, R., 2013. Accelerating the tempo of the segmentation clock by reducing the number of introns in the Hes7 gene. *Cell Rep*. 3(1): 1-7.

Harms, E., Young, M.W., Saez, L., 2003. CK1 and GSK3 in the Drosophila and mammalian circadian clock. *Novartis Found Symp*. 253:267-77; discussion 102-9, 277-84.

He, G., Siddik, Z.H., Huang, Z., Wang, R., Koomen, J., Kobayashi, R., Khokhar, A.R., Kuang, J., 2005. Induction of p21 by p53 following DNA damage inhibits both Cdk4 and Cdk2 activities. *Oncogene* 24(18):2929-43.

Hedequist, D., and Emans, J., 2007. Congenital scoliosis: a review and update. *J. Pediatr. Orthop.* 27, 106–116.

Heemskerk, J., DiNardo, S., Kostriken, R., O'Farrell, P.H., 1991. Multiple modes of engrailed regulation in the progression towards cell fate determination. *Nature* 352: 404–410.

Hendzel, M.J., Wei, Y., Mancini, M.A., Van Hooser, A., Ranalli, T., Brinkley, B.R., Bazett-Jones, D.P., Allis, C.D., 1997. Mitosis-specific phosphorylation of histone H3 initiates primarily within pericentromeric heterochromatin during G2 and spreads in an ordered fashion coincident with mitotic chromosome condensation. *Chromosoma* 106(6):348-60.

Henrique, D., Adam, J., Myat, A., Chitnis, A., Lewis, J., Ish-Horowicz, D., 1995. Expression of a Delta homologue in prospective neurons in the chick. *Nature* 375, 787–790.

Herrgen, L., Ares, S., Morelli, L.G., Schro¨ ter, C., Ju¨ licher, F., and Oates, A.C., 2010. Intercellular coupling regulates the period of the segmentation clock. *Curr. Biol*. 20, 1244–1253.

Hirata, H., Bessho, Y., Kokubu, H., Masamizu, Y., Yamada, S., Lewis, J., Kageyama, R., 2004. Instability of Hes7 protein is crucial for the somite segmentation clock. *Nat Genet* 36, 750-754.

Holley, S.A., Geisler, R., Nusslein-Volhard, C., 2000. Control of her1 expression during zebrafish somitogenesis by a Delta-dependent os- cillator and an independent wavefront activity. *Genes Dev*. 14, 1678–1690.

Hoyle, N.P., Ish-Horowicz, D., 2013. Transcript processing and export kinetics are rate-limiting steps in expressing vertebrate segmentation clock genes. *PNAS* 110(46):E4316-24.

Huang, S.M., Mishina, Y.M., Liu, S., Cheung, A., Stegmeier, F., Michaud, G.A., Charlat, O., Wiellette, E., Zhang, Y., Wiessner, S., Hild, M., Shi, X., Wilson, C.J., Mickanin, C., Myer, V., Fazal, A., Tomlinson, R., Serluca, F., Shao, W., Cheng, H., Shultz, M., Rau, C., Schirle, M., Schlegl, J., Ghidelli, S., Fawell, S., Lu, C., Curtis, D., Kirschner, M.W., Lengauer, C., Finan, P.M., Tallarico, J.A., Bouwmeester, T., Porter, J.A., Bauer, A., Cong, F., 2009. Tankyrase inhibition stabilizes axin and antagonizes Wnt signalling. *Nature* 461(7264):614-20.

Hülskamp, M., Pfeifle, C., Tautz, D., 1990. A morphogenetic gradient of hunchback protein organizes the expression of the gap genes Krüppel and knirps in the early Drosophila embryo. *Nature* 346(6284):577-80.

Huppert, S.S., Ilagan, M.X., De Strooper, B., Kopan, R., 2005. Analysis of Notch function in presomitic mesoderm suggests a gamma-secretase-independent role for presenilins in somite differentiation. *Dev Cell*. 8(5):677-88.

Ingham, P. W., Taylor, A.M., Nakano, Y., 1991. Role of *Drosophila patched* gene in positional signalling. *Nature* 353: 184–187.

Itoh, M., Kim, C.H., Palardy, G., Oda, T., Jiang, Y.J., Maust, D., Yeo, S.Y., Lorick, K., Wright, G.J., Ariza-McNaughton, L., Weissman, A.M., Lewis, J., Chandrasekharappa, S.C., Chitnis, A.B., 2003. Mind bomb is a ubiquitin ligase that is essential for efficient activation of Notch signaling by Delta. *Dev. Cell* 4, 67–82.

Izpisúa-Belmonte, J.C., Falkenstein, H., Dollé, P., Renucci, A., Duboule, D., 1991. Murine genes related to the Drosophila AbdB homeotic genes are sequentially expressed during development of the posterior part of the body. *EMBO J.* 10(8):2279-89.

Jaskwhich, D., Ali, R.M., Patel, T.C., Green, D.W., 2000. Congenital scoliosis. *Curr. Opin. Pediatr*. 12: 61–66.

Jiang, Y.-J., Aerne, B.L., Smithers, L., Haddon, C., Ish-Horowicz, D., Lewis, J., 2000. Notch signalling and the synchronization of the somite segmentation clock. *Nature* 408, 475–479.

Jin, Y.H., Kim, H., Oh, M., Ki, H., Kim, K., 2009. Regulation of Notch1/NICD and Hes1 Expressions by GSK-3α/β. *Mol. Cells* 27, 15-19.

Johnson, J., Rhee, J., Parsons, S.M., Brown, D., Olson, E.N., Rawls, A., 2001. The anterior/posterior polarity of somites is disrupted in paraxis-deficient mice. *Dev Biol*. 229(1):176-87.

Jouve, C., Iimura, T., Pourquie, O., 2002. Onset of the segmentation clock in the chick embryo: evidence for oscillations in the somite precursors in the primitive streak. *Development* 129(5):1107-17.

Jouve, C., Palmeirim, I., Henrique, D., Beckers, J., Gossler, A., Ish-Horowicz, D., Pourquie, O., 2000. Notch signalling is required for cyclic expression of the hairy-like gene HES1 in the presomitic mesoderm. *Development* 127, 1421–1429.

Jülich, D., Mould, A. P., Koper, E. and Holley, S. A., 2009. Control of extracellular matrix assembly along tissue boundaries via Integrin and Eph/Ephrin signaling. *Development* 136, 2913-2921.

Katoh, M., 2002. Molecular cloning and characterization of human WINS1 and mouse Wins2, homologous to Drosophila segment polarity gene Lines (Lin). *Int J Mol Med*. 10(2):155-9.

Kawamura, A., Koshida, S., Hijikata, H., Sakaguchi, T., Kondoh, H., and Takada, S., 2005. Zebrafish hairy/enhancer of split protein links FGF signaling to cyclic gene expression in the periodic segmentation of somites. *Genes Dev*. 19, 1156–1161.

Kerszberg, M., and Wolpert, L., 2000. A clock and trail model for somite formation, specialization and polarization. *J. Theor. Biol.* 205, 505–510.

Kessel, M., Gruss, P., 1991. Homeotic transformations of murine vertebrae and concomitant alteration of Hox codes induced by retinoic acid. *Cell* 67(1):89-104.

Keynes, R.L, Stern, C.D., 1988 Mechanisms of vertebrate segmentation. *Development* 103: 413-429.

Kim, W., Matsui, T., Yamao, M., Ishibashi, M., Tamada, K., Takumi, T., Kohno, K., Oba, S., Ishii, S., Sakumura, Y., and Bessho, Y., 2011. The period of the somite segmentation clock is sensitive to Notch activity. *Mol. Biol. Cell* 22, 3541–3549.

Komarnitsky, P., Cho, E.J., Buratowski, S., 2000. Different phosphorylated forms of RNA polymerase II and associated mRNA processing factors during transcription. *Genes Dev*. 14(19):2452-60.

Kopan, R., Ilagan, X.G., 2009. The canonical Notch signalling pathway: unfolding the activation mechanism. *Cell* 137, 216-233.

Kouhara, H., Hadari, Y., Spivak-Kroizman, T., Schilling, J., Bar-Sagi, D., Lax, I., Schlessinger, J., 1997. A lipid-anchored Grb2-binding protein that links FGF-receptor activation to the Ras/MAPK signaling pathway. *Cell* 89, 693–702.

Krol, A.J., Roellig, D., Dequeant, M.-L., Tassy, O., Glynn, E., Hattem, G., Mushegian, A., Oates, A.C., Pourquie, O., 2011. Evolutionary plasticity of segmentation clock net- works. *Development* 138, 2783–2792.

Krucher, N.A., Meijer, L., Roberts, M.H., 1997. The cyclin-dependent kinase (cdk) inhibitors, olomoucine and roscovitine, alter the expression of a molluscan circadian pacemaker. *Cell Mol Neurobiol*. 17(5):495-507.

Kyriakis, J.M., App, H., Zhang, X.F., Banerjee, P., Brautigan, D.L., Rapp, U.R., Avruch, J., 1992. Raf-1 activates MAP kinase-kinase. *Nature* 358(6385):417-21.

Lanz, T.A., Hosley, J.D., Adams, W.J., Merchant, K.M., 2004. Studies of Abeta pharmacodynamics in the brain, cerebrospinal fluid, and plasma in young (plaque-free) Tg2576 mice using the gamma-secretase inhibitor N2-[(2S)-2-(3,5-difluorophenyl)-2-hydroxyethanoyl]-N1-[(7S)-5-methyl-6-oxo-6,7-dihydro-5H-dibenzo[b,d]azepin-7-yl]-L-alaninamide (LY-411575). *J Pharmacol Exp Ther.* 309(1):49-55.

Lauschke, V.M., Tsiairis, C.D., François, P., Aulehla, A., 2013. Scaling of embryonic patterning based on phase-gradient encoding. *Nature* 493(7430):101-5.

Lehmann, R., Nüsslein-Volhard, C., 1987. Hunchback, a gene required for segmentation of an anterior and posterior region of the Drosophila embryo. *Dev Biol*. 1987 Feb;119(2):402-17.

Leimeister, C., Dale, J.K., Fischer, A., Klamt, B., Hrabe de Angelis, M., Radtke, F., McGrew, M.J., Pourquie, O., Gessler, M., 2000. Oscillating expression of c-hey2 in the presomitic mesoderm suggests that the segmentation clock may use combinatorial signaling through multiple interacting bHLH factors. *Dev*. *Biol*. 227, 91–103.

Levine, M. S., Harding, K.W., 1989. *Drosophila*: The zygotic contribution. *In* D. M. Glover and B. D. Hames (eds.), *Genes and Embryos*. IRL, New York, pp. 39–94.

Lewis, J., 2003. Autoinhibition with transcriptional delay: a simple mechanism for the zebrafish somitogenesis oscillator. *Curr. Biol.* 13, 1398–1408.

Liao, Y., G. K. Smyth and W. Shi, 2013. The Subread aligner: fast, accurate and scalable read mapping by seed-and-vote. *NAR* 41(10): e108.

Lopez, T.P, Fan, C-M., 2013. Dynamic CREB family activity drives segmentation and posterior polarity specification in mammalian somitogenesis. *PNAS* 110(22):E2019-27.

MacCallum, D.E., Melville, J., Frame, S., Watt, K., Anderson, S., Gianella-Borradori, A., Lane, D.P., Green, S.R., 2005. Seliciclib (CYC202, R-Roscovitine) induces cell death in multiple myeloma cells by inhibition of RNA polymerase II-dependent transcription and down-regulation of Mcl-1. *Cancer Res*. 65(12):5399-407.

Malumbres, M., Barbacid, M., 2009. Cell cycle, CDKs and cancer: a changing paradigm. *Nat. Rev. Cancer* 9(3): 153-166.

Mansouri, A., Yokota, Y., Wehr, R., Copeland, N.G., Jenkins, N.A., Gruss, P., 1997. Paired-related murine homeobox gene ex- pressed in the developing sclerotome, kidney, and nervous system. *Dev Dyn* 210:53–65.

Maroto, M., Bone, R.A., Dale, J.K, 2012. Somitogenesis. *Development* 139, 2453-2456.

Maroto, M., Reshef, R., Münsterberg, A.E., Koester, S., Goulding, M., Lassar, A.B., 1997. Ectopic Pax-3 activates MyoD and Myf-5 expression in embryonic mesoderm and neural tissue. *Cell* 89(1):139-48.

Marshall, N.F., Peng, J., Xie, Z., Price, D.H., 1996. Control of RNA polymerase II elongation potential by a novel carboxyl-terminal domain kinase. *J Biol Chem*. 271(43):27176-83.

Martinez-Arias, A., Lawrence, P.A., 1985. Parasegments and compartments in the Drosophila embryo. *Nature* 313(6004):639-42.

McClue, S.J., Blake, D., Clarke, R., Cowan, A., Cummings, L., Fischer, P.M., MacKenzie, M., Melville, J., Stewart, K., Wang, S., Zhelev, N., Zheleva, D., Lane, D.P., 2002. In vitro and in vivo antitumor properties of the cyclin dependent kinase inhibitor CYC202 (R-roscovitine). *Int J Cancer* 102(5):463-8.

McGill, M.A., McGlade, C.J., 2003. Mammalian numb proteins promote Notch1 receptor ubiquitination and degradation of the Notch1 intracellular domain. *J Biol Chem*. 278(25):23196-203.

McGinnis, W., Krumlauf, R., 1992. Homeobox genes and axial patterning. *Cell* 68 (2): 283–302.

McGrew M.J., Dale J.K., Fraboulet S., Pourquie O., 1998. The lunatic fringe gene is a target of the molecular clock linked to somite segmentation in avian embryos. *Curr Biol* 8:979 – 982.

McGrew, M. J., Sherman, A., Lillico, S. G., Ellard, F. M., Radcliffe, P. A., Gilhooley, H. J., Mitrophanous, K. A., Cambray, N., Wilson, V. and Sang, H., 2008. Localised axial progenitor cell populations in the avian tail bud are not committed to a posterior Hox identity. *Development* 135, 2289-2299.

McMahon, J.A., Takada, S., Zimmermann, L.B., Fan, C.M., Harland, R.M., McMahon, A.P., 1998. Noggin-mediated antagonism of BMP signaling is required for growth and patterning of the neural tube and somite. *Genes Dev* 12:1438–1452.

Meinhardt, H., 1986. Models of segmentation. In: *Somites in Developing Embryos*, R. Bellairs, D.A. Ede, and J.W. Lash, eds. (New York: Plenum press), pp. 179–191.

Meinhardt, H.,1982. *Models of Biological Pattern Formation*. London: Academic Press

Minowada, G., Jarvis, L.A., Chi, C.L., Neubüser, A., Sun, X., Hacohen, N., Krasnow, M.A., Martin, G.R., 1999. Vertebrate Sprouty genes are induced by FGF signaling and can cause chondrodysplasia when overexpressed. *Development* 126(20):4465-75.

Mitsiadis, T.A., Henrique, D., Thesleff, I., Lendahl, U., 1997. Mouse Serrate-1 (Jagged1): expression in the developing tooth is regulated by epithelial-mesenchymal interactions and fibroblast growth factor-4. *Development* 124:1473-1483.

Monk, N. A. M., 2003. Oscillatory expression of Hes1, p53 and NF‐kB driven by transcriptional time delays. *Curr. Biol.* 13, 1409–1413.

Morales, A. V., Yasuda, Y. & Ish-Horowicz, D., 2002. Periodic lunatic fringe expression is controlled during segmentation by a cyclic transcriptional enhancer responsive to Notch signaling. *Dev. Cell* 3, 63–74.

Morimoto, M., Takahashi, Y., Endo, M. & Saga, Y., 2005. The Mesp2 transcription factor establishes segmental borders by suppressing Notch activity. *Nature* 435, 354–359.

Muñoz Descalzo, S., Martinez Arias, A., 2012. The structure of Wntch signalling and the resolution of transition states in development. *Semin Cell Dev Biol*. 23(4):443-9.

Münsterberg, A.E., Kitajewski, J., Bumcrot, D.A., McMahon, A.P., Lassar, A.B., 1995. Combinatorial signaling by Sonic hedgehog and Wnt family members induces myogenic bHLH gene expression in the somite. *Genes Dev*. 9(23):2911-22.

Murata, Y., Wharton, R.P., 1995. Binding of pumilio to maternal hunchback mRNA is required for posterior patterning in Drosophila embryos. *Cell* 80(5):747-56.

Murray, P.J., Maini, P.K., Baker, R.E., 2011. The clock and wavefront model revisited. *J Theor Biol*. 283(1):227-38.

Murtaugh, L.C., Chyung, J.H., Lassar, A.B., 1999. Sonic hedgehog promotes somitic chondrogenesis by altering the cellular response to BMP signaling. *Genes Dev*. 13(2):225-37.

Mutoh, H., Naya, F. J., Tsai, M. J., and Leiter, A. B., 1998. The basic helix-loop-helix protein BETA2 interacts with p300 to coordinate differentiation of secretin-expressing enteroendocrine cells. *Genes Dev.* 12, 820–830.

Naiche, L.A., Holder,N., Lewandoski, M., 2011. FGF4 and FGF8 comprise the wavefront activity that controls somitogenesis. *PNAS* 108, 4018–23.

Neidhardt, L. M., Kispert, A. and Herrmann, B. G., 1997. A mouse gene of the paired-related homeobox class expressed in the caudal somite compartment and in the developing vertebral column, kidney and nervous system. *Dev. Genes Evol*. 207: 330-339.

Nitanda, Y., Matsui, T., Matta, T., Higami, A., Kohno, K., Nakahata, Y., Bessho, Y., 2014. 3'-UTR-dependent regulation of mRNA turnover is critical for differential distribution patterns of cyclic gene mRNAs. *FEBS J*. 281(1):146-56.

Niwa, Y., Masamizu, Y., Liu, T., Nakayama, R., Deng, C.X., Kageyama, R., 2007. The initiation and propagation of Hes7 oscillation are cooperatively regulated by Fgf and notch signaling in the somite segmentation clock. *Dev Cell* 13:298-304.

Niwa, Y., Shimojo, H., Isomura, A., Gonzalez, A., Miyachi, H., Kageyama, R., 2011. Different types of oscillations in Notch and Fgf signaling regulate the spatiotemporal periodicity of somitogenesis. *Genes Dev* 25:1115-1120.

Nusslein-Volhard, C. & Wieschaus, E., 1980. Mutations affecting segment number and polarity in Drosophila. *Nature* 287, 795–801.

Oates, A.C., Ho, R.K., 2002. Hairy/E(spl)-related (Her) genes are central components of the segmentation oscillator and display redundancy with the Delta/Notch signaling pathway in the formation of anterior segmen- tal boundaries in the zebrafish. *Development* 129, 2929–2946.

Oginuma, M., Niwa, Y., Chapman, D.L., Saga, Y., 2008. Mesp2 and Tbx6 cooperatively create periodic patterns coupled with the clock machinery during mouse somitogenesis. *Development* 135(15):2555-62.

Ong, S. H., Guy, G. R., Hadari, Y. R., Laks, S., Gotoh, N., Schlessinger, J., Lax, I., 2000. FRS2 proteins recruit intracellular signaling pathways by binding to diverse targets on fibroblast growth factor and nerve growth factor receptors. *Mol. Cell Biol.* 20, 979–89.

Palmeirim I., Henrique D., Ish-Horowicz D., Pourquie O., 1997. Avian hairy gene expression identifies a molecular clock linked to vertebrate segmentation and somitogenesis. *Cell* 91:639 – 648.

Pinhero, R., Liaw, P., Yankulov, K., 2004. A uniform procedure for the purification of CDK7/CycH/MAT1, CDK8/CycC and CDK9/CycT1. *Biol Proced Online* 6:163-172.

Potter, S.W., Morris, J.E., 1985. Development of mouse embryos in hanging drop culture. *Anat Rec*. 211(1):48-56.

Poulton, J.S., Huang, Y.C., Smith, L., Sun, J., Leake, N., Schleede, J., Stevens, L.M., Deng, W.M., 2011. The microRNA pathway regulates the temporal pattern of Notch signaling in Drosophila follicle cells. *Development* 138(9):1737-45.

Pourquié, O. & Tam, P. P., 2001. A nomenclature for prospective somites and phases of cyclic gene expression in the presomitic mesoderm. *Dev. Cell* 1, 619–620.

Pownall, M.E., Isaacs, H.V. (eds.), 2010. FGF Signalling in Vertebrate Development. In: *Developmental Biology*. Morgan & Claypool Life Sciences. San Rafael (CA).

Primmett DR, Norris WE, Carlson GJ, Keynes RJ, Stern CD., 1989. Periodic segmental anomalies induced by heat shock in the chick embryo are associated with the cell cycle. *Development*. 1989 Jan;105(1):119-30.

Psychoyos, D. and Stern, C. D., 1996. Fates and migratory routes of primitive streak cells in the chick embryo. *Development* 122, 1523-1534.

Puri, P. L., Avantaggiati, M. L., Balsano, C., Sang, N., Graessmann, A., Giordano, A., and Levrero, M., 1997. p300 is required for MyoD-dependent cell cycle arrest and muscle-specific gene transcription. *EMBO J.* 16, 369 –383.

Ramsköld, D., Wang, E.T., Burge, C.B., Sandberg, R., 2009. An abundance of ubiquitously expressed genes revealed by tissue transcriptome sequence data. *PLoS Comput Biol*. 5(12):e1000598.

Reaume, A.G., Conlon, R., Zimgibl, T.P., Yamaguchi, Rossant. J., 1992. Expression analysis of a Notch homologue in the mouse embryo. *Dev. Biol*. 154:377-387.

Remak R., 1850. *Untersuchungen über die Entwicklung der Wirbelthiere*. Reimer, Berlin.

Resende, T. P., Ferreira, M., Teillet, M. A., Tavares, A. T., Andrade, R. P. and Palmeirim, I., 2010. Sonic hedgehog in temporal control of somite formation. *PNAS* 107, 12907-12912.

Rida, P.C., Le Minh, N., Jiang, Y.J., 2004. A Notch feeling of somite segmentation and beyond. *Dev. Biol.* 265, 2–22.

Riley, M.F., Bochter, M.S., Wahi, K., Nuovo, G.J., Cole, S.E., 2013. Mir-125a-5p-mediated regulation of Lfng is essential for the avian segmentation clock. *Dev. Cell* 24(5):554-61.

Rivera-Pomar, R., Niessling, D., Schmidt-Ott, U., Gehring, W.J., Jäckle., H., 1996. RNA binding and translational suppression by *bicoid*. *Nature* 379: 746–749.

Saga Y., Hata N., Koseki H., Taketo M.M., 1997. Mesp2: a novel mouse gene expressed in the presegmented mesoderm and essential for segmentation initiation. *Genes Dev* 11: 1827 – 1839.

Sancho, R., Blake, S.M., Tendeng, C., Clurman, B.E., Lewis, J., Behrens, A., 2013. Fbw7 repression by hes5 creates a feedback loop that modulates Notch-mediated intestinal and neural stem cell fate decisions. *PLoS Biol*. 11(6):e1001586.

Sasaki, N., Kiso, M., Kitagawa, M., Saga, Y., 2011. The repression of Notch signaling occurs via the destabilization of mastermind-like 1 by Mesp2 and is essential for somitogenesis. *Development* 2011, 138:55-64.

Sato, T., Rocancourt, D., Marques, L., Thorsteinsdóttir, S., Buckingham, M., 2010. A Pax3/Dmrt2/Myf5 regulatory cascade functions at the onset of myogenesis. *PLoS Genet*. 6(4):e1000897.

Schlessinger, J., 2000. Cell signaling by receptor tyrosine kinases. *Cell* 103,211–225.

Schoenwolf, G. C., 1984. Histological and ultrastructural studies of secondary neurulation in mouse embryos. *Am. J. Anat.* 169, 361-376.

Schoenwolf, G. C., 1991. Cell movements in the epiblast during gastrulation and neurulation in avian embryos. *In* R. Keller, W. H. Clark, Jr. and F. Griffin (eds.), *Gastrulation: Movements, Patterns, and Molecules*. Plenum, New York, Pp. 1–28.

Schröter, C., Ares, S., Morelli, L.G., Isakova, A., Hens, K., Soroldoni, D., Gajewski, M., Jülicher, F., Maerkl, S.J., Deplancke, B., Oates, A.C., 2012. Topology and Dynamics of the Zebrafish Segmentation Clock Core Circuit. *PLoS Biol* 10(7): e1001364.

Schröter, C., Oates, A.C., 2010. Segment number and axial identity in a segmentation clock period mutant. *Curr Biol*. 20(14):1254-8.

Schulz, C., Tautz, D., 1995. Zygotic caudal regulation by hunchback and its role in abdominal segment formation of the *Drosophila* embryo. *Development* 121: 1023–1028.

Shankaran, S. S., Sieger, D., Schröter, C., Czepe, C., Pauly, M.C., Laplante, M.A., Becker, T.S., Oates, A.C., Gajewski, M., 2007. Completing the set of h/E(spl) cyclic genes in zebrafish: her12 and her15 reveal novel modes of expression and contribute to the segmentation clock. *Dev. Biol*. 304, 615–632.

Sherr, C.J. and Roberts, J.M., 1999. CDK inhibitors: Positive and negative regulators of G1-phase progression. *Genes & Dev*. 13: 1501–1512.

Sieger, D., Tautz, D. & Gajewski, M., 2004. her11 is involved in the somitogenesis clock in zebrafish. *Dev. Genes Evol.* 214, 393–406.

Smyth, G. K., 2005. Limma: Linear models for microarray data. *Bioinformatics and Computational Biology Solution Using R and Bioconductor*: 397-420.

Sparrow, D. B. et al., 2006. Mutation of the LUNATIC FRINGE gene in humans causes spondylocostal dysostosis with a severe vertebral phenotype. *Am. J. Hum. Genet.* 78, 28–37.

Sparrow, D. B., Sillence, D., Wouters, M. A., Turnpenny, P. D. and Dunwoodie, S. L., 2010. Two novel missense mutations in HAIRY-ANDENHANCER-OF-SPLIT-7 in a family with spondylocostal dysostosis. *Eur. J. Hum. Genet.* 18, 674-679.

Sparrow, D.B., Chapman, G., Smith, A.J., Mattar, M.Z., Major, J.A., O'Reilly, V.C., Saga, Y., Zackai, E.H., Dormans, J.P., Alman, B.A., McGregor, L., Kageyama, R., Kusumi, K., Dunwoodie, S.L., 2012. A mechanism for gene-environment interaction in the etiology of congenital scoliosis. *Cell* 149(2):295-306.

Sparrow, D.B., Guillén-Navarro, E., Fatkin, D., Dunwoodie, S.L., 2008. Mutation of Hairy-and-Enhancer-of-Split-7 in humans causes spondylocostal dysostosis. *Hum Mol Genet*. 17(23):3761-6.

Stein, S., Niss, K., Kessel, M., 1996. Differential activation of the clustered homeobox genes CNOT2 and CNOT1 during notogenesis in the chick. *Dev Biol*. 180(2):519-33.

Stern, C.D., 2004. Gastrulation in the chick. In *Gastrulation: From Cells to Embryo*. Cold Spring Harbor Laboratory Press. Cold Spring Harbour, NY. Pp. 219-232.

Stern, C.D., Fraser, S.E., Keynes, R.J., and Primmett, D.R., 1988. A cell lineage analysis of segmentation in the chick embryo. *Development* 104, 231–244.

Stulberg, M.J, Lin, A., Zhao, H., Holley, S.A., 2012. Crosstalk between Fgf and Wnt signalling in the zebrafish tailbud. *Dev. Biol*. 369, 298-307.

Takahashi, J., Ohbayashi, A., Oginuma, M., Saito, D., Mochizuki, A., Saga, Y. and Takada, S., 2010. Analysis of Ripply1/2 deficient mouse embryos reveals a mechanism underlying the rostro-caudal patterning within a somite. *Dev. Biol*. 342, 134-145.

Takahashi, Y., Inoue, T., Gossler, A., Saga, Y., 2003. Feedback loops comprising Dll1, Dll3 and Mesp2, and differential involvement of Psen1 are essential for rostrocaudal patterning of somites. *Development* 130:4259–4268.

Takahashi, Y., Koizumi, K., Takagi, A., Kitajima, S., Inoue, T., Koseki, H., Saga, Y., 2000. Mesp2 initiates somite segmentation through the Notch signalling pathway. *Nat Genet* 25:390-396.

Takashima Y., Ohtsuka T., González A., Miyachi H., Kageyama R., 2011. Intronic delay is essential for oscillatory expression in the segmentation clock. *PNAS* 108(8):3300-5.

Tautz, D., 1988. Regulation of the *Drosophila* segmentation gene hunchback by two maternal morphogenetic centers. *Nature* 332: 281–284.

Tenin, G., Wright, D., Ferjentsik, Z., Bone, R., McGrew, M. J. and Maroto, M., 2010. The chick somitogenesis oscillator is arrested before all paraxial mesoderm is segmented into somites. *BMC Dev. Biol.* 10, 24.

Towers, M., Tickle, C., 2009. Growing models of vertebrate limb development. *Development* 136, 179-190.

Trofka, A., Schwendinger-Schreck, J., Brend, T., Pontius, W., Emonet, T., Holley, S.A., 2012. The Her7 node modulates the network topology of the zebrafish segmentation clock via sequestration of the Hes6 hub. *Development* 139(5):940-7.

Turnpenny, P., Alman, B., Cornier, A. S., Giampietor, P. F., Offiah, A., Tassy, O., Pourquie, O., Kusumi, K. and Dunwoodie, S., 2007. Abnormal vertebral segmentation and the notch signalling pathway in man. *Dev. Dyn.* 236, 1456-1474.

van Eeden, F.J.M., Granato, M., Schach, U., Brand, M., Furutani-Seiki, M., Haffter, P., Hammerschmidt, M., Heisenberg, C.-P., Jiang, Y.-J., Kane, D.A., Kelsh, R.N., Mullins, M.C., Odenthal, J., Warga, R.M., Allende, M.L., Weinberg, E.S., Nusslein-Volhard, C., 1996. Mutations affecting somite formation and patterning in the zebrafish *Danio rerio*. *Development* 123, 153–164.

Vermot J, Pourquié O., 2005. Retinoic acid coordinates somitogenesis and left-right patterning in vertebrate embryos. *Nature* 435(7039):215-20.

Vermot, J., Gallego Llamas, J., Fraulob, V., Niederreither, K., Chambon, P., Dollé, P., 2005. Retinoic acid controls the bilateral symmetry of somite formation in the mouse embryo. *Science* 308(5721):563-6.

Wada, T., Takagi, T., Yamaguchi, Y., Ferdous, A., Imai, T., Hirose, S., Sugimoto, S., Yano, K., Hartzog, G.A., Winston, F., Buratowski, S., Handa, H., 1998. DSIF, a novel transcription elongation factor that regulates RNA polymerase II processivity, is composed of human Spt4 and Spt5 homologs. *Genes Dev*., 12, 343–356.

Wahl, M.B., Deng, C., Lewandoski, M., Pourquie, O., 2007. FGF signalling acts upstream of the NOTCH and WNT signalling pathways to control segmentation clock oscillations in mouse somitogenesis. *Development* 134, 4033–4041.

Wellik, D.M., Capecchi, M.R., 2003. Hox10 and Hox11 genes are required to globally pattern the mammalian skeleton. *Science* 301(5631):363-7.

Wharton, R.P., Struhl, G., 1991. RNA regulatory elements mediate control of Drosophila body pattern by the posterior morphogen nanos. *Cell* 67(5):955-67.

Whittock, N.V., Sparrow, D.B., Wouters, M.A., Sillence, D., Ellard, S., Dunwoodie, S.L., Turnpenny, P.D., 2004. Mutated MESP2 causes spondylocostal dysostosis in humans. *Am J Hum Genet*. 74(6):1249-54.

Wilson, V., Olivera-Martinez. I., Storey, K.G., 2009. Stem cells, signals and vertebrate body axis extension. *Development* 136(10):1591-604.

Wolff, C., Schröder, R., Schulz, C., Tautz, D., Klingler, M., 1998. Regulation of the Tribolium homologues of caudal and hunchback in Drosophila: evidence for maternal gradient systems in a short germ embryo. *Development* 125(18):3645-54.

Wright, D., Ferjentsik, Z., Chong, S-W., Qiu, X., Jiang, Y-J., Malapert, P., Pourquie, O., Van Hateren, N., Wilson, S.A., Franco, C., Gerhardt, H., Dale, J.K., Maroto, M., 2009. Cyclic Nrarp mRNA expression is regulated by the somitic oscillator but Nrarp protein levels do not oscillate. *Dev. Dyn*. 238, 3043–3055.

Wu, L. H., Lengyel, J.A., 1998. Role of caudal in hindgut specification and gastrulation suggests homology between *Drosophila* amnioproctodeal invagination and vertebrate blastopore. *Development* 125: 2433–2442.

Yusuf, F. and Brand-Saberi, B., 2006. The eventful somite: patterning, fate determination and cell division in the somite. *Anat. Embryol*. (Berl.) 211, 21-30.

Zákány J, Kmita M, Alarcon P, de la Pompa JL, Duboule D., 2001. Localized and transient transcription of Hox genes suggests a link between patterning and the segmentation clock. *Cell* 106(2):207-17.

Zandomeni, R., Mittleman, B., Bunick, D., Ackerman, S., Weinmann, R., 1982. Mechanism of action of dichloro-β-D-ribofuranosyl- benzimidazole: effect on in vitro transcription. *PNAS* 79, 3167–3170.

Zhang, N. and Gridley, T., 1998. Defects in somite formation in lunatic fringe- deficient mice. *Nature* 394, 374-377.

Zhang, T., Jiang, T., Zhang, F., Li, C., Zhou, Y.A., Zhu, Y.F., Li, X.F., 2010. Involvement of p21Waf1/Cip1 cleavage during roscovitine-induced apoptosis in non-small cell lung cancer cells. *Oncol Rep*. 23(1):239-45.

Zwartjes, C.G., Jayne, S., van den Berg, D.L., Timmers, H.T., 2004. Repression of promoter activity by CNOT2, a subunit of the transcription regulatory Ccr4-not complex. *J Biol Chem*. 279(12):10848-54.